INVESTIGATING CHANGES IN ANGIOTENSIN II SIGNALLING, RESPIRATORY VARIABILITY AND CAROTID BODY FUNCTION IN RESPONSE TO CHRONIC HYPOXIA

By

HAYYAF SAAD ALDOSSARY

A thesis submitted to

The University of Birmingham

For the degree of

DOCTOR OF PHILOSOPHY

School of Biomedical Sciences
Institute of Clinical Sciences
The University of Birmingham
March 2024

Abstract

Chronic hypoxia (CH) and rises in circulating angiotensin II (Ang II) are key features of chronic obstructive pulmonary disease (COPD), an illness associated with respiratory dysfunction. Hypertension is an important co-morbidity in COPD. It has recently been suggested that the carotid body (CB) has an important role in causing vascular dysfunction in COPD patients. In response to CH, the CB undergoes extensive structural and functional adaptation, leading to hyperactivity. It is proposed that CB hyperactivity contributes to hypertension development in CH/COPD.

The CB serves as a peripheral chemoreceptor located at the common carotid artery bifurcation, sensing and reacting to alterations in arterial O_2, CO_2, and pH levels. Previous studies have suggested the involvement of Ang II and its G Protein-Coupled Receptor (GPCR) member, AT_1R, in mediating CB activity. It is currently unknown if the membrane arrangement of AT_1Rs is altered by CH. It is not clear if Ang II stimulation involves activation of TRPC channels. Furthermore, a role for heightened Ang II-AT_1R-TRPC signalling in mediating CB hyperactivity in response to CH remains uncertain. Key aims of this thesis were to: 1. Assess if AT_1R membrane protein expression is increased in CH, 2. Explore how single molecule organisation of AT_1R is modified by CH, 3. Provide a detailed evaluation of respiratory changes induced by CH, 4. Identify if CB Ang II-TRPC signalling is upregulated in CH and 5. Determine if targeting Ang II-TRPC signalling *in vivo* decreases the blood pressure in CH animals.

In Chapter 2 and 3, utilizing the PC12 cell line as a surrogate for CB type I cells, it was revealed that AT_1R protein expression was elevated by CH, accompanied by modifications in cell size, suggesting adaptive responses to prolonged hypoxia. Subsequent investigations utilising super-resolution microscopy

demonstrated that AT$_1$Rs form distinct clusters in the cell membrane. Furthermore, the maximum cluster size is increased under CH, indicating enhanced supercluster formation.

In Chapter 4, expanding beyond cellular responses, the impact of CH on respiratory variables was evaluated using whole body plethysmography. It revealed key alterations, such as rises in respiratory frequency, shortening of respiratory timings and elevations in inspiratory and expiratory drive. Furthermore, a decrease in breath to breath interval variability was observed after CH exposure.

In Chapter 5, carotid sinus nerve (CSN) activity measurements showed augmented, more consistent responses to Ang II that were apparent in a greater proportion of fibres in the CH group, suggesting increased Ang II sensitivity. In the presence of Ang II, the TRPC channel blocker, specifically 2-APB, produced exaggerated inhibition of CB activity in the CH group, suggestive of a rise in Ang II-TRPC signalling.

Lastly, **in Chapter 6**, cardiovascular measurements showed that single bolus injection of 2-APB did not successfully decrease the mean arterial pressure (MAP) or heart rate (HR) in CH animals. This is likely due to it not reaching a high enough concentration in the CB.

These investigations provide comprehensive information regarding AT$_1$R, CB and respiratory adaptations to CH. The findings should help guide the development of novel therapeutic interventions, based on targeting Ang II-AT$_1$R-TRPC signalling, to treat CB hyperactivity in conditions such as COPD.

Dedication

This thesis is dedicated to my incredible parents, Saad Aldossary and Nawal Albiabi, for their belief in me and their limitless sacrifices. Your endless love and support have been the motivating power behind my academic success. Thank you for being my guiding lights and for shaping me into the person I am today.

Acknowledgment

Throughout my research journey, I have been fortunate to receive invaluable support and guidance from numerous individuals and groups, without whom this work would not have been possible.

of motivation throughout this journey. I am also truly grateful for the number of friends I made in this journey, who became family to me.

My heartfelt and sincere gratitude goes to my father and my mother, whose consistent support, which I would never survive without, and encouragement have been the cornerstone and the driving force behind pursuing my PhD. I am also grateful to my sister and brothers, who have been invaluable sources of support throughout my PhD journey.

I am profoundly grateful to my wife and children, Rawaf and Refan, whose support, understanding, and patience have been the source of my power. Their support has made this journey even more meaningful and rewarding.

Finally, I would like to express my gratitude to King Saud bin Abdulaziz University for Health Sciences for their scholarship, which has been instrumental in making my academic pursuits possible.

Table of contents

List of figures

Chapter 7:

List of abbreviations

2-APB	2-Aminoethoxydiphenyl borate
5-HT	Serotonin
AB	Antibody
ABP	Arterial Blood Pressure
AC	Adenylyl cyclase
ACE	Angiotensin-converting enzyme
Ang II	Angiotensin II
ANOVA	Analysis of Variance
AT$_1$R	Angiotensin II type 1 receptor
B-B interval	Breath-to-breath interval
BL	Baseline
cAMP	Cyclic adenosine monophosphate
CAs	Catecholamines
CB	Carotid body
CcO	Cytochrome c oxidase
CD39	Ecto-nucleosidetriphosphate diphosphohydrolase
CD73	Ecto-5'-nucleotidase
CH	Chronic hypoxia
CIH	Chronic intermittent hypoxia
CO$_2$	Carbon dioxide
COPD	Chronic Obstructive Pulmonary Disease
CSN	Carotid sinus nerve
CSNDR	Carotid sinus nerves discharge rate
DA	Dopamine
DAG	Diacylglycerol
DBSCAN	Density-based spatial clustering of applications with noise
DPT	Differential pressure transducer
dSTORM	Direct stochastic optical reconstruction microscopy
ENT	Equilibrative nucleoside transporter
EPACs	Exchange proteins activated by cAMP
ER	Endoplasmic reticulum
ET	Endothelin
FBS	Foetal Bovine Serum
GA	General anaesthesia
GPCR	G-Protein-Coupled Receptor
Hc	Hypercapnia
HF	Heart failure
HIF	Hypoxia-inducible factor
HIF-1α	Hypoxia-inducible factor 1α
HPC	Human Placental Collagen
HR	Heart Rate
HTN	Hypertension

HV	High voltage
HVR	Hypoxic ventilatory response
Hx	Hypoxia
IP$_3$	Inositol trisphosphate
IP$_3$Rs	Inositol trisphosphate receptors
IQR	Interquartile range
LTF	Long term facilitation
LTP	Long-term potentiation
MAP	Mean arterial pressure
NA	Noradrenaline
NOX	NADPH oxidase
NTM	Neurotransmitter
Nx	Normoxia
OSA	Obstructive sleep apnea
PAC1	Pituitary adenylate cyclase-activating polypeptide type 1
PACAP	Pituitary adenylate cyclase-activating polypeptide
PBS	Phosphate-buffered saline
PHDs	Prolyl hydroxylases
PKC	Protein kinase C
PLC	Phospholipase C
RAS	Renin-angiotensin system
Rf	Respiratory frequency
ROS	Reactive oxygen species
SH	Spontaneous/essential hypertension
SIDS	Sudden infant death syndrome
sLTF	Sensory long-term facilitation
SNS	Sympathetic nervous system
TCT	Total cycle times
Te	Expiratory time
TH	Tyrosine hydroxylase
Ti	Inspiratory time
Ti/Te	Inspiratory to expiratory ratio
TIRF	Total internal reflection fluorescence microscopy
tmAC	Transmembrane adenylyl cyclase
TRP	Transient receptor potential
TRPC	Transient receptor potential Canonical
VCO$_2$	CO_2 production
VE	Minute ventilation
VEGF	Vascular endothelial growth factor
VMAT1	Vesicular monoamine transporter 1
VT	Tidal volume
Vt/Te	Expiratory drive
Vt/Ti	Inspiratory drive
WBP	Whole body plethysmography
WT	Wild type

Chapter 1. Introduction

Part of this Chapter has been published:

Hayyaf S. Aldossary [1,3], Abdulaziz A. Alzahrani [1,4], Demitris Nathanael [1], Eyas A. Alhuthail [1,5], Clare J. Ray [1], Nikolaos Batis [2], Prem Kumar [1], Andrew M. Coney [1] and Andrew P. Holmes [1,6].

[1]Institute of Clinical Sciences, University of Birmingham, Birmingham, UK; HXA807@student.bham.ac.uk (H.S.A.); AAA717@student.bham.ac.uk (A.A.A.); demitris.nathanael@gmail.com (D.N.); EXA833@student.bham.ac.uk (E.A.A.); c.j.ray@bham.ac.uk (C.J.R.); p.kumar@bham.ac.uk (P.K.); a.m.coney@bham.ac.uk (A.M.C.)
[2]Institute of Cancer and Genomic Sciences, University of Birmingham, Birmingham, UK; N.Batis@bham.ac.uk
[3]College of Medicine, Basic Medical Sciences, King Saud bin Abdulaziz University for Health Sciences, Riyadh, Saudi Arabia
[4]Respiratory Care Department, Faculty of Applied Medical Sciences, Umm Al-Qura University, Makkah, Saudi Arabia
[5]Collage of Sciences and Health Professions, Basic Sciences Department, King Saud bin Abdulaziz University for Health Sciences, Riyadh, Saudi Arabia
[6]Institute of Cardiovascular Sciences, University of Birmingham, Birmingham, UK

1.1 Carotid body (CB) physiology in normoxia and hypoxia

The CB ensures adequate oxygen supply to tissues by modulating respiratory rate and depth through neural pathways (Lopez-Barneo et al., 2008). Under normal oxygen conditions, oxygen-sensitive, TASK and BK potassium channels in type I cells are open and maintain a resting membrane potential (Buckler, 2015a, Buckler, 2015b).

During hypoxia, the inhibition of these potassium channels leads to cell depolarization (Pulgar-Sepulveda et al., 2018, Patel and Honoré, 2001). This depolarization opens voltage-gated calcium channels, causing an influx of calcium ions (Pulgar-Sepulveda et al., 2018, Patel and Honoré, 2001). The increased intracellular calcium triggers the exocytosis of neurotransmitters such as acetylcholine, dopamine, and ATP from the type I cells into the synaptic cleft (Pulgar-Sepulveda et al., 2018, Patel and Honoré, 2001).

The released neurotransmitters bind to receptors on the afferent nerve endings of the glossopharyngeal nerve and this interaction generates action potentials that are transmitted to the respiratory centers in the medulla oblongata of the brainstem (Gold et al., 2022). The brainstem processes these signals and responds by increasing the rate and depth of breathing, which enhances oxygen uptake and carbon dioxide excretion, thereby normalizing blood gas levels (Iturriaga et al., 2021).

1.2 CB O$_2$ sensing and chemoreflex activation

Acute O$_2$ sensing by the CB is a complex process governed by unique cellular and molecular mechanisms within the sensory type I/glomus cells (Ortega-Saenz et al., 2020). One of the specialisations appears to be the presence of unique mitochondria and the presence of multiple mitochondrial related signalling pathways (Holmes et al., 2018a, Holmes et al., 2022). These mitochondria are distinct in structure and function, enabling them to play a critical role in the detection of changes in O$_2$ levels (Ortega-Saenz et al., 2020).

The type I cell mitochondria contain unique subunits, such as those within the O$_2$-sensitive enzyme cytochrome c oxidase (CcO), which is suggested to serve as the primary O$_2$ sensor (McElroy and Chandel, 2017, Buckler and Turner, 2013, Gao et al., 2017). CcO, a key component of the mitochondrial electron transport chain, undergoes changes in its redox state in response to variations in O$_2$ levels (Srinivasan and Avadhani, 2012). When O$_2$ concentrations decrease (hypoxia), the CcO and electron transport chain become more reduced, leading to a proposed increase in production of reactive O$_2$ species (ROS) within the mitochondria at complex I and III, possibly mediated via enhanced succinate metabolism (Srinivasan and Avadhani, 2012, Fernandez-Aguera et al., 2015, Cabello-Rivera et al., 2022, Swiderska et al., 2021, Arias-Mayenco et al., 2018).

The increased ROS levels are suggested to cause type I cell depolarization thereby contributing to the opening of voltage-gated Ca^{2+} channels, leading to Ca^{2+} influx (Yamamoto et al., 2006). This rise in intracellular Ca^{2+} triggers the release of neurotransmitters, including dopamine, acetylcholine and ATP, with the latter two being responsible for the generation of post-synaptic action potentials in sensory fibres

of the carotid sinus nerve (Leonard et al., 2018). These cellular events result in the activation of the chemoreflex including a strong rise in ventilation, an increase in heart rate (HR), peripheral vasoconstriction and adrenaline release (Beckhauser et al., 2016, Kumar, 2009, Fernandez-Aguera et al., 2015, Swiderska et al., 2021). In addition to ROS, it has also been suggested that numerous other mitochondrial related signalling pathways are initiated in response to the depression in mitochondrial electron transport (Holmes et al., 2022). These include: a fall in ATP leading to TASK channel blockade, (Varas et al., 2007), an increase in lactate generation, (Chang et al., 2015), and a change in the overall cellular redox status (Bernardini et al., 2020). Other potential O_2 signalling mechanisms independent of the mitochondria include direct O_2 sensitive K^+ channels and increased generation of H_2S (Peng et al., 2010, Lopez-Barneo et al., 1988).

During hypoxia, the mitochondrial-derived ROS may activate various signaling pathways, including those related to stabilization of hypoxia-inducible factor (HIF) (Sena and Chandel, 2012). HIF is a transcription factor that plays a central role in cellular adaptation to low O_2 levels (Sena and Chandel, 2012). In normoxic conditions, HIF is hydroxylated by O_2-dependent prolyl hydroxylases (PHDs), leading to its degradation (Marxsen et al., 2004). However, under hypoxic conditions, the activity of PHDs is inhibited, allowing HIF to accumulate and translocate to the nucleus (Marxsen et al., 2004). In the nucleus, HIF induces the expression of genes involved in adaptive responses to hypoxia, such as erythropoietin and vascular endothelial growth factor (VEGF) (Ramakrishnan et al., 2014). Although some evidence does suggest that HIF2 is needed for the CB to respond acutely to low O_2, this may be linked to its development rather than it being involved in the acute O_2 signalling mechanism (Bishop et al., 2013, Macias et al., 2018).

The complex interplay of mitochondrial O_2 sensing, Ca^{2+} signaling, and potential HIF activation highlights the complexity of the CB response to hypoxia. However, this unique mechanism ensures a rapid and coordinated adjustment of respiratory and cardiovascular functions to maintain O_2 delivery to the brain and vital organs before their metabolism starts to be severely impaired (Kumar, 2009).

While the CB primarily senses alterations in O_2 levels, it also responds to changes in carbon dioxide (CO_2) and pH levels (Iturriaga et al., 2021). Indeed, it is thought that the primary mechanism of CO_2 induced chemoexcitation is mediated by intracellular generation of H^+ and a fall in pH. The diversity of these stimuli demonstrates the adaptability of the CB and the chemoreflex to maintain blood gases and pH. Dysregulation of these mechanisms is implicated in various respiratory and cardiovascular disorders such as obstructive sleep apnoea, obesity, essential hypertension and heart failure, emphasizing the clinical significance of understanding the molecular and cellular processes underlying acute O_2 sensing and overall CB function.

1.3 CB adaptation to chronic hypoxia (CH)

Prolonged exposure to low O_2 environments triggers a series of complex mechanisms that allow the CB to modulate its function, contributing to the overall physiological adaptation of the respiratory and cardiovascular systems (Prabhakar et al., 2022).

One of the central players in the CBs adaptation to CH is the HIF signalling pathway (Powell and Fu, 2008). In CH, the sustained reduction in O_2 availability inhibits PHD activity, preventing HIF degradation (Semenza

and Prabhakar, 2018). Consequently, stabilized HIF translocates to the nucleus, where it acts as a transcription factor, orchestrating changes in expression of genes involved in various adaptive responses.

One notable adaptation involves an increase in the number (hyperplasia) of type I cells (Lopez-Barneo et al., 2008). It remains unclear if this co-insides with an elevation in single type I O_2 sensitivity. A heightened O_2 sensitivity could be achieved through the upregulation/modification of key components in the O_2-sensing pathway, such as CcO as has been observed in other cell types (Castello et al., 2008). In other tissues, an upregulated 'hypoxic' phenotype of CcO enhances the responsiveness of cells to changes in O_2 levels, ensuring a more robust detection of hypoxia (Castello et al., 2008). Whether further mitochondrial isoform switching occurs in the CB type I cell in response to CH remains to be determined.

What is more well established is that CH induces structural changes in the CB, including hypertrophy and hyperplasia of type I cells (Prabhakar et al., 2009). There are currently three main ideas of where an increase in TH-positive type I cells come from. The first is that the type I cells themselves divide in response to the CH stimulus and this is dependent on PHD2-HIF2α signalling (Fielding et al., 2018). The second is that the type II cells in the CB differentiate into type I cells in response to CH, acting as a type of glial-like stem cell (Pardal et al., 2007). The third is that CH activates fast neurogenesis of immature (normally quiescent) catecholaminergic (TH-positive) neuroblasts such that they develop into new type I cells with acute O_2 sensitivity (Sobrino et al., 2018). Clearly, more research is needed to reconcile these findings, although it may be that each is partially responsible for the overall rise in type I cell number. This morphological adaptation is accompanied by an increased vascularity within the CB, enhancing blood flow to support heightened metabolic demands (Prabhakar et al., 2009). The enhanced vascularization is, in part, facilitated by HIF-mediated upregulation of angiogenic factors, such as vascular endothelial growth

factor (VEGF) (Krock et al., 2011). Although much work has been done in this area there is still much to uncover regarding the full CB adaptation to CH. In particular, more work is needed to better understand specific changes in ion channel and GPCR expression/function and neuromodulation. Part of this thesis explores the importance of angiotensin signalling and TRP channels in mediating CB hyperactivity associated with CH.

In addition to cellular and structural adaptations, the CB influences systemic responses to CH through the elevated release of neurotransmitters and increased sensory action potential input into the brainstem (Powell, 2007). Increased production and release of neurotransmitters, such as dopamine, acetylcholine and ATP, contribute to an increase in the hypoxic ventilatory response (HVR)(Powell, 2007). In some species, such as the mouse, it appears that the rise in HVR is only apparent in the presence of 3% CO_2. This is likely due to some animals e.g. rodents, being more susceptible to respiratory alkalosis (Bishop et al., 2013). The increased CB type I cell neurotransmitter release is linked to HIF-dependent changes in intracellular Ca^{2+} rises during acute hypoxia and changes in the expression of relevant ion channels (Pulgar-Sepulveda et al., 2018).

Whilst it is known that breathing is enhanced in response to CH, previous reports have mainly focused on parameters such as respiratory frequency (Rf), tidal volume (VT) and minute ventilation (VE). Much less is known about specific changes in respiratory timings such as inspiratory (Ti) and expiratory (Te) times and overall changes in inspiratory and expiratory drive (VT/Ti and VT/Te). Furthermore, it is unclear whether there are modifications in the patterning or variability of breathing in response to CH. Identifying such changes would be helpful in providing a more detailed characterization of the respiratory adaptation that occurs in CH. In addition, these changes could be linked to the extent of CB hyperplasia/hypersensitivity.

Therefore, one of the aims of this thesis to provide a more detailed characterization of the respiratory adaptation that takes place in response to CH.

The adaptive responses to CH are not limited to the CB. For instance, CH stimulates erythropoiesis, mediated by HIF-induced production of erythropoietin, leading to an increased red blood cell count and haematocrit (Haase, 2010). This systemic response enhances the O_2-carrying capacity of the blood, facilitating improved O_2 delivery to tissues. In addition, in response to sustained hypoxia there is pulmonary vasoconstriction which often leads to right ventricular hypertrophy (Prieto-Lloret et al., 2021). There are also modifications in endothelial function, vascular reactivity, vascular sympathetic nerve activity and blood pressure (Rook et al., 2014, Marshall, 2015, Walsh and Marshall, 2006). Exposure to hypoxia may also increase the risk of fatal cardiac arrhythmias (Plant et al., 2020).

In summary, the CB demonstrates a sophisticated process to adapt to CH, orchestrated by the HIF pathway and encompassing changes at cellular, whole-organ, and whole-body levels. The interaction of these mechanisms ensures a comprehensive cardiovascular-respiratory adjustment to prolonged low O_2 conditions, ultimately contributing to the maintenance of whole-body metabolism in this challenging environment.

1.4 A potential role for the CB in mediating cardiovascular disease in chronic obstructive pulmonary disease (COPD)

1.4.1 COPD overview

COPD is one of the leading causes of morbidity and mortality globally, with its prevalence progressively rising over the past few decades (Chen et al., 2023). According to the World Health Organization (WHO), an estimated 251 million people suffer from COPD worldwide. This number is expected to increase further due to factors such as aging populations, continued exposure to risk factors, and improved diagnostic techniques leading to better detection rates (Boers et al., 2023).

The pathophysiology of COPD involves chronic inflammation and structural changes in the airways and lung tissue (Hogg and Timens, 2009). Prolonged exposure to irritants leads to airway inflammation, mucus hypersecretion, and remodelling of the airway walls, seen in chronic bronchitis (Hogg and Timens, 2009). Additionally, destruction of alveolar walls in emphysema reduces lung elasticity, causing air trapping and hyperinflation (Hogg and Timens, 2009). With the destruction of alveolar walls, the surface area available for gas exchange is diminished (Baraldo et al., 2012), this impairs the O_2 and CO_2 gas exchange, contributing to chronic hypoxia (CH) and hypercapnia.

Clinically, COPD presents with symptoms such as chronic cough, sputum production, dyspnoea, and wheezing, significantly impacting patients' quality of life and potentially leading to respiratory failure and cardiovascular complications (Devine, 2008). COPD patients frequently demonstrate altered breathing aimed at optimizing gas exchange and reducing dyspnoea (Yentes et al., 2020). These changes often include prolonged expiration, increased respiratory rate, and the use of accessory muscles (Sarkar et al., 2019).

Techniques like pursed-lip breathing help alleviate symptoms by maintaining airway patency and facilitating more effective gas exchange (Sarkar et al., 2019).

1.4.2 CH and cardiovascular consequences in COPD

COPD presents many challenges beyond respiratory impairment, including significant cardiovascular implications induced by CH (Kent et al., 2011). In COPD, compromised lung function leads to inadequate oxygenation of tissues, resulting in persistent hypoxia, which triggers various systemic responses with major cardiovascular consequences (Kent et al., 2011).

One of the primary cardiovascular effects of CH in COPD is pulmonary hypertension (Kent et al., 2011). Hypoxic pulmonary vasoconstriction, a physiological response to low oxygen levels, causes constriction of pulmonary arterioles, leading to increased pulmonary vascular resistance (Dunham-Snary et al., 2017). Over time, this can ultimately lead to right ventricular hypertrophy and heart failure (Dunham-Snary et al., 2017, Rosenkranz et al., 2016).

Furthermore, CH in COPD exacerbates existing cardiovascular conditions, such as ischemic heart disease and arrhythmias. Reduced oxygen delivery to the myocardium worsens ischemia and impairs cardiac function, increasing the risk of myocardial infarction and cardiac arrhythmias (Morgan et al., 2018a). Relatively little is known about cardiac autonomic activity in COPD and whether this contributes to an increase in arrhythmia incidence.

Beyond the heart and pulmonary vasculature, CH in COPD also impacts systemic blood vessels. The number one symptom associated with COPD is the development of systemic hypertension (Kim et al., 2017, Finks et al., 2020, Greulich et al., 2017) . Increased sympathetic nervous system activity, driven by hypoxia, encourages peripheral vasoconstriction and heightened vascular tone (Kent et al., 2011). This can exacerbate peripheral vascular disease and contribute to complications such as peripheral artery disease and eventually systemic hypertension (Kim et al., 2017).

1.4.3 Interaction of CH and CB hyperactivity in mediating cardiovascular complications of COPD

The interplay between CH and CB activation plays a significant role in exacerbating cardiovascular dysfunction in COPD, worsening peripheral vascular disease and other related complications (Phillips et al., 2018).

CH, a key feature of COPD, initiates a series of adaptive responses within the body, including the persistent stimulation of the CB (Phillips et al., 2018). This is proposed to contribute to the persistent rise sympathetic nerve activity (Prabhakar et al., 2022). This heightened sympathetic outflow may encourage greater vasoconstriction and heightened vascular tone, ultimately contributing to neurogenic hypertension, a form of hypertension driven by neural factors rather than by renal or hormonal mechanisms (Prabhakar et al., 2022). Thus, targeting the CB in patients with COPD may offer a novel strategy for treating hypertension and improving cardiovascular outcomes.

In COPD, the adaptation to CH, mainly in the CB, is thought to contribute to the observed increase in the hypoxic ventilatory response (HVR) (Kobayashi et al., 1996). While this response initially aims to maintain

adequate O_2 levels in the short/mid term, prolonged activation may contribute to the development of cardiovascular complications, including systemic hypertension and cardiac arrhythmias.

1.4.4 Inflammatory pathways and vascular dysfunction in COPD

Systemic inflammation is another feature of COPD, contributing to disease progression and exacerbations, as well as cardiovascular complications (King, 2015). The chronic inflammatory state observed in COPD involves the release of various inflammatory mediators, including cytokines and ROS, which may also have effects on vascular function and structure (Barnes and Celli, 2009, Agusti and Faner, 2012).

Endothelial dysfunction, characterized by impaired vasodilation and increased vascular permeability, is a key consequence of systemic inflammation in COPD (Theodorakopoulou et al., 2021). Inflammatory cytokines such as tumour necrosis factor-alpha (TNF-α) and interleukin-6 (IL-6) disrupt endothelial function by reducing nitric oxide bioavailability and promoting oxidative stress, contributing to vasoconstriction and vascular stiffness (Neunhauserer et al., 2021, Theodorakopoulou et al., 2021).

Moreover, systemic inflammation in COPD promotes atherosclerosis, a chronic inflammatory disease of the arteries characterized by the accumulation of plaques (Hughes et al., 2020). Inflammatory cells infiltrate the arterial wall, promoting plaque formation and destabilization, increasing the risk of myocardial infarction and stroke (Brassington et al., 2022). In addition to atherosclerosis, systemic inflammation in COPD contributes to vascular remodelling, characterized by structural changes in blood vessels (Karnati et al., 2021). These alterations may exacerbate vascular dysfunction and increase the risk of cardiovascular events.

The interaction between CH-induced CB hyperactivation and systemic inflammation are both likely to contribute to the overall increases risk of cardiovascular morbidity and mortality in COPD. Whilst endothelial dysfunction, vascular remodelling, and inflammation, are known critical components of hypertension in COPD patients, much less is known about the potential neurogenic component of hypertension driven by the CB. This thesis aims to assess some of the potential CB adaptations mediated by CH, that contribute to its hyperactivity, focusing on Ang II and TRPC signalling. This should help guide future CB-targeted therapies for potential treatment of COPD patients.

1.5 G-Protein-Coupled Receptor (GPCR) Signaling in the Carotid Body: Roles in Hypoxia and Cardiovascular and Respiratory Disease (adapted from Aldossary et al., 2020).

The CB is a critical sensory organ, located near the carotid bifurcation, that constantly monitors blood supplying the brain (Kumar and Prabhakar, 2012a). The CB is stimulated by acute hypoxia, upon which it rapidly activates vital cardiovascular and respiratory reflexes, including peripheral vasoconstriction, elevated heart rate and increased breathing (Kumar, 2009). It is essential in initiating a rapid response to Hx and alter physiological function aiming to correct this reduction and improve O_2 levels. It is now apparent that there are numerous G-protein-coupled receptors (GPCRs) expressed in the CB, and that modulation of these receptors is able to alter baseline CB activity and the sensitivity to hypoxia. Indeed, components of GPCR signaling pathways represent some of the most highly expressed genes in the rodent CB (Zhou et al., 2016). Three different types of GPCR alpha subunit have been identified to date in the CB: $G_{\alpha s}$, $G_{\alpha i}$ and $G_{\alpha q}$, and each one of these subtypes has a unique mechanism of action. Activation of $G_{\alpha s}$ will lead to transmembrane adenylyl cyclase (tmAC) activation, which in turn leads to an increase in intracellular cAMP. In contrast, the activation of $G_{\alpha i}$ will lead to the inhibition of tmAC activity, which in turn decreases cAMP (Nunes et al., 2013, Nunes et al., 2014). The activation of $G_{\alpha q}$ activates phospholipase C

(PLC), leading to the production of diacylglycerol (DAG) and IP_3, which can modify $[Ca^{2+}]_i$, protein kinase activity, ion channel function and potentially also ROS generation (Kumar and Prabhakar, 2012a). Importantly, the CB has gained attention clinically due to its hyperactivity in a number of conditions, including obstructive sleep apnea (OSA) (Prabhakar, 2016) and heart failure (HF) (Schultz and Li, 2007), in which it promotes neurogenic hypertension and arrhythmia (Iturriaga et al., 2021). Multiple GPCRs have been implicated in CB hyperactivity, and these may offer key targets for novel drug discovery or repurposing. However, as yet, there are no drugs used clinically that directly target the CB, and this will be required in order to provide better and more personalized treatment of CB-mediated cardiovascular and respiratory disease. The aim of this chapter is to briefly explore the role of the major GPCRs and associated ligands in the CB, both in mediating normal CB function, hypoxic sensitivity and CB hyperactivity.

1.5.1 $G_{\alpha q}$-Protein-Coupled Receptor Signaling in the CB

Angiotensin II

Angiotensin II (Ang II) is a powerful hormone that influences many organs, and its level is increased in important cardiovascular diseases including HF, hypertension, COPD and chronic kidney disease. A wealth of evidence has also shown that Ang II acutely increases CB chemoafferent frequency with a threshold in the pico/nano-molar range (Allen, 1998c, Peng et al., 2011b). Rises in $[Ca^{2+}]_i$ initiated by Ang II can be attenuated by losartan, an AT_1R antagonist (Fung et al., 2001). RT-PCR analysis revealed that both AT_{1a} and AT_{1b} subtypes are expressed in type I cells and immunohistochemistry has confirmed the presence of AT_1R protein (Fung et al., 2001, Atanasova et al., 2018c). Combined with the finding that an AT_2-receptor antagonist was not able to prevent the Ang II-induced increase in $[Ca^{2+}]_i$ [+], these results suggest that AT_1Rs are responsible for modifying CB activity via Ang II.

Although AT_1R mRNA increases in CH, it isn't known if this translates into an increase in membrane protein expression. It is now known that GPCRs tend to form clusters or hotspots in the cell membrane rather than being randomly expressed (Aldossary et al., 2023). Changes in such cluster number, size or density may enhance local microdomain signalling. A key aim of this thesis is to establish if AT_1Rs are present in distinct clusters in CB type I cells (or in similar cell lines derived from the same neural crest origin). Furthermore, how exposure to CH may modify the cluster characteristics of AT_1Rs is unknown and will therefore also be explored.

AT_1Rs are coupled to the $G_{\alpha q}$ protein and its activation leads to the generation of IP_3, via phospholipase C, causing the release of Ca^{2+} from intracellular stores (Leung et al., 2003). It is now thought that this rise in Ca^{2+} is sufficient to activate the non-selective cation channel which contributes to cellular depolarization (Wang et al., 2017b), Figure 1.3. Interestingly, in other tissues it has been reported that Ang II can cause activation of TRPC channels, leading to increased cellular excitability and intracellular Ca^{2+} (Ilatovskaya et al., 2014). A number of studies have reported that TRP channels are expressed in the CB (Buniel et al., 2003a, Shirahata et al., 2015, Iturriaga et al., 2021). However, it remains to be seen if Ang II stimulation of the CB type I cell involves TRPC channel activation. Identifying a link between Ang II and TRPC in the CB will be explored in this thesis and it will be determined if this pathway is upregulated in response to CH.

Repetitive application of Ang II can also promote sensory long-term facilitation (sLTF) of chemoafferent nerve activity in CIH CBs, an effect reliant on activation of NADPH-oxidase and ROS generation (Peng et al., 2011b). AT_1R signalling is also key to causing CB sLTF and persistent sympathoexcitation following acute intermittent hypoxia, in a PKC, ROS-dependent manner (Kim et al., 2018, Roy et al., 2018). This suggests that even in healthy CBs, Ang II maybe able to induce LTF under the right circumstances. In this thesis it

will be determined whether or not multiple repetitive applications of Ang II are able to produce LTF of the baseline carotid sinus nerve activity in healthy CBs.

An interesting concept is regarding the kinetics or time course of the response to Ang II. Most studies up to now have only applied Ang II for brief periods, making it difficult to establish if the response is well sustained. Many GPCRs can internalise upon prolonged agonist stimulation leading to termination/run-down of the acute response and initiating activation of secondary signalling pathways. Whether the response to prolonged Ang II in the CB desensitizes due to receptor phosphorylation, β-arrestin recruitment and internalization is yet to be studied. Therefore, some experiments in this thesis will use sustained application of Ang II to examine the detailed kinetics of the CB response to Ang II, and establish if this is modified by CH.

Recent reports have indicated that AT_1R inhibition does not reduce the HVR or chemoreflex in healthy humans before or after a short period (8 h) of hypoxia (Brown et al., 2020). Furthermore, raising serum Ang II in healthy individuals does not lead to chemoreflex sensitization (Solaiman et al., 2014). This possibly indicates that Ang II and AT_1R signaling might be more important in pathology or short/long-term CB adaptation rather than setting chemosensitivity in healthy individuals. *In vivo* experiments in this thesis will target Ang II-TRPC signalling using 2-APB signalling to identify if heightened chemoreflex activation in CH (e.g. rise in HR and changes in ABP) is dependent on an upregulation in Ang II related signalling pathways.
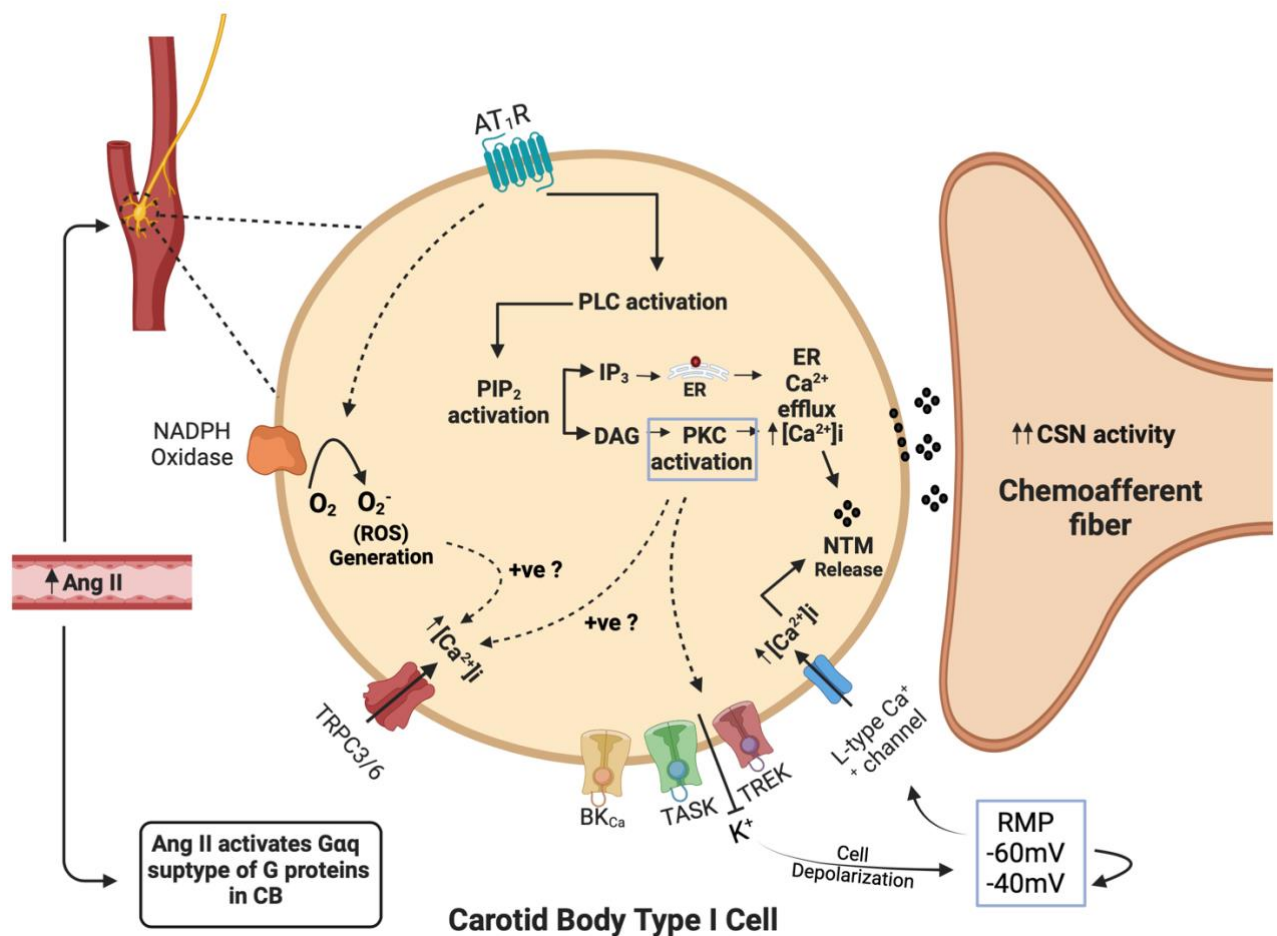
Figure 1.1 Illustrates the process following the activation of AT1R due to increase in circulatory Ang II.

The activation of AT_1R will cause an activation of phospholipase C (PLC), this activation will in turn activates phosphatidylinositol 4,5 bisphosphate (PIP_2). Hydrolysis of PIP_2 by PLC produces intracellular mediators such as inositol triphosphate (IP_3) and diacylglycerol (DAG). IP_3 will bind to the endoplasmic reticulum (ER), causing ER Ca^{2+} efflux and cell depolarization. DAG will activate protein kinase C (PKC), and the activation will in turn block K^+ channels, leading to further depolarization. PKC activation might contribute to TRP channels activation, leading to more Ca^{2+} efflux. Cell depolarization will eventually lead to neurotransmitter release. On the other hand, AT_1R activation could directly affect NADPH oxidase and lead to ROS generation.

1.5.2 A role for Angiotensin II in CB hyperactivity?

CH has been shown to increase AT_{1a} and AT_{1b}-receptor mRNA expression in type I cells as well as CSN sensitivity to Ang II (Leung et al., 2000). As yet, it is unknown if this correlates with an elevation in membrane AT_1R protein expression. In situ hybridization, PCR and Western blot analysis have confirmed the presence of components of the renin-angiotensin system (RAS), including angiotensinogen and angiotensin-converting enzyme (ACE), in type I cells of the CB, indicative of a local system (Lam et al., 2004b). These components are elevated in rat CBs exposed to CH and CIH (Lam et al., 2004b, Lam et al., 2014). AT_1R protein is also increased in CBs following CIH (Marcus et al., 2010). It has therefore been suggested that Ang II may play a role in causing CB hyperactivity in diseases associated with CH and/or CIH, e.g., in OSA. To support this, heightened sympathetic activity following exposure to CIH is prevented in rats treated with losartan, an AT_1R inhibitor (Marcus et al., 2010). Translational findings in humans are currently limited. However, in a recent clinical trial, it was observed that losartan reduced systolic and diastolic blood pressure in OSA patients without modifying muscle-sympathetic outflow or ventilation during hypoxia (Morgan et al., 2018b). OSA was fairly well established in these patients and as such, there may have been irreversible epigenetic remodelling of CB function (Nanduri et al., 2017b), accounting for the apparent lack of impact of losartan on CB function. Future studies could evaluate if losartan or similar agents are more effective in protecting against the development of hypertension in newly diagnosed or more-mild OSA patients.

In animal models of HF, augmented CB Ang II signalling is also suggested to increase basal and hypoxic sympathetic outflow and contribute to neurogenic hypertension (Li et al., 2006). AT_1-receptor antagonists reduce chemoafferent discharge frequency and renal sympathetic nerve activity in rabbits with HF but not controls (Li et al., 2006). Furthermore, The AT_1R antagonist, L-158,809 (1 µM), significantly decreases the

sensitivity of voltage-dependent K$^+$ current to hypoxia in type I cells isolated from HF but not control rabbits (Li and Schultz, 2006). These increased actions of Ang II in HF are reported to be mediated by increased NADPH-oxidase activity and ROS generation (Li et al., 2007). Clinical trials are now called for to directly assess the role of Ang II and Ang II antagonists in mediating CB hyperactivity and hypertension in human patients with HF.

It is established that Ang II is important in driving CB hyperactivity in CIH and HF. However, its importance in mediating CB hyperactivity in CH is less clear. A key aim of this thesis is to examine if CH increases AT$_1$R protein expression and/or modifies single AT$_1$R organisation/cluster characteristics. This will be done using a combination of confocal and super-resolution microscopy. In addition, work will be performed to determine whether heightened CB activity associated with CH is dependent on changes in the sensitivity and response kinetics to Ang II. The work also aims to better characterise a link between Ang II signalling and TRPC channel activation in the CB, and determine if this is augmented by exposure to CH. *In vivo* experiments will be performed to evaluate if targeting AngII-TRPC signalling may improve cardiovascular function in CH animals. This should therefore provide a more detailed picture of the adaptations associated with CH that are mediated by Ang II signalling in the CB.

1.5.2 GPCR Summary

G-proteins play a crucial role in CB function both in normal physiology and pathology. Activation of GPCRs in the CB can cause either stimulation or the inhibition of chemoafferent activity dependent on intricate balance between numerous different neuromodulators, GPCRs and second messenger systems. Ultimately, changes in the output from the CB mediated by GPCRs will have important systemic effects, including variations in ventilation, heart rate, blood vessel vasoconstriction and blood glucose. Importantly, GPCRs have a very significant part in evoking CB hyperactivity, hypertension and cardiac arrhythmia associated with key conditions such as OSA and HF. Despite this, there is still no therapy used clinically that directly targets the CB. Thus, translational studies are urgently required to evaluate if drugs targeting GPCRs can effectively protect against or reverse CB-mediated cardiovascular disease in humans.

1.6 Transient Receptor Potential (TRP) channels in the CB

TRP channels represent a diverse family of ion channels involved in the detection and transduction of various sensory stimuli (Zhang et al., 2023). Among the numerous TRP channel subtypes, several have been identified as key players in mediating responses within the CB (Buniel et al., 2003a). TRP channels contribute significantly to the complex processes governing O_2 sensing and the subsequent reflex responses initiated by the CB (Buniel et al., 2003a). The Transient Receptor Potential Canonical (TRPC) channels, belonging to the larger TRP superfamily, are key components in the intricate machinery of O_2 sensing within the CB (Mori et al., 2016). TRPC channels, particularly TRPC1, TRPC3, and TRPC6, have been identified in the type I cell of the CB using Western Blotting and PCR, potential playing a crucial role in transducing signals associated with changes in blood O_2 levels (Iturriaga et al., 2021).

TRPC channels are activated by a variety of stimuli, including G protein-coupled receptors (Kim et al., 2012). In the CB, these channels are implicated in mediating the influx of Ca^{2+} ions in response to hypoxic conditions (Mori et al., 2017). The activation of TRPC channels initiates downstream signaling events, including cellular depolarisation, rises in Ca^{2+}, and the release of neurotransmitters, which orchestrate the CB reflex (Iturriaga et al., 2021).

In addition to TRPC channels, the vanilloid subfamily, which includes TRPV1, TRPV3, and TRPV4, also play a significant role in CB O_2 sensing (Jendzjowsky et al., 2021, Numata et al., 2013). TRPV1, expressed in type I cell, responds to various stimuli, including heat, acidic pH, and certain chemicals (Jendzjowsky et al., 2021). In the context of the CB, TRPV1 activation is associated with increased intracellular Ca^{2+}, contributing to the modulation of neurotransmitter release and the subsequent activation of whole-body reflex responses (Jendzjowsky et al., 2021).

Similarly, TRPV4 channels, sensitive to changes in osmotic pressure, temperature, and mechanical stress, are expressed in the CB (Numata et al., 2013, Phan et al., 2009). Activation of TRPV4 channels contributes to an elevation in intracellular Ca^{2+} concentration, thereby participating in the overall response of the CB to environmental stimuli (Randhawa and Jaggi, 2015). The presence of TRPV4 channels in type I cell underscores their role in transducing multiple signals, enhancing the sensitivity of the CB to O_2 fluctuations.

Beyond the vanilloid subfamily, the melastatin subfamily, including TRPM3, TRPM6, and TRPM7 channels are reported to be present in the CB (Shirahata et al., 2015). In the CB, these channels may contribute to sensory responses crucial for maintaining homeostasis. TRPM3 channels are known to be expressed in sensory neurons and have been associated with thermal and chemical sensitivity (Su et al., 2021). TRPM6, primarily recognized for its role in magnesium homeostasis, might also play a role in cellular processes within the CB (Luongo et al., 2018). TRPM7, with its dual function as an ion channel and kinase, has been suggested to participate in O_2 sensing and cellular signalling pathways in other tissues through its sensitivity to ATP, and potentially could influence the CBs response to changes in O_2 levels (Touyz, 2008).

Additionally, the ankyrin subfamily, represented by TRPA1, is expressed in the CB (Chen et al., 2020a). TRPA1 channels are activated by various chemical stimuli, including ROS (Taylor-Clark, 2016, Taylor-Clark et al., 2008). Their involvement in the CB remains to be defined.

The presence of diverse TRP channel subtypes in the CB indicates a potential involvement in O_2 sensing. Understanding the specific contributions of TRP channel subtypes in the CB should enhance our grasp of the molecular mechanisms governing CB O_2 sensing and reflex regulation, with potential implications for

respiratory and cardiovascular health. This thesis will investigate a potential link between Ang II signalling and TRPC activation in the CB and evaluate if this is enhanced following exposure to CH.

1.7 The involvement of the CB in CH pathophysiology: the role of Ang II and TRPC channels

The CB plays a significant role in conditions like COPD, HTN, and HF due to its sensitivity to hypoxia and its influence on SNS activity (Iturriaga et al., 2016b & Somers, 2016b). In COPD, characterized by chronic airflow limitation and significant lung inflammation, impaired gas exchange leads to CH (Albert and Calverley, 2007), causing sustained activation of the CB (Iturriaga et al., 2016b & Somers, 2016a). This triggers an increase in respiratory drive and SNS activity, resulting in heightened ventilatory responses, elevated heart rate, and increased blood pressure (Iturriaga et al., 2016b & Somers, 2016a). Similarly, in hypertension, the CB's heightened sensitivity to hypoxia contributes to increased SNS activity, promoting vasoconstriction, elevated heart rate, and impaired baroreflex sensitivity, which exacerbate blood pressure control (Felippe et al., 2023). In heart failure, reduced cardiac output leads to systemic hypoxia, prompting the CB to increase SNS drive, which results in higher heart rate, vasoconstriction, and fluid retention, worsening heart failure symptoms (Schultz and Li, 2007). CH in these conditions induces adaptive changes in the CB, enhancing its reactivity and maintaining elevated SNS activity, thereby sustaining cardiovascular and respiratory complications.

Angiotensin II is known to sensitize the CB to hypoxia, enhancing its chemoreceptive function (Leung et al., 2003). In COPD, elevated levels of ANG II can exacerbate carotid body activity, further increasing sympathetic output and contributing to the systemic effects of the disease (van Gestel et al., 2012).

TRPC channels are involved in the CB's response to hypoxia (Buniel et al., 2003b). These channels mediate calcium influx in response to hypoxic conditions, playing a crucial role in the depolarization and activation of carotid body glomus cells (Buniel et al., 2003b). The increased expression or activity of TRPC channels may enhance the CB's sensitivity to hypoxia, amplifying its output.

Ang II not only acts on the vasculature to increase blood pressure but also sensitizes the carotid body (Li and Schultz, 2006). By enhancing the chemoreceptive functions of the CB, Ang II plays a crucial role in the maladaptive sympathetic activation seen in these chronic conditions (Li and Schultz, 2006). On the other hand, TRPC channels mediate calcium entry in response to hypoxic stimuli, a key step in carotid body activation (Lopez-Barneo et al., 2016). Their role is critical in the context of CH conditions like COPD and heart failure, where increased TRPC activity can lead to persistent CB stimulation and subsequent sympathetic activation.

1.8 The PC12 cell-line as a model of CB type I cells

The PC12 cell line, derived from a pheochromocytoma of the rat adrenal medulla, has proven to be an invaluable tool in neurobiological research (Oprea et al., 2022). The adrenal medullary chromaffin cells and CB type I cells share the same neural crest embryological origin. They are both neurosecretory cells, with large amounts of dense core vesicles containing dopamine and ATP (Westerink and Ewing, 2008). PC12 cells share physiological similarities with type I cells of the CB, particularly in their responsiveness to O_2 levels leading to neurotransmitter release (Greene and Tischler, 1976). PC12 cells possess characteristics that mimic some of the O_2-sensing mechanisms observed in CB type I cell, making them a suitable *in vitro* model for studying O_2 sensing and neurosecretion (Conforti et al., 2000).

One of the key similarities lies in the expression of O_2-sensitive enzymes, including cytochrome c oxidase (CcO). PC12 cells, like CB type I cells, exhibit the presence of CcO, which plays a crucial role in the cellular response to changes in O_2 levels (Zhdanov et al., 2008). The upregulation and unique nature of CcO in both cell types contribute to their unusually acute sensitivity to hypoxia.

Furthermore, PC12 cells, similar to CB type I cell, respond to changes in O_2 levels by modulating intracellular Ca^{2+} concentrations (Westerink and Ewing, 2008). The influx of Ca^{2+} ions is a common feature in both cell types under hypoxic conditions (Green et al., 2002). This elevation in intracellular Ca^{2+} serves as a trigger for downstream events, including the release of neurotransmitters, such as dopamine and ATP (Koizumi et al., 2002).

While PC12 cells do not fully replicate the complex cellular and structural architecture of the CB, their physiological similarities make them a valuable model for investigating fundamental aspects of O_2 sensing and adaptation to CH. The use of PC12 cells as an alternative for CB type I cells can still contribute to the understanding of O_2-sensing and adaptive mechanisms in a simplified *in vitro* setting when access to animal tissue is restricted. In this thesis PC12 cells were used to evaluate changes in AT_1R protein expression and clustering in response to CH. PC12 cells were used in the early-stages of the project when access to animal tissue was not possible due to restrictions implemented during the COVID-19 pandemic.

1.9 Key thesis aims

- Assess if CH increases AT_1R protein expression in PC12 cells

- Determine whether AT_1Rs are organised in distinct clusters in the cell membrane of PC12 cells rather than being randomly distributed, using super-resolution microscopy

- Evaluate if AT_1R cluster characteristics are altered by exposure to CH

- Using *in vivo* measurements of animal breathing, validate my animal model of CH and observe whether CH induces changes in inspiratory/expiratory timings, inspiratory/expiratory drive and breathing variability.

- Assess if AngII-TRPC signalling is enhanced in CBs isolated from CH animals, using *ex vivo* recordings of carotid sinus nerve activity

- Determine if alterations cardiovascular function caused by CH can be alleviated by *in vivo* targeting of AngII-TRPC signalling in the CB i.e. by use of a TRPC channel blocker.

Chapter 2. Investigating the impact of chronic hypoxia on angiotensin II receptor type 1 (AT$_1$R) protein expression in PC12 cells

2.1 Chapter introduction and overview

The CB is a small sensory organ located bilaterally at the bifurcation of the common carotid artery (Kumar and Prabhakar, 2012b). Thus, the CB is perfectly positioned to continuously monitor the components of the blood perfusing the brain. The CB sensory function is mainly driven by type I ''glomus'' cells and supported by type II cells (Lever et al., 1959).

Type I cells originate from the neural crest and contain large amount of catecholamines which explains the presence of established cell markers, such as tyrosine hydroxylase (TH), a rate-limiting enzyme of catecholamine synthesis (Kameda, 1996). Type I cells are primarily stimulated by any acute changes in blood contents and classical stimuli include acidic pH, hypoxia and hypercapnia (Lopez-Barneo et al., 2016). Type I cells have a round shape, approximately 10 μm diameter, and contain a dense arrangement of neurosecretory vesicles and mitochondria (Kumar and Prabhakar, 2012b).

COPD is a pathological condition, characterized by chronic hypoxia (CH). Patients with COPD live with a $P_aO_2 < 60$ mmHg (Cukic, 2014). This level of oxygen will lead to persistent activation of CB and possibly cell growth and hypersensitivity (Cukic, 2014). CB hyperactivity during COPD could lead to other consequences in the long-term, such as a chronic reflex activation of the sympathetic nervous system (SNS) which could drive neurogenic hypertension. Indeed, in a small cohort of COPD patients, it has been shown that CB hyperactivity promotes vascular dysfunction in these patients (Phillips et al., 2018). Thus, effective

targeting of the CB could offer a novel approach to treating hypertension in patients with COPD. To do this, a better understanding of CB adaptation to CH is needed.

It has become apparent that the CB can be stimulated by a host of other blood-borne stimuli, including hormones, cytokines, hypoglycaemia and lactate (Kumar and Prabhakar, 2012b, Chang et al., 2015, Allen, 1998b, Bin-Jaliah et al., 2004, Thompson et al., 2016). Ang II is a critical hormone that influences many organs and its level is increased in many important cardiovascular diseases; such as heart failure (HF) and hypertension (HTN) (Opie and Sack, 2001). Ang II and its receptor, AT_1R, play crucial roles in the CB (Aldossary et al., 2020). AT_1R is located on type I cells, endothelial cells, and afferent nerve fibres within the CB (Aldossary et al., 2020) and enables Ang II to enhance the chemosensitivity to hypoxia, modulate blood flow, and influence neurotransmitter release (Kumar and Prabhakar, 2012b). Ang II also promotes angiogenesis within the CB, improving blood supply and enhancing chemosensory function, particularly under chronic hypoxic conditions (Li et al., 2006). This interaction supports respiratory control, blood pressure regulation, and adaptive responses to chronic hypoxia, thereby maintaining homeostasis under varying oxygen conditions (Forrester et al., 2018). Ang II is also known to be elevated in COPD and it is possible that an increase in Ang II signalling augments CB sensory activity in these patients (Cho et al., 2011).

Evidence has shown that exogenous Ang II acutely stimulates the CB, causing a rise in $[Ca^{2+}]_i$, which in turn triggers the release of neurotransmitters from their vesicles, leading to the increase of the CB chemoafferent discharge frequency (Allen, 1998a, Fung et al., 2001, Peng et al., 2011a). RT-PCR analysis has revealed that both AT_{1a} and AT_{1b} subtypes are expressed in type I cells and immunohistochemistry

has confirmed the presence of AT_1R protein (Atanasova et al., 2018a, Fung et al., 2001). AT_1R are coupled to the $G_{\alpha q}$ protein and overall stimulation is thought to be a consequence of PLC-mediated IP_3 and DAG generation, release of Ca^{2+} from intracellular stores, PKC stimulation and ion channel activation (Figure 2.1) (Leung et al., 2003), (Wang et al., 2017a). In other tissue, AT_1R signalling acts to modify the activity of TRP channels including TRPC3 (Nishida et al., 2015).
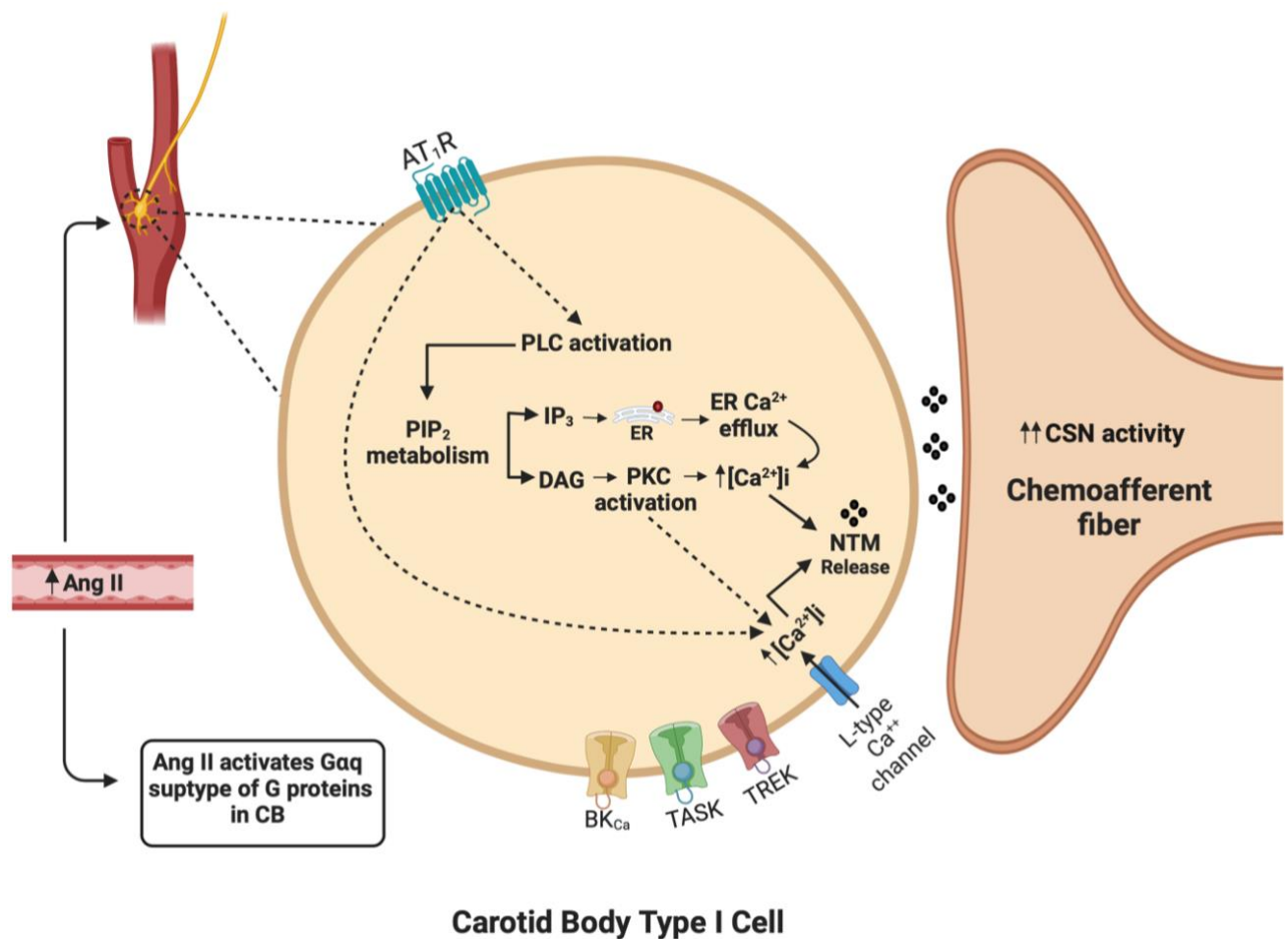
Figure 2.1 The mechanism of angiotensin II type 1 receptor (AT_1R) stimulation of the carotid body (CB) by Angiotensin II (Ang II).

Adapted from (Aldossary et al., 2020).

It has been suggested by (Lam et al., 2014) and others that the CB locally facilitates Ang II generation, due to its expression of angiotensinogen. They have shown that CIH induces an upregulation of renin-angiotensin system expression in the CB, including an increase in angiotensinogen and angiotensin-converting enzyme (ACE) signalling in type I cells (Lam et al., 2004a). They reported that angiotensinogen and angiotensin-converting enzyme mRNA expression were significantly increased after the induction of CIH and measurements of $[Ca^{2+}]_i$ revealed that the CB becomes more sensitive to Ang II (Lam et al., 2014). It has also been reported that CH increases AT_{1a} and $AT_{1b}R$ mRNA expression in type I cells (Leung et al., 1998) as well as CB sensitivity to Ang II (Lam et al., 2004a, Leung et al., 2000). However, it is not yet clear if AT_1R protein is increased in response to CH and which mechanisms are responsible for the increase in sensitivity to Ang II.

Although AT_1R mRNA expression is known to increase in response to CH, little is known about the specific changes in AT_1R protein expression and membrane organisation in the CB. Cellular imaging such as confocal microscopy and direct stochastic optical reconstruction microscopy (dSTORM) could provide a clearer indication about AT_1R protein expression changes after exposure to CH. The aim of this Chapter was initially to measure AT_1R protein expression and organisation in the CB before and after exposure to CH. However, these plans were disrupted due to the inability to perform animal experiments during the COVID-19 pandemic. Furthermore, no such CB cell line was available. Therefore, the PC12 cell line was used to determine the impact of CH on AT_1R expression. The PC12 cell line is a cell line derived from a tumour of rat adrenal medullary chromaffin cells. These cells have the same embryological origin as CB type I cells and have many similarities such as very high content of catecholamines and acute O_2 sensitivity.

Tyrosine hydroxylase (TH) is expressed in all CB type I cells and is essential as the rate-limiting enzyme in catecholamine synthesis, converting tyrosine to L-DOPA (Daubner et al., 2011). Catecholamines produced by these cells are crucial for the chemoreceptive function of the carotid body, mediating responses to hypoxia by signalling respiratory and cardiovascular adjustments (Iturriaga et al., 2021). The presence of TH indicates that type I cells can produce catecholamines, necessary for their role in detecting and responding to changes in blood oxygen levels (Kato et al., 2010).

Due to its ubiquitous presence in CB type I cells, TH is commonly used to identify this cell type in immunofluorescent experiments. Additionally, in disease states such as COPD, hypertension, and heart failure, altered TH expression in the CB can indicate pathophysiological changes (Kato et al., 2010). CH, a common feature in these conditions, often leads to increased TH levels, reflecting enhanced chemosensitivity and sympathetic activity (Czyzyk-Krzeska et al., 1992). Monitoring TH expression provides insights into the functional status of the CB, the progression of these diseases, and the effectiveness of therapeutic interventions aimed at reducing CB hyperactivity.

2.1.1 Chapter hypotheses

- CH increases AT$_1$R protein expression in PC12 cells.

- CH alters TH expression in PC12 cells.

- The exposure to CH augments PC12 cell size.

2.1.2 Chapter aims

- Develop and optimise a method of immunocytochemistry to visualise AT$_1$R and TH expression in PC12 cells using confocal microscopy.

- Determine the impact of CH on AT$_1$R and TH expression in PC12 cells as measured using immunocytochemistry.

- Test whether CH has an impact on PC12 cell size.

2.2 Methods

2.2.1 PC12 cell culture and establishing growth rates

PC12 cells are a rat pheochromocytoma cell line that share many similarities with CB type I cells. These cells were used to optimise immunostaining techniques for assessment of AT_1R protein expression.

Undifferentiated PC12 cells were purchased from Sigma-Aldrich, Gillingham, UK. Lot: 88022401) via the "European Collection of Authenticated Cell Cultures". The initial cell count was around 5000 cells in total. Cell number had to be increased to approximately ($1.0X10^6$/ml) to be able to perform subsequent functional experiments. PC12 cells were grown in RPMI media (1X) Gluta MAX+ (ThermoFisher, Paisley, UK), supplemented with 10% Horse Serum (ThermoFisher, Paisley, UK), 5% Foetal Bovine Serum (FBS) (ThermoFisher, Paisley, UK); Penicillin (50μg/ml, ThermoFisher, Paisley, UK) and Streptomycin (50μg/ml, ThermoFisher, Paisley, UK), incubated at 37°C and equilibrated with 5% CO_2 in air, pH 7.35-7.45. Cells were originally placed in flasks lying horizontally and rat tail collagen (5μg/cm^2, ThermoFisher, Paisley, UK) was used to adhere cells to the flask's surface. After two days, cell number increased from approximately $6.0X10^4$/ml to $1.0X10^5$/ml, with doubling time of approximately 71 hours, which indicate a relatively slow growth rate.

PC12 cells may not grow well when they are adhered to a surface (Wiatrak et al., 2020). Therefore, cells were subsequently cultured in suspension without the addition of rat tail collagen. In this experiment, the cell growth improved, from $1.0X10^5$/ml to $1.2X10^5$/ml per week, but this was still slower than expected.

One of the other unique characteristics of PC12 cells is that they usually grow in clusters (Wiatrak et al., 2020). This characteristic led to the decision of keeping the flasks in a vertical position during the

incubation time, allowing cells to cluster together in suspension rather than forming a monolayer on the flask surface. This modification led to a significant rise in the growth rate with cell density increasing from $1.2X10^5$/ml to $9.5X10^5$/ml in one week. After optimizing the foundation of cell growth, follow up with regular cell counts and cell maintenance started. Cells were supported and monitored by changing the media as well as counting the cells three times per week.

As seen in the cell growth chart (Figure 2.2), PC12 cell number continued to increase up to the minimum targeted cell count for staining and imaging, which is approximately ($1X10^6$/ml). The cell number continued to increase after the passage 26 (P26). At (P38) the cell count plateaued at ($8X10^7$/ml) after which cell number started to decline very gradually (Figure 2.2). The targeted starting point to perform experiments was at least $1X10^6$/ml, ensuring that enough cells would be in each well/dish and targeted number of cells/ml was reached at P26 (Wiatrak et al., 2020).
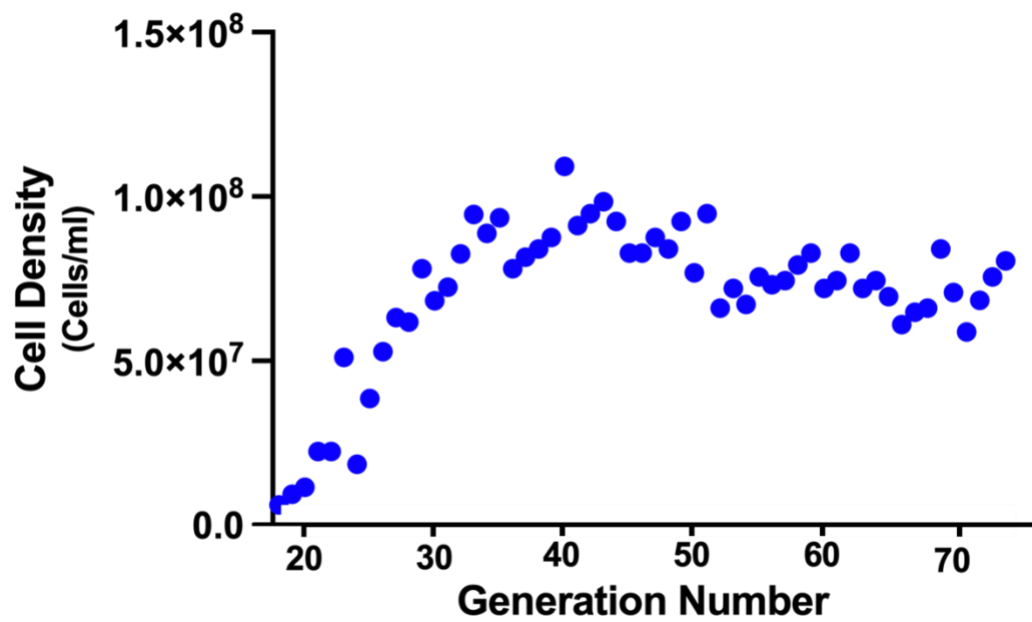
Figure 2.2 An example of the cell growth timeline for a single batch of PC12 cells.

The figure shows PC12 cell growth, the y axis represents the number of cells per ml, while the x axis represents the generation (passage) number.

2.2.2 Immunocytochemistry

A subset of cells was taken out of suspension media and plated on 10 mm microwell imaging dish (MatTek Corporation, Ashland, USA. Lot: P35G-1.5-10-C) containing 400 μg/ml Human Placental Collagen (Sigma-Aldrich, Gillingham, UK. Lot: SLBN2983V). Cells were allowed to adhere to the coverslip in normoxia (20% O_2) and 37°C, for 1 hour. Cells were then incubated in either normoxia (control) (20% O_2) or hypoxia, (1% O_2) for a further 4, 12 or 24 hours and 3 repeated experiments for each group was performed. Cells were then immediately fixed in 4% paraformaldehyde (Alfa Aesar, Lancashire, UK. Lot: S04F501) for 90 minutes to ensure maximal immobilization of cellular proteins. Cells were permeabilised with a 0.1% Triton (VWR, Lutterworth, UK. Lot: 437002A) in PBS solution for 5 minutes and blocked in a 5% BSA in PBS solution for 60 minutes. The primary AT_1R antibody (abcam, Cambridge, UK. Lot: ab124734-16) (1:500) and Tyrosine

Hydroxylase (TH) (abcam, Cambridge, UK. Lot: ab129991) (1:500) were diluted in blocking solution and incubated overnight at 4°C. Cells were washed three times in PBS, blocked again for 30 minutes and then incubated in secondary antibodies (Alexa Fluor 647 F(ab')2 fragment of goat anti-rabbit IgG (H+L), 1:1000, ThermoFisher Scientific, Waltham, MA, USA. Lot: 2147629) and (Alexa fluor 488 F(ab')2 fragment donkey anti-mouse IgG (H+L), 1:1000, ThermoFisher Scientific, Waltham, MA, USA. Lot: 2229195) for 90 minutes at room temperature.

The antibody ab124734 from Abcam is a rabbit monoclonal antibody that targets the AT_1R. It specifically binds to an epitope within the extracellular N-terminal domain of AT_1R (abcam, Cambridge, UK, RRID: AB_11156128). This region is critical for the receptor's interaction with Ang II. The antibody's binding to this extracellular segment makes it valuable for functional studies involving AT_1R (abcam, Cambridge, UK), (Bian et al., 2019, Joshi et al., 2019). While the antibody ab129991 is a rabbit monoclonal antibody that targets TH (abcam, Cambridge, UK, RRID: AB_11156128). This antibody specifically targets an amino acid sequence within the N-terminal region of the TH protein. (abcam, Cambridge, UK), (Li et al., 2021, Cheng et al., 2020, Nakashima et al., 2009).

2.2.3 Confocal Imaging

Confocal microscopy is an advanced method to look at cells or tissues at higher spatial resolution than conventional wide-field microscopy. A laser is used to excite the fluorescently labelled specimen at a desired wavelength. Emitted fluorescence is filtered as it passes through a dichromatic mirror and needs to pass through a pinhole before reaching the detector (Fellers.T.J.; and Davidson.M.W., 2021). As such fluorescence will only be captured from a single focal plane (depth) in the sample (Fellers.T.J.; and

Davidson.M.W., 2021). Fluorescence will not be captured that is emitted at different depths within the sample (different focal planes). This reduces the amount of background/out of focus light, increasing the ability to resolve the point of origin of the emitted fluorescence. However, this method is still limited due to the diffraction limit of light with a resolution in the hundreds of μms (Wu et al., 2021). The principal of confocal microscopy is demonstrated in Figure 2.3.
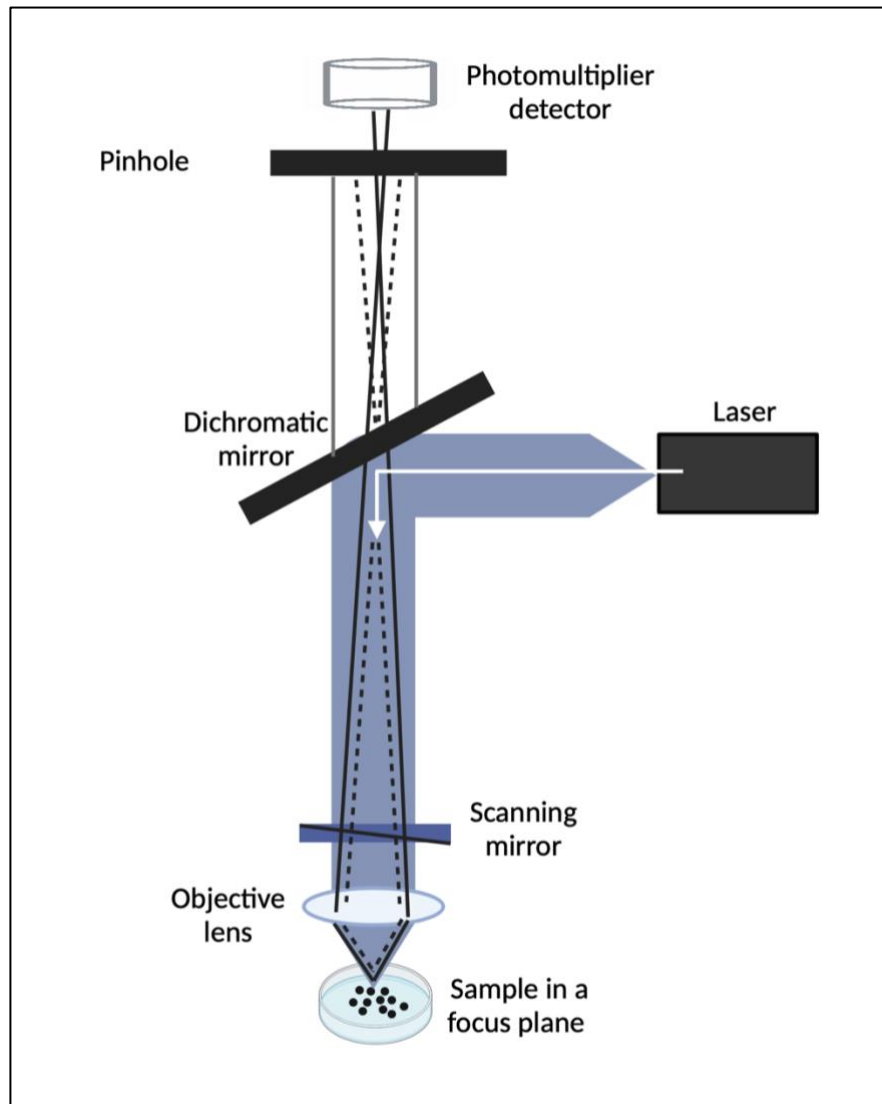
Figure 2.3 Confocal microscopy principle.

Confocal microscopy offers higher spatial-resolution imaging of cells and tissues. Emission light passes through a dichroic mirror and then a pinhole before reaching the detector. Emitted fluorescence from different depths of the specimen will not pass through the pinhole. Thus, this method allows for imaging in a single focal plane.

Single cells in this experiment were imaged using a confocal microscope (Olympus Fluoview FV1000) fitted with a water immersion objective (Olympus FV1000; 40×, NA 1.3) using (Olympus FV10-ASW 4.2) imaging software. All images were acquired at 512 x 512 pixels using one-way mode at 2.0 μs/pixel. The sample

was excited at 650 nm and emission captured at 665 nm (Alexa Fluor 647). Additional imaging settings were: 1) High voltage (HV), which controls the signal amplification, set at 720V (Scherer, 2019); 2) Gain, a digital value multiplication factor applied to all of the the pixels, set at 4.5x (Scherer, 2019); 3) Black level control (offset) (Scherer, 2019) was set at -4% and 4) Laser intensity set at 11%. Alexa fluor 488 was excited at 490nm and emission measured at 525nm. For Alexa fluor 488 imaging settings were: HV of 720V, Gain of 4.0x, offset of 0% and laser intensity of 17%. These settings were consistent for all cells imaged, allowing for quantification and comparison of fluorescent intensity between different experimental groups. After cell imaging, analysis was performed using ImageJ. The whole cell area was carefully selected using the freehand selection feature in ImageJ. After selecting the targeted cell, the mean intensity of fluorescent emitted was quantified across the whole cell area. This accounted for any change in cell area that may have occurred. The fluorescent intensity was measured twice, first for Alexa 647 then for Alexa 488 for each cell. Cells were chosen randomly, based on their location in the dish. The non-selective staining creating background was calculated and compared within groups. The amount of background was equal between groups (Figure 2.4) and was therefore not subtracted.
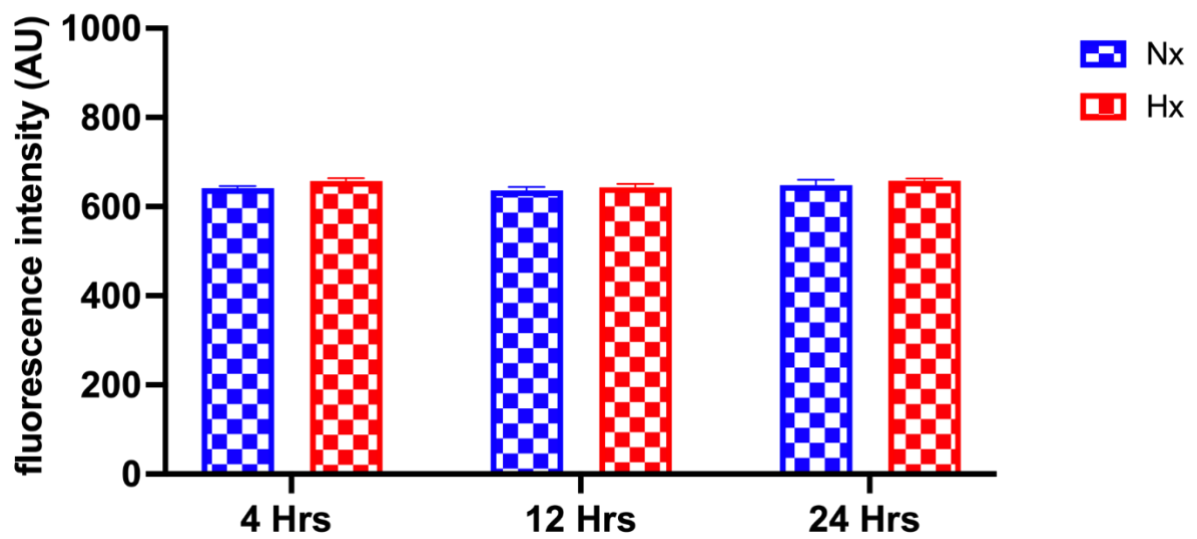
Figure 2.4 Background fluorescence intensity across all experiments.

The background intensity was consistent and not significantly different across all the experimental conditions. A (2 X 2 µm^2) was selected randomly for 6 cells in each group. (Data is presented as mean±SEM) and were tested using Two-way ANOVA with Bonferroni post-hoc analysis.

2.2.4 Analysis of data

For this experiment, the analysis was done per experimental repeat (3 repeats per group/condition) and per cell repeat (all cells on the same group/condition), this method is described in (Table 2.1). Data is presented as box-whisker plots, where the box represents the 25 to 75 percentiles, the line in the box represents the median, and the whiskers represent the minimum and maximum values. Statistical analysis was performed using a two-way Analysis of Variance (ANOVA) and Bonferroni Post-hoc test (Prism v8-10, GraphPad Software, Boston, MA, USA). Significance was considered as p<0.05. Data is presented in the text as mean ± SEM.

		First Experiment *	Second Experiment *	Third Experiment *	Total Cell Number **
4 Hrs	Nx	30 Cells	22 Cells	40 Cells	92 Cells
	Hx	15 Cells	18 Cells	32 Cells	65 Cells
12 Hrs	Nx	24 Cells	24 Cells	45 Cells	93 Cells
	Hx	21 Cells	28 Cells	32 Cells	81 Cells
24 Hrs	Nx	13 Cells	21 Cells	38 Cells	72 Cells
	Hx	32 Cells	23 Cells	37 Cells	92 Cells

* Cells were stained in the same days
** Cells were stained in differant days

Table 2.1 Demonstration of experimental design. For analysis the mean of each experimental repeat was taken along with the mean of the total cell number (by averaging all the cells from the same group together from the 3 experiments at each individual time point and experimental condition). Nx- normoxia (20% O_2), Hx-hypoxia (1% O_2).

2.3 Results

2.3.1 PC12 adherent substrate optimisation and selection of optimal antibody concentrations

After reaching the target cell count per ml and initially starting to image PC12 cells using confocal microscopy, it was noted that cells were not adhering well to the imaging dish coverglass. Initially, Poly-L-Lysine 1.0 mg/ml was used as an adherent substrate (Figure 2.5 A). Despite Poly-L-Lysine being the most frequently used adherent material in cellular staining protocols (Mazia et al., 1975), it was not optimal for PC12 cells in these experiments; only a few cells adhered to the imaging dish compared to cell count when in suspension. Next, two concentrations of Poly-D-Lysine 0.1 mg/ml (Figure 2.5 B) and 1.0 mg/ml (Figure 2.5 C) were used as a potential alternative adherent substrate. Based on cell count monitoring, using pilot experiments and light microscopy, Poly-D-Lysine proved to be a better substrate than Poly-L-Lysine, but the number of cells adhered was still far lower than compared to those grown in suspension, again indicating sub-optimal adherence. Two concentrations of Human Placental Collagen (HPC) were also tested, 200μg/ml (Figure 2.5 D) and 400μg/ml (Figure 2.5 E). HPC improved cell adherence and allowed the cells to remain in clusters (Figure 2.5 D & E). HPC 400 μg/ml was therefore the substrate used for further imaging studies. After the confirmation of optimum substrate type and concentration, the optimisation of the primary antibody concentrations was also needed, to ensure the optimal signal intensity. For the confocal microscopy experiments, 1:200, 1:500 and 1:1000 anti-AT$_1$R and anti-TH concentrations were tested (Figure 2.6). The 1:200 concentration produced a saturated/overexposed AT$_1$R and TH signal, compromising the information obtained from the experiment (Figure 2.6 A). The 1:1000 concentration produced a very low signal (especially for the AT$_1$R) (Figure 2.6 C). The 1:500 concentration was selected as the optimum concentration for both AT$_1$R and TH (Figure 2.6 B). It was also confirmed that the secondary antibody alone does not produce a significant signal, indicative of negligible non-selective staining (figure 2.6 D).
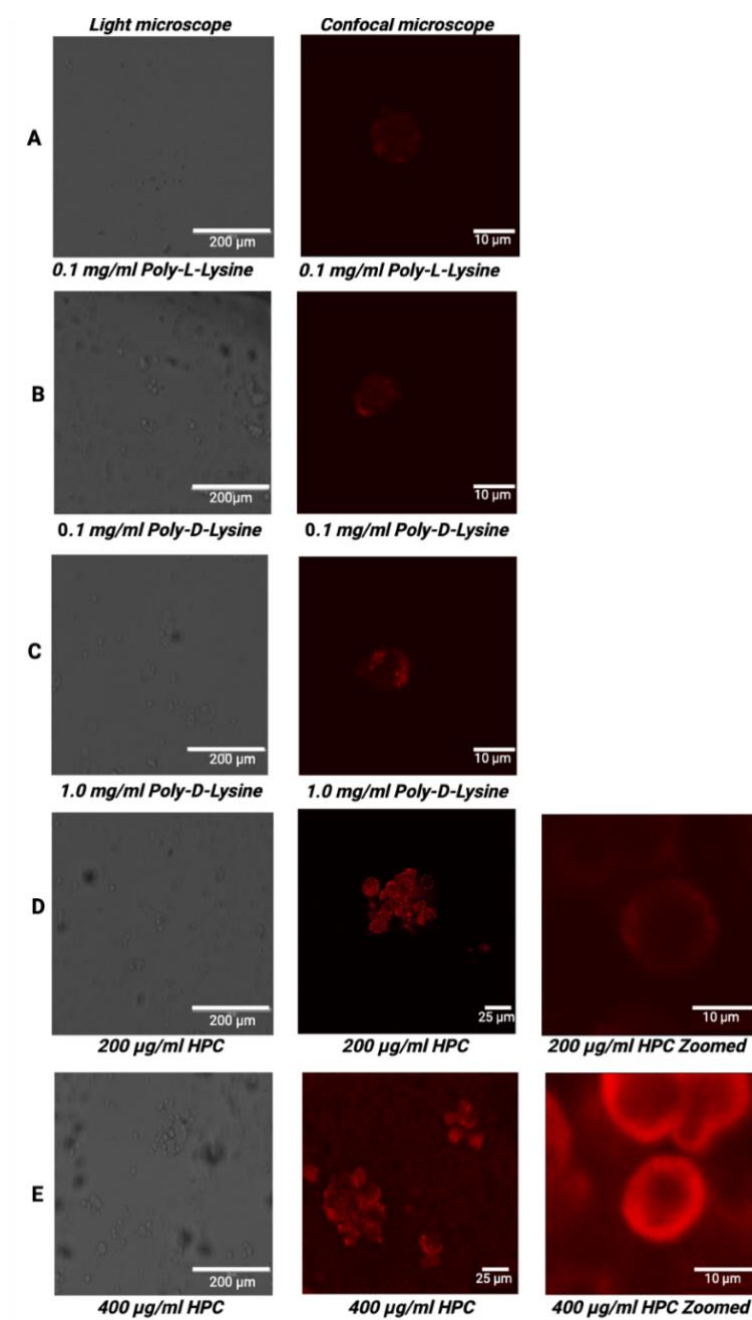
Figure 2.5 Comparing adherent substrates for cell imaging.

All images of PC12 cells were stained with primary antibody (AB); anti-AT$_1$R AB (1:500) and secondary AB Alexa fluor 647 (1:500). A) PC12 cells after using 0.1% Poly-L-Lysine imaged using a light microscope (**left**) and confocal microscope (**right**). B) PC12 cells after using 0.1 mg/ml Poly-d-Lysine imaged using a light microscope image (**left**) and a confocal microscope (**right**). C) PC12 cells imaged after using 1.0 mg/ml Poly-d-Lysine with a light microscope (**left**) and a confocal microscope (**right**). D) PC12 cells imaged after using 200µg/ml human placental collagen (HPC) with a light microscope (**left**), confocal microscope image (**middle**), and magnified confocal image (**right**). E) PC12 cells imaged after using 400µg/ml HPC with a light microscope (**left**), a confocal microscope (**middle**) and a magnified confocal image (**right**). The scale bars are 200 µm for the light microscope and 10 or 25 µm and confocal microscope, unless otherwise stated.
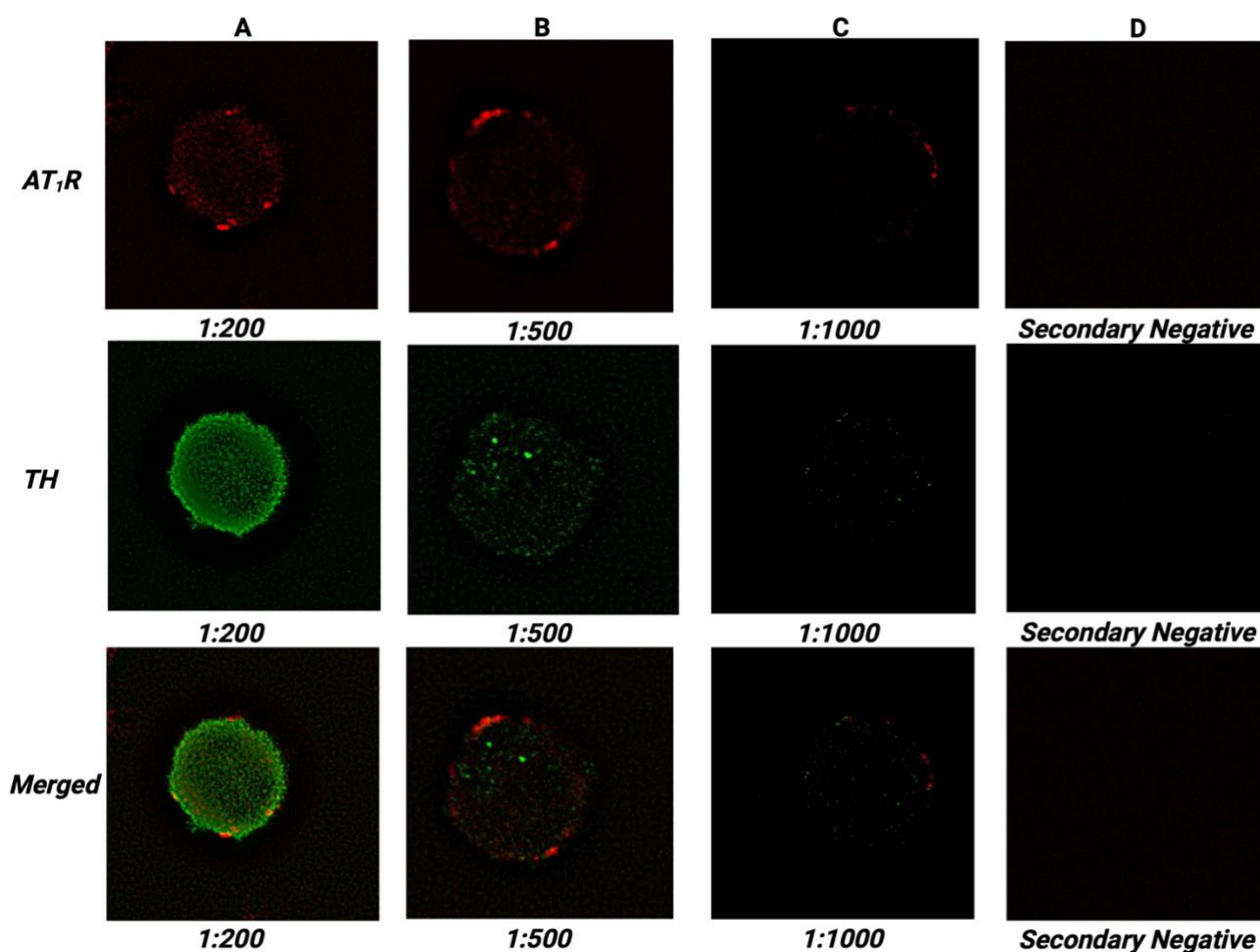
Figure 2.6 Comparing primary antibody concentrations.

A) PC12 cells stained with (1:200) concentrations of anti-AT$_1$R and anti-TH primary antibodies and conjugated secondary antibodies (Alexa Fluor 647 1:1000 and Alexa Fluor 488 1:1000). B) PC12 cells stained with (1:500) concentrations of anti-AT$_1$R and anti-TH primary antibodies and conjugated secondary antibodies (Alexa Fluor 647 1:1000 and Alexa Fluor 488 1:1000). C) PC12 cells stained with (1:1000) concentrations of anti-AT$_1$R and anti-TH primary antibodies and conjugated secondary antibodies (Alexa Fluor 647 1:1000 and Alexa Fluor 488 1:1000). D) Shows PC12 cells stained with only conjugated secondary antibodies (Alexa Fluor 647 1:1000 and Alexa Fluor 488 1:1000).

2.3.2 Hypoxia increases PC12 cell size in a time dependent manner

4 hours of hypoxic (1% O_2) exposure, produced no significant alteration in cell area when compared to normoxic conditions. Both normoxic, 155.5±7.4 μm^2 (n=92), and hypoxic cells, 150.9±8.2 μm^2 (n=65), exhibited similar cell areas, and the difference was not statistically significant (p=0.67), Figure 2.7 A-C.

However, as the duration of hypoxia exposure increased, changes in cell area became evident. 12 hours of hypoxia exposure caused a significant increase in cell area (Figure 2.7 A-C). Under normoxic conditions, the cell area was 142.9±5.8 μm^2 (n=93), while in 12 hours hypoxia, it increased to 165.0±6.8 μm^2 (n=81). This difference was statistically significant (p=0.01), indicating that prolonged exposure to 1% O_2 for 12 hours caused an increase in cell area, Figure 2.7 A-C.

Moreover, 24 hours of hypoxia exposure, showed similar trend. The cell area remained significantly increased compared to normoxia. In normoxic cells, the mean cell area was 143.4±6.2 μm^2 (n=72), while after 24 hours hypoxia, it increased to 183.2±8.5 μm^2 (n=92). This difference was statistically significant (p=0.0005), indicating a substantial increase in cell area after 24 hours of hypoxia exposure, Figure 2.7 A-C.
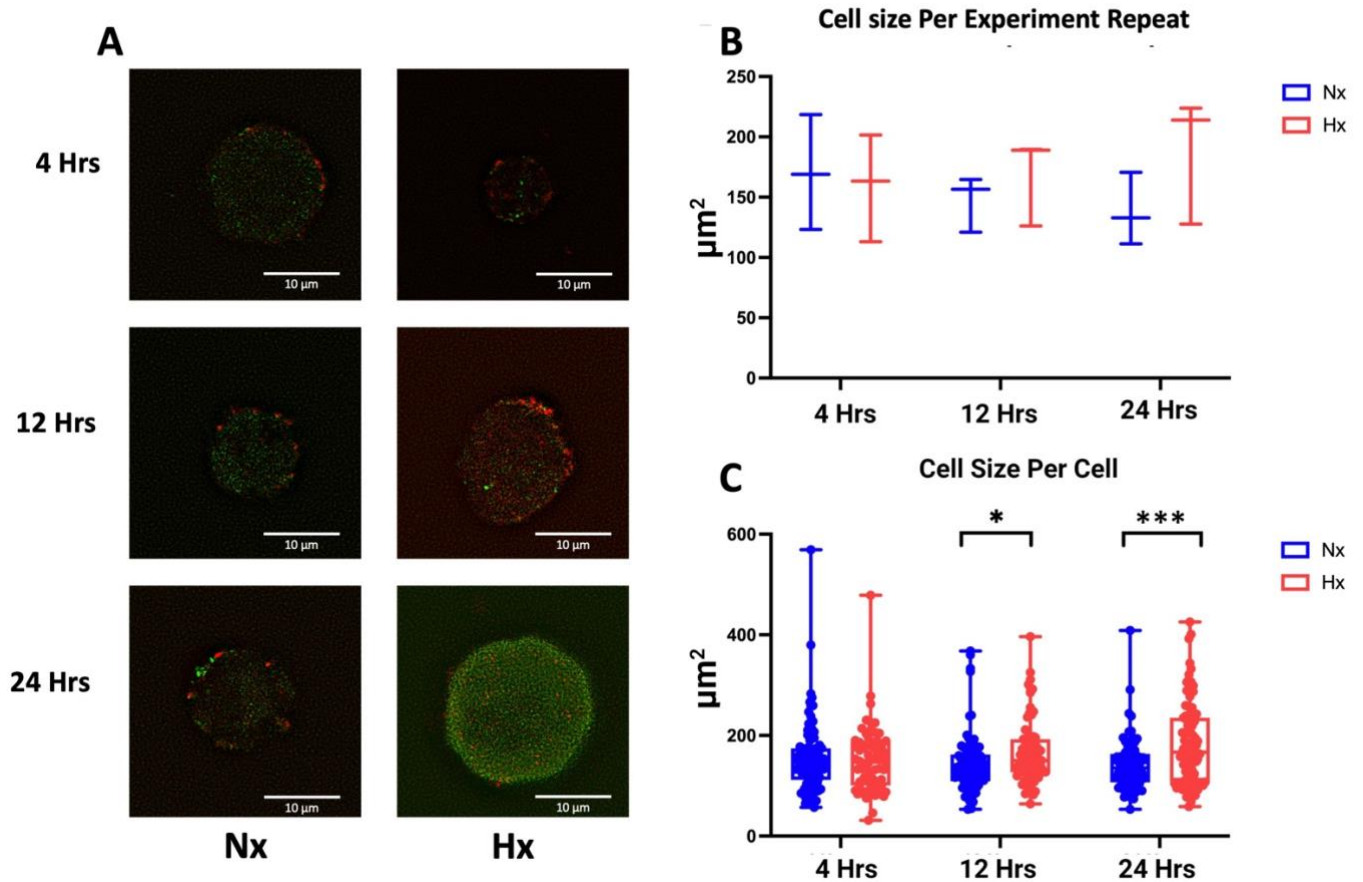
Figure 2.7 Comparing PC12 cell size in normoxia (Nx) and hypoxia (Hx).

This figure compares PC12 cell area when incubated in hypoxic (1% O_2) and normoxic (20% O_2) conditions for 4, 12 and 24 hours. A) Raw data examples of PC12 cells incubated for 4, 12 and 24 hours in either normoxia or hypoxia. B) and C) show group data for each experimental repeat and each cell respectively. After 4 hours of hypoxia exposure, no significant alteration in cell area was observed compared to normoxic cells (P=0.67, n=92 normoxic cells, n=65 hypoxic cells). However, with extended exposure, cell area significantly increased after 12 hours (P=0.01, n=93 normoxic cells, n=81 hypoxic cells) and 24 hours (P=0.0005, n=72 normoxic cells, n=92 hypoxic cells) of hypoxia. Data is presented as boxplots, with box limits indicating the interquartile range, the horizontal line indicating the median and the whiskers extending to the maximum and minimum points. For C, all individual cell measurements are shown as single points. Significance was tested using Two-way ANOVA with Bonferroni post-hoc analysis. * and *** denotes p<0.05 and p<0.001 respectively.

2.3.3 Hypoxia increases cytosolic TH expression in PC12 cells in a time dependent manner

The confocal imaging results showed that, initially, after 4 hours of exposure to hypoxia, there was no significant change in cytosolic TH fluorescence levels. At this early time point, both normoxic and hypoxic cells had comparable fluorescence intensities, with no statistically significant difference between them, normoxia (n=92) 1764±117 AU and hypoxia (n=65) 1523±113.5 AU (P=0.15), Figure 2.8 A-C.

After 12 hours of exposure to hypoxia, the cytosolic TH fluorescence levels were significantly elevated when compared to normoxic conditions. The mean fluorescence intensity was 1904±135.4 AU in hypoxic cells (n=81), while it was 1334±93.5 AU in normoxic cells (n=93). This increase was statistically significant (p=0.0005), indicating that a longer exposure to low oxygen levels led to an increase in TH fluorescence within the cytosol, Figure 2.8 A-C.

Similarly, after 24 hours of hypoxia, the cytosolic TH fluorescence levels remained significantly elevated compared to normoxia. During this extended period of low oxygen exposure, the fluorescence intensity was measured at 1766±116 AU in hypoxic cells (n=92), while it was 1176±61.3 AU in normoxic cells (n=72). Once again, this difference was statistically significant (p<0.0001), indicating that the elevation in cytosolic TH fluorescence persisted with prolonged hypoxia, Figure 2.8 A-C.
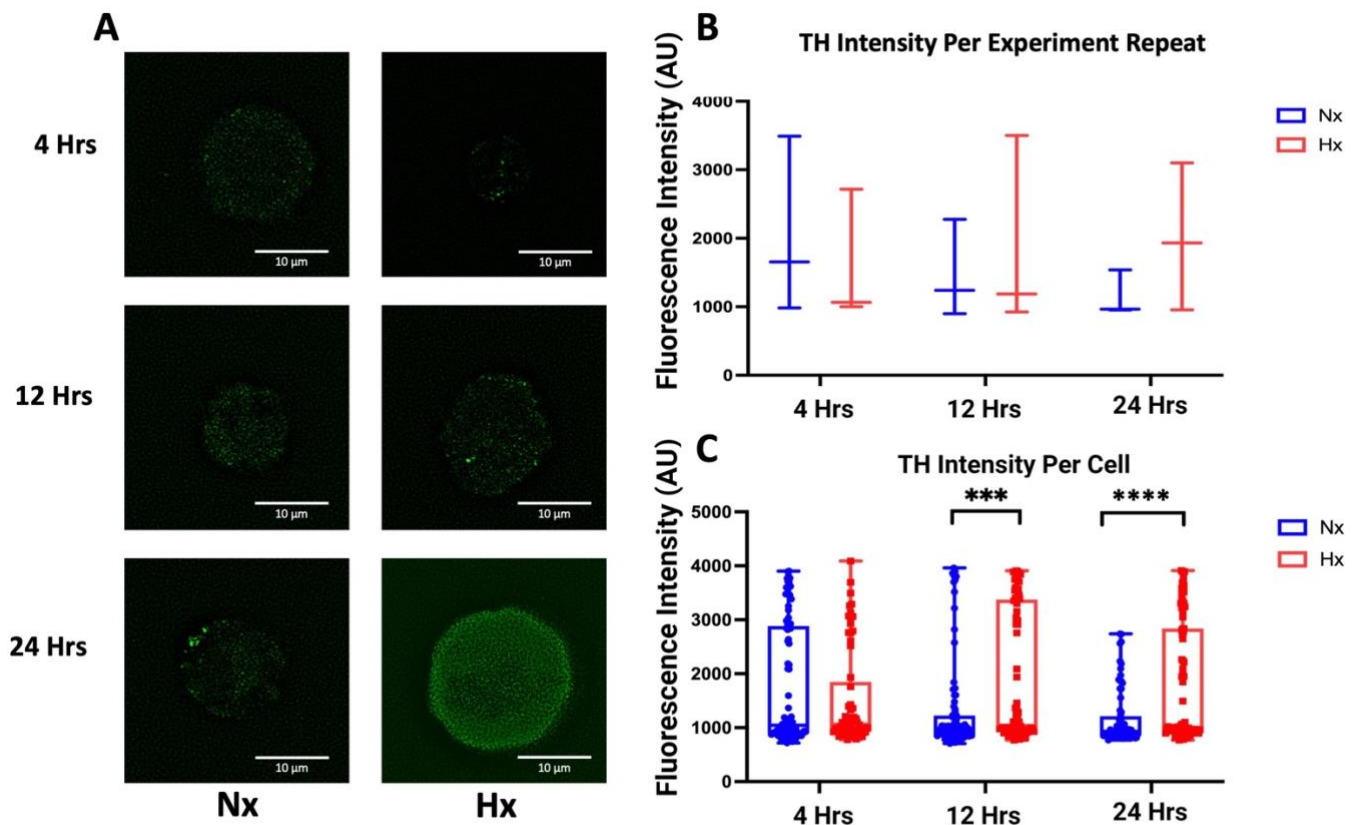
Figure 2.8 Comparing PC12 cytosolic TH expression levels in normoxia (Nx) and hypoxia (Hx).

This figure demonstrates cytosolic TH fluorescence levels in PC12 cells under varying oxygen conditions and exposure durations. A) Raw data example of TH fluorescence measured in different PC12 cells measured following incubation in 4, 12 and 24 hours of normoxia (20% O_2) or hypoxia (1% O_2). B) and C) show grouped TH-fluorescence data for each experimental repeat and each cell respectively. Grouped data is presented as boxplots, with box limits indicating the interquartile range, the horizontal line indicating the median and the whiskers extending to the maximum and minimum points. For C, all individual cell measurements are shown as single points. Significance was tested using Two-way ANOVA with Bonferroni post-hoc analysis. *** and **** denote $p < 0.001$ and $p < 0.0001$ respectively.

2.3.4 1% Hypoxia elevates PC12 AT$_1$R expression in a time dependent manner

After 4 hours of exposure to hypoxia, there was no significant change in AT$_1$R fluorescence when compared to normoxic cells, normoxic cells (n=92) 1444±40.8 AU, while hypoxic cells (n=65) have a mean AT$_1$R fluorescence intensity of 1353±35.6 AU. The fluorescence intensity remained relatively consistent, and there was no statistically significant difference between the two groups at this time point (p=0.11), Figure 2.9 A-C.

For 12 hours hypoxia exposure, AT$_1$R fluorescence intensity was significantly increased. Under normoxic conditions (n= 93) the fluorescence intensity was measured at 1316±35.1 AU, while under hypoxic condition (n= 81) it increased to 1547.3±53.4 AU. This increase was statistically significant (p=0.0003), Figure 2.9 A-C.

For 24 hours hypoxia exposure, a similar increase was observed. The AT$_1$R fluorescence levels remained significantly elevated compared to normoxia. In normoxic cells (n= 72) the fluorescence intensity was 1287±33.5 AU, whereas under hypoxia (n=92) it increased to 1592±46.6 AU. Once again, this difference was statistically significant (p<0.0001), indicating that AT$_1$R expression is enhanced with prolonged hypoxia, Figure 2.9 A-C.
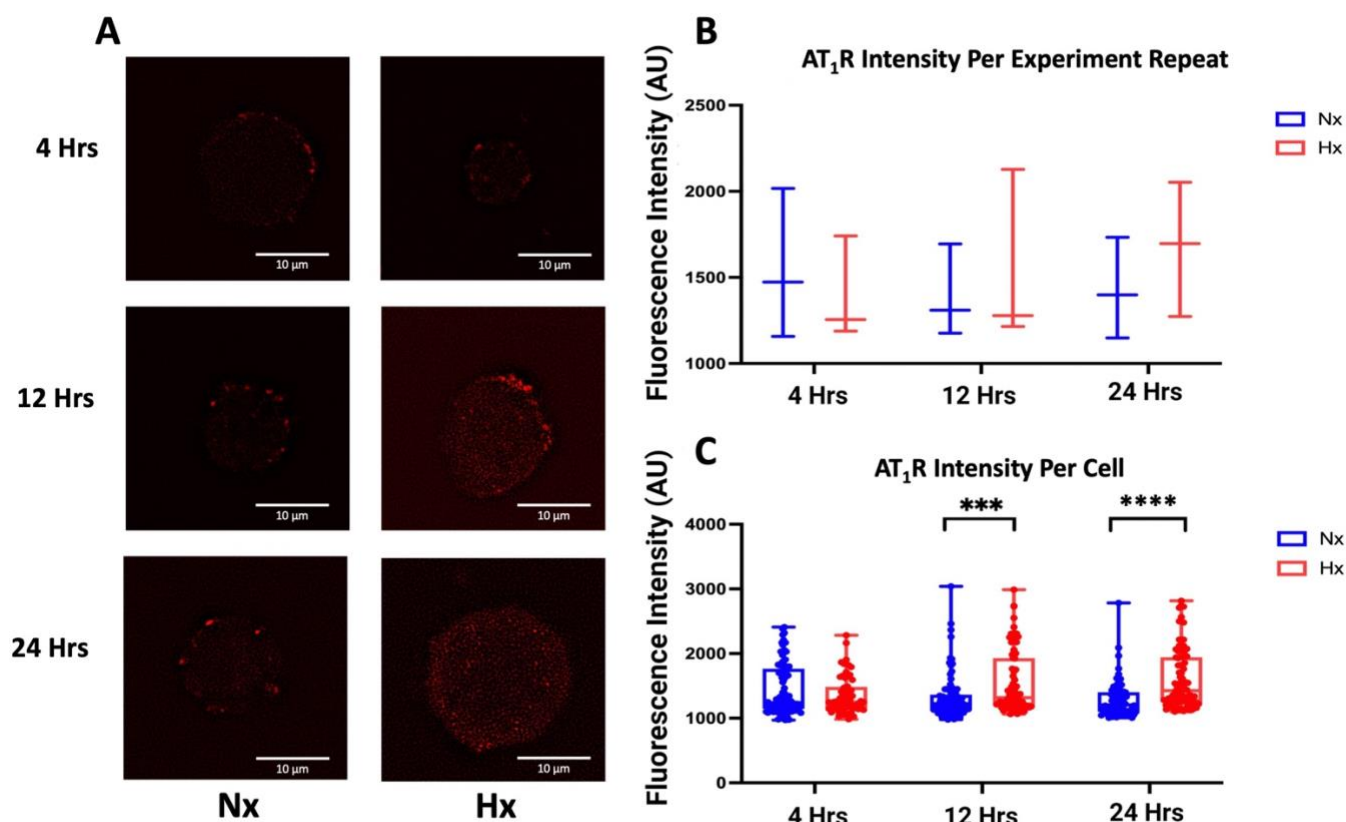
Figure 2.9 Comparing PC12 AT$_1$R fluorescence levels in normoxia (Nx) and hypoxia (Hx).

This figure illustrates AT$_1$R fluorescence levels in PC12 cells under varying oxygen conditions and exposure durations. A) Raw data example of AT$_1$R fluorescence measured in different PC12 cells measured following incubation in 4, 12 and 24 hours of normoxia (20% O$_2$) or hypoxia (1% O$_2$). B) and C) show grouped AT$_1$R fluorescence data for each experimental repeat and each cell respectively. Grouped data is presented as boxplots, with box limits indicating the interquartile range, the horizontal line indicating the median and the whiskers extending to the maximum and minimum points. For C, all individual cell measurements are shown as single points. In B and C Significance was tested using Two-way ANOVA with Bonferroni post-hoc analysis. *** and**** denotes p<0.001 and p<0.0001, respectively.

2.4 Chapter synopsis and discussion

2.4.1 List of main findings

- PC12 cell optimisation studies revealed that the optimal growth condition is achieved when cells are cultured in suspension.

- The optimal adherent substrate for PC12 cells, needed for imaging, was 400μg/ml of HPC.

- For immunostaining studies on PC12 cells, 1:500 was the optimum primary antibody concentration for both anti-AT_1R and anti-TH.

- 12 and 24 hours of hypoxia was sufficient to increase PC12 cell size along with AT_1R and TH protein expression.

2.4.2 HPC is the optimum adherent substrate for imaging PC12 cells

In the pursuit of optimizing the adherent substrate for imaging PC12 cells, the comparative analysis between HPC, Poly-L-Lysine, and Poly-D-Lysine provided valuable insights. Notably, Poly-L-Lysine at 0.1 mg/ml revealed minimal cell adhesion, prompting concerns about its effectiveness for PC12 cells. While Poly-D-Lysine at 0.1 mg/ml showed a modest improvement, the escalation to 1.0 mg/ml demonstrated increased favourability, yet a significant portion of cells observed before substrate application remained unattached. HPC at 200 μg/ml displayed improved adherence yet still not at the desired level. The application of HPC at 400 μg/ml, provided much improved adherence, indicating its superiority as a substrate over Poly-L-Lysine and Poly-D-Lysine for PC12 cells.

The superior adherence capacity of HPC compared to Poly-L-Lysine and Poly-D-Lysine can be attributed to several factors. Firstly, the biological origin of HPC may provide a more biocompatible and physiologically relevant environment for PC12 cells (Chua and Lim, 2023). The extracellular matrix of the human placenta contains a complex mixture of proteins, growth factors, and signalling molecules that could support cell adhesion and growth (Chua and Lim, 2023). This natural composition might mimic the *in vivo* conditions more closely than synthetic substrates like Poly-L-Lysine and Poly-D-Lysine. Secondly, HPC may possess a greater affinity for cell adhesion receptors present on the surface of PC12 cells. The molecular structure of HPC could facilitate stronger interactions with integrins or other adhesion molecules on the cell membrane, promoting a more stable attachment compared to Poly-L-Lysine and Poly-D-Lysine. Additionally, the optimal concentration of HPC (400 μg/ml) used in the study might be critical for providing an appropriate microenvironment for PC12 cells. The concentration-dependent effect observed suggests that higher concentrations of HPC may offer a more conducive substrate for cell adhesion, possibly by presenting a greater number of binding sites for cell surface receptors (Vandenberg et al., 1991). Finally, HPC might offer a more useful and adaptable substrate that accommodates the specific requirements of PC12 cells. The complexity of the extracellular matrix derived from human placenta could provide a range of cues and signals that support cell adhesion, proliferation, and differentiation (Xing et al., 2020).

2.4.3 Increase in PC12 cell area after CH induction

To date, there is no literature available that has directly tested the influence of hypoxia on PC12 cell size per se but rather its ability to alter cell viability and neurite outgrowth. There are many potential reasons that can increase cell area. One of the possible explanations of the cell area increase is that hypoxia causes a rapid increase in nerve growth factor induced neurite outgrowth (O'Driscoll and Gorman, 2005). Another

possible explanation is that adenosine, specifically through the activation of A_2 receptors that become elevated under hypoxic conditions, is linked to promoting cell growth and proliferation by triggering signalling pathways that elevate intracellular cAMP levels (Sheth et al., 2014). However, in the studies described in this Chapter, cells seemed to maintain a round morphology with no obvious evidence of neurite outgrowth. Another reason for the area increase is a potential overexpression of GPCRs and modifications in ion channel expression/activity (Aldossary et al., 2020). An increase in GPCR's and/or ion channel expression/activity could lead to an cell stimulation and elevated intracellular Ca^{2+}, and this may contribute in cell size change (Boyle and Pompeiano, 1981). Cell growth could also be a possible reason in the PC12 size rise after hypoxia, most likely mediated subsequent to HIF stabilisation. In studies where hypoxia has initiated neurite outgrowth and neuronal-like differentiation (Bork et al., 2015), HIF-1a stabilisation is a key mediator and it is most likely responsible for the change in cell size seen here. Another possibility could be attributed to generalized cell swelling. The dysregulation of ion channels and transporters in hypoxia disrupts cellular ionic and osmotic balance, leading to the accumulation of intracellular ions and subsequent water influx (Boutilier, 2001). This could indicate cellular stress and dysfunction (Boutilier, 2001).

These suggestions could be explored to identify the exact reason/s behind PC12 cell size increase after hypoxia induction. Cell growth factors linked to HIF and downstream signalling could be measured and compared between Nx and Hx groups. In CB type I cells, it is known that there is a rise in growth factors during hypoxia, driven by HIF-1 and HIF-2 stabilisation (Prabhakar and Jacono, 2005, Lopez-Barneo et al., 2001, Platero-Luengo et al., 2014, Pardal et al., 2007, Fielding et al., 2018).

2.4.4 Increase in TH expression after CH

Large amounts of catecholamines (CAs) are stored in the CB and PC12 cells (Aldossary et al., 2020, Zapata et al., 1969) and Dopamine (DA) accounts for more than half of CA stored in type I cells (Aldossary et al., 2020, Chiocchio et al., 1966). Dopamine synthesis, for example, starts with phenylalanine hydroxylase, which converts phenylalanine to tyrosine. Tyrosine will then be converted to L-DOPA via TH and subsequently to dopamine via DOPA decarboxylase. TH is considered a rate-limiting enzyme in this pathway (Nagatsu, 2007).

During CB type I cell stimulation by hypoxia, DA will endogenously be released from type I cells and its action is to act as an inhibitory regulator (Wakai et al., 2015) to balance overall excitation and cAMP concentration (Conde et al., 2008). It was shown that CB stimulation by hypoxia, significantly increases DA release (Urena et al., 1994, Fidone et al., 1982). Whether or not persistent cellular stimulation during CH and release of DA then directly leads to an increase in TH expression is unknown. However, it is clear that TH expression does increase in response to CH in the rat CB (Schmitt et al., 1992).

The role of TH is to initiate the synthesis of CAs from tyrosine and is therefore widely used as a marker of dopaminergic neurones (Nurse and Fearon, 2002, Weihe et al., 2006). The use of TH identification/expression in CB studies is mainly to identify dopaminergic type I cells and/or to assess alterations in the ability to produce CAs. TH protein expression is significantly increased after CH induction in the CB type I cell, and this increase leads to a significant rise in CA biosynthesis (Schmitt et al., 1992). CH also increases TH mRNA expression in both the CB (Czyzyk-Krzeska et al., 1992, Mosqueira and Iturriaga, 2019) and PC12 cells (Hempleman, 1996). In the current Chapter, there was a significant rise in TH expression in PC12 cells after 12 and 24 Hrs of Hx exposure but not after 4 Hrs. This suggests that the

hypoxic stimulus intensity was sufficient to activate signalling pathways needed to initiate increases in TH expression. However, there was a delay of at least 12 hours before there were quantifiable elevations in TH protein expression which then tended to remain stable for at least another 12 hours. This information will be used to guide experiments in the next Chapter where similar exposure of PC12 cells to CH will be performed.

2.4.5 Increase in AT_1R expression after CH

The influence of Ang II and AT_1R expression on CB type I cell is well established. It was shown that Ang II significantly increases the CB chemoafferent discharge frequency (Allen, 1998a, Peng et al., 2011a). It was also confirmed using RT-PCR that both AT_{1a} and AT_{1b} receptors are expressed in CB type I cells as well as AT_1R protein (Atanasova et al., 2018a, Fung et al., 2001).

It was reported that CH leads to an increase in AT_{1a} and AT_{1b} -receptor mRNA expression in type I cells (Leung et al., 2000). AT_1R protein was shown to be increased in type I cells following CIH (Marcus et al., 2010), indicating that Ang II may play a role in causing CB hyperactivity in diseases associated with hypoxia. However, this study is the first to show that AT_1R protein is elevated in response to hours of hypoxia in PC12 cells which are closely related to CB type I cells. As with TH, rises in AT_1R expression were apparent after 12 and 24 Hrs of Hx exposure but not after 4 Hrs. This suggests that the level of hypoxia used (1% O_2) is sufficient to evoke alterations in AT_1R expression, but that measurable increases only start to appear after at least 12 hours. After this AT_1R protein expression levels remain elevated (but do not rise further) for at least another 12 hours. This information will help to guide study design in the next Chapter which

will evaluate single molecule organisation and clustering of AT_1R in response to sustained hypoxia. Further experiments are required to directly validate this in CB type I cells.

2.4.6 The role of HIF Stabilization in Hypoxia-Induced Changes in PC12 Cell Size, TH, and AT_1R Expression

Under normoxic conditions, Hypoxia-inducible factor (HIF) is rapidly degraded, but in Hx it is stabilized due to the inhibition of its degradation pathway, allowing it to accumulate and translocate to the nucleus to activate target gene transcription (Hu et al., 2003). This stabilization plays a crucial role in the cellular response to hypoxia (Hu et al., 2003) and can lead to an increase in PC12 cell size due to the upregulation of genes involved in cell survival and adaptation to low oxygen levels. One of the primary responses is the activation of genes that regulate ionic balance and water homeostasis, which can result in generalized cell swelling (Cramer and Johnson, 2003).

Additionally, HIF stabilization significantly impacts the expression of TH and AT_1R in PC12 cells after 24 hours of hypoxia. HIF directly upregulates TH expression, enhancing the synthesis of catecholamines necessary for the adaptive response to hypoxia (Paulding et al., 2002). Increased catecholamine production is crucial for maintaining cellular and systemic functions under low oxygen conditions (Paulding et al., 2002). Moreover, HIF upregulates AT_1R expression, which is involved in the renin-angiotensin system and contributes to vasoconstriction and blood pressure regulation (Szczepanska-Sadowska et al., 2018). The elevated AT_1R levels enhance the cell's sensitivity to Ang II, further promoting adaptive responses such as increased sympathetic activity (Miller and Arnold, 2019). Together, these changes orchestrated by HIF stabilization enable PC12 cells to adapt with the challenges posed by CH.

2.4.7 Integrating Western blot analysis for more comprehensive understandings

The inclusion of Western blotting analysis as an additional confirmation tool could offer valuable insights into the presence and/or alteration of AT_1R or TH expression in normoxia versus hypoxia. While immunocytochemistry provides qualitative information on protein localization, Western blotting complements this by offering quantitative data on overall protein expression levels (Mishra et al., 2017). By detecting specific protein bands, Western blotting could enhance the understanding of AT_1R or TH expression dynamics under hypoxic conditions. Moreover, the validation of immunocytochemistry findings through Western blot analysis would strengthen the reliability and robustness of the observed protein expression alteration. Incorporating Western blot analysis into future experimental designs as a confirmation technique would provide comprehensive approach to studying protein expression changes in hypoxia-related contexts.

2.4.8 Limitations

2.4.8.1 Confocal microscopy and the use of antibodies to measure protein expression

The application of confocal microscopy has significantly advanced the ability to visualize cellular and subcellular structures with exceptional detail. However, like any scientific technique, confocal microscopy is not without its limitations. A primary limitation of confocal microscopy is the issue of photobleaching. The intense laser light used to illuminate the specimen during imaging can lead to the degradation of fluorescent dyes over time. This phenomenon can compromise the integrity of the signal and limit the ability to capture dynamic cellular processes or prolonged observations. In this Chapter, the same settings regarding laser intensity and time taken to capture sample fluorescence were the same for every cell tested, limiting variation caused by photobleaching. However, its impact on making quantitative

measurements of protein expression cannot be ruled out and so these results should be treated with some caution and strengthened by additional techniques (see next Chapter). Additionally, the technique's reliance here on antibodies and fluorescence poses challenges in terms of specificity. Antibodies and fluorophores may exhibit non-specific binding or undesired interactions with cellular components, leading to false-positive signals. This limitation underscores the importance of careful antibody and fluorophore selection and controls to ensure the accuracy of the observed fluorescence patterns. Whilst primary negative controls were not performed, it was shown that the addition of secondary antibodies alone produced very little fluorescence, consistent with very limited non-specific secondary binding. That said some non-specific primary antibody binding cannot be ruled out.

The depth of penetration is another significant constraint in confocal microscopy. While it excels in imaging thin sections of specimens, its ability to visualize deep within tissues is limited. This is due to the scattering of light, which reduces both the resolution and signal intensity with increasing depth. This limitation restricts the applicability of confocal microscopy for imaging three-dimensional structures in thick samples. However, this should not have been a major problem in the current experiments as images were taken from single cells rather than tissue sections.

2.4.8.2 PC12 vs type I cell differences

Using PC12 cells as a model for CB type I cells has been a valuable approach in studying cellular responses and mechanisms associated with oxygen sensing. However, it is crucial to acknowledge certain limitations and differences between PC12 cells and native CB type I cells that may impact the translational relevance and interpretation of findings.

PC12 cells, originally derived from a rat pheochromocytoma, are of neural crest origin but may not perfectly replicate the physiological characteristics of CB type I cells. CB type I cells are specialized chemoreceptor cells that respond to changes in arterial blood oxygen levels. PC12 cells lack some of the specific features of CB cells, including unique gene expression and mitochondrial function. The expression of other molecular markers, ion channels and receptors associated with oxygen sensing may differ between PC12 cells and native CB type I cells. Furthermore, PC12 cells may lack the complex cellular interactions and communication present in the CB tissue (such as connections between supporting type 2 cells). The complex microenvironment of the CB, including interactions with neighbouring cells, vascular components, and the extracellular matrix, cannot be fully replicated in a cultured cell line. Thus, whilst the results may suggest that O_2 sensitive cells from the same neural crest origin are likely to increase AT_1R expression in response to sustained hypoxia, experiments evaluating this specifically in CB type I cells are still warranted.

2.4.8.3 Level and duration of hypoxia

The limitation regarding the level and duration of hypoxia used in this study stems partially from practical constraints associated with maintaining a controlled hypoxic environment for PC12 cells. The experimental setup imposed a maximum duration of 24 hours for hypoxic exposure, and the minimum O_2 concentration achievable was 1%. This limitation arose from the necessity to regularly replace the nitrogen cylinders supplying the hypoxic chamber to sustain a consistent 1% oxygen environment within the incubator. The logistical challenge of changing nitrogen cylinders to maintain the desired hypoxic conditions-imposed constraints on the duration of continuous hypoxia that could be administered to PC12 cells. This limitation may impact the ability to observe longer-term cellular responses or assess the effects of extended hypoxic exposure, which could be relevant in understanding adaptive mechanisms over prolonged periods.

Additionally, the choice of a minimum oxygen concentration of 1% reflects a compromise between achieving a hypoxic environment and the practical considerations of gas exchange in the experimental setup. While 1% O_2 provides a hypoxic challenge, it is essential to acknowledge that more severe hypoxic conditions may be encountered in certain physiological or pathological contexts, and the current experimental setup may not fully replicate such extreme or alternatively more mild conditions. The fact that significant changes in cell size, TH and AT_1R expression were observed does however suggest that the duration and level of hypoxia used was sufficient to modify protein expression and cell growth.

2.4.9 Conclusion

CH in PC12 cells increased TH and AT_1R protein expression. This highlights a link between O_2 availability and neurotransmitter synthesis. Furthermore, the upregulation of AT_1R expression in response to CH in PC12 highlights a complex signalling pathways in cellular responses to O_2 deprivation and suggests a role for the renin-angiotensin system in mediating adaptive changes.

Chapter 3. Analyzing angiotensin II receptor type 1 clustering in PC12 cells in response to hypoxia using direct stochastic optical reconstruction microscopy (dSTORM)

Hayyaf S. Aldossary [1,2], Daniel J. Nieves [3], Deirdre M. Kavanagh [4], Dylan Owen [5], Clare J. Ray [1], Prem Kumar [1], Andrew M. Coney [1], and Andrew P. Holmes [1]

[1] School of Biomedical Sciences, Institute of Clinical Sciences, University of Birmingham, Birmingham, UK.
[2] College of Medicine, Basic Medical Sciences, King Saud bin Abdulaziz University for Health Sciences, Riyadh, Saudi Arabia.
[3] Institute of Immunology and Immunotherapy and Centre of Membrane Proteins and Receptors (COMPARE), University of Birmingham, Birmingham, UK.
[4] Micron Bioimaging Facility, University of Oxford, Oxford, UK.
[5] School of Mathematics, University of Birmingham, Birmingham, UK.

3.1 Introduction

3.1.1 Chapter introduction and overview

Angiotensin II (Ang II) is a critical peptide hormone that has a direct impacts on the function of many organs and it is increased in numerous cardiorespiratory diseases including heart failure, hypertension and chronic obstructive pulmonary disease (COPD) (Andreas et al., 2006, Opie and Sack, 2001, van de Wal et al., 2006). Ang II stimulates the carotid body (CB) type I cells, which in turn increases CB chemoafferent discharge frequency (Allen, 1998b, Fung et al., 2001, Peng et al., 2011a). RT-PCR analysis has revealed that the mRNA for both AT_1a and AT_1b subtypes is expressed in type I cells and immunohistochemistry has confirmed the presence of angiotensin II receptor type 1 (AT_1R) protein (Atanasova et al., 2018b, Fung et al., 2001).

Studies have shown that the mRNA expression and activity of AT_1R can be altered in response to CH (Lam et al., 2014). CH can lead to an upregulation of AT_1R mRNA expression in the CB (Lam et al., 2014). This upregulation of AT_1R may enhance the sensitivity of the CB to Ang II and further amplify its response to hypoxia (Lam et al., 2014, Leung et al., 2000). It is believed that this adaptive response may contribute to the increased ventilatory drive observed in individuals exposed to CH.

Dysregulation of AT_1R signalling in the CB during CH may have implications for cardiovascular health (McMurray et al., 2014). Excessive AT_1R activation in response to prolonged hypoxia has been linked to conditions such as pulmonary hypertension and COPD (Devaux and Lagier, 2023).

AT_1Rs are members of the G-protein-coupled receptor (GPCR) family, key players in mediating CB activity (Aldossary et al., 2020, Holmes et al., 2019). Recent data obtained using novel super-resolution imaging techniques suggest that GPCRs are not uniformly distributed but are present in distinct clusters located in

specific compartments or 'hot spots' in the cell membrane (Sungkaworn et al., 2017). This allows for downstream intracellular signalling to be localised to specific regions within the cell. Different cluster characteristics may modify responses to pharmacological agents (Duke and Graham, 2009). Although AT_1Rs are known to be expressed in CB type I cells and the closely associated PC12 cell line, there is currently little information regarding the detailed single-molecule spatial organisation of these receptors in either of these O_2 sensitive cell types. Furthermore, it is not clear if the single-molecule distribution and cluster characteristics of AT_1Rs can be modified by exposure to other stimuli, such as sustained hypoxia. In the previous Chapter a protocol was developed to demonstrate that exposure to 12-24 Hrs of Hx augmented AT_1R protein expression in PC12 cells. However, confocal microscopy does not have the resolution capable of detecting changes in single molecule organization or clustering. Furthermore, it was not clear if this increase in expression was throughout the cell or specifically on the cell membrane. A key aim of this Chapter is to use super-resolution imaging to explore the impact of hypoxia on the single molecule arrangement of AT_1R on the cell membrane.

Direct Stochastic Optical Reconstruction Microscopy (dSTORM) stands as a transformative innovation within the domain of super-resolution microscopy (Endesfelder and Heilemann, 2015). This cutting-edge technique enables exploration of the nanoscale complexity of biological specimens, providing an understanding of cellular structures, subcellular dynamics, and molecular interactions in unprecedented detail (Endesfelder and Heilemann, 2015). In particular, when used in combination with total internal reflection fluorescence microscopy (TIRF), it allows for detailed assessment of the nanoscale organization of receptors and ion channels at or within 200nm of the cell membrane (Chang et al., 2023, Lelek et al., 2021).

The findings from the previous Chapter that CH leads to increased AT_1R can be explored further by quantifying the single molecule organization and cluster characteristics of AT_1R using dSTORM and TIRF, and investigating if CH modifies these cluster characteristics. dSTORM imaging technique will allow precise measurement and visualization of AT_1R organization on the cell membrane (Klein et al., 2023), revealing if increased AT_1R expression under CH corresponds to changes in density, distribution, or clustering, which could have important implications for local AngII-signalling. Understanding these mechanisms is critical for addressing hypoxia-related conditions like COPD, potentially guiding targeted therapies.

The original aim of this chapter was to quantify the single molecule organisation and clustering of AT_1R on the cell membrane of CB type I cells before and after exposure to CH. However, similar to Chapter 2, these plans were unable to be carried out due to the inability to perform animal experiments during the COVID-19 pandemic. Therefore, as in Chapter 3, the PC12 cell line was instead used as a surrogate for a dopaminergic O_2-sensitive cell, sharing many similarities with the CB type I cell.

3.1.2 Chapter hypothesis

- Exposure of PC12 cells to CH significantly alters the single molecule arrangement and clustering of AT_1Rs on the cell membrane.

3.1.3 Aims of this Chapter

- To quantify the single molecule organization and cluster characteristics of AT_1R on the cell membrane of PC12 cells using a combination of dSTORM and TIRF

- To investigate if exposure to sustained hypoxia (CH) modifies the cluster characteristics of AT_1R on the membrane surface of PC12 cells

1- To investigate AT_1Rs clustering characteristics in O_2 sensitive PC12 cells

A

B

?

Hx

C

2- To identify if hypoxia (Hx) alters AT_1Rs cluster characteristics?
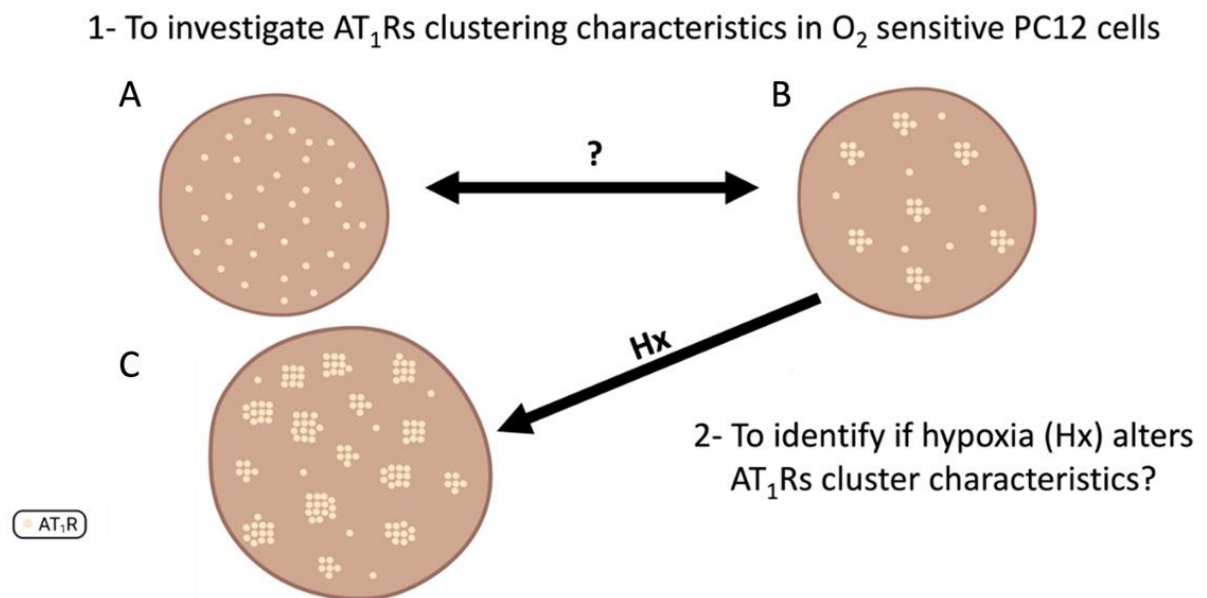
AT_1R

Figure 3.1 Summary of Chapter hypothesis and aims

A) Illustrates the conventional idea of AT_1R being randomly distributed across the cell membrane of PC12 cells. B) Proposes a hypothesis that AT_1Rs are found in a distinct clusters or 'hotspots' in the cell membrane of PC12 cells. C) Introduces the idea that these clusters may undergo significant adaptive alterations in response to sustained/chronic hypoxic conditions.

3.2 Methods

3.2.1 PC12 cell culture, hypoxic protocol, and immunocytochemistry

The protocol used was described in chapter 2. After cell adherence, cells were incubated in either normoxia (Nx; 20% O_2) or hypoxia; (Hx, 1% O_2) for 24 hours. After 24 hours, cells were immediately fixed in 4% paraformaldehyde (Alfa Aesar, Lancashire, UK) for 90 minutes, permeabilized for 5 minutes and blocked for 60 minutes. The primary rabbit anti-AT_1R antibody (abcam, Cambridge, UK) (1:500) was diluted in blocking solution and incubated overnight at 4°C. Cells were washed three times in PBS, blocked again for 30 minutes and incubated in secondary antibody Alexa Fluor 647 F(ab')2 fragment of goat anti-rabbit IgG (H+L), 1:2000, (ThermoFisher Scientific, Waltham, MA, USA) for 90 minutes at room temperature, Figure 3.2.
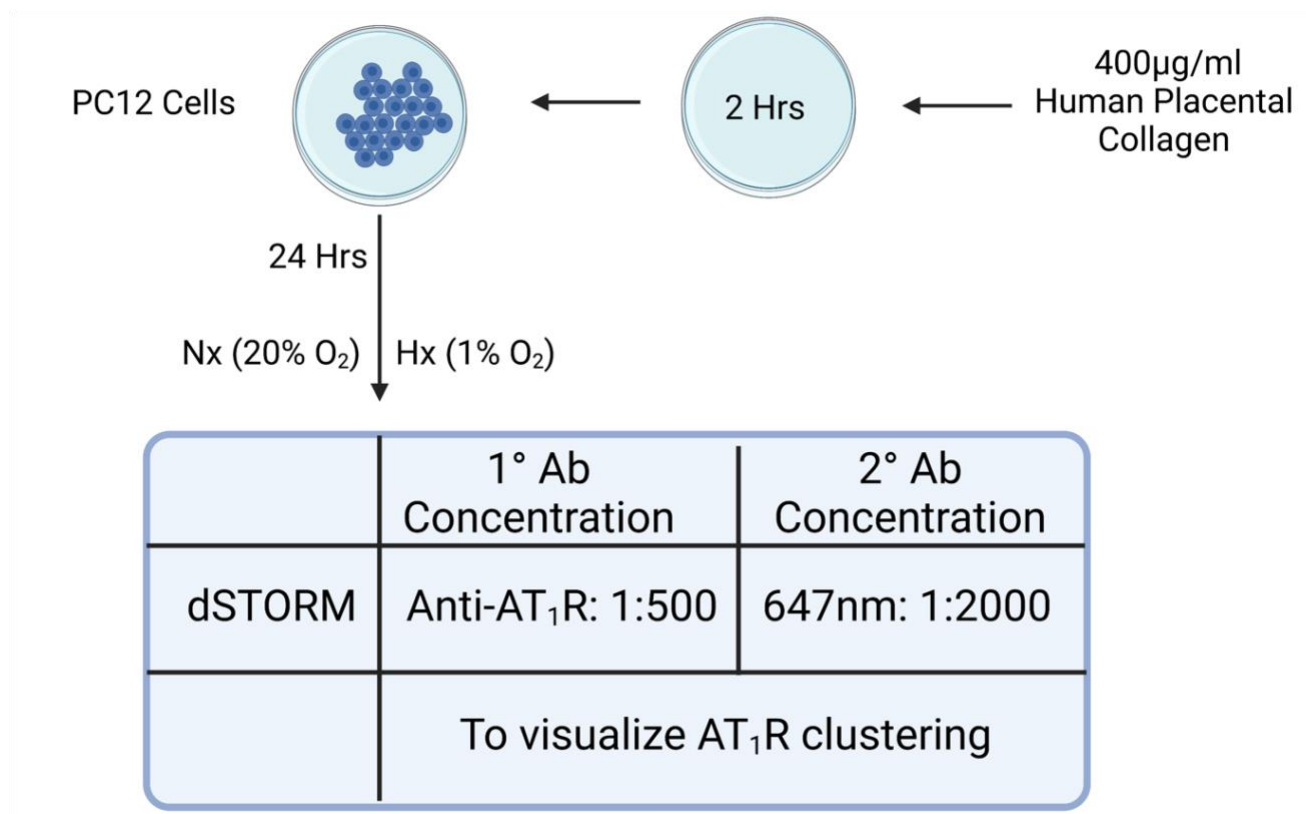
Figure 3.2 Summary of PC12 cell hypoxic exposure and immunocytochemistry staining protocol

The 10 mm microwell in the imaging dish was initially coated with human placental collagen for 2 hours. Cells were then plated on human placental collagen-coated microwell dishes and allowed to adhere for 1 hour at 37°C in normoxia (20% O_2). Following this, they were exposed to either normoxia (Nx; 20% O_2) or hypoxia (Hx; 1% O_2) for 24 hours. After fixation, permeabilization, and blocking, cells were stained with a rabbit anti-AT$_1$R antibody (1:500) overnight at 4°C. Subsequently, a secondary Alexa Fluor 647 (1:2000) antibody was applied for 90 minutes before final washing and dSTORM.

3.2.2 dSTORM principles

dSTORM is a super-resolution microscopy technique that allows to achieve higher spatial resolution in imaging biological samples beyond the diffraction limit of light (Klein et al., 2023). It relies on the switching properties of certain fluorophores between dark and bright states, and the use of excitable and non-excitable fluorophores is an important aspect of this technique (Requejo-Isidro, 2013). The key principles of dSTORM is the use of dark and bright states, where in a dark state cells emit little to no fluorescence and during a bright state cells emit strong fluorescence (Requejo-Isidro, 2013). As different fluorophores

switch from the dark to light state at different times (termed blinking), this allows for more precise localization of each individual molecule in the sample.

dSTORM typically uses two types of fluorophores, one that is excitable and can be turned on by specific excitation light, and another that is non-excitable and undergoes spontaneous switching between dark and bright states (Xu et al., 2017).

Standard excitable fluorophores are typically used as activator molecules. Under normal low intensity laser illumination the majority of flurophores are turned on. However, after a brief period of continuous high intensity laser excitation (in the presence of appropriate reducing agents in the dSTORM buffer), the vast majority of fluorophores switch into the dark or off state. As the fluorophores randomly transition back to the ground (on) state they emit a photon which can be detected. The fluorescence emitted by the bright-state fluorophores is captured using a high-resolution microscope with precise localization capabilities (Baddeley et al., 2009, Jensen and Crossman, 2014). Images are captured in a time series of approximately 5,000-20,000 frames. Importantly, in any one image only a small number of fluorophores are in the on state. There is an extremely low probability of two fluorophores within a close vicinity coming on together within the same frame of the image series. This therefore acts to overcome the problems caused by the diffraction limit of light. The positions of individual fluorophores in their bright states are determined with high precision and collating all the imaging frames together allows for the construction of a super-resolved image of the sample (Jensen and Crossman, 2014), Figure 3.3.
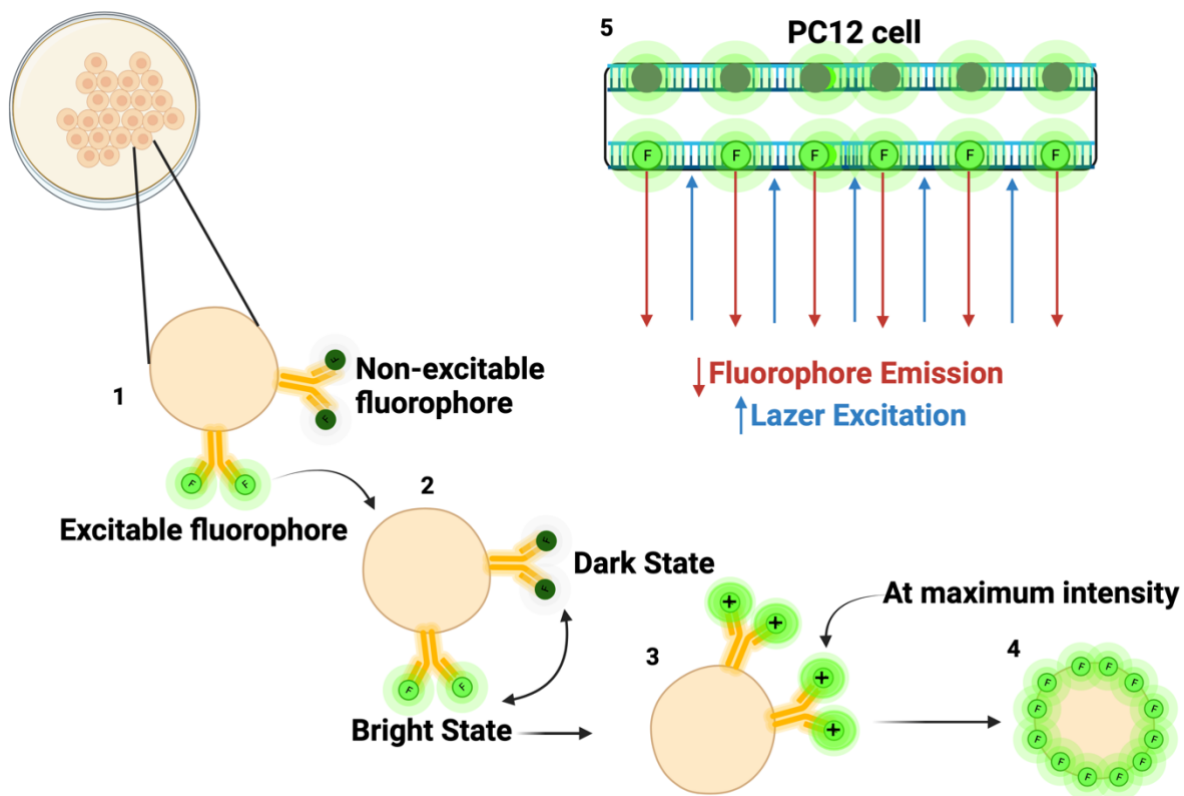
Figure 3.3 dSTORM and image reconstruction principles

dSTORM employs two types of fluorophores: excitable activator molecules temporarily excited by specific laser wavelengths and non-excitable reporter molecules that emit fluorescence in the bright state (1). dSTORM utilizing the switching properties of certain fluorophores between dark and bright states (2). The imaging process involves selective activation of excitable fluorophores, followed by high-resolution microscopy to capture emitted fluorescence (3). At maximum intensity, a precise localization of bright-state fluorophores enables the construction of super-resolved images with nanoscale detail (4).

3.2.3 dSTORM imaging and cluster analysis

dSTORM experiments were performed on a NIKON N-STORM microscope equipped with a Nikon x 100 1.49

NA total internal reflection fluorescence (TIRF) oil objective, Perfect Focus Ti-E stand, Agilent MLC400 laser

bed and Andor iXon Ultra EM-CCD camera. Laser illumination was provided using a fully motorised TIRF

combiner. The use of the TIRF combiner allows for the laser to illuminate the sample at an angle that will

only excite fluorophores that are within 200 nm of the cell surface membrane. Immunolabelled samples

were imaged in 0.5 mg/ml glucose oxidase, 40 μg/ml catalase, 10% wt/vol glucose and 100 mM MEA in

PBS, pH 7.4 to induce Alexa 647 blinking. During dSTORM acquisition, the sample was continuously illuminated at 640 nm for 20,000 frames (256 x 256 pixels, 9.2 ms exposure time). For the image sequence, single molecules were localised using the density estimation approach and an initial reconstructed image was generated as an average shifted histogram. The image sequence was then drift corrected and compensated for multiple blinking. After merging, a normalized 2D Gaussian image was produced and a colour from a predefined table (LUT) was applied. This process was performed using the ThunderSTORM plugin in FIJI (ImageJ) (Figure 3.4).

A density-based spatial clustering of applications with noise (DBSCAN) algorithm was used to detect and quantify AT_1R clusters (Ester et al., 1996, Pageon et al., 2016). DBSCAN is an unsupervised learning method, whereby points are classified as clustered according to two parameters; epsilon – the radius of search, and minPts – the minimum number of points required to be classified as a cluster (Ester et al., 1996, Pageon et al., 2016). This process was performed using MATLAB software, and epsilon and minPts were set to 20 nm and 10, respectively.
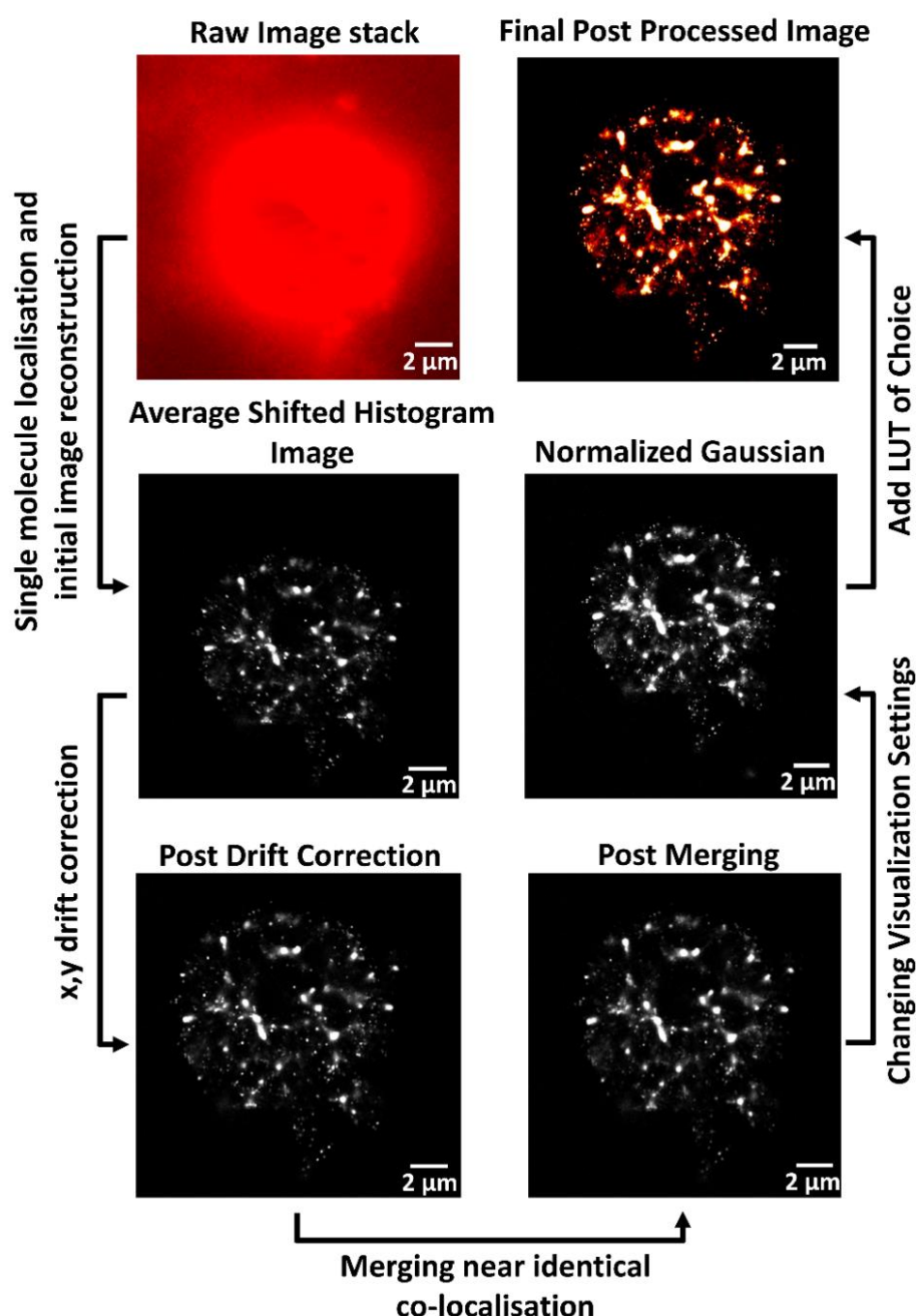
Figure 3.4 Summary of image processing used to generate super resolution images of angiotensin II receptor type 1 (AT₁R) distributions across the cell membrane of PC12 cells.

The **left top** image shows a single raw pre-processed PC12 cell. **Left middle** image shows the same cell after the localisation of single molecules and the generation of an average shifted histogram image. **Left bottom** image shows the cell after drift correction. Merging near identical coordinates was done next and the post merging image is shown in **right bottom**. After merging, a normalized 2D Gaussian image was produced **right middle**. A colour was applied as shown in the **right top** image. Processing was performed using the ThunderSTORM plugin in FIJI (ImageJ).

3.2.4 Statistical analysis

Data is presented in the text as mean±SEM. In figures, data is presented as box-whisker plots with the median, a box representing the interquartile range (IQR) and the whiskers extending to outliers. Single points represent mean data from an individual cell. Significance was taken as $p<0.05$ using an unpaired 2-tailed Student's t-test. Distribution figures were presented as 95th percentile, to eliminate outliers.

3.3 Results

3.3.1 AT$_1$Rs are clustered on the cell membrane of PC12 cells with measurable characteristics

The initial aim was to determine if AT$_1$Rs were randomly distributed on the cell membrane of PC12 cells or if they were found in clusters. An example reconstructed super-resolution image demonstrating the spatial organization of AT$_1$Rs across the entire PC12 cell surface is presented in Figure 3.5 A along with a magnified region of interest in Figure 3.5 C.

There are regions on the cell surface with an increased local density of AT$_1$R whilst there are other areas where AT$_1$R expression is absent. DBSCAN analysis confirmed the presence of distinct AT$_1$R cluster formation, Figure 3.5 B and 3.5 D. Analysis revealed a mean of 2.8±0.7 AT$_1$R clusters/μm^2 cell membrane when averaged across the entire cell surface, although there was some variation between cells (range 0.8-6.8 AT$_1$R clusters/μm^2), Figure 3.5 E. Mean AT$_1$R cluster area was 9.8±0.6 x 10^{-3} μm^2, (range 1.1 x 10^{-4} to 43.9 x 10^{-2} μm^2), with more than 50% of clusters being less than 3.7 x 10^{-3} μm^2, Figure 3.5F. More than 50% of clusters contained fewer than 100 localisations (range; 10 to 1041, mean; 252±15, median 45±15 localisations), Figure 3.5 G. The cluster density (a measure of how tightly packed together molecules are within the cluster) identified by DBSCAN showed a range of 1.5 x 10^4 to 3.6 x 10^4 localisations/μm^2, mean: 2.5±0.01 x 10^4 localisations/μm^2 and median 2.4±0.01 x 10^4 localisations/μm^2, Figure 3.5 H. Identification of AT$_1$R clustering was apparent in every cell tested (n=10). Additional demonstration of AT$_1$R clusters being present in PC12 cells is presented in Figure 3.6.
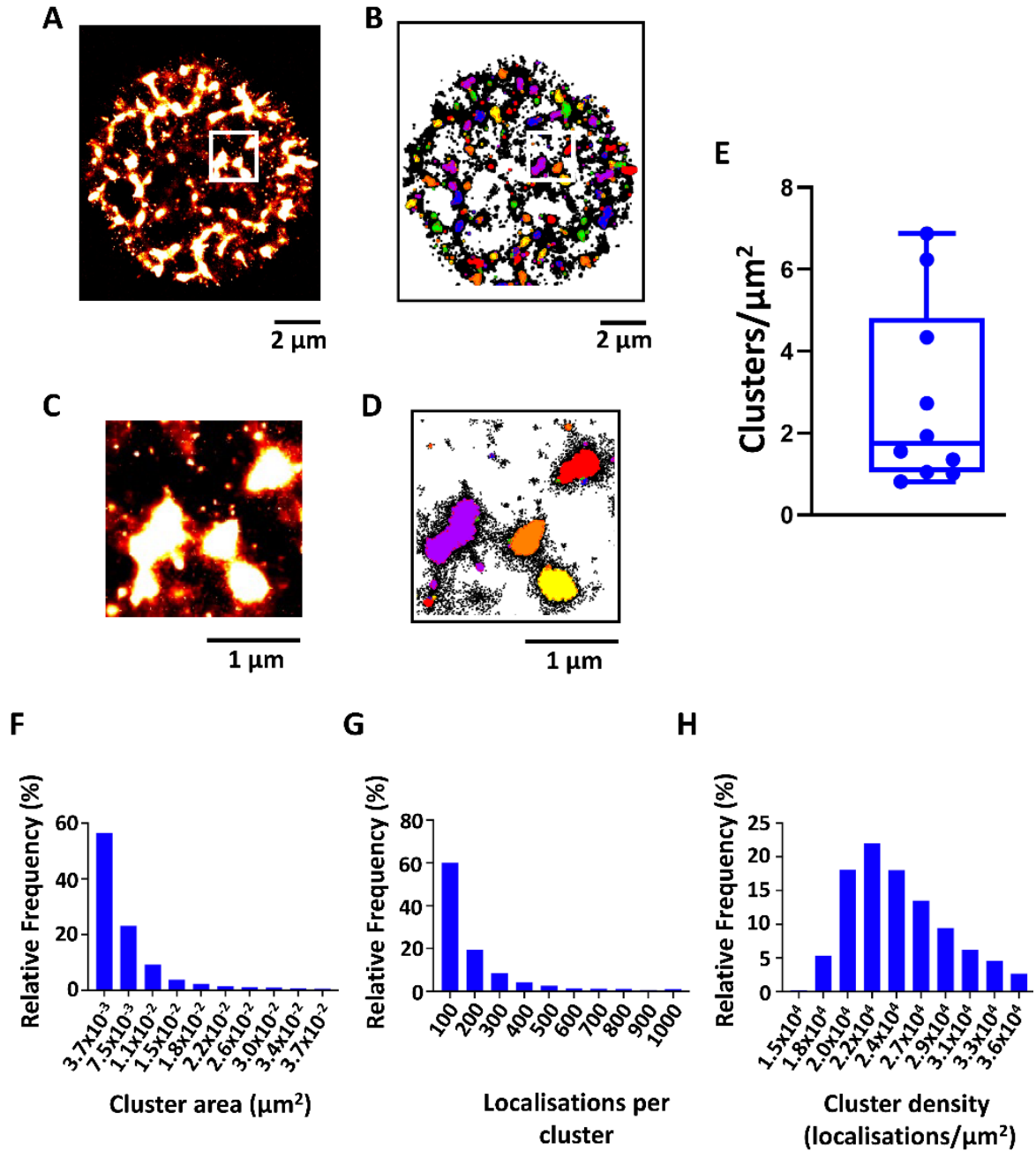
Figure 3.5 Quantification of angiotensin II receptor type 1 (AT$_1$R) cluster parameters on the cell surface membrane of PC12 cells.

Direct stochastic optical reconstruction microscopy (dSTORM) images (A & C) of AT$_1$R clustering on the cell surface membrane of PC12 cells along with corresponding cluster maps (B & D). (E) The number of AT$_1$R clusters detected per μm^2 when averaged across the entire cell surface membrane for 10 individual PC12 cells. Box-whiskers denote IQR and max-min values respectively. Horizontal line is the median. Individual dots denote data from a single cell. (F-H) Relative frequency distribution plots of cluster area (F), the number of localisations per cluster (G) and the number of localisations per μm^2 within the cluster (cluster density) (H). For F-H, data has been distributed into 10 equally sized bins. For F-H data is from N=3219 clusters taken from n=10 PC12 cells.
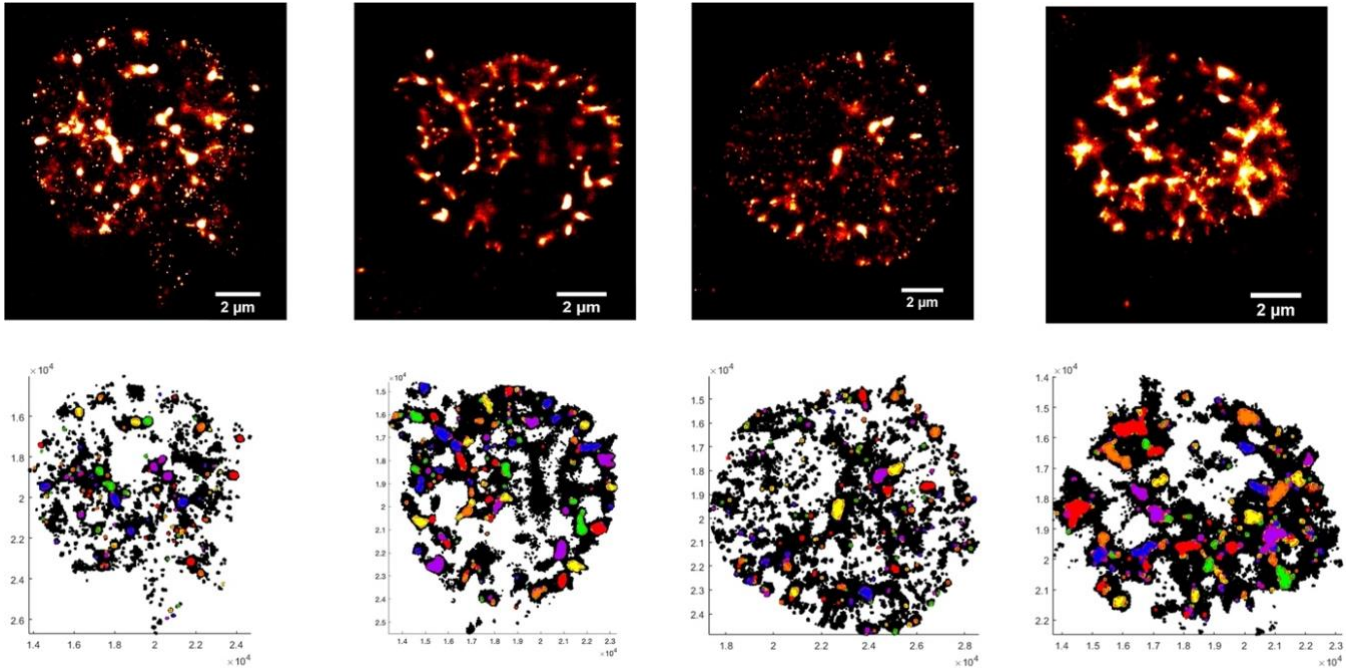
Figure 3.6 Distinct Angiotensin II receptor type 1 (AT₁R) clusters are consistently identified in PC12 cells.

(Top) Direct stochastic optical reconstruction microscopy (dSTORM) image examples showing significant AT$_1$R hotspots in 4 PC12 cells. (Bottom) The corresponding DBSCAN cluster maps, confirming the presence of AT$_1$R clusters in all 4 PC12 cells.

3.3.2 Maximum AT$_1$R cluster area is increased by chronic/sustained hypoxia

A comparison of the normoxic (Nx, 20% O$_2$) data was made against PC12 cells subjected to 24 hours of 1% O$_2$ (Hx) to evaluate whether any of the AT$_1$R cluster parameters would change in response to sustained hypoxia. In terms of the spatial arrangement of AT$_1$R, an initial reflection seen in the examples in Figure 3.7 A, suggests that AT$_1$R clusters were still apparent following 24 hours hypoxia with no obvious differences in the single molecule organisation. The mean spacing of AT$_1$R clusters throughout the entire cell membrane surface was consistent between Nx (2.8±0.7 clusters per μm^2, n=10 cells) and Hx (2.3±0.3 clusters per μm^2 n=10 cells, p>0.5). The mean and minimum cluster area was similar between groups, Figure 3.7 B & C. However, the maximum cluster area was significantly increased by 24 hours of sustained hypoxia, Figure 3.7 D.
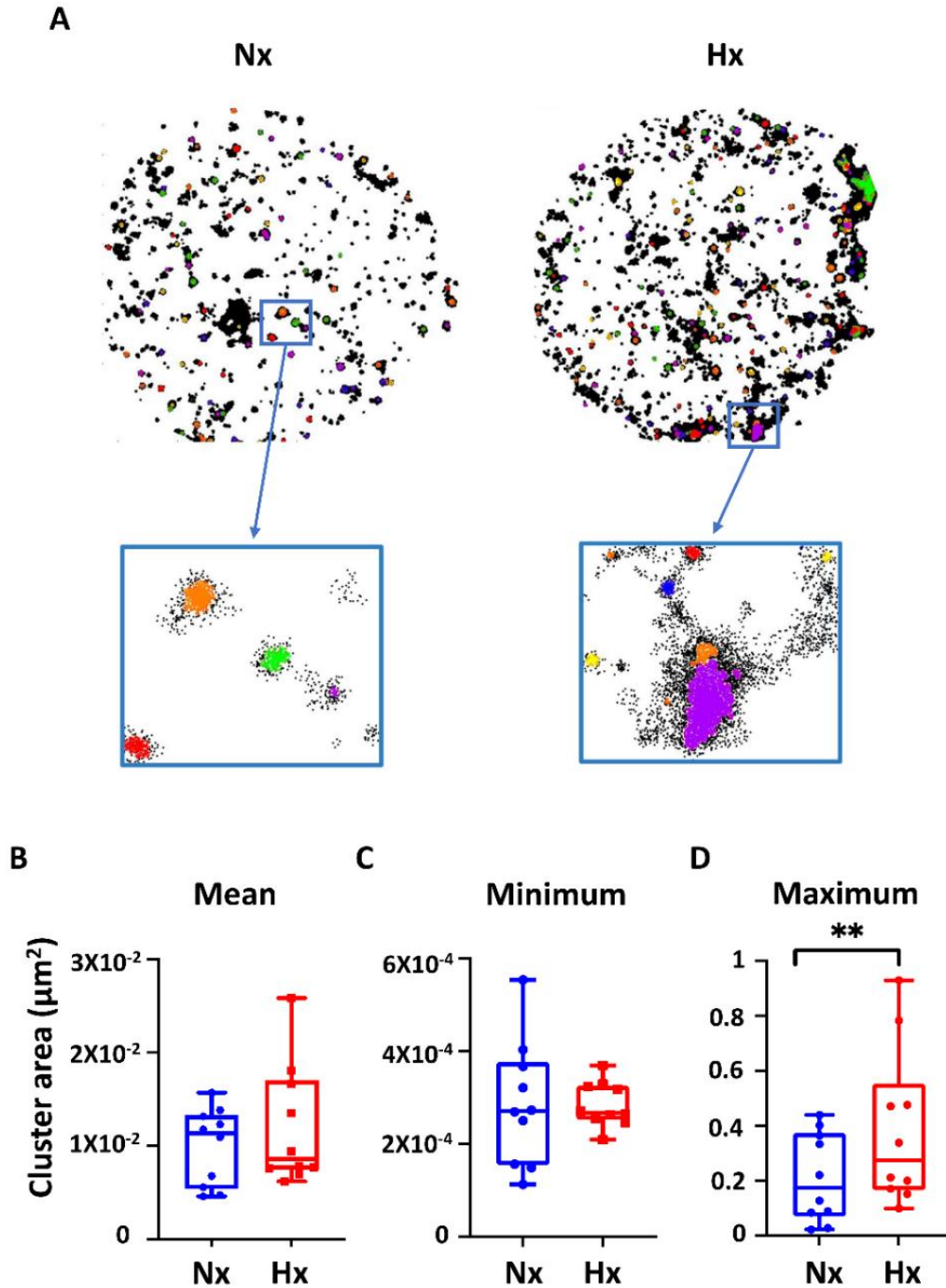
Figure 3.7 Hypoxia increases the maximum angiotensin II receptor type 1 (AT₁R) cluster area in PC12 cells.

(A) Example single molecule AT$_1$R cluster maps created by MATLAB using the DBSCAN algorithm, for cells exposed to 24 hours normoxia (Nx, 21% O_2, left) and hypoxia (Hx, 1% O_2, right). Insets: magnified ROIs showing individual clusters. (B-D) Box-whisker plots comparing the mean (B), minimum (C) and maximum (D) cluster area between Nx and Hx groups. Box-whiskers denote IQR and max-min values respectively. All data points (representing individual cells, n=10 cells Nx, n=10 cells Hx) are shown as well as the median. ** denotes $p < 0.01$, unpaired 2-tailed Student's t-test.

3.3.3 AT$_1$R cluster parameters are modestly altered by hypoxia:

Based on the previous findings, which indicated that the maximum cluster size is significantly increased after hypoxia, a comparison between Nx (N=3219) and Hx (N=2430) AT$_1$R cluster distributions was performed. For cluster area, the distribution follows a negative exponential for both Nx and Hx, with the majority of clusters being 7.5×10^{-3} μm^2 or less, Figure 3.8 A. However, there does appear to be a slightly greater proportion of clusters with particular large areas in the Hx group compared to the Nx group, Figure 3.8 B. Similarly, Hx slightly elevates the proportion of clusters with a particularly high number of localisations when compared to Nx, Figure 3.8 C & D.

Hypoxia did not significantly modify the distribution of cluster densities suggesting that hypoxia does not modify how tightly packed together AT$_1$R receptors are within the cluster, Figure 3.8 E. Collectively, this data is indicative of an increased generation of large area super-clusters in response to sustained hypoxia, which is dependent on an increase in AT$_1$R number rather than augmented spacing between the receptors.
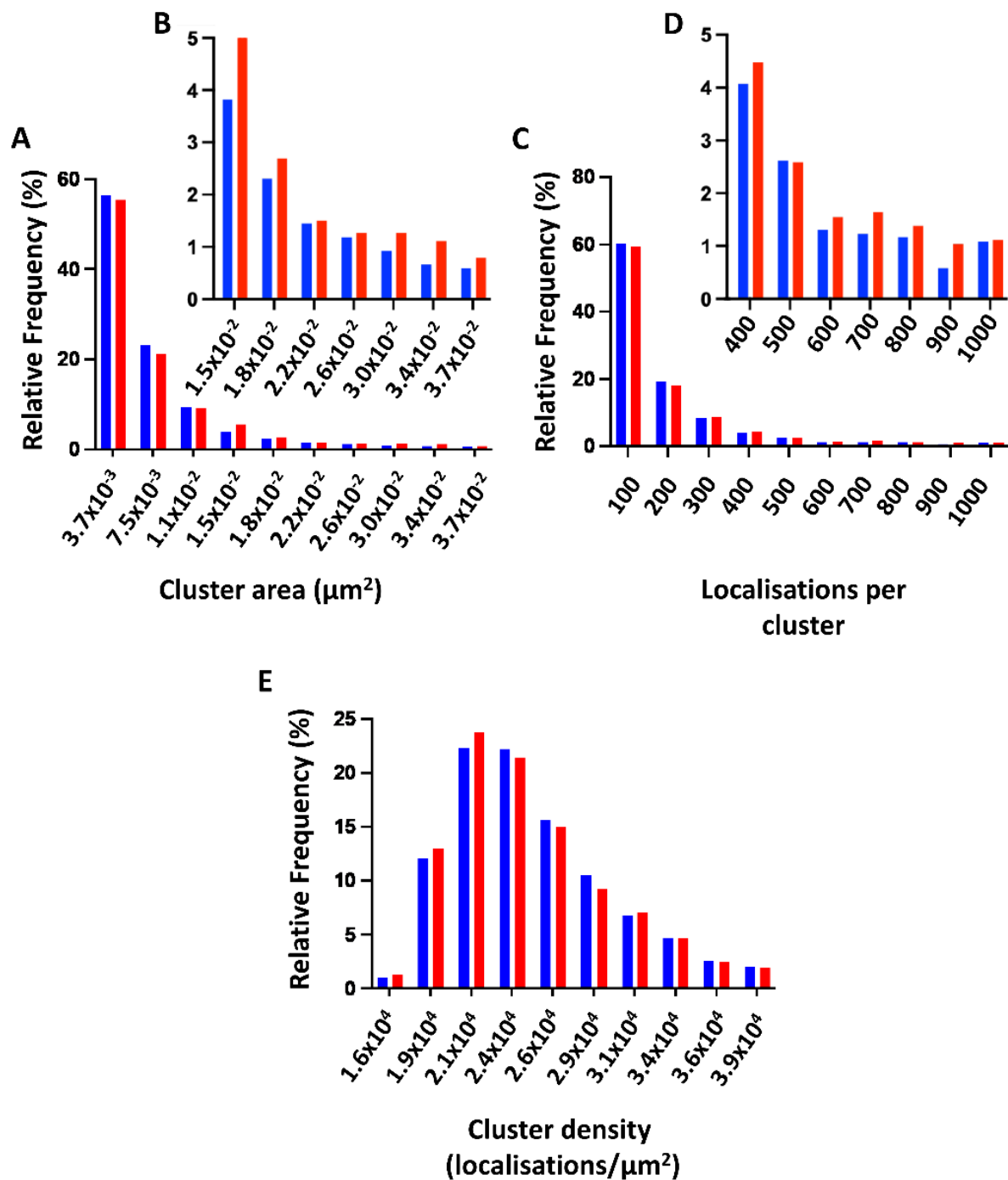
Figure 3.8 Hypoxia increases the proportion of large area angiotensin II receptor type 1 (AT₁R) clusters.

(A-E) Relative frequency distribution plots of AT$_1$R cluster area (A & B), the number of localisations per cluster (C & D) and the number of localisations per µm^2 within the cluster (cluster density) (E) for PC12 cells exposed to either 24 hours normoxia (Nx, N=3219 clusters) or hypoxia (Hx, N=2430 clusters). Data has been distributed into 10 equally sized bins. The y-axis has been confined in B and D to magnify data in the final 7 bins.

3.4 Chapter synopsis and discussion

3.4.1 List of main finding

- AT_1Rs are found in distinct clusters rather than being randomly distributed on the cell membrane of PC12 cells and have measurable characteristics.

- Maximum AT_1R cluster area is increased by hypoxia.

- Hypoxia induced AT_1R super-cluster formation.

3.4.2 The potential importance of AT_1R cluster formation and adaptation to hypoxia

AT_1R is a member of the GPCRs family, which are integral membrane proteins localized in the cell membrane, where they play a crucial role in signal transduction (Aldossary et al., 2020). These receptors span the cell membrane and are involved in detecting extracellular signals, such as hormones, neurotransmitters, and other signalling molecules (Tuteja, 2009). Upon binding to their specific ligands, GPCRs undergo conformational changes that activate intracellular G-proteins, initiating a cascade of downstream signalling events (Aldossary et al., 2020). This localization in the cell membrane allows GPCRs to effectively mediate communication between the external environment and the cell's interior, making them essential for various physiological processes (Fasciani et al., 2022).

TIRF microscopy is particularly effective at imaging membrane-associated proteins by using the evanescent wave created during total internal reflection at the interface between a glass slide and the aqueous

medium (Fish, 2009). This wave penetrates only a short distance (100-200 nm), selectively exciting fluorophores near the cell membrane and minimizing background fluorescence from deeper cell regions (Fish, 2009). While it excels at visualizing membrane proteins, TIRF can also image other structures within this thin region, such as cytoskeletal elements and vesicles, by enhancing contrast and resolution close to the cell surface (Li et al., 2015). Whilst it is therefore likely that the measurements obtained indicate the membrane distribution of AT$_1$Rs, this data could have been validated using a membrane marker, and should still be viewed with some caution.

Alterations in Ang II signalling in response to CH, CIH and heart failure have been implicated in mediating CB plasticity and hyperactivity (Kumar and Prabhakar, 2012b). It has been reported that CH increases AT$_{1a}$ and AT$_{1b}$-receptor mRNA expression in type I cells (Leung et al., 1998) as well as enhancing chemoafferent sensitivity to exogenous Ang II (Lam et al., 2004a, Leung et al., 2000). Given the link between the CB and augmented vascular sympathetic nerve activity in COPD patients (Iturriaga et al., 2016b, Phillips et al., 2018), selective targeting of the Ang II signalling pathway in the CB could be a novel approach to treat neurogenic hypertension of this aetiology.

In the current study, when a comparison was made between Nx and Hx groups, the results showed that Hx increased the maximum AT$_1$R cluster area and altered the cluster distribution, slightly increasing the proportion of large area clusters and the number of clusters with a very high number of localisations (superclusters). These findings are consistent with CH increasing AT$_1$R gene expression. In addition, our findings open up the possibility of CH inducing a more intense local Ang II microdomain signal. AT$_1$R activation is suggested to promote IP$_3$ dependent release of Ca^{2+} from intracellular stores (Leung et al.,

2003), as well as increasing the activity of NADPH oxidase (Garrido and Griendling, 2009, Peng et al., 2011a) both of which account for acute and sustained type I cell activation. An interesting next step would be to explore the nanoscale relationship between AT_1Rs and IP_3 receptors on the endoplasmic reticulum as well as with NADPH oxidases. This may underpin local Ang II mediated Ca^{2+} and ROS signalling microdomains within the PC12 cell which could be enhanced in response to CH.

CH has been shown to have a significant influence upon many aspects of the CB type I cell, which shares a number of similar properties to PC12 cells, including acute and specialised O_2 sensitivity. CH can impact on ion channel mRNA expression, enhancing cell excitability, alter neurotransmitter (NTM) secretion (Powell, 2007) and increase the action of neuromodulators, which collectively will facilitate afferent activity (Powell, 2007). These changes are associated with an increase in hypoxia-inducible factor 1α (HIF-1α) expression (Powell, 2007, Soulage et al., 2004). As well as changes in gene expression there is the possibility that hypoxia and HIF-1α related signalling may modify AT_1R degradation, trafficking or internalization (Collingridge et al., 2004, Drake et al., 2006). Understanding such modifications would help to explain the increase of AT_1R cluster size and super-cluster formation in PC12 cells after CH.

3.4.3 Chapter limitations

3.4.3.1 PC12 cell-line as a model of the CB type I cells

A limitation of this study was performing the experiments on PC12 cells rather than isolated CB type I cells. Similar work performed on type I cells would help extend our understanding of how changes in AT_1R clustering correlate against CB hyperactivity. It would be interesting to observe if the AT_1R clustering seen

here in PC12 cells resembles that of the type I cell and if the responses to hypoxia are consistent. A more extensive understanding of the single-molecule distribution of other GPCR and ion clustering in PC12 cells and isolated CB type I cells is also needed. Furthermore, in the current study, cells were only exposed to single level of hypoxia for 24 hours. It is probable that the extent of cluster re-modelling is dependent on both the intensity and duration of the hypoxic stimulus. *In vivo* cellular/tissue normoxia varies between different organs but it is estimated that the majority of cell types are exposed to somewhere between 2 and 5% O_2 (Lee et al., 2020). Cell lines which have been cultured over many generations, often in 20-21% O_2, may well have adapted to survive and grow at much higher O_2 levels. For most cells, cellular hypoxia ranges between 0.5 and 2% (Lee et al., 2020). However, for specialised O_2 sensing cells such as the PC12 cell and CB type I cell, acute responses to hypoxia are initiated at much higher levels, possibly as high as 5% O_2. However, even in these cells, long term adaptation to hypoxia is likely to be dependent on an alternative O_2 sensing mechanism involving HIF stabilisation and alterations in gene expression. Prolyl hydroxylase inhibition and HIF stabilisation occurs at a lower O_2 level estimated to be between 0.5 to 2% (Lee et al., 2020). Thus, it is accepted that the level of O_2 used in this study (1% O_2) can be considered as a relatively severe hypoxic stimulus but was used to initiate considerable HIF stabilisation which I hypothesised would lead to more long-term changes in AT_1R gene and protein expression. Indeed, in a previous study using PC12 cells, 1% O_2 was shown to cause the maximum increase in $HIF2\alpha$ stabilisation (Seta et al., 2002). That said it would be interesting to see if alterations in AT_1R cluster characteristics are still observed under more mild hypoxic conditions.

3.4.3.2 The use of dSTORM imaging technique

Although dSTORM imaging is a powerful technique, it has its limitations. One major limitation is the potential reduction in spatial resolution in densely labelled samples, where overlapping signals can affect the accurate representation of molecular arrangements, while low labelling density requires more attempts to reveal local protein architecture of cellular compartments (Venkataramani et al., 2018). Another concern is the susceptibility of dSTORM to photobleaching and phototoxicity. Prolonged exposure to intense light, necessary for super-resolution images, can damage fluorophores and harm cells, limiting the observation of cellular processes (Valli et al., 2021). Moreover, one of the additional limitations is using antibodies for labelling in dSTORM. Antibody specificity and affinity are crucial, as non-specific binding or low affinity can result in false signals, affecting the reliability of results (Xu et al., 2017). Thus, it was important to have performed some secondary-only negative controls to identify the absence of non-selective secondary binding, in the previous Chapter. The widespread use of dSTORM is limited, due to the need for highly specialized equipment, such as advanced microscopy setups and sensitive detectors.

3.4.4 Chapter conclusion

In conclusion, this work demonstrates that AT_1Rs are present in distinct clusters located in specific compartments or 'hot spots' in the cell membrane of O_2 sensitive PC12 cells. Exposure to hypoxia augments the maximum cluster area and elevates the proportion of large area clusters. Stronger Ang II microdomain signalling is therefore likely to be apparent in response to hypoxia although this needs to be verified.

Chapter 4. Investigating the influence of CH on respiratory timings, variability and sigh frequency

4.1 Introduction

4.1.1 Chapter introduction and overview

CH is a condition characterized by prolonged and inadequate O_2 supply to tissues and organs, causing a complex cascade of physiological responses aimed at maintaining cellular homeostasis and viability under O_2-deprived conditions (Lee et al., 2020). CH is a key feature of COPD. Over time, CH can lead to structural and functional alterations in various organ systems, influencing cardiovascular dynamics, pulmonary function, and metabolic processes (Barnes et al., 2022). During chronic exposure to hypoxia, as in COPD patients, baseline ventilation progressively increases due to persistent activation of the CB (Walsh and Marshall, 2006). In CH and COPD, there is also an increase in sympathetic nerve activity, which adjusts cardiac output and vascular conductance to ensure adequate O_2 delivery to the brain and vital organs (Marshall, 2015, Heindl et al., 2001). However, the most common comorbidity in COPD patients is the emergence of hypertension (Finks et al., 2020). The mechanisms for this are not fully understood but there is some evidence of involvement of heightened chemoreceptor activity and elevated sympathetic nerve activity (Phillips et al., 2019, van Gestel and Steier, 2010). Targeting the CB chemoreceptors may offer a novel therapy for treating hypertension in COPD patients.

In the previous chapters there were noticeable changes in AT_1R clustering in O_2 sensitive PC12 cells, a close surrogate of CB type I cells, in response to sustained hypoxia. These *in vitro* experiments used 24 hours of 1% O_2 as the hypoxic stimulus. Before moving on to look at Ang II signalling in the CB in response to CH, it was necessary to first validate an *in vivo* model of CH that will be used throughout the rest of the thesis.

Given the observed increase in AT_1R expression, TH expression and modifications in AT_1R clustering, observed in PC12 cells (a surrogate for the O_2 sensitive type I cells), in the previous chapters, transitioning to whole body plethysmography (WBP) would enable the identification of whether these changes could be observable at a systemic level and there for be responsible for pathological consequences. WBP allows for a comprehensive assessment of respiratory function and can clarify the physiological impacts of CH on respiratory parameters *in vivo*. By integrating WBP, changes in respiratory frequency, minute ventilation and breathing patterns can be quantified, thereby linking molecular and cellular alterations to functional respiratory outcomes. This approach enhances the understanding of how CH influences systemic physiology.

CH alters many physiological aspects in rats including alterations in chemoreceptor activity and a rise in baseline minute ventilation (Thomas and Marshall, 1995). A key initial aim of this Chapter is to make sure my model of CH does indeed lead to an expected elevation in baseline ventilation and inspiratory drive, consistent with heightened CB chemoreceptor activity.

Prolonged exposure to reduced O_2 levels may also be expected to introduce significant changes in the rhythmicity of respiratory patterns. Apart from a general increase in ventilation, relatively little is known about other variations in breathing in CH such as inspiratory/expiratory timings, breath-to-breath interval (B-B interval) variability and breath-to-breath tidal volume (VT) variability. The regulatory mechanisms governing respiratory adaptation to the demands of CH, and in particular CB hypersensitivity, are hypothesised to cause modifications in the dynamics of B-B interval variability and inspiratory/expiratory timings. A better understanding of these adaptations should provide valuable insights into the respiratory system's capacity to cope with chronic O_2 deficiency. Furthermore, changes in such parameters could be

useful predictors/markers of disease severity and/or the extent of chemoreceptor hyperactivity. Therefore, a second aim is to quantify the alterations in inspiratory/expiratory timings, breath-to-breath interval variability and breath-to-breath tidal volume (VT) variability in animals exposed to CH.

Another breathing parameter that is commonly studied is sigh frequency, which is characterized by a deep and exaggerated inhalation followed by a prolonged exhalation, and sometimes a post-expiratory pause. Sighs are thought to play a role in optimizing lung function by enhancing lung recruitment and preventing alveoli collapse (Hess and Bigatello, 2002). There are some suggestions that a sigh is generated as a controlling mechanism, primarily to reset breathing regularity (Ramirez, 2014). Interestingly, during acute hypoxia, there is an observed increase in the number of sighs (Ramirez, 2014). This probably reflects the respiratory system's response to the reduced availability of O_2. The heightened occurrence of sighs during acute hypoxia is likely a compensatory mechanism aimed at preserving efficient gas exchange and lung function when challenged by decreased O_2 levels (Cherniack et al., 1981).

Often following a sigh there is a ventilatory pause (apnoea). Ventilatory pauses, which represent temporary periods of suspended breathing within the respiratory cycle, are shorter during acute hypoxia (Xu et al., 2003), which could suggest an adaptive response of the respiratory system to maintain a more continuous breathing pattern. This is possibly due to an increase in inspiratory drive mediated by heightened input from the CB and helps to ensure a consistent supply of oxygen to vital tissues and organs in the context of decreased oxygen availability.

At present, it is not clear whether the frequency or morphology of sighs is disturbed in COPD patients or in response to CH. Furthermore, there is little evidence regarding how post-sigh ventilatory pauses are

impacted by CH when it is assumed there is an exaggerated inspiratory drive. The final aim of this chapter is therefore to quantify sigh activity and post-sigh ventilatory pauses in animals exposed to normoxia and CH.

4.1.2 Chapter hypotheses

- CH alters breathing parameters by increasing respiratory frequency, minute ventilation and inspiratory drive at baseline and during acute hypoxia.

- Exposure to CH produces changes in respiratory cycle timings and breath-breath respiratory patterns at baseline and during acute hypoxia.

- CH modifies sigh initiation and post-sigh ventilatory pause duration at baseline and during acute hypoxia.

4.1.3 Aims of this Chapter

After 10 days of CH (12% F_iO_2) or normoxia (21% F_iO_2) whole body plethysmography will be used to:

1. Examine the influence of CH on basic ventilatory parameters, such as respiratory frequency, tidal volume and minute ventilation, in normoxia, acute hypoxia or upon reoxygenation.

2. Investigate the impact of CH on inspiratory and expiratory times, breath-breath interval variability and breath-breath tidal volume variability, in normoxia, hypoxia or upon reoxygenation.

3. Test whether sigh induction and ventilation pauses, are affected in CH rats during normoxia, acute hypoxia or upon reoxygenation

4.2 Chapter methods

4.2.1 Animals and exposure to CH

All animal procedures were performed in accordance with UK Animals (Scientific Procedures) Act 1986 and approved by the UK Home Office (PPL number PP9019875) and by the Animal Welfare and Ethical Review Body (AWERB) at the University of Birmingham. A total of 13 adult male Wistar rats (240-333 g) were randomly split into two groups (normoxia (N) n= 7 and chronic hypoxia (CH) n= 6). All animals were housed in individually ventilated cages, (n = 2-4 per cage) with free access to food and water and under standard conditions: 12:12 hour light:dark cycle (lights on at 0700), 22 °C and 55 % humidity. Only male rats were used in the experiments to minimize hormonal variability that could influence the results (Lovick and Zangrossi, 2021, Arakawa et al., 2014). To determine the number of animals required to establish a definitive outcome, a power calculation is required. However, the experiments described here is a preliminary one and so the number of animals used was in line with those previously used by our research group.

For the CH group, CH (F_iO_2 = 12%) was induced continuously for 10 days using a dynamic O_2 controller and dedicated small animal chamber (BioSpherix, Parish, NY, USA) (Figure 4.1). On the first day the F_iO_2 was gradually reduced over a period of 2 hours from 21% to 12%, by decreasing F_iO_2 levels approximately 0.05 to 0.1% every minute until reaching 12% (Figure 4.2). It is then maintained at 12% for 9-10 days, Figure 4.2. To maintain cage humidity and prevent rises in CO_2, silica gel and soda lime were used inside each cage and were changed on a daily basis. Every day at 10 am, animal welfare checks were completed, CO_2 and humidity levels were documented, silica gel and soda lime were changed, and food and water were replenished.

Figure 4.1 Hypoxia chamber

Photograph of dynamic O_2 controller and dedicated small animal chamber (BioSpherix, Parish, NY, USA). A single chamber could house 1 cage containing 2 animals.
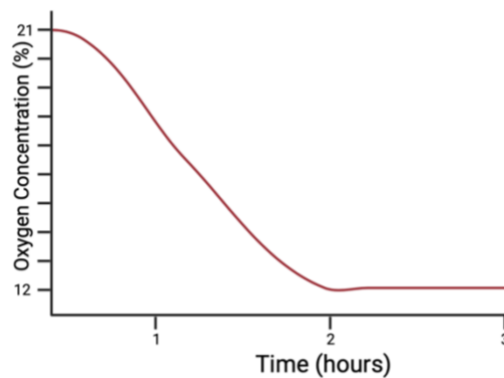
Figure 4.2 Gradual hypoxic ramp used for induction of CH on the first day

The figure demonstrates the O_2 ramp used for induction of CH within the hypoxic chamber, where O_2 concentration is decreased by 0.05 to 0.1% every minute to go from 21 to 12% in two hours. After reaching 12%, a control protocol will be initiated, where the O_2 level will be maintained at 12% until the end of 10 days.

4.2.2 Whole body plethysmography (WBP)

WBP is a technique used to evaluate respiratory function in animals. It's particularly important for understanding the role of CBs in regulating breathing responses to acute hypoxia. WBP was used in the current Chapter to assess how breathing is affected by CH. The WBP system, developed by Emka Technologies, allows for various respiratory parameters to be calculated non-invasively, including tidal volume (Vt), respiratory frequency (Rf), minute ventilation (VE) and respiratory timings (inspiratory time – Ti and expiratory time - Te).

The WBP system operates based on barometric principles. The animal breathes in a sealed chamber with two compartments: the subject chamber, where the animal is placed, and a reference chamber that reduces external noise interference. Changes in chamber pressure caused by the animal's breathing are detected using a differential pressure transducer (DPT). This setup cancels out external disturbances like

room pressure fluctuations. The DPT has ports connected to both chambers, helping differentiate animal-generated pressure changes from external noise, Figure 4.3.

In a controlled environment, the animal's breathing causes pressure changes within the sealed chamber. During inspiration, the animal inhales air, resulting in an increase in lung volume (Emka Technologies, Paris, France). This increase in lung volume leads to a decrease in chamber pressure due to Boyle's law, which states that the pressure of a gas is inversely proportional to its volume when temperature is held constant (Sorbello et al., 2018). As the animal continues to breathe in, the decrease in chamber pressure is recorded by sensors within the plethysmography chamber (Emka Technologies, Paris, France). Conversely, during expiration, the rat exhales air, causing a decrease in lung volume. This decrease in lung volume leads to an increase in chamber pressure according to Boyle's law. Sensors within the plethysmography chamber detect this increase in pressure as the rat exhales (Emka Technologies, Paris, France).

The shift volume is essential during both inspiration and expiration (Kraemer et al., 2024). When a rat inhales during inspiration, the shift volume represents the extra air entering the lungs, aiding in assessing lung compliance and respiratory function by revealing understandings into lung tissue elasticity and expansion (Criée et al., 2011). Conversely, during expiration, the shift volume mirrors the decrease in lung volume as air is exhaled, aiding in detecting changes in airway resistance and lung mechanics (Criée et al., 2011). Abnormalities in shift volume may indicate respiratory disorders or altered lung function (Kraemer et al., 2024).

The DPT captures these pressure changes, which are amplified and converted by an Emka Technologies usbAMP amplifier and recorded using iox2 acquisition software (Emka Technologies, Paris, France).

Before each experiment, calibration is crucial for accurate measurements. This involves both high and low calibrations. Normally, the low value is set at 0, indicating no flow, and the high value corresponds to the injected volume, which is 20 mL. The recommended calibration range for rats is (±8500 to ±13500 ml/s) by Emka Technologies. If calibration is initially out range, troubleshooting will be performed (such as identifying and sealing small leaks) to ensure a controlled and accurate recording environment is established for all subjects before starting the experiment.
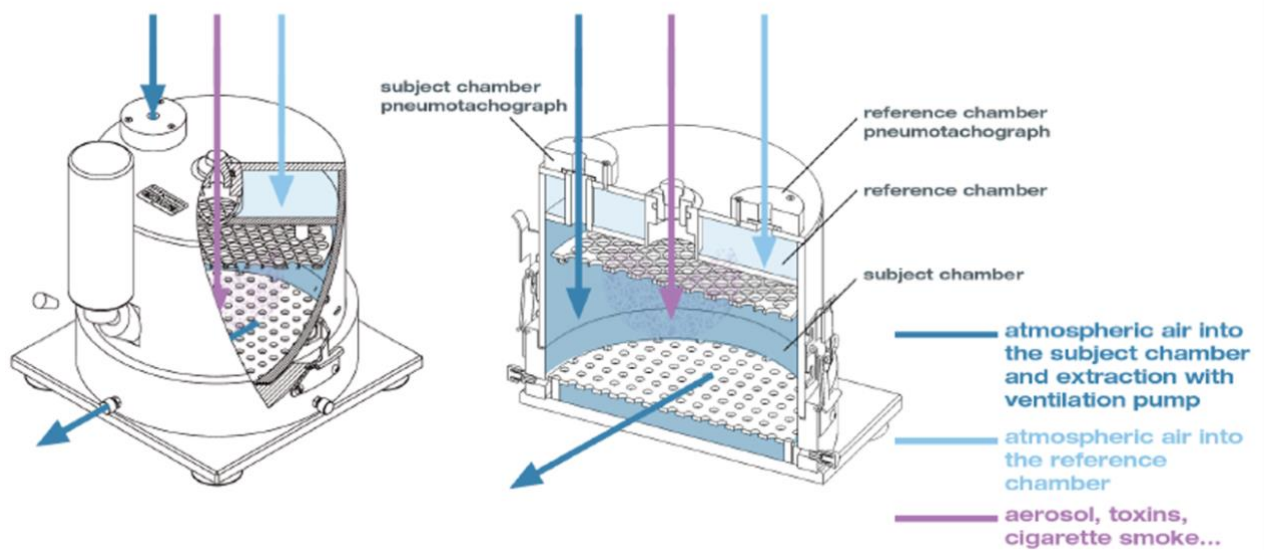
Figure 4.3 Whole body plethysmography (WBP) system

The WBP system, supplied by EMKA Technologies, Paris, France, consisting of two chambers: the subject chamber, where the animal is placed during the experiment, and the reference chamber that plays a crucial role in minimizing the transmission of noise and unwanted signals. Gas mixtures are delivered through the gas inlet located on both sides of the chamber.

4.2.3 WBP protocol

The experiments took place between 9:00 AM and 4:00 PM. To administer a desired hypoxic/hypercapnic gas mixture, high precision O_2, N_2, and CO_2 mass flow controllers were programmed to deliver gases at varying flow rates whilst ensuring that the total flow rate delivered to the ventilation input port of the subject chamber was always 2 L min^{-1} (Vent2 Emka Technologies, Paris, France). O_2, N_2, and CO_2 cylinders from BOC Limited, Surrey, UK, were used to deliver the desired gas mixture. Connected to the chamber, there was a ventilation pump, which aims to extract air from the chamber at the same flow rate (2 L min^{-1}), to prevent CO_2 and humidity accumulation inside the recording chamber.

Right before starting the experiment, animal weight was measured, to allow for normalization of Vt and VE to body mass. Animal bedding was added to minimise stress and improve acclimatisation. Fresh, unsaturated silica gel was replenished to minimize large changes in humidity. After placing the rat in the chamber, a settlement period will start, where rats acclimatize to the new environment. Acclimatization takes approximately 30 minutes. When the animal is fully acclimatized and respiratory flow signals become steady, and unaffected by significant movement artefacts, a 5-minute baseline will be recorded, followed by exposure to hypoxia. After switching to the hypoxic gas mixture, it takes 5 minutes for the F_iO_2 inside the subject chamber to ramp down from 21% to 10% (Figure 4.4). An F_iO_2 of 10% (hypoxia) was then maintained for 5 minutes, followed by 10 minutes of reoxygenation. A summary of the whole protocol is presented in Figure 4.5. After the WBP experiment was performed, animals were returned to the CH chamber. This was done because the cardiovascular measurements, described in Chapter 6, were scheduled to be conducted the following day.
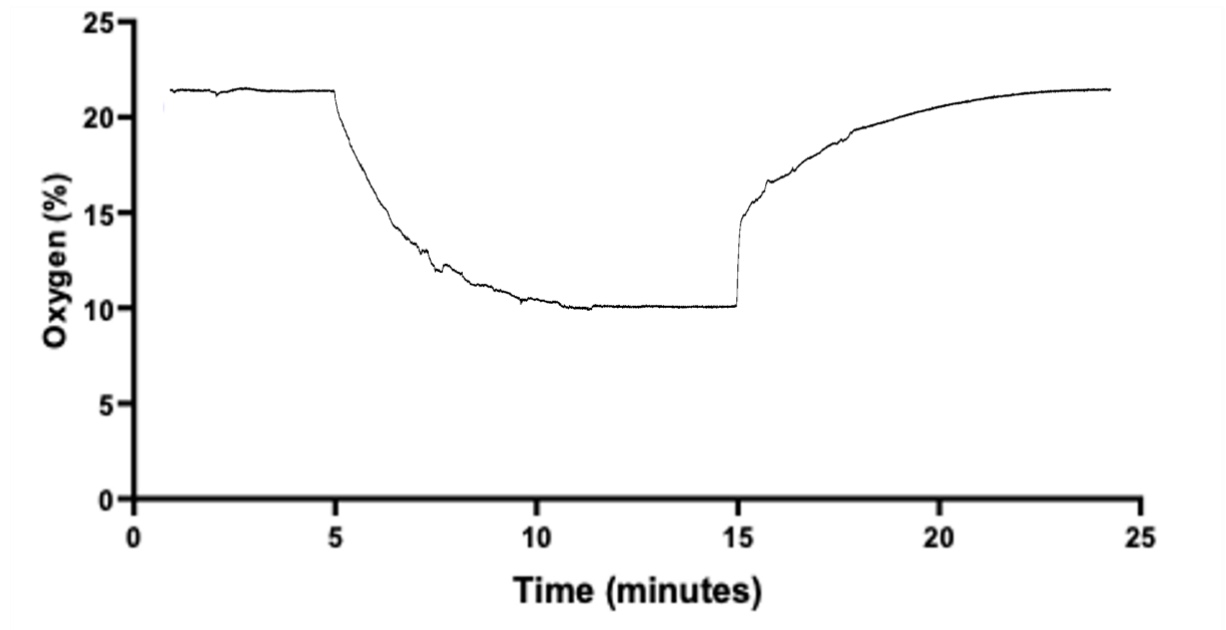
Figure 4.4 Example O₂ ramp raw trace measurement in the subject chamber

A raw trace of O_2 measured using an O_2 electrode placed in the subject chamber illustrates the exact time required for the O_2 level to go from 21% to 10%, which, as shown, was approximately 5 minutes. The 10% hypoxia was then sustained for 5 minutes. Similarly it takes over just 5 minutes for the O_2 to return to 21%.
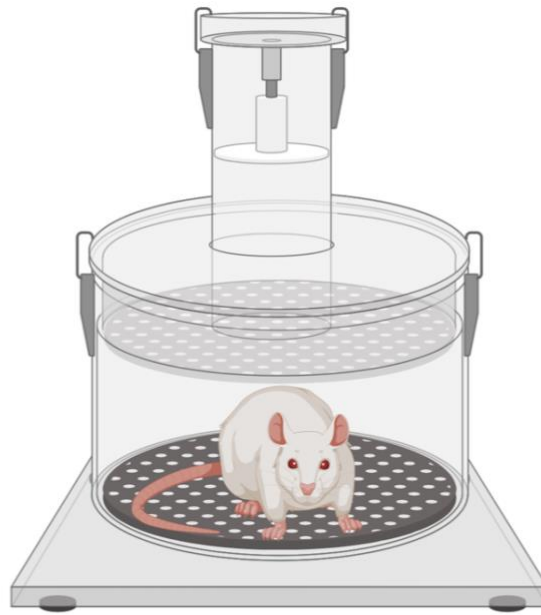
Figure 4.5 Whole body plethysmography protocol

Following a settling period (rat acclimatization and breathing stabilization) upon rat placement in the chamber, a 5-minute baseline (BL) recording of breathing was conducted. To induce hypoxia (Hx) it took 5 minutes to gradually ramp from 21% to 10% F_iO_2, (see Figure 4.4). 10% Hx was then sustained for 5 minutes. Following this, breathing was recorded during a reoxygenation period of 10 minutes to allow enough time for the F_iO_2 to return to 21% and for the breathing to restabilize.

4.2.4 Data analysis

Data acquisition was obtained using iox2 software (Emka Technologies, Paris, France), which calculates the basic respiratory parameters, such as, Vt, Rf, Ti and Te, while other parameters, including body-mass normalized VE and Vt, were calculated using excel. Data analysis was performed using Prism v8-10 (GraphPad, Boston, MA, USA), where data was presented as mean ± SEM. For baseline (normoxic) analysis, the last 4 minutes of steady state breathing were averaged. For hypoxia, the last 3 minutes of breathing 10% F_iO_2 were averaged once a steady state had been achieved. During the reoxygenation period, the last 2 minutes were used for analysis, again once breathing had achieved a steady state.

Pre- and post- sigh breathing analysis was performed by taking 5 breaths immediately before and after the sigh. Sigh amplitude and pause duration after the sigh were also analysed (Figure 4.6). For respiratory variability analysis, the whole data trace in an iox2 file format was converted into a labChart compatible file format. In LabChart the raw data signal was smoothed and filtered to allow for identification of each individual breath across the entire trace. Breath-breath variability data was assessed by initially calculating individual B-B intervals, then by taking measurements of B-B interval standard deviation and finally by producing Poincaré plots of the $B-B_n$ interval (x axis) vs $B-B_{n-1}$ interval (y-axis).
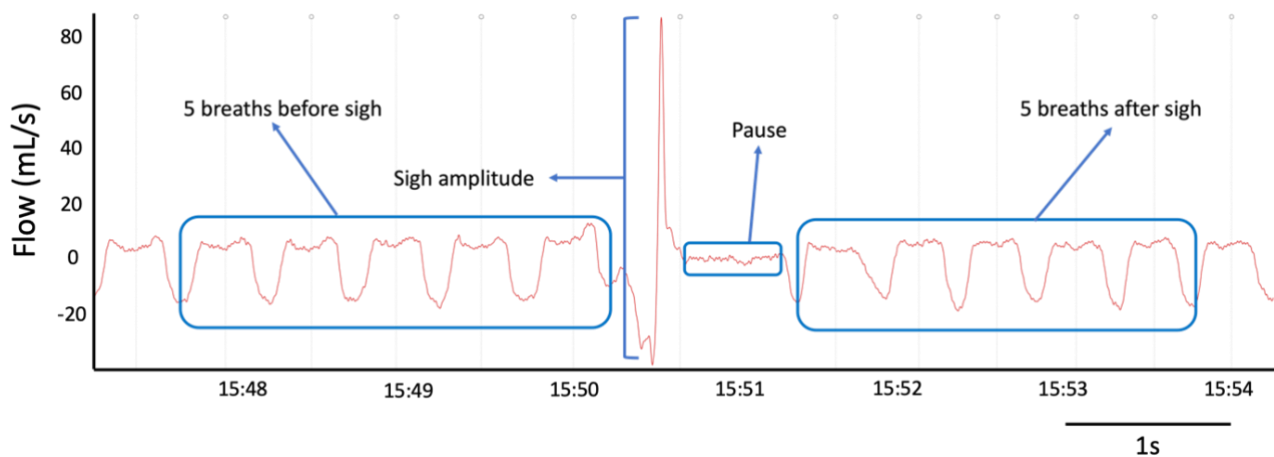
Figure 4.6 A demonstration of breathing pre and post sigh, sigh amplitude and a post sigh ventilatory pause.

A breathing raw trace that shows where exactly data points were taken. The pre sigh breathing was considered to be the last 5 breaths before the sigh, while post sigh breathing is the 5 breaths immediately after the sigh. The ventilatory pause length is determined by the time between the end of a sigh to the initiation of a new breath.

4.2.5 Statistical analysis

Data is presented in the text and figures as mean ± SEM. Individual subject (animal) data is shown as single

dots. Significance was taken as $p<0.05$, using an unpaired two-tailed Student's t-test or 2-way repeated

measures ANOVA, as appropriate. In some instances, a Sidak's post hoc test was performed to identify

significant differences between individual groups within the dataset.

4.3 Results

4.3.1 CH alters VE at baseline, during hypoxia and upon reoxygenation and this is mainly driven by an elevated Rf

Before a comprehensive assessment of the experimental time course, a raw trace exemplifying the impact of exposure to 12% hypoxia for 10 days on respiratory parameters is shown in Figure 4.7. Flow traces are presented under the 3 conditions: baseline (normoxia, 21% F_iO_2), hypoxia (10% F_iO_2) and reoxygenation (return to 21% F_iO_2), for an N and CH animal. This raw trace serves as a visual illustration of the observed changes in Rf, VE and respiratory cycle timings between N and CH animals.

Assessment of the whole experimental time course shows that exposure to 12% hypoxia for 10 days (CH) increases Rf; the overall effect of CH on Rf is significant ($p < 0.0001$) (Figure 4.8 A). There was no overall effect of CH on Vt ($p = 0.5542$) (Figure 4.8 B). VE was significantly increased in the CH group ($p = 0.0083$), which is a consequence of the rise in Rf (Figure 4.8 C).

To examine when breathing changes were most prominent, further comparisons were made between N and CH at baseline, during the final 3 minutes of 10% hypoxia and during the last 2 minutes of reoxygenation. CH significantly increases the baseline Rf, N=87.13±6.395 bpm, while the CH group had a baseline Rf of 121.8±5.164 bpm, (Student's t test, $p = 0.0017$). During 10% acute hypoxia exposure, Rf was significantly increased in CH group, N Rf was 129.7±5.142 bpm and CH Rf was 155.0±8.091 bpm, (Student's t test, $p = 0.0200$). Upon reoxygenation and once breathing had reached a steady state, the Rf was significantly higher in CH, 113.5±4.530 bpm, compared with N rats, 71.54±2.533 bpm, (Student's t test, $p < 0.0001$) (Figure 4.9 A). The normalized Vt does not show any alteration between the groups in all condition; baseline- N Vt was 0.006675±0.0008527 mL g^{-1} and CH Vt was 0.006273±0.0004953 mL g^{-1},

acute hypoxia- N Vt was 0.008145 ± 0.0008505 mL g^{-1} and CH Vt was 0.009706 ± 0.001070 mL g^{-1} , and reoxygenation, where N Vt was 0.007586 ± 0.0009161 mL g^{-1} and CH Vt was 0.007810 ± 0.0009420 mL g^{-1}, (Student's t-tests, p=0.7044, p=0.2719 and p=0.8681, respectively), Figure 4.9 B. There was a strong tendency for baseline VE to be augmented in CH animals, 0.7575 ± 0.05313 mL min^{-1} g^{-1} compared to N animals, 0.5731 ± 0.07063 mL min^{-1} g^{-1}, (Student's t test, p=0.0676). VE was significantly increased in CH group during acute hypoxia, N 1.032 ± 0.09899 mL min^{-1} g^{-1} vs CH $1.4710.1500$ mL min^{-1} g^{-1}, and reoxygenation, N 0.5393 ± 0.05901 mL min^{-1} g^{-1} and CH, 0.8774 ± 0.09749 mL min^{-1} g^{-1}, (Student's t-test, p=0.0288 and p=0.0107, respectively), Figure 4.9 C. The changes in Rf, Vt and VE were measured by comparing hypoxia or reoxygenation against baseline breathing, and it showed no significant alteration between N and CH, Figure 4.10 A, B and C.
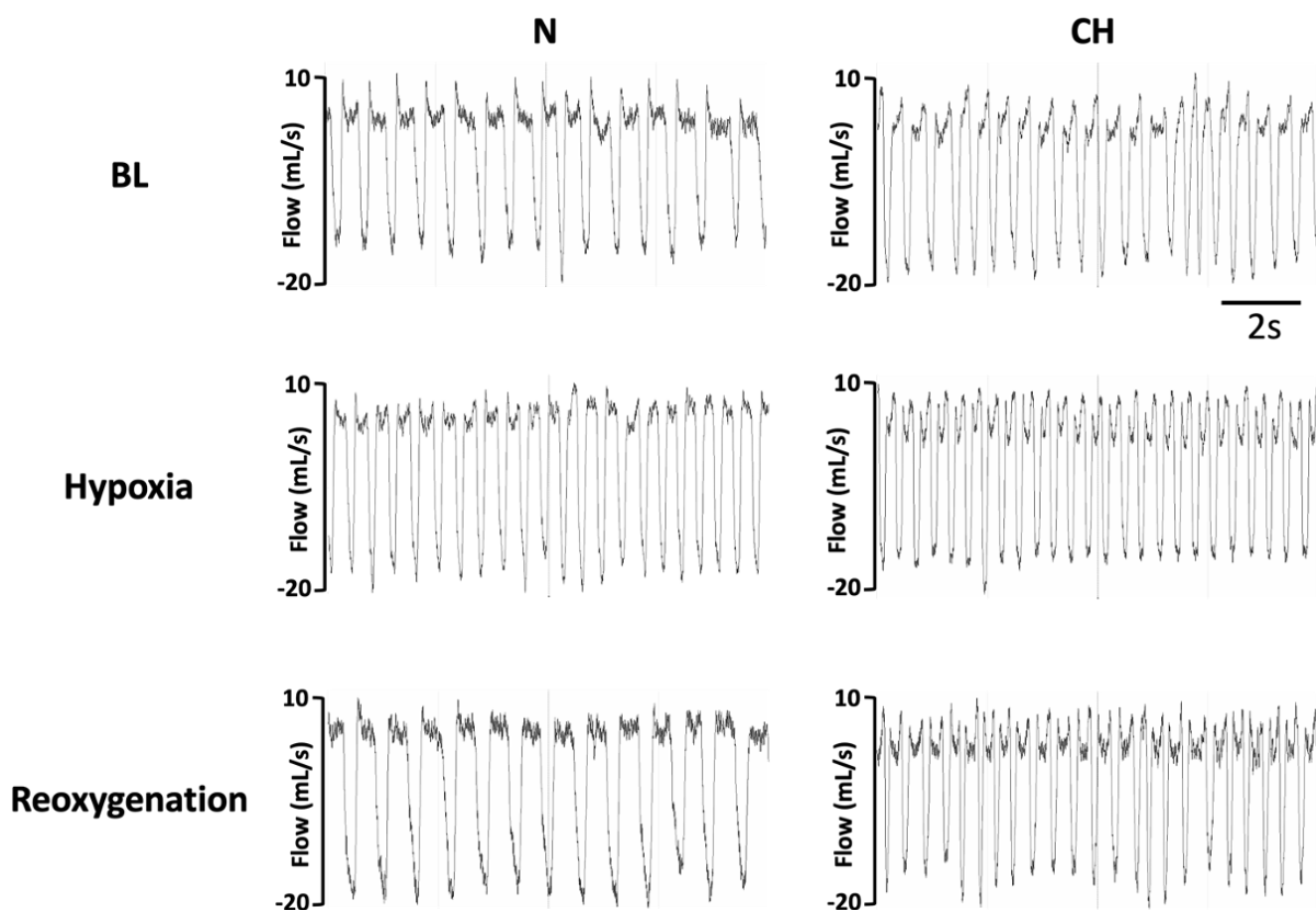
Figure 4.7 Raw respiratory trace comparison for a normoxic (N) and chronically hypoxic (CH) animal.

Raw traces showing the respiratory flow in normoxic (N) and chronic hypoxia (CH) groups during baseline (21% F_iO_2), hypoxia (10% F_iO_2), and during the reoxygenation period (21% F_iO_2). The traces provide a visual insight into the differences in breathing for N and CH, at different time points/experimental conditions throughout the experimental protocol.
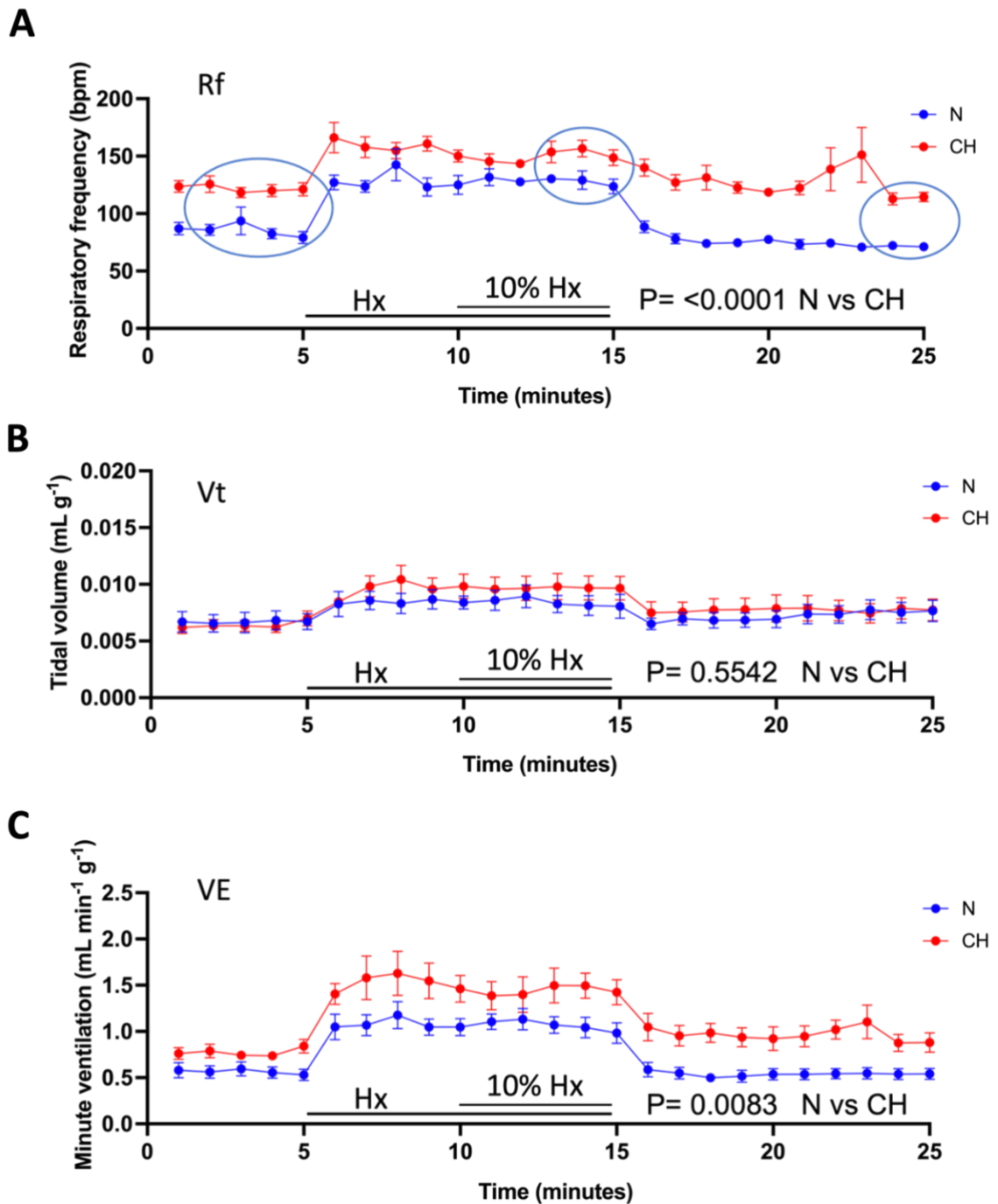
Figure 4.8 Exposure to chronic hypoxia (CH) increases minute ventilation (VE) by augmenting respiratory frequency (Rf).

(A-C) Time courses demonstrating minute-to-minute measurements of Rf (A), tidal volume (Vt) (B), and (VE) (C) recorded at baseline, in response to 10% O_2 (hypoxia, Hx) and upon reoxygenation, in normoxic (N; n=7) and CH (n=6) animal groups. The first 5 minutes are baseline breathing measurements, minutes 5 to 10 is when the O_2 ramps down from 21 to 10%, minutes 10 to 15 is when the animal is exposed to 10% F_iO_2 and minutes 15 to 25 is where the reoxygenation takes place, gradually returning to 21% F_iO_2. Data presented as mean±SEM, statistical tests performed using 2-way repeated measures ANOVA.
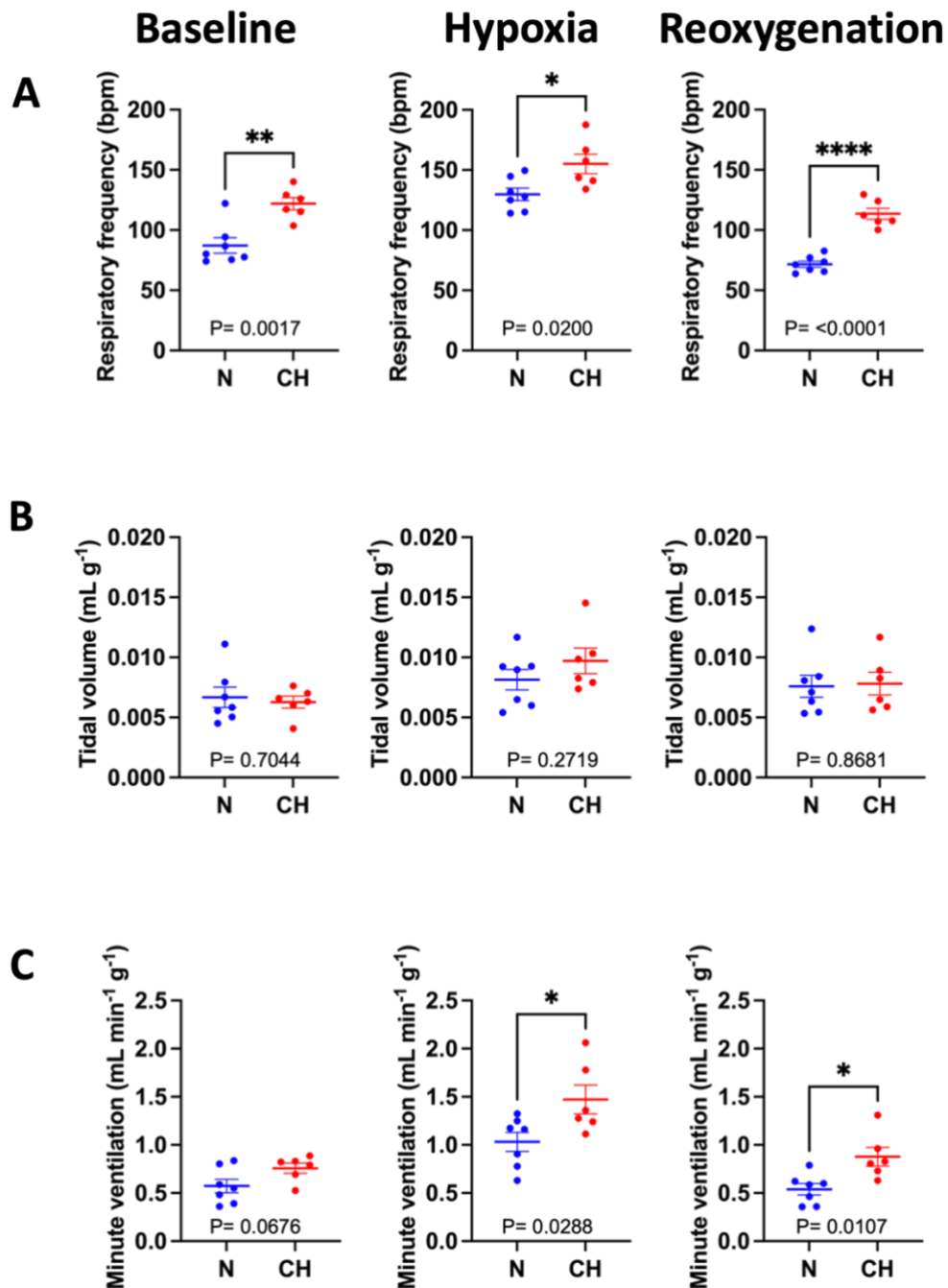
Figure 4.9 Chronic hypoxia (CH) increases respiratory frequency (Rf) and minute ventilation (VE) at baseline, during the response to acute hypoxia (Hx) induction and upon reoxygenation.

(A) Rf measured in normoxic (N, n=7) and CH (n=6) animal groups at baseline (left), during acute hypoxia (Hx) (middle) and upon reoxygenation (right). (B) Tidal volume (Vt) measured at baseline (left), during acute hypoxia (Hx) (middle) and upon reoxygenation (right) for N and CH. (C) VE measured at baseline (left), during acute hypoxia (Hx) (middle) and upon reoxygenation (right) for N and CH. Data presented as mean±SEM. Analysis performed using unpaired Student's t-test. Individual dots represented single animal data.
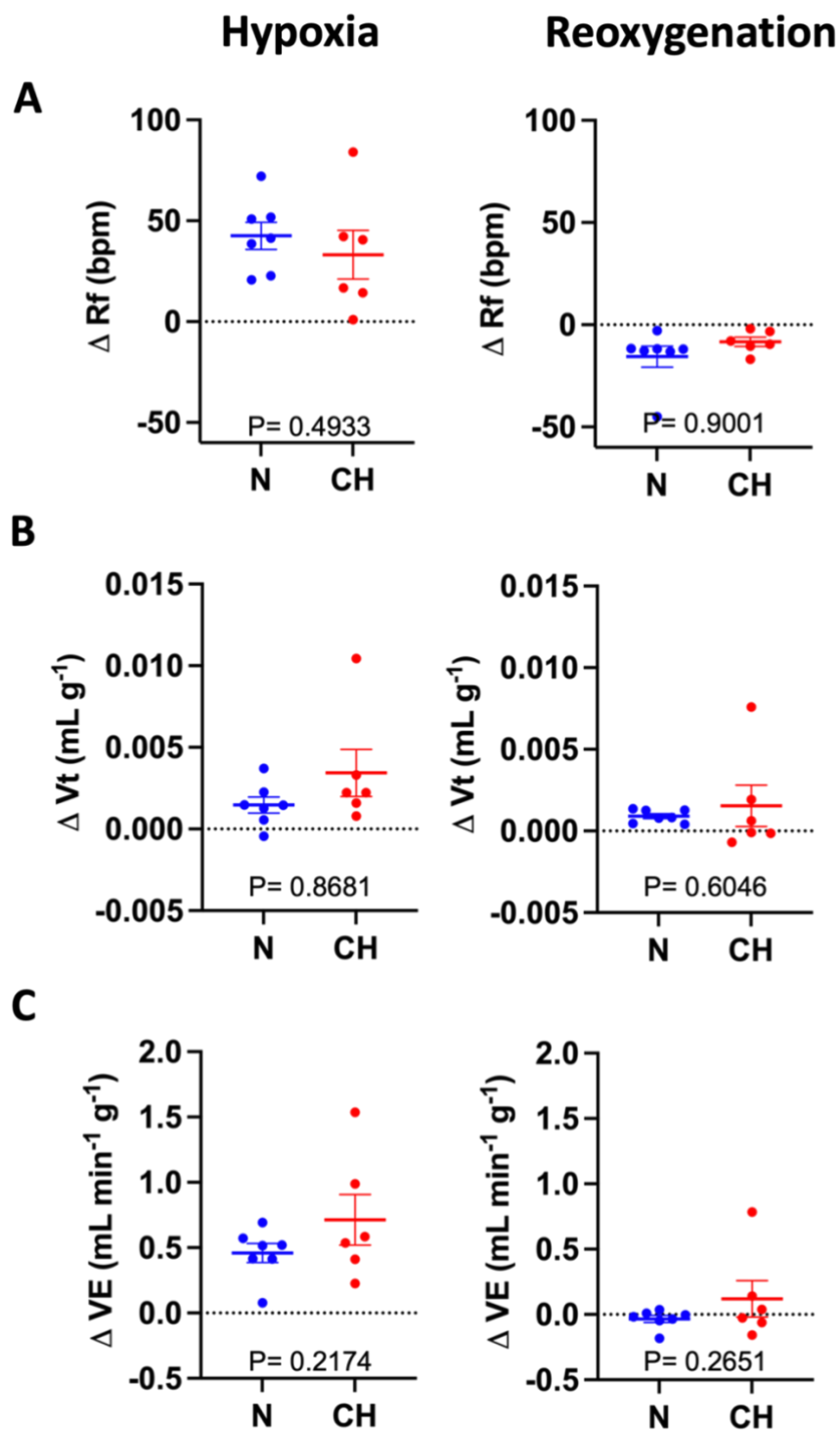
Figure 4.10 Measuring changes in respiratory frequency (Rf), tidal volume (Vt) and minute ventilation (VE) caused by hypoxia (Hx) and reoxygenation compared to baseline, in normoxic (N) and chronic hypoxic (CH) animals.

(A-C) The change in Rf, Vt and VE, respectively, during Hx (left) and upon reoxygenation (right) compared to baseline, measured in N (n=7) and CH (n=6) groups. Data presented as mean±SEM. Analysis performed using unpaired Student's t-test. Individual dots represented single animal data.

4.3.2 CH decreases inspiratory, expiratory, and total cycle times predominantly at baseline and during reoxygenation

After confirming that CH alters Rf and VE, compared to normal subjects, the breathing timings were analysed to establish a more detailed understanding of breathing alterations driven by CH. When measured across the whole experiment, the overall effect of CH was to significantly reduce the Ti ($p<0.0001$) (Figure 4.11 A). The impact of CH was also to significantly reduce Te ($p=0.0118$) (Figure 4.11 B). The Inspiratory to expiratory ratio (Ti/Te) was also analysed and there were no significant differences between the groups ($p=0.1202$) (Figure 4.11 C). The total cycle time (TCT) was significantly shorter in the CH group compared to N ($p<0.0001$) (Figure 4.11 D).

These respiratory timings were then analysed at specific time-points; at baseline (normoxia), during hypoxia and upon reoxygenation. During baseline ventilation, the Ti was significantly reduced in the CH group (173.1±6.57ms) compared to N group (238.1±13.30ms), $p=0.0016$ (Figure 4.12 A). This difference in Ti was not as evident but was still significantly lower in CH group during acute hypoxia (CH 144.8±2.83ms compared to N 171.9±8.65ms, $p=0.0180$) (Figure 4.12 A). After acute hypoxia, and during the reoxygenation period, the difference in Ti became more apparent between the two groups, CH 178.7±4.617ms compared to N 261.8±9.16ms, $p<0.0001$ (Figure 4.12 A). At baseline, the Te was significantly shorter in the CH group compared to N, (335.2±14.97ms vs 466.6±43.74ms respectively, $p=0.0224$) (Figure 4.12 B). However, during hypoxia this reduction was diminished, CH 268.3±11.95ms and N 304.4±32.47ms, $p=0.3495$ (Figure 4.12 B). In reoxygenation, the differences in Te between CH and N emerged again, 361.1±16.99ms and 548.0±54.82ms respectively, $p=0.0114$ (Figure 4.12 B). The shortening of both Ti and Te meant that the Ti/Te (I/E) ratio was not changed in CH compared to N, at baseline, during hypoxia or in reoxygenation (Figure 4.12 C). However, this did mean that there was a large reduction in the

TCT (baseline- CH 508.3±19.40 ms vs N 729.6±40.25 ms, p=0.0007; hypoxia- CH 413.1±12.13 ms compared to N 502.4±26.13 ms, p=0.0138; reoxygenation- CH 539.8±21.08 ms vs N 861.4±32.07 ms, p<0.0001) (Figure 4.12 D).

Changes in respiratory timings produced by hypoxia and reoxygenation compared to baseline were also calculated and compared between N and CH. The shortening of Ti caused by hypoxia was significantly smaller in CH vs N (p=0.0433) (Figure 4.13 A). Similarly, there was a trend for the abbreviation of Te caused by hypoxia to be less apparent in CH (p=0.0604) (Figure 4.13 B). Any variations in the I/E ratio produced by hypoxia and reoxygenation were consistent between N and CH (Figure 4.13 C). However, there was a striking attenuation of the shortening of TCT produced by hypoxia in the CH group (p=0.0273) and a much less obvious rebound prolongation of TCT upon reoxygenation in the CH group (p=0.0089) (Figure 4.13 D).
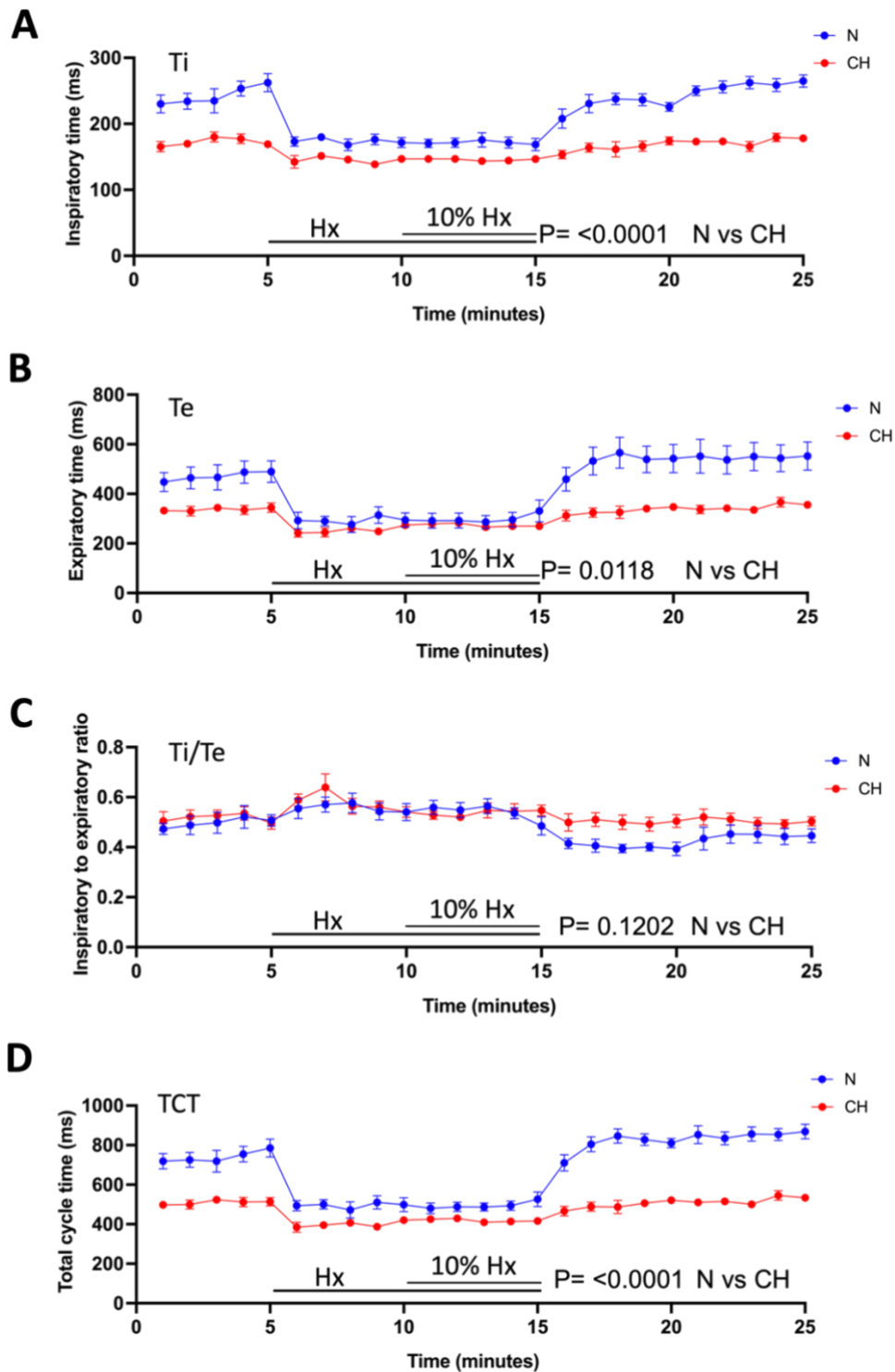
Figure 4.11 Chronic hypoxia (CH) modifies respiratory cycle timings.

Time courses demonstrating recordings of inspiratory time (Ti) (A), expiratory time (B), Ti/Te (C), and total cycle time (D) at baseline, in response to 10% O_2 (hypoxia, Hx) and upon reoxygenation, in normoxic (N; n=7) and CH (n=6) animal groups. Data presented as mean±SEM, statistical tests performed using using 2-way repeated measures ANOVA.
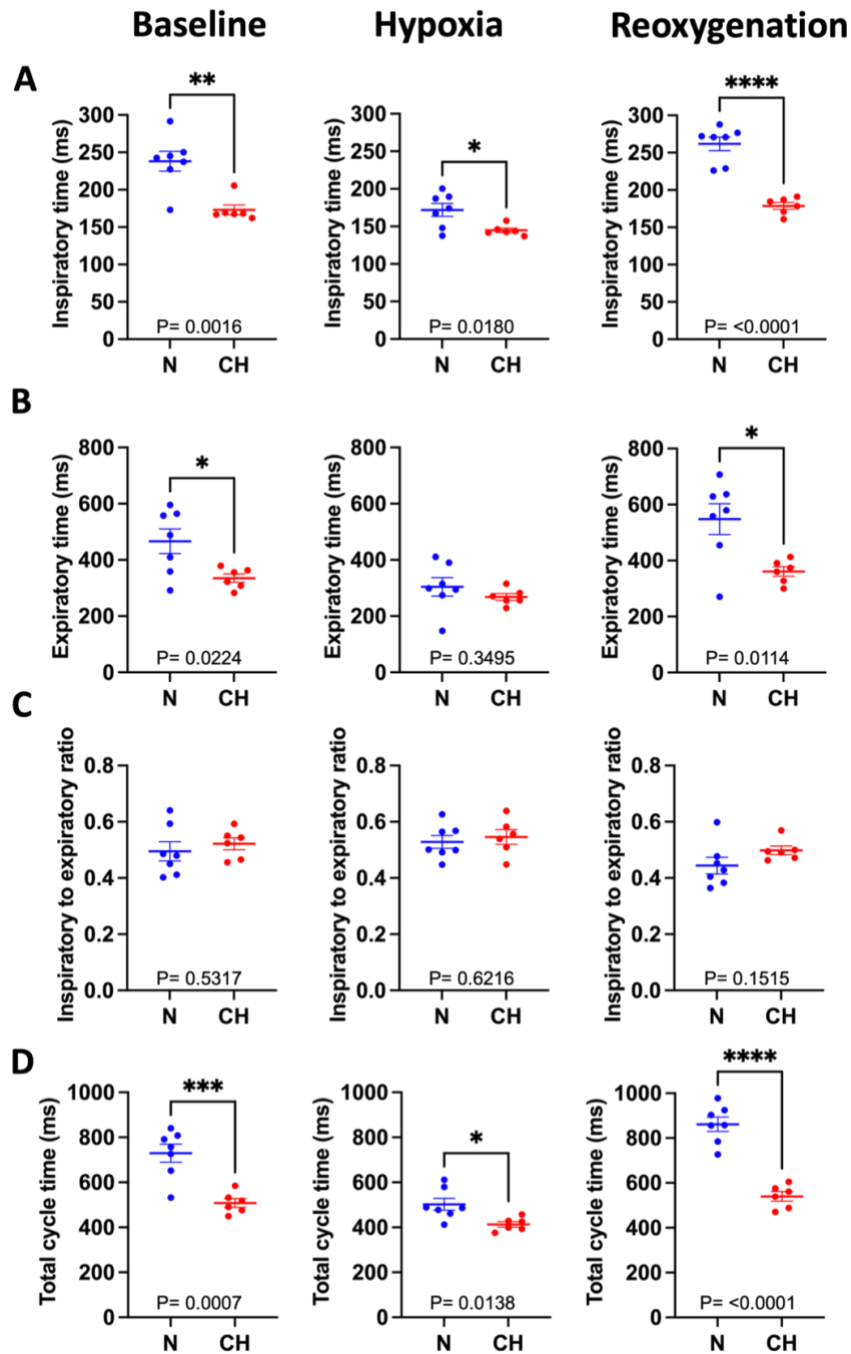
Figure 4.12 Chronic hypoxia (CH) shortens respiratory timings at baseline, during the response to acute hypoxia (Hx) and upon reoxygenation.

(A) Inspiratory time (Ti) recorded in normoxic (N, n=7) and CH (n=6) animal groups at baseline (left), during acute hypoxia (Hx) (middle) and upon reoxygenation (right). (B) Expiratory time (Te) measured at baseline (left), during acute hypoxia (Hx) (middle) and in reoxygenation (right) for N and CH. (C) Ti/Te (I/E) ratio calculated at baseline (left), during acute hypoxia (Hx) (middle) and in reoxygenation (right) for N and CH. (D) Total cycle time measured at baseline (left), during acute hypoxia (Hx) (middle) and in reoxygenation (right) for N and CH. Data presented as mean±SEM. Analysis performed using unpaired Student's t-test. Individual dots represented single animal data.
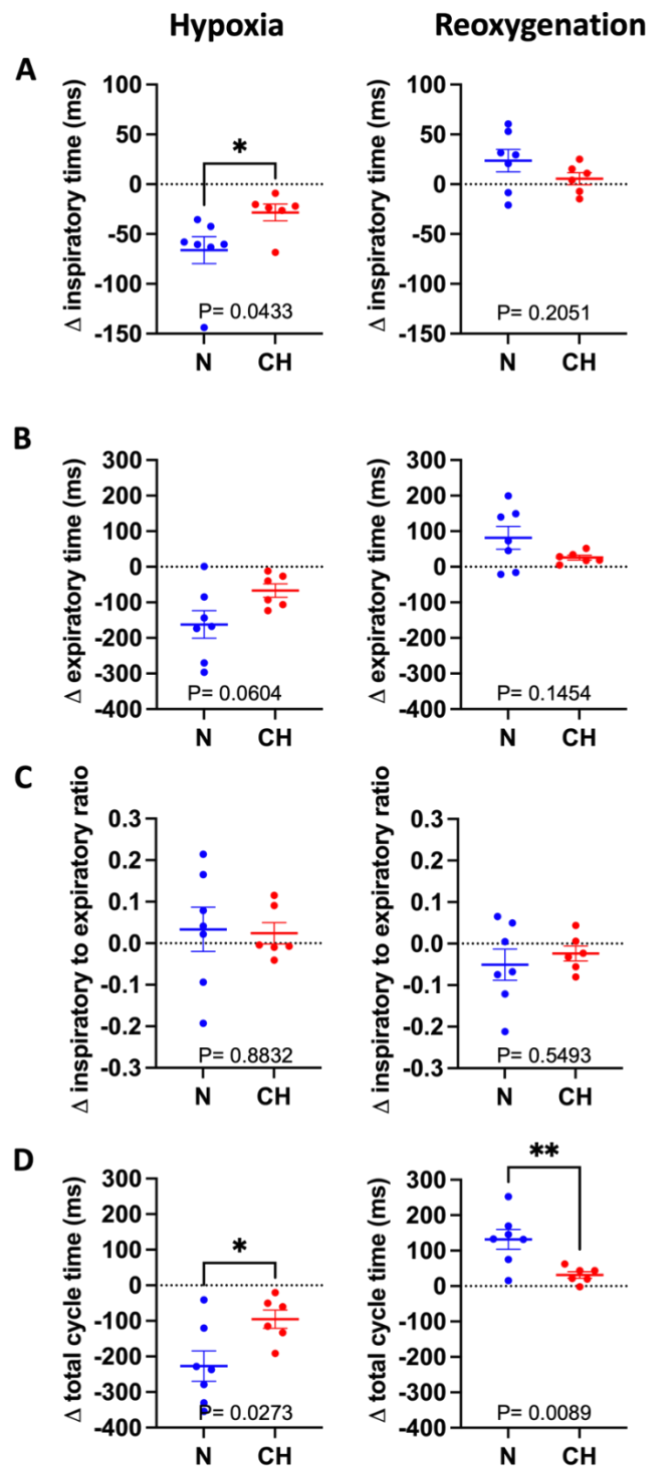
Figure 4.13 Changes in inspiratory times (Ti), expiratory times (Te), inspiratory to expiratory (I/E) ratios and total cycle times (TCT) produced by hypoxia (Hx) and reoxygenation compared to baseline, in normoxic (N) and chronic hypoxic (CH) animals.

The change in Ti, Te, I/E and TCT, respectively, during Hx (left) and upon reoxygenation (right) compared to baseline, measured in N (n=7) and CH (n=6) groups. Data presented as mean±SEM. Analysis performed using unpaired Student's t-test. Individual dots represented single animal data.

4.3.3 CH significantly augments VT/Ti and VT/Te suggestive of an elevation in inspiratory and expiratory drives

The inspiratory and expiratory drives indicate the intensity or strength of the neural signals that stimulate the muscles responsible for inspiration and active expiration respectively. An indirect measure of inspiratory and expiratory drive is the VT/Ti and VT/Te slopes respectively. This could help (particularly the VT/Ti) in determining the extent of CB hyperactivity caused by CH. When analysed across the whole time course the VT/Ti was significantly increased in the CH group (p=0.0346) (Figure 4.14 A).

Comparison at specific time points showed that VT/Ti is elevated at baseline in CH animals, where the VT/Ti in N group was $2.878e\text{-}005 \pm 3.898e\text{-}006$ mL g^{-1} ms^{-1}, and VT/Ti in CH group was $3.627e\text{-}005 \pm 2.579e\text{-}006$ mL g^{-1} ms^{-1}, however, this difference was not statistically significant (Student's t-test, p=0.1508). Similarly, VT/Ti is elevated in acute hypoxia in CH animals, the VT/Ti for the N group was $4.793e\text{-}005 \pm 5.099e\text{-}006$ mL g^{-1} ms^{-1} and $6.751e\text{-}005 \pm 7.909e\text{-}006$ mL g^{-1} ms^{-1} for the CH group, however, this increase was not statistically significant (Student's t-test, p=0.0554) and was significantly increased upon reoxygenation, where it was $2.921e\text{-}005 \pm 3.542e\text{-}006$ mL g^{-1} ms^{-1} for the N group and $4.368e\text{-}005 \pm 5.023e\text{-}006$ mL g^{-1} ms^{-1} for the CH group, (Student's t-test, p=0.0347), Figure 4.15 A. The change in VT/Ti caused by hypoxia and reoxygenation from baseline was consistent between N and CH (Figure 4.15 B).

Across the whole experiment, the overall effect of CH was to increase VT/Te compared to N (2-way repeated measures ANOVA, p=0.0076) (Figure 4.14 B). At all experiment stages, baseline ventilation, acute hypoxia and reoxygenation, the CH group had significantly higher VT/Te, compared to the N group. At baseline, the N group has a VT/Te of $1.380e\text{-}005 \pm 1.604e\text{-}006$ mL g^{-1} ms^{-1} and the CH group had a VT/Te of $1.880e\text{-}005 \pm 1.340e\text{-}006$ mL g^{-1} ms^{-1}, (Student's t-test, p=0.0389) (Figure 4.16 A). During acute hypoxia, the

N group had a VT/Te of $2.537\text{e-}005 \pm 2.819\text{e-}006$ mL g^{-1} ms^{-1} whereas the CH group had a Vt/Te of $3.616\text{e-}005 \pm 3.344\text{e-}006$ mL g^{-1} ms^{-1}, (Student's t-test, p=0.0303) (Figure 4.16 A). Upon reoxygenation, the N group had a Vt/Te of $1.274\text{e-}005 \pm 1.381\text{e-}006$ mL g^{-1} ms^{-1}, while the CH group had a Vt/Te of $2.165\text{e-}005 \pm 2.441\text{e-}006$ mL g^{-1} ms^{-1}, (Student's t-test, p=0.0071) (Figure 4.16 A). However, the change in VT/Te caused by acute hypoxia- $N=1.157\text{e-}005 \pm 2.497\text{e-}006$ mL g^{-1} ms^{-1} and $CH=1.735\text{e-}005 \pm 4.478\text{e-}006$ mL g^{-1} ms^{-1}, and reoxygenation- $N=-1.055\text{e-}006 \pm 7.465\text{e-}007$ mL g^{-1} ms^{-1} and $CH=2.852\text{e-}006 \pm 3.409\text{e-}006$ mL g^{-1} ms^{-1}, (compared to baseline) was similar for N and CH (p=0.2655 and p=0.2526, respectively) (Figure 4.16 B). This data suggests that inspiratory and expiratory drive are elevated by CH but this is not exaggerated by acute hypoxia.
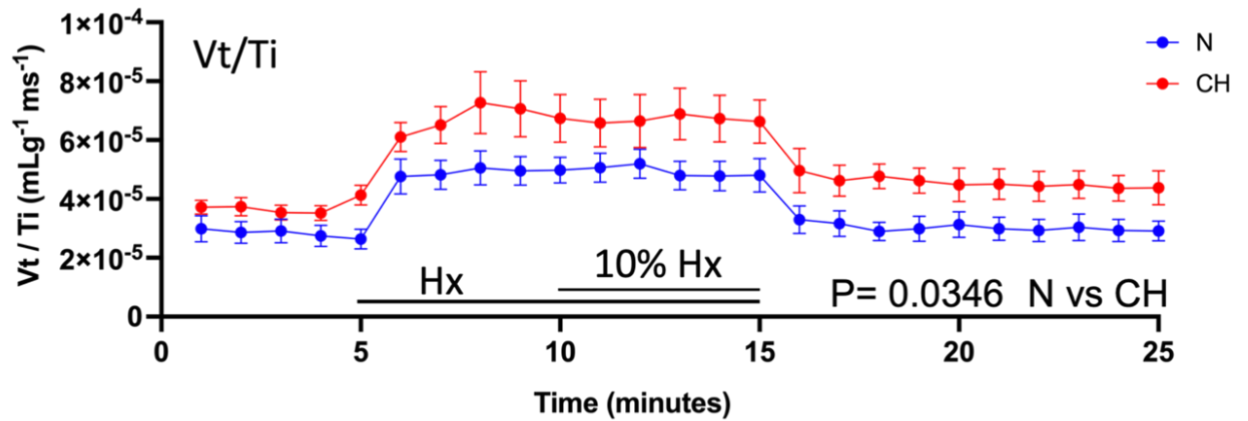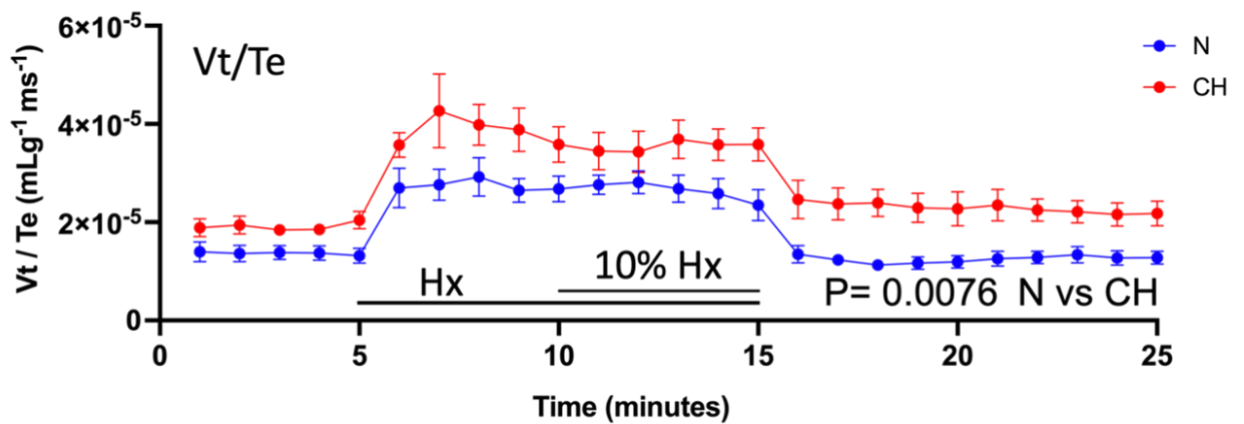
Figure 4.14 Chronic hypoxia (CH) augments inspiratory and expiratory drives

Time courses demonstrating minute to minute measurements of tidal volume/inspiratory time (Vt/Ti) (A) and tidal volume/expiratory time (Vt/Te) (B), at baseline, in response to 10% O_2 (hypoxia, Hx) and upon reoxygenation, in normoxic (N; n=7) and CH (n=6) animal groups. Data presented as mean±SEM, statistical tests performed using 2-way repeated measures ANOVA.
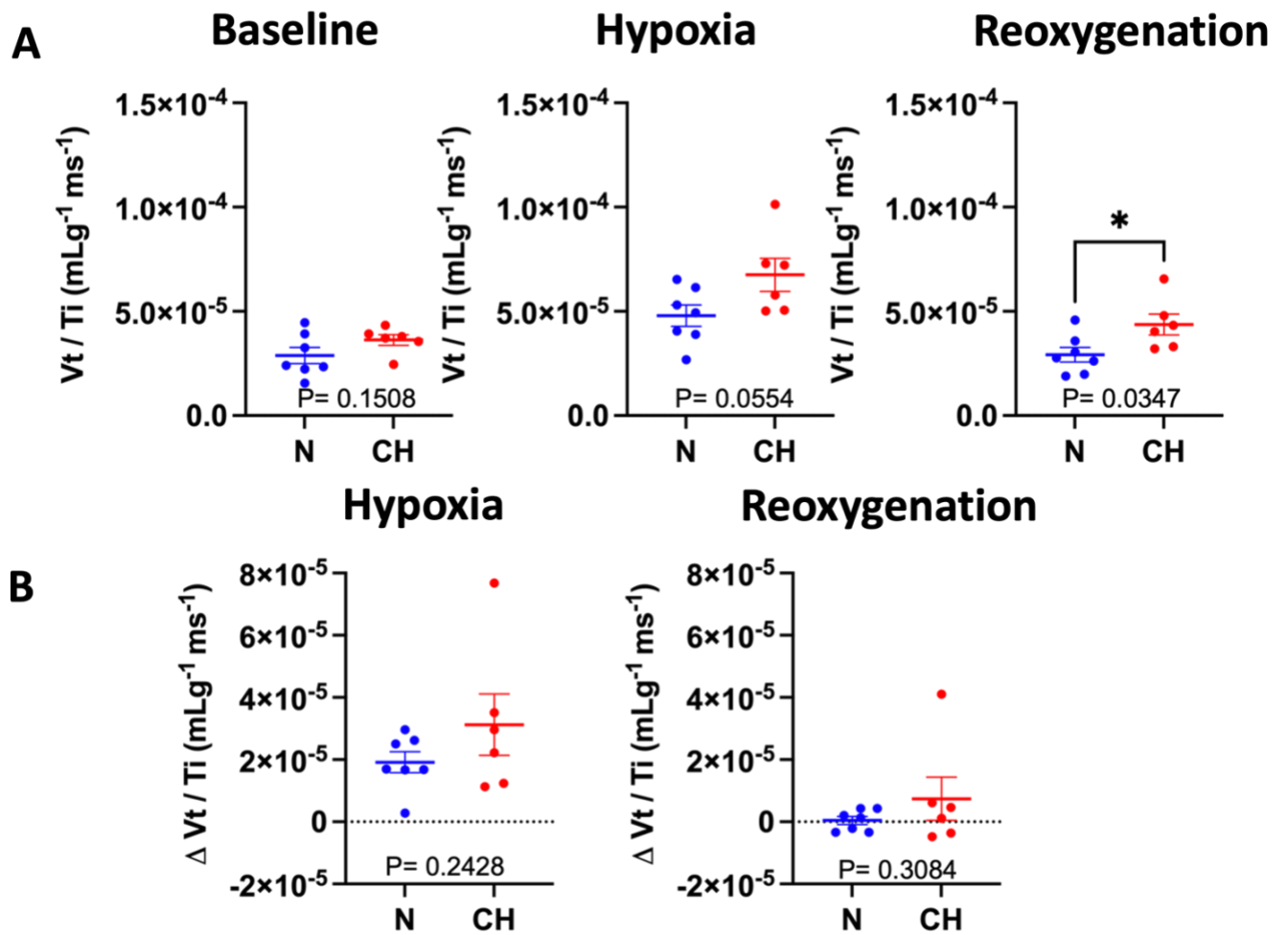
Figure 4.15 Rises in inspiratory drive caused by chronic hypoxia (CH) are not exaggerated during acute hypoxia but are more evident upon reoxygenation.

(A) Grouped recordings of tidal volume/inspiratory time (Vt/Ti) (inspiratory drive) measured at baseline (left), in hypoxia (middle) and in reoxygenation (right) for normoxic (N, n=7) and CH (n=6) animals. (B) Alteration in Vt/Ti induced by hypoxia (left) and reoxygenation (right) vs baseline for normoxic (N, n=7) and CH (n=6) animals. Data presented as mean±SEM. Analysis performed using unpaired Student's t-test. Individual dots represented single animal data.
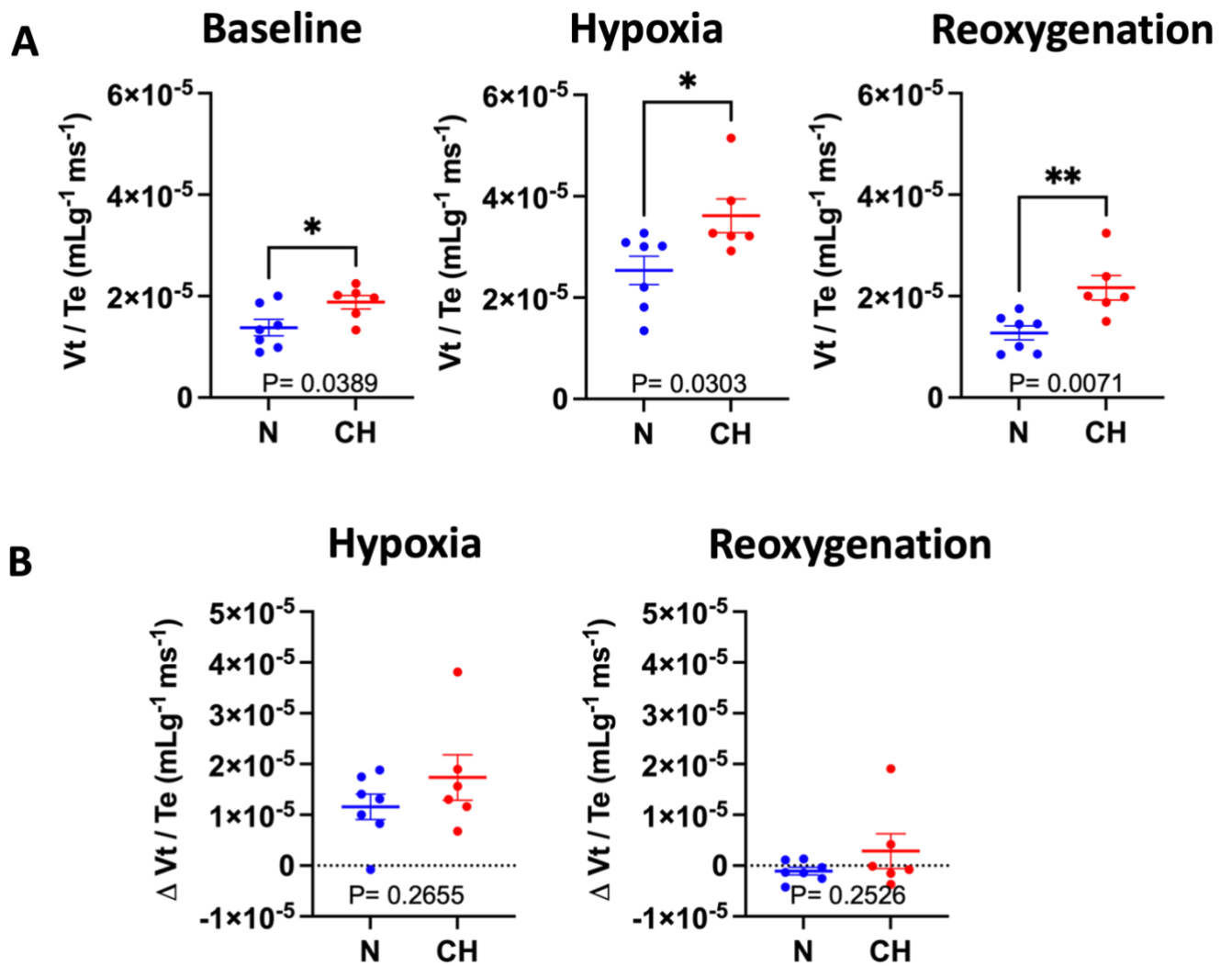
Figure 4.16 The elevation in expiratory drive caused by chronic hypoxia (CH) is not exaggerated during acute hypoxia or upon reoxygenation.

(A) Grouped data of tidal volume/expiratory time (Vt/Te) (expiratory drive) recorded at baseline (left), in hypoxia (middle) and during reoxygenation (right) for normoxic (N, n=7) and CH (n=6) animals. (B) Alteration in Vt/Te induced by hypoxia (left) and reoxygenation (right) vs baseline for normoxic (N, n=7) and CH (n=6) animals. Data presented as mean±SEM. Analysis performed using unpaired Student's t-test. Individual dots represented single animal data.

### 4.3.4. Breath to breath interval variability is significantly lower in CH animals.

The next aim was to investigate if the breathing variability was altered in CH animals. This was done by looking at the variability of the B-B intervals and Vt across the entire experiment in the 3 different conditions, normoxia (baseline), acute hypoxia and reoxygenation. Consistent with Rf and TCT data the mean B-B interval was consistently shorter in CH animals Figure 4.17 A.

Furthermore, the CH group seemed to have a more regular breathing pattern as indicated by the, B-B interval standard deviation being significantly decreased in the CH group (p<0.0001) (Figure 4.17 B). During baseline breathing the CH group had a B-B interval SD of 0.06764±0.003 ms, while N group had an SD of 0.1163±0.011 ms (Figure 4.17 B). In acute hypoxia the B-B interval SD for CH was 0.04674±0.003 ms, and for N 0.05099±0.006 ms (Figure 4.17 B). Reoxygenation's B-B interval SD for CH was 0.05527±0.008 ms vs 0.1156±0.014 for N (Figure 4.17 B). Thus, the SD BBI was significantly lower in CH animals at baseline (normoxia) and upon reoxygenation but not during acute hypoxia (Figure 4.17B). When normalised to the mean BBI, (SD/mean BBI ratio), differences between N and CH were not significantly different although still tended to be lower in the CH group (p= 0.1533) (Figure 4.17 C). This is possibly indicative that the main driver of the more regular breathing pattern in CH is the overall elevation in Rf.

Further analysis was performed looking at variability of Vt. Consistent with data presented earlier on the in Chapter, there was no overall difference in the Vt between N and CH (p=0.221) although there was a significant increase in Vt for both groups during acute hypoxia (Figure 4.18 A). Furthermore, the SD Vt was also consistent between groups when measured as absolute values (p=0.1328) (Figure 4.18 B) and when normalised to the mean Vt (SD/mean ratio) (p=0.2290) (Figure 4.18 C). Therefore these data suggest that whilst the breathing is more regular in CH animals, fluctuations in Vt are unaffected, being similar to N.
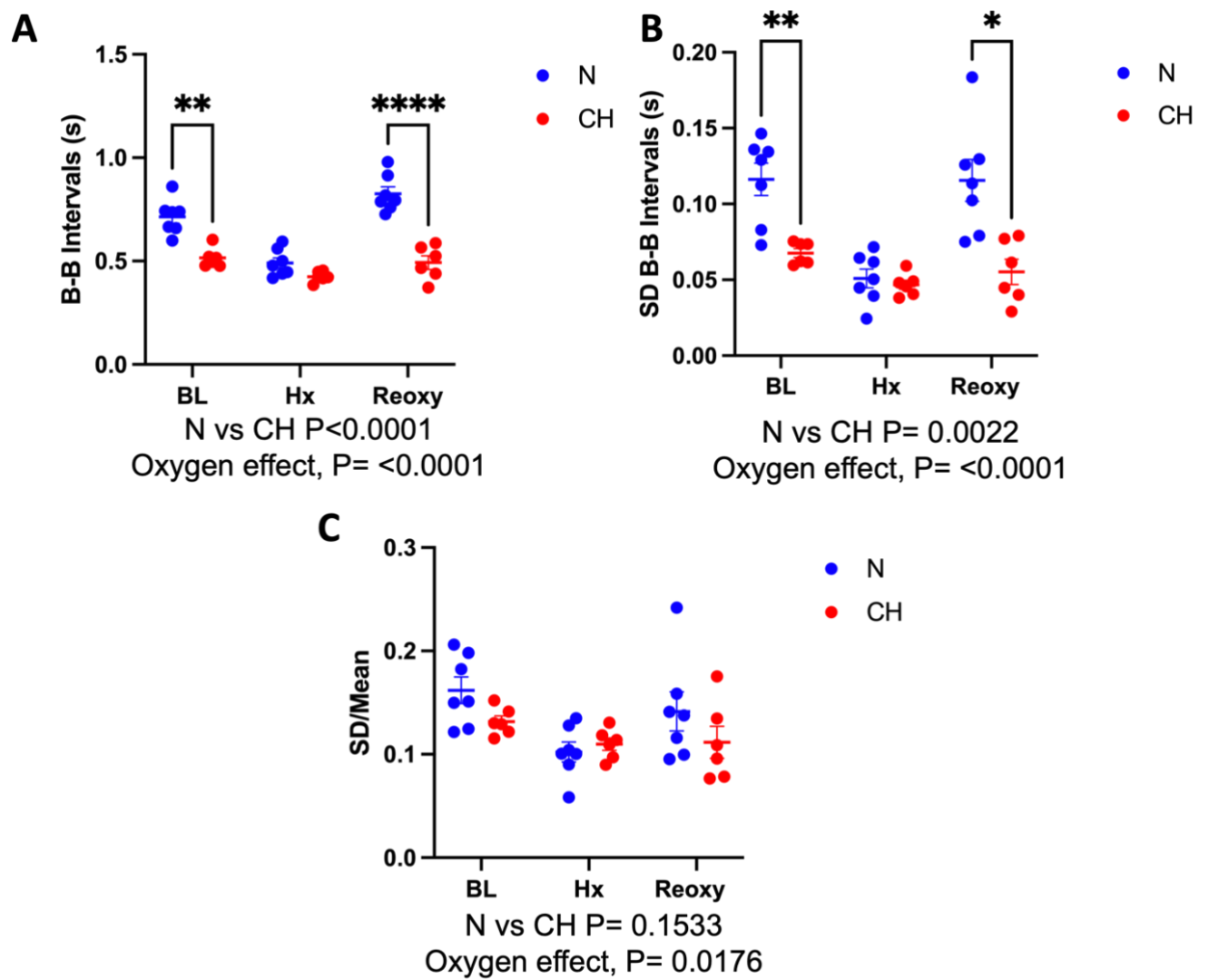
Figure 4.17 The breath to breath (B-B) interval is shorter and less variable in chronic hypoxic (CH) animals compared to normoxic (N) animals

A) Mean B-B intervals measured in CH (n=6) and N (n=7) animals at baseline (BL, normoxia, 21% F_iO_2), during acute hypoxia (Hx, 10% F_iO_2) and upon reoxygenation (Reoxy, 21% F_iO_2). B) SD of B-B intervals for N and CH measured at BL, Hx and Reoxy. C) SD/Mean B-B interval ratio for N and CH at BL, Hx and Reoxy. For A-C data presented as mean±SEM. Statistical tests performed using 2-way repeated measures ANOVA with Sidak's post-hoc analysis. *, ** and **** denote p<0.05, p<0.01 and p<0.0001 respectively. Individual dots represented single animal data.
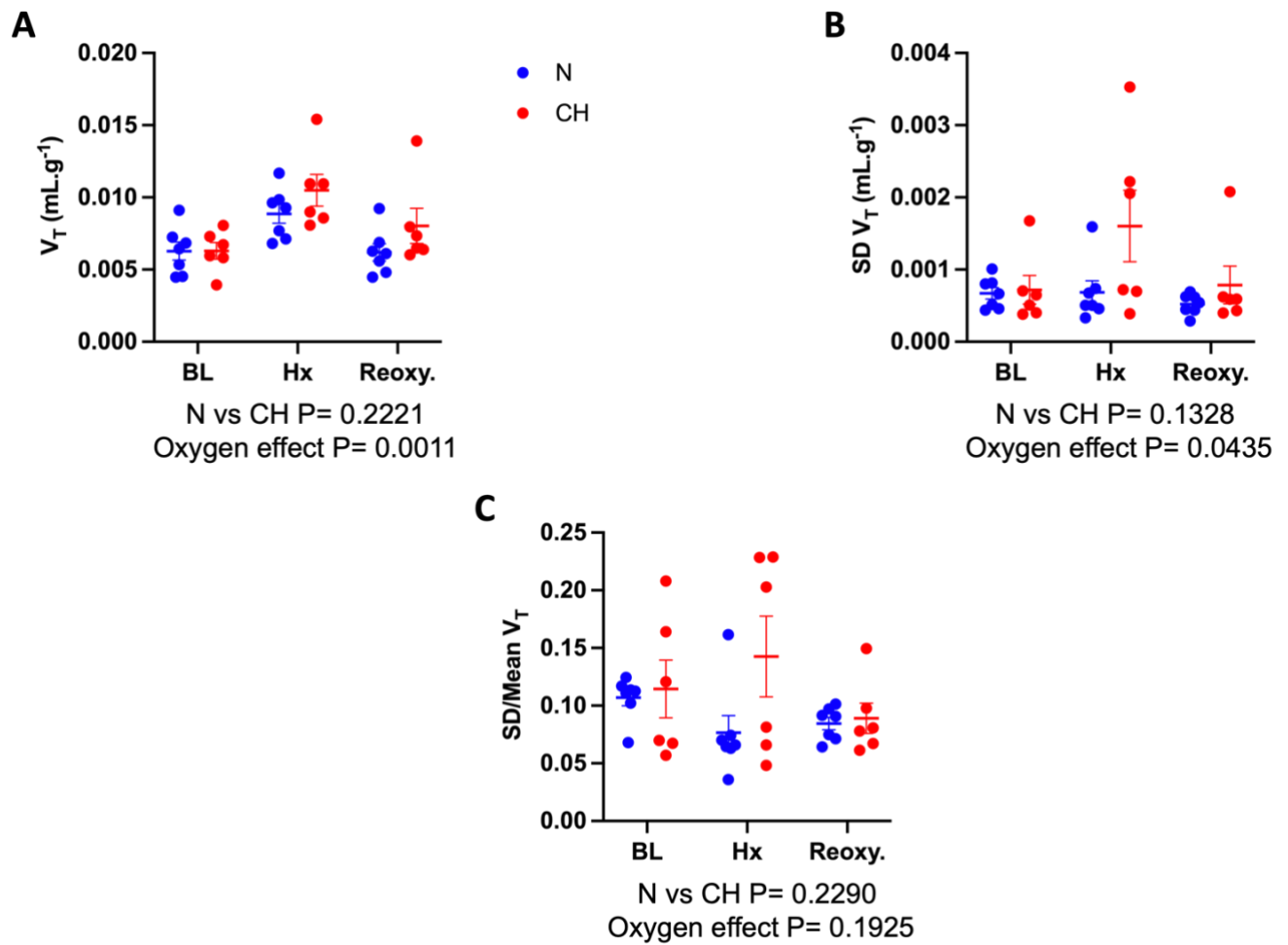
Figure 4.18 The tidal volume (Vt) size and variability is similar between normoxic (N) and chronically hypoxic (CH) animals.

A) Mean Vt measured in CH (n=6) and N (n=7) animals at baseline (BL, normoxia, 21% F_iO_2), during acute hypoxia (Hx, 10% F_iO_2) and upon reoxygenation (Reoxy, 21% F_iO_2). B) SD of Vt for N and CH measured at BL, Hx and Reoxy. C) SD/Mean Vt ratio for N and CH at BL, Hx and Reoxy. For A-C data presented as mean±SEM. Statistical tests performed using 2-way repeated measures ANOVA. Individual dots represented single animal data.

4.3.5 Assessing short and long term breath to breath variabilities in N and CH

One of the aims of this experiment is to identify breathing variability. Previously it was seen that 12% of CH induction for 10 days (CH group) resulted in an obvious overall decrease in SD of B-B interval. In this next section poincare plot analysis was performed by plotting each breath (n) (x axis) against its previous breath (n-1) (y axis). This analysis has been used previously to examine short and long term heart rate variability, but a similar method can be applied to examine breathing variability. This analytical technique provides a visible way to interpret the B-B interval variability. SD1 is used to represent short term variability and SD2 longer term variability. Every measured B-B interval is plotted for N and CH animals, in the 3 conditions (baseline/normoxia, hypoxia and reoxygenation) in Figure 4.19 A. The distribution of breaths during baseline ventilation appears to be much less variable in CH group, compared to N, figure 4.19 A (left). This pattern continues during acute hypoxia but the difference between N and CH is not as obvious, mainly due to a very large reduction in variability in the N group, Figure 4.19 A (middle). During reoxygenation, breathing variability returned to be much more pronounced in the N group, compared with CH group, which retains a degree of regularity, Figure 4.19 A (right). Quantitative analysis showed that SD1 is significantly decreased in CH group, compared to N group, (p=0.0056), and this is most evident at baseline (normoxia) and upon reoxygenation, Figure 4.19 B (left). However, SD2 was not significantly changed between the groups, although it did tend to be lower in the CH animals (p=0.0656), Figure 4.19 B (middle). The SD1/SD2 ratio was also not significantly altered between the groups but again did tend to be decreased in the CH group (p=0.0786), Figure 4.19 B (right). Thus, a key finding is that CH animals have a significant reduction in short term B-B interval variability.
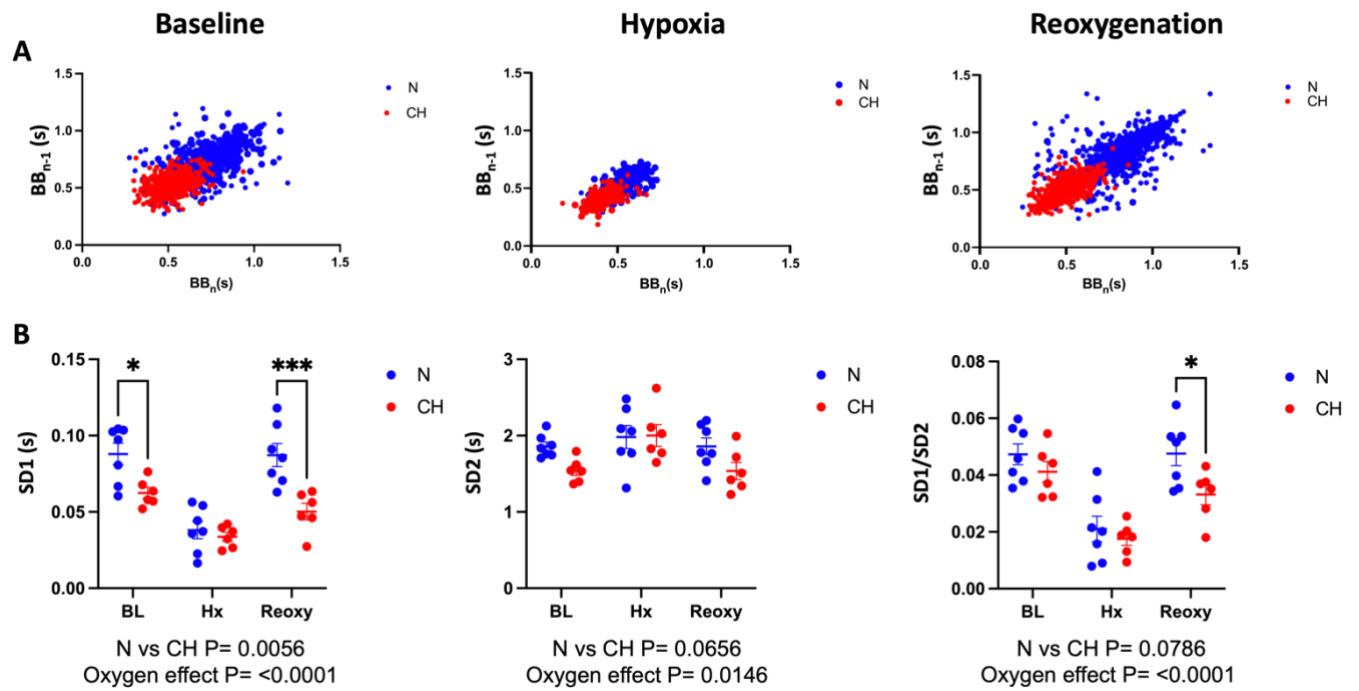
Figure 4.19 Chronic hypoxic (CH) animals have reduced short term breath to breath (B-B) interval variability.

A) Poincare plots for current (B-B) and previous (B-B$_{n-1}$) breath-to-breath intervals for N and CH animals measured during baseline (normoxia, BL, 21% F$_i$O$_2$), acute hypoxia (Hx, 10% F$_i$O$_2$) and upon reoxygenation (Reoxy, 21% F$_i$O$_2$). B) Grouped data for SD1 (left), SD2 (middle) and SD1/SD2 (right) during baseline, acute Hx and reoxygenation, for CH, n=6, compared to N, n=7. Data presented as mean±SEM. Statistical tests performed using 2-way repeated measures ANOVA with Sidak's post-hoc analysis. *, *** denote p<0.05, p<0.001 respectively.

4.3.6 Assessment of sigh number, amplitude and post sigh pause duration in N and CH animals.

To further understand the physiological changes induced by CH, the number of sighs were calculated. The N group, n=7, had a mean number of 3.286±0.64 sighs in the 5-minute baseline (normoxic) period, which significantly increased during the final 5 minutes hypoxia to 10.86±1.143, before decreasing back to 4.429±0.997 sighs, during the final 5 minutes of reoxygenation, Figure 4.20 A. On the other hand, the CH group, n=6, has a baseline sigh number of 2.833± 0.79, which was increased during acute hypoxia to 11.67±2.71, and went back during the reoxygenation period to 2.167±0.31, Figure 4.20 A. However, the overall effect of CH on the number of sighs was not significant (p=0.5165) (Figure 4.20 A).

Further sigh analysis was done to determine whether acute Hx would alter sigh amplitude and if this was different between N and CH. In N animals, sigh amplitude was not modified by the F_iO_2. The baseline sigh amplitude for N was 0.01777±0.002 mL g^{-1}, while in acute hypoxia it was 0.02083±0.002mL g^{-1}, and in reoxygenation 0.01886± 0.0023 mL g^{-1} (Figure 4.20 B). Similarly, the data showed that sigh amplitude was not changed in the CH group, in either hypoxia (0.02607±0.003 mL g^{-1}) or reoxygenation (0.02322±0.0026 mL g^{-1}) when compared to baseline (0.02159±0.0017 mL g^{-1}) (Figure 4.20 B). The overall effect of CH on sigh amplitude was not significantly altered but it did tend to produce a small elevation (p=0.0905) (Figure 4.20 B).

One of the noticeable physiological phases of ventilation is a pause following the sigh. For further understanding, the pause time was analysed. The N group had mean post-sigh pause times of 1.218±0.15 s, 0.8203±0.086 s and 1.149±0.21 s during baseline (normoxia), acute hypoxia and reoxygenation respectively (Figure 4.20 C). The CH group exhibits the same consistency measuring 0.8192±0.20 s, 0.6135±0.068 s, and 1.290±0.31 s in baseline (normoxia), acute hypoxia and reoxygenation respectively.

The overall effect of CH on pause time was calculated using 2-way repeated measures ANOVA, and demonstrated no significant difference between N and CH (p=0.2943) (Figure 4.20 C). The overall effect of O_2 was also not significant (p=0.0595) although for both groups there was a numerical increase between baseline (normoxia) and hypoxia, Figure 4.20 C. Collectively therefore CH does not seem to produce major effects on sigh number, amplitude or post-sigh ventilatory pause duration.
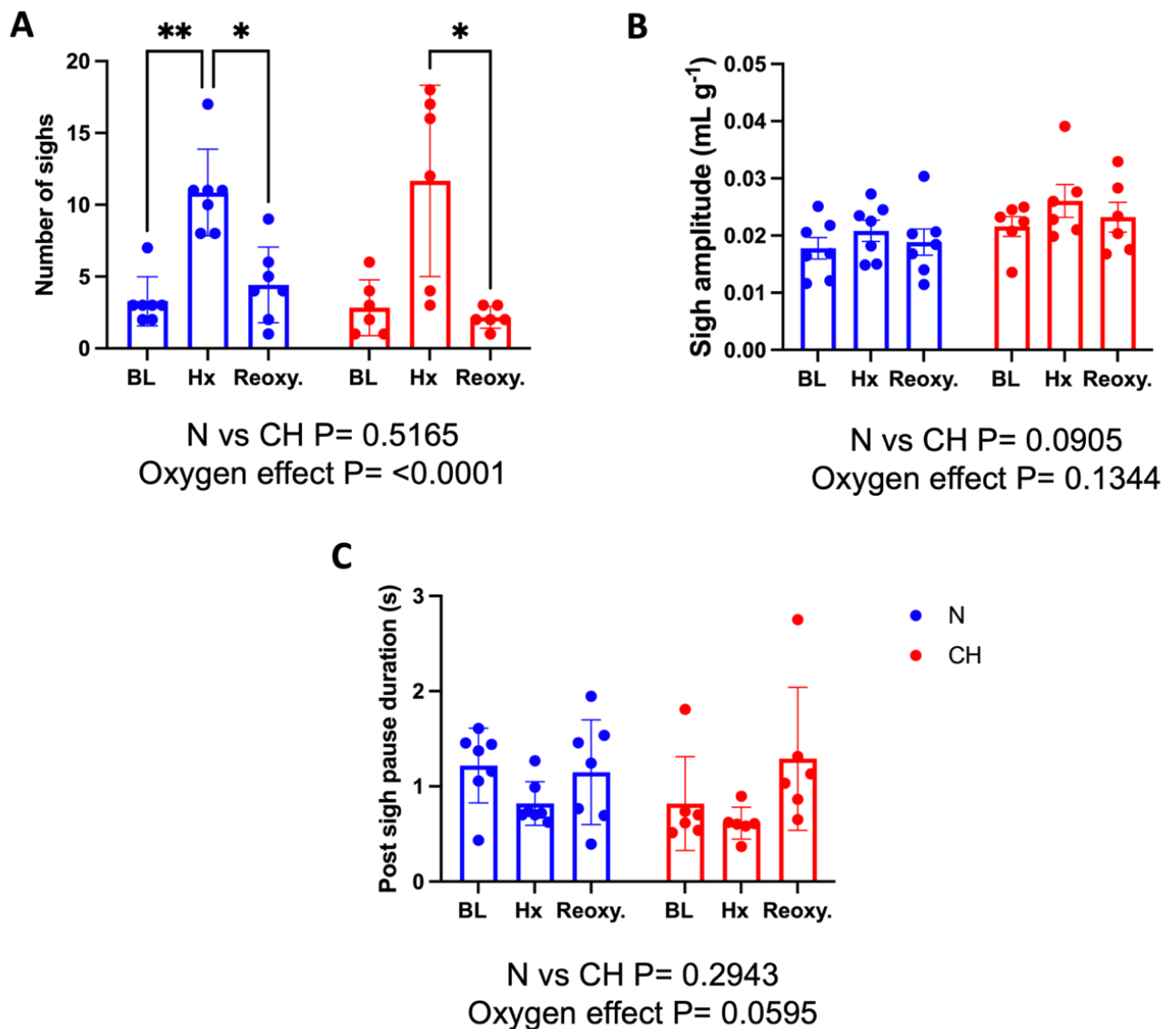
Figure 4.20 Sigh number are higher during acute hypoxia in both normoxic (N) and chronically hypoxic (CH) animals.

A) Mean number of sighs measured in CH (n=6) and N (n=7) animals at baseline (BL, normoxia, 21% F_iO_2), during acute hypoxia (Hx, 10% F_iO_2) and upon reoxygenation (Reoxy, 21% F_iO_2). B) Mean sigh amplitude for N and CH measured at BL, Hx and Reoxy. C) Mean post-sigh ventilatory pause duration for N and CH at BL, Hx and Reoxy. For A-C data presented as mean±SEM. Individual data points represent single animals. Statistical tests performed using 2-way repeated measures ANOVA with Sidak's post-hoc analysis. * and ** denote p<0.05 and p<0.01 respectively. Individual dots represent data from a single animal.

4.3.7 CH animals do not exhibit pre-sigh shortening of the B-B interval

Measurements of the 5 breaths immediately before and after a sigh where analysed and compared to mean control breaths. This was compared under the 3 different conditions (baseline/normoxia, hypoxia and reoxygenation) and between N and CH. At baseline there was a significant shortening of the B-B interval in the 5 breaths before a sigh in the N group (Figure 4.21 A). The 5 breaths after a sigh had an increase in B-B interval and were consistent with control (Figure 4.21 A). In N, this pre-sigh shortening of the B-B interval was absent during acute hypoxia (Figure 4.21 B) but returned upon reoxygenation (Figure 4.21 C). On the other hand, CH animals did not display any evidence of pre-sigh shortening of B-B interval at baseline (normoxia), during hypoxia or upon reoxygenation (Figure 4.21 A-C).

After identifying the B-B interval shortening immediately before a sigh in N group, and how CH eliminates this, it was critical to identify whether Vt was also altered 5 breaths immediately before or after a sigh. Based on the data obtained at baseline (normoxia) it appears that overall Vt is affected by the presence of a sigh (p=0.0158), driven by a general increase in pre and post sigh Vt (Figure 4.22 A). There is also a general effect of a sigh on Vt during hypoxia but in this case both pre- and post-sigh Vt are slightly decreased compared with the control (Figure 4.22 B). Upon reoxygenation, Vt does not appear to be impacted on by a sigh (p=0.0842) (Figure 4.22 C). Under all conditions, there was no significant difference between the N and CH groups suggesting that small alterations in pre- and post sigh Vt are consistent in N and CH (Figure 4.22 A-C).
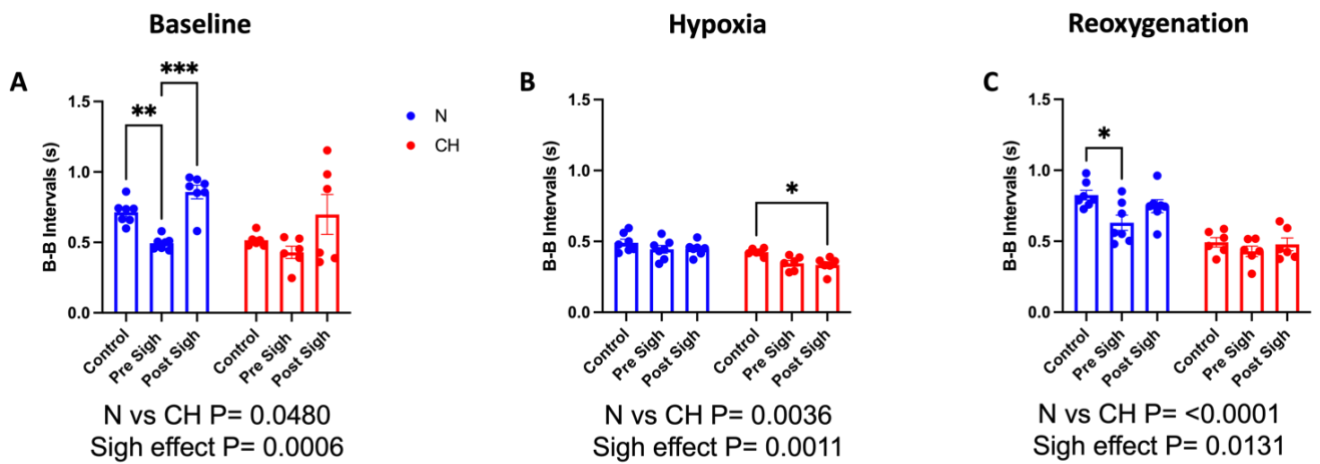
Figure 4.21 Breath to breath (B-B) interval shortening immediately before a sigh in normoxic (N) animals is absent in chronically hypoxic (CH) animals.

(A-C) Mean breath-breath (B-B) interval measured in periods of breathing without sighs (control), in the 5 breaths immediately before a sigh (Pre Sigh) and in the 5 breaths immediately after a sigh in CH (n=6) and N (n=7) animals, under baseline (normoxia, 21% F_iO_2) conditions (A), during acute hypoxia (10% F_iO_2) (B) and upon reoxygenation (21% F_iO_2) (C). Data presented as mean±SEM. Individual data points represent single animals. Statistical tests performed using 2-way repeated measures ANOVA with Sidak's post-hoc analysis. *, ** and *** denote $p<0.05$, $p<0.01$ and $p<0.001$ respectively.
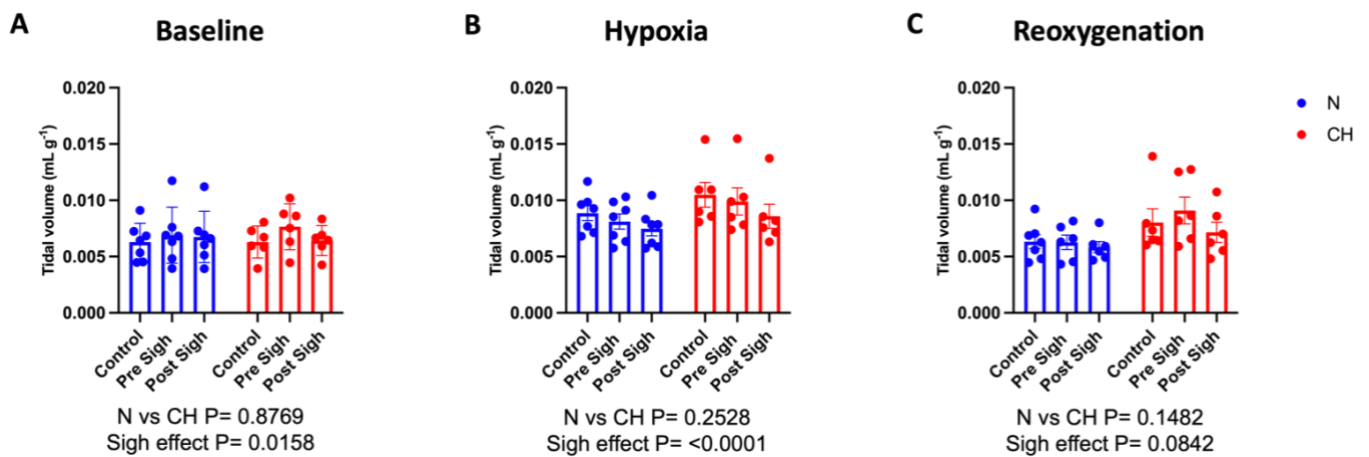
Figure 4.22 Comparison of tidal volume changes immediately before and after a sigh in normoxic (N) and chronically hypoxic (CH) animals.

(A-C) Mean tidal volume measured in periods of breathing without sighs (control), in the 5 breaths immediately before a sigh (Pre Sigh) and in 5 breaths immediately after a sigh (Post Sigh) in CH (n=6) and N (n=7) animals, under baseline (normoxia, 21% F_iO_2) conditions (A), during acute hypoxia (10% F_iO_2) (B) and upon reoxygenation (21% F_iO_2) (C). Data presented as mean±SEM. Individual data points represent single animals. Statistical tests performed using 2-way repeated measures ANOVA.

4.3.8 Assessing recovery kinetics of Vt immediately after a sigh, in N and CH animals

As an observational analysis, the recovery of Vt immediately following a large volume sigh was assessed. This was done by plotting Vt against Vt-1 in the breaths immediately before and after a sigh. This was done under all 3 conditions (baseline/normoxia, hypoxia and reoxygenation) for N and CH animals. Every single recovery of the Vt following a sigh for N and CH is presented in this way in Figure 4.23. Regardless of condition or animal group the majority of restoration of a normal Vt consistently takes place in the breath immediately following a sigh (Figure 4.23 A-F), suggestive of a rapid recovery of Vt following a sigh with only a very small persistent error signal.
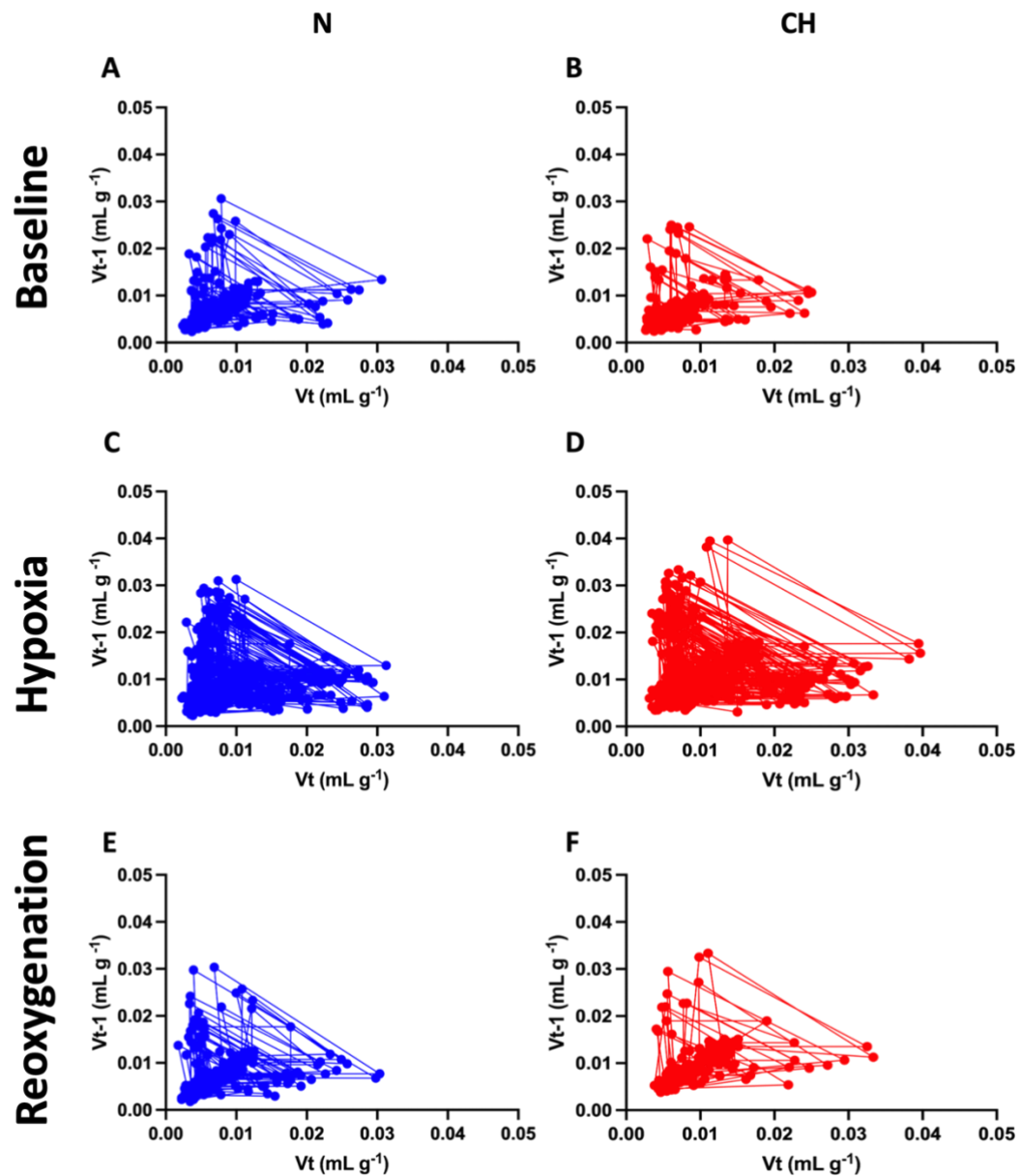
Figure 4.23 Assessing the recovery of tidal volume (Vt) immediately after a sigh in normoxic (N) and chronically hypoxic (CH) animals.

(A-F) Vt is plotted against Vt-1 for the breath immediately before the sigh, followed by the sigh itself and finally the 2-3 breaths immediately after the sigh, for N and CH at baseline (normoxia, 21% F_iO_2) (A & B), during acute hypoxia (10% F_iO_2) (C & D) and upon reoxygenation (21% F_iO_2) (E & F). Every Vt recovery from a sigh observed in every animal is presented.

4.4 Chapter synopsis and discussion

4.4.1 List of main finding

- CH significantly increases Rf during baseline (normoxia), acute hypoxia and reoxygenation, which drives an overall elevation in VE

- Ti and Te are significantly reduced in CH animals, which promotes a large decrease in TCT

- The overall effect of CH is to significantly elevate Vt/Ti and Vt/Te, suggestive of an increase in both inspiratory and expiratory drive.

- B-B interval variability was decreased in CH animals, suggestive of a more regular breathing pattern in the short-term

- The number of sighs noticeably increases during acute hypoxia for both N and CH animals

- Pre-sigh B-B interval shortening (a key feature in N animals), is absent in CH animals

- Vt recovery following a sigh is not gradual but predominantly occurs in the first breath immediately after a sigh, in both N and CH animals

4.4.2 CH produces changes in respiratory parameters and timings that are consistent with CB hyperactivity

One of the first goals of this Chapter was to validate that the CH method used was sufficient to induce ventilatory changes that are consistent with CB hyperactivity. The CH model was selected based on literature, which suggested that between one week (Bisgard, 2000) and three weeks (Mills and Nurse, 1993) of 12% O_2 was effective in producing alterations in the hypoxic ventilatory response (HVR). Therefore, a decision of exposing animals to 12% O_2 for 10 days was taken. This level of O_2 (12%) was also predicted to cause O_2 desaturation that is more in line with what is seen in the majority of COPD patients,

rather than a more excessive desaturation what would be seen if a more severe stimulus (e.g. 10%) had been applied, thereby increasing translational relevance.

After CH exposure, ventilatory measurements taken using WBP were used to assess the model. At baseline, during acute hypoxia and upon reoxygenation, CH animals had an elevation in VE, which was dependent on a rise in Rf. These initial findings, such as an increase in Rf and VE, were in line with results previously described in the literature (Thomas and Marshall, 1995, Bavis et al., 2020, Reeves et al., 2003). This more rapid breathing pattern is likely an adaptive response mediated by CB hyperactivity that allows for greater VE and thus improved O_2 availability to tissues.

Alterations in breathing cycle time play a critical role in adapting to the challenges induced by decreased O_2 availability (Brinkman et al., 2023). The observed decrease in Ti, Te, and TCT in CH rats is likely an adaptive response linked to the body's attempt to enhance O_2 uptake and minimize CO_2 retention. The decrease in Ti and Te results in more breaths per minute and is therefore responsible for the elevation in Rf. As Vt was not modified by CH the decrease in Ti and Te also produced an increase in both Vt/Ti and Vt/Te. This is suggestive of a rise in inspiratory and expiratory drive.

CH triggers neural adaptations in the medullary respiratory centres (Powell, 2007). The increase in sensitivity of the CB leads to an augmented sensory input into the NTS (Dwinell and Powell, 1999, Powell, 2007, Guyenet et al., 2010, Nattie and Li, 2012). The brainstem's inspiratory motor output is augmented as it integrates these heightened chemoreceptor signals (Ikeda et al., 2017). This produces an increase in the frequency (but in this case not strength) of diaphragmatic contractions (McMorrow et al., 2011, Mirabile et al., 2023).

Interestingly, it has been suggested that as CH persists, the CB becomes more sensitive to hypoxia, which in turn exaggerates the hypoxic ventilatory response (HVR) (Dempsey and Forster, 1982, Prabhakar et al., 2022, Smith et al., 1986). Upon exposure to CH, the CB undergoes structural and functional adaptations (Prabhakar and Jacono, 2005). These include increased vascularization (Wang and Bisgard, 2002), augmented expression of HIF-1α (Tipoe and Fung, 2003), and alterations in neurotransmitter release (Pulgar-Sepulveda et al., 2018). These changes collectively justify the CBs major role in adaptive ventilatory changes after CH exposure.

However, the data described in this Chapter suggest that most of the adaptive ventilatory changes are present in normoxia and are mostly preserved (but not exaggerated) in acute hypoxia. This could be due to enhanced CB activity at baseline, and whilst this is retained in acute hypoxia, it is not further exaggerated i.e. the CB O_2 sensitivity isn't altered. Alternatively, it could be that a further amplification of the HVR in CH animals is not observed due to a greater respiratory alkalosis, despite augmented CB O_2 sensitivity and a greater rise in CB sensory activity into the NTS. Measurements of arterial blood gases and/or pH would have helped to clarify this but were not measured in these set of experiments due to the non-invasive nature of the technique. Importantly, it has been shown that to observe a sustained rise in the HVR in CH mice, addition of 3% CO_2 is required (presumably to prevent the respiratory alkalosis) (Bishop et al., 2013). It is possible that this is also needed for rats. In addition, there could be alterations in the *in vivo* tissue PO_2 within the CB between N and CH at an F_iO_2 of 10% due to adaptions such as a greater haematocrit (and therefore greater O_2 delivery) that is known to be present in CH rats. In the next Chapter direct measurements of CB sensory nerve activity will be measured to clarify if hypoxic sensitivity of the CB is indeed increased by this model of CH.

In parallel with the increased inspiratory drive, CH rats also demonstrated an increase in expiratory drive. This increase in expiratory efforts involves a combination of mechanisms. One of the key contributors is a shift to an active expiration, involving the recruitment of expiratory motor output from the brainstem medulla, leading to the engagement of expiratory muscles, which include the abdominal muscles (Barer et al., 1978). These muscles contract more forcefully during expiration, enhancing the removal of CO_2 (Barer et al., 1978). It is unlikely that the CB would be responsible for this more active expiration. More likely candidates would be those centres in the brainstem medulla, that show plastic changes during CH exposure. This would be an interesting future area to explore.

In normal rats, the normoxic respiratory frequency ranges from 70 to 110 bpm, with a normalized tidal volume of 0.004 to 0.007 mL g^{-1} (Thomas and Marshall, 1995, Alzahrani et al., 2021b). This results in a baseline VE of approximately 0.5 to 0.7 mL min^{-1} g^{-1}. The Ti typically ranges from 230 to 250 ms, while the Te ranges from 450 to 500 ms. In contrast, CH rats exhibit a respiratory frequency of 110 to 130 bpm, with a reduced tidal volume of 0.003 to 0.006 mL g^{-1} (Thomas and Marshall, 1995). Consequently, their baseline minute ventilation is slightly increased ranges from 0.7 to 0.75 mL min^{-1} g^{-1}. Their Ti decreases to between 170 to 180 ms, and their Te ranges from 330 to 340 ms (Thomas and Marshall, 1995). These differences highlight the physiological adaptations that occur in response to CH.

4.4.3 B-B interval analysis using Poincaré Plots: insights into breathing variability modifications in CH rats

There is some small scale clinical data suggesting that individuals with COPD may have an altered breathing pattern, including reduced inspiratory times, which may be a relevant manifestation of respiratory symptoms and the progression of the disease (Yentes et al., 2020). The Poincaré plot, is a powerful tool for

analysing physiological time series data, and whilst it has mostly been used to assess HRV, it can be used to monitor breathing variability (Fishman et al., 2012). It was used here to analyse the B-B intervals of successive breaths. The plot visually illustrates the extent of B-B interval variability, as well as allowing for quantification of specific parameters, providing insights into the rhythmicity and regularity of breathing.

Findings from this work demonstrate that CH rats have a more regular pattern of breathing. During normoxic breathing, in comparison to N animals, where B-B intervals are relatively more scattered, CH rats exhibit a greater clustering of B-B intervals around a central point in their Poincaré plots. This more clustered pattern suggests an increased regularity in respiration, indicating a more rhythmic inspiratory drive (Fishman et al., 2012). One interpretation is that this clustered pattern reflects another important adaptation to CH mediated by the CB. It is tempting to speculate that this rise in breathing regularity in CH is dependent on a more regular pattern of action potentials delivered from the CB into the NTS via the carotid sinus nerve. It is well known that the normoxic sensory output from the CB in healthy CBs is random. There is some suggestion that during hypoxia, as well as increasing in frequency this pattern becomes more regular (Coney et al., 2022). Here, in acute hypoxia, the B-B interval in N animals becomes more regular (similar to CH) and is more centred around a single point, possibly related to this change in CB patterning. A less variable and more rhythmic CB sensory pattern could be present in normoxia in CH animals thereby promoting greater synchronisation with inspiratory motor activity and a more regular breathing pattern. Comparison of CB spike patterning/variability between N and CH warrants further investigation. Functionally, the synchronization of breaths could facilitate O_2 uptake by limiting fluctuations in alveolar gases, optimizing gas exchange.

The Poincaré plot can be more helpful by providing different standard deviations: SD1 and SD2. SD1 reflects short-term variability, while SD2 represents is associated with long-term variability (Fishman et al., 2012). Data analysis shows that SD1 but not SD2 is significantly reduced in CH rats compared to N rats. This reduction suggests a decrease in short-term variability of the B-B interval. An interesting idea is that decreases in the B-B interval SD1 could act as a novel marker of CB hyperactivity. Clinically, Poincaré plots are used to analyse HRV (Mourot et al., 2004), where SD1 is often associated with changes in the parasympathetic nervous system activity (Navarro-Lomas et al., 2020). As well as affecting ventilation, a more regular CB activity could influence the autonomic nervous system and possibly contribute to changes in HRV associated with CH. Although the CB is known to trigger systemic increases in sympathetic nerve activity, as part of the body's adaptive response (Badoer, 2020), a direct link between the CB and cardiac sympathetic nerve activity is still to be defined.

4.4.4 Sigh analysis in N and CH animals

The phenomenon of sighing, characterized by the occurrence of larger than normal breaths, has been studied extensively across various species, including rodents (Ramirez, 2014). Sigh generation is a complex respiratory phenomenon, arising from complex interactions within the neural circuits of the brainstem (Ramirez, 2014). The process involves the coordination of various brainstem nuclei, including the preBötzinger complex (Ramirez, 2014). This neural interaction results in the periodic activation of inspiratory muscles, leading to an augmented breath (Ramirez, 2014).

In the context of acute hypoxia, it is known that the CB becomes involved in sigh generation (Yao et al., 2023). An increased firing rate of CB chemoreceptor neurons (Lindsey et al., 2018) is transmitted to the

brainstem's respiratory centres, including the preBötzinger complex and evokes sigh generation (Severs et al., 2022, Yao et al., 2023). Accordingly, both N and CH rats exhibited an increased frequency of sighs during acute hypoxic challenges as has been observed previously (Yao et al., 2023). Functionally, this response is believed to be a compensatory mechanism to counteract the decreased oxygen availability in the environment (Yao et al., 2023). As well as an elevation in CB activity, the neural circuits responsible for sigh generation in the brainstem could be sensitized by low O_2 levels, contributing to an increase in sigh occurrence and enhancing O_2 intake.

Sigh amplitude refers to the magnitude of the Vt that constitutes a sigh. The number and amplitude of sighs was not significantly different between N and CH. There was however a tendency for sigh amplitude being augmented in CH animals, possibly suggesting that that chronic exposure to low oxygen levels leads to small adaptations in the respiratory neural networks that govern sigh generation. It must be noted that relatively few animals were included in this study and increasing the sample size is likely to have uncovered a significant effect. Similarly in both N and CH, the sigh amplitude during acute hypoxia tended to increase, suggesting that hypoxia plays a role in determining sigh amplitude as well as sigh number.

Something that is hardly studied is the ability to predict sigh occurrence. Here, the analysis of the B-B interval and Vt immediately before a sigh, were evaluated. In N rats, the pre-sigh B-B interval during baseline (normoxic) ventilation and reoxygenation significantly reduced immediately before a sigh. Interestingly, this pre-sigh shortening of the B-B interval was not apparent in the CH group. As such it may be easier to predict the occurrence of a sigh in N rats. It could be that in N rats during normoxia, some degree of hypoxia and/or a burst of CB activation leads to a shortening of the B-B interval immediately before a sigh is generated. This is supported by the fact that in N animals there was no shortening of the

B-B interval before a sigh during acute hypoxia when the CB is continuously stimulated. In the CH group, since they are persistently experiencing the chronic stimulation of the CB in both normoxia and hypoxia, there was no shortening of the B-B interval immediately before a sigh in either condition.

On the other hand, similar patterns of Vt changes before and after a sigh were present in N and CH groups during baseline, acute hypoxia and reoxygenation. At baseline, there was a slight and general rise in Vt immediately before and after a sigh in both N and CH. In contrast, during acute hypoxia there was a small overall decrease in Vt immediately before and after a sigh in both N and CH. Furthermore, it appears that Vt recovery from a large volume sigh is not graded, but mostly occurs in the very first breath following a sigh. This suggests that Vt recovery from a sigh is tightly regulated and occurs with hardly any error signal, possibly indicative of a feed-forward or learnt response.

4.4.5 Conclusion

The findings of this Chapter delve into the complex respiratory adaptations induced by CH, shedding light on several key findings. The observed alterations in VE across various conditions; baseline, hypoxia, and reoxygenation, underline the significant impact of CH, primarily driven by an elevated Rf. This highlights the adaptability of the respiratory system in response to CH. The decrease in Ti, Te and TCT during baseline and reoxygenation in CH animals points towards a restructuring of the respiratory pattern as a potential compensatory mechanism. Moreover, the significant augmentation of VT/Ti and VT/Te in CH animals suggests an elevation in both inspiratory and expiratory drives. The consistent reduction in B-B interval variability in CH animals particularly in the short term, further emphasizes the increased stability in respiratory patterns in CH animals, potentially mediated by the CB. Additionally, the findings highlight a

distinctive response to acute hypoxia, with higher sigh numbers observed in both N and CH rats. The absence of B-B interval shortening before a sigh in CH animals implies unique regulatory mechanisms, but makes sigh prediction more difficult. Finally, it appears that Vt recovery following a sigh is not gradual but predominantly occurs in the first breath immediately after a sigh, in both N and CH animals.

Chapter 5. Evaluating Ang II and TRPC signalling in CBs of N and CH animals

5.1 Chapter introduction and overview

The complex regulation of blood pressure and cardiovascular homeostasis is a fundamental aspect of human physiology. Among the key players in this complex system is Ang II, a peptide hormone that exerts its effects through a multitude of mechanisms, one of which is to influence carotid sinus nerve activity (Allen, 1998b). This neuroendocrine interaction holds crucial importance in the regulation of blood pressure, chemoreceptor function, and the overall responsiveness of the cardiovascular system (Shanks and Ramchandra, 2021).

It has been suggested that even in control healthy animals, Ang II can modify carotid sinus nerve activity dose-dependently (Allen, 1998b). Allen (1998) showed that Ang II significantly increases the activity of the CB chemoreceptor afferents through the activation of AT_1R, suggesting a role for Ang II in enhancing the sensitivity of CB chemoreceptors, thereby influencing respiratory reflexes and blood pressure regulation, particularly in conditions where the renin-angiotensin system is active. In addition, the augmented carotid sinus nerve activity, could also contribute to the increased in sympathetic nerve activity and subsequently lead to vasoconstriction (Shanks and Ramchandra, 2021).

What is less clear is the kinetics of the CB response to Ang II. Like all GPCRs, AT_1R can internalise upon agonist binding potentially making responses transient and poorly sustained. A first aim of this Chapter is therefore to consider whether the CB response to Ang II is well maintained or transient. This will be tested at different concentrations. It will also be determined whether Ang II causes any longer-term alterations i.e. any rebound potentiation of carotid sinus nerve activity once the Ang II stimulus is removed.

Furthermore, it remains to be determined if the sensitivity of Ang II is dependent on the background level of O_2 (Ang II-hypoxia interaction) and/or CO_2 (Ang II-hypercapnia interaction).

Pathological conditions characterized with CH, such as COPD, can stimulate the release of renin and subsequently increase the systemic production of Ang II (Kaparianos and Argyropoulou, 2011). In these patients, there is a cascade of events that can cause elevated Ang II levels. As Ang II rises in CH, it may act to further intensify the CB signalling (Allen, 1998b). In Chapters 2 and 3 it was shown that cellular exposure to sustained hypoxia increases AT_1R expression and AT_1R supercluster formation. Thus, in CH and COPD patients, in addition to an elevation in circulating Ang II, there may be augmented AT_1R expression, leading to amplifications of microdomain Ang II signalling in the CB. In Chapter 4 a model of CH was validated suggestive of CB hyperactivity. In this Chapter a key aim is to see if CBs isolated from these CH animals exhibit exaggerated responses to Ang II. As well as monitoring the size of stimulation, the proportion of nerve fibres that demonstrate measurable responses to Ang II will be compared between N and CH. Furthermore, it will be determined whether Ang II has a greater effect on CB hypoxic sensitivity in CH CBs compared with N. This should provide information regarding whether targeting Ang II signalling in the CB of CH animals is likely to have a significant impact on sympathetic nerve activity, which could underpin changes in vasoconstriction and HR (Iturriaga et al., 2021).

Interestingly, in other tissues a clear link has been established between Ang II signalling and activation of TRPC channels (Hamdollah Zadeh et al., 2008, Liu et al., 2009, Takahashi et al., 2007). TRPC channels are a family of ion channels involved in a wide range of cellular processes, including Ca^{2+} signalling and the regulation of the resting membrane potential (Abramowitz et al., 2007). Many TRP channel subtypes are expressed in the CB, where they have been identified as key players in mediating responses within the CB

(Buniel et al., 2003b), including TRPC, which may act to regulate basal activity and O_2 sensitivity (Iturriaga et al., 2021, Kumar et al., 2006a). Furthermore, in other tissues it has been suggested that Ang II directly regulates the activity of TRPC channels (Ilatovskaya et al., 2014, Onohara et al., 2006). However, such an interaction has not been explored in the CB.

What is not known is whether CB responses to Ang II may be modified by inhibition of TRPC channels and if this is more apparent in CH animals. 2-Aminoethoxydiphenyl borate (2-APB) is well-known for its modulation of TRPC channels (Colton and Zhu, 2007), with its effects varying depending on the specific TRPC channel subtype and cell class (Chen et al., 2020b). In some cases, 2-APB acts as an agonist, activating TRPC channels and allowing Ca^{2+} ions to enter the cell (Colton and Zhu, 2007). In other situations, it can function as an antagonist, inhibiting TRPC channel activity, reducing calcium influx and lowering cellular excitability (Colton and Zhu, 2007). The exact mechanisms of 2-APB's effects on TRPC channels can be complex and may depend on factors such as TRPC channel subtype and the specific cellular environment (Colton and Zhu, 2007). 2-APB has been used previously to monitor its effects on CB nerve activity, and to provide insights into TRPC as a potential modulator of Ca^{2+} signalling in chemoreceptor cells (Kim et al., 2020). It is generally regarded as an inhibitory modulator of CB function (Sundin et al., 2007, Kim et al., 2015, Kumar et al., 2006b) . However, a link between Ang II and TRPC signalling is yet to be characterised in the CB or an upregulation of such a signalling pathway in CH. Therefore, final experiments were performed to see if 2-APB was able to reverse the effects of Ang II in modifying sensitivity to hypoxia and if this was more effective in CH CBs.

5.1.1 Chapter hypotheses

- CB responses to Ang II are dose dependent, well sustained, reversible and exaggerated in the presence of mild steady state hypoxia and/or hypercapnia

- A greater proportion of CB nerve fibres from CH animals respond to Ang II and responses are larger.

- Ang II has a greater effect on CB O_2 sensitivity in those isolated from CH animals.

- Blocking TRPC channels reverses the effects of Ang II and this is more apparent in CH CBs

5.1.2 Aims of this chapter

Measurements of single fibre carotid sinus nerve activity will be recorded to:

- Observe if the CB response to Ang II is dose dependent, well-sustained, rapidly reversible and modified by steady-state O_2 and/or CO_2

- Assess if CB Ang II sensitivity is enhanced after the exposure to CH.

- Determine if 2-APB modifies O_2 sensitivity in the presence of Ang II more in CBs isolated from CH than N.

5.2 Chapter methods

5.2.1. Animals

Similar to Chapter 4, all animal procedures were performed in accordance with UK Animals (Scientific Procedures) Act 1986 and approved by the UK Home Office (PPL number PP9019875) and by the Animal Welfare and Ethical Review Body (AWERB) at the University of Birmingham. A total of 45 rats were used in this chapter, of which 26 were N and 19 were CH. The N rats' mean wight was 292.5±4.701 g and the CH rats' average weight was 260.0±4.402 g. All animals were housed in individually ventilated cages, either in normoxic or hypoxic environments, 2-4 per animals per cage, with free access to food and water.

CH protocols were the same as those described in Chapter 4. Briefly, CH rats breathed an F_iO_2 of 12% for 10 days using a dynamic O_2 controller and dedicated small animal chamber (BioSpherix, Parish, NY, USA). Animal welfare checks, CO_2 and humidity levels, replacement of silica gel and soda lime, and food and water replenishment were performed daily.

5.2.2. Extracellular recordings of CB sensory activity

CB isolation and microdissection of the carotid sinus nerve were not performed by the author of this thesis, but by other members of the research team. The author performed the extracellular nerve recording experimental protocols, acquired data and performed all data analysis.

Rats were induced with 5% isoflurane in O_2, flow rate 1.5 L min^{-1} using an anesthesia induction chamber. The animal was then moved to the surgical table and anesthesia was maintained via face mask (2.5 to 5% in O_2, 1.5 L min^{-1}) throughout the surgery. To ensure adequate depth of surgical anesthesia, a toe pinch technique was performed to test for the absence of a withdraw reflex. An anatomically identified area in the neck was removed, to expose the common carotid artery and its branches. Two cuts were made, one on the common carotid artery, before it branches, and the other across the internal and external carotid arteries, above the glossopharyngeal nerve. This ensured that a block of tissue was isolated containing the common carotid artery, the internal carotid artery, the external carotid artery, the CB, carotid sinus nerve, the superior cervical ganglion, a branch of the vagus nerve and the glossopharyngeal nerve. After removing the tissue, it was immediately placed into an ice-cold bicarbonate buffered Krebs solution, equilibrated with 95% O_2, 5% CO_2, to preserve the tissue, described in Table 5.1. Animals were killed by cervical dislocation, confirmed by the termination of circulation.

Compound	Final Concentration (mM)
NaCl	119
NaHCO$_3$	25
KCl	4.5
MgSO$_4$.7H$_2$O	1.2
NaH$_2$PO$_4$	1.2
Glucose	11
CaCl$_2$	2.4

Table 5.1*: **Krebs solution components**
A table describing components of the Krebs solution used to preserve carotid body (CB) tissue after surgical removal and to perform extracellular recordings of carotid sinus nerve activity.

A randomly selected CB, either right or left, as there is no evidence of differences between them, was then placed under a dissection microscope and connective tissue along with most other structures were

removed to just leave the carotid bifurcation, CB, the carotid sinus nerve and glossopharyngeal nerve. Further connective tissue was removed from the carotid sinus nerve and it was then sectioned before entering into the glossopharyngeal nerve. To purify the electrical signals, the tissue was then incubated in a bicarbonate buffer enzyme Krebs solution containing: 0.075 mg/ml collagenase type II, 0.0025 mg/ml dispase type I (Sigma, St. Louis, Missouri, United States) in a heated water bath (37 °C) for 20-30 minutes, to remove connective tissue and increase the signal:noise ratio of electrical signals.

After incubation, the tissue was placed into a small volume recording chamber, approximately 0.1 mL, and continuously infused with a bicarbonate buffered extracellular Krebs solution, maintained at a temperature of 37 °C, equilibrated with 5% CO_2, pH 7.4 (Table 5.1) (Holmes et al., 2018b, Swiderska et al., 2021). The O_2 was continuously measured using a standard O_2 electrode (ISO2) and O2 meter (OXELP) (World Precision Instruments, Sarasota, FL, USA). High precision flow meters (Cole-Palmer, St Neots, UK) were used to adjust gas concentrations and to induce hypoxia or hypercapnia.

A glass suction electrode was used to record extracellular action potentials from the cut end of the carotid sinus nerve. Glass electrodes were pulled from borosilicate capillary glass using a microelectrode puller (Ealing, UK). The glass microelectrode contains a silver recording electrode attached to the head stage. Another silver reference electrode is placed in the same solution/recording chamber and the voltage difference between the recording and reference electrodes will be measured. The voltage is pre-amplified x100 (NeuroLog 104, Digitimer, UK) and then filtered (NeuroLog 125/126, Digitimer, UK). The signal is low pass filtered at 50,000 Hz and high pass filtered at 50 Hz. After filtering, the signal is amplified again (x50) (NeuroLog 106), which makes the total signal amplification (x5000). The signals were converted using an analogue to digital converter (micro-1401, Cambridge Electronic Design, Cambridge, UK). Signals were

acquired at 15,000 Hz on a PC using Spike2 v7-9 software (Cambridge Electronic Design, Cambridge, UK) (Figure 5.1).

Normally, the carotid sinus nerve (CSN) will always have some baseline/normoxic activity (0.25-1.5 Hz) (Holmes et al., 2014), which reflects the communication between the CB and the brain, and is important in mediating basal ventilation. In these nerve recording experiments, the baseline CB activity was measured and, in addition, the single fibre frequency responses were observed when stimulated by hypoxia and/or hypercapnia.
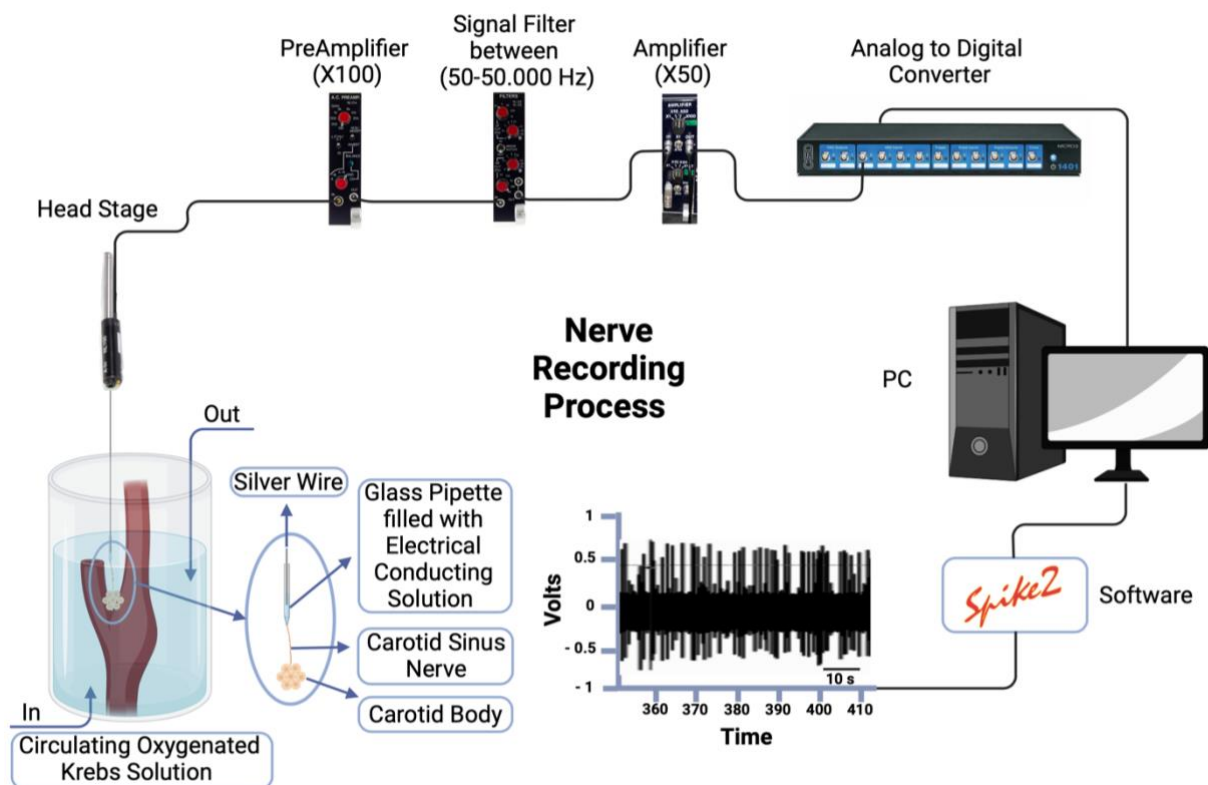
Figure 5.1 A schematic describing the signal acquisition process when performing extracellular carotid sinus nerve recordings.

This figure illustrates the experimental setup for carotid sinus nerve recordings. A glass microelectrode covers a silver recording electrode attached to a head stage. A silver reference electrode is placed in the same solution. The voltage difference between the recording and reference electrodes is measured. The voltage signal is first pre-amplified (x100), filtered, and then amplified again (x50) for a total amplification of x5000. The signal is digitised at 15,000 Hz using a CED micro 1401 and acquired on a PC using Spike2 software. The frequency of action potentials is used as a measure of carotid body function.

5.2.3 Experimental protocols:

In this Chapter, more than one protocol was used, based on the experimental aim. The first protocol aimed to measure the dose dependency of Ang II on the carotid sinus nerve activity. In this protocol, 4 concentrations of Ang II were used, 0.1, 1.0, 10 and 100 nM. Figure 5.2 illustrates how the experiment was conducted. For each concentration, the drug was prepared and added to the normoxic, normocapnic Krebs solution, 37°C, pH 7.4. Each concentration was applied for 5 minutes followed by 5 minutes of recovery/washout. To assess responses kinetics, measurements of nerve discharge frequency were taken for the first minute, the peak response and the last minute. The mean baseline (BL) discharge frequency before Ang II and following exposure to the 4 concentrations was also assessed to determine any long-term potentiation/preparation run-down. In the first protocol, 10 normal rats were used.
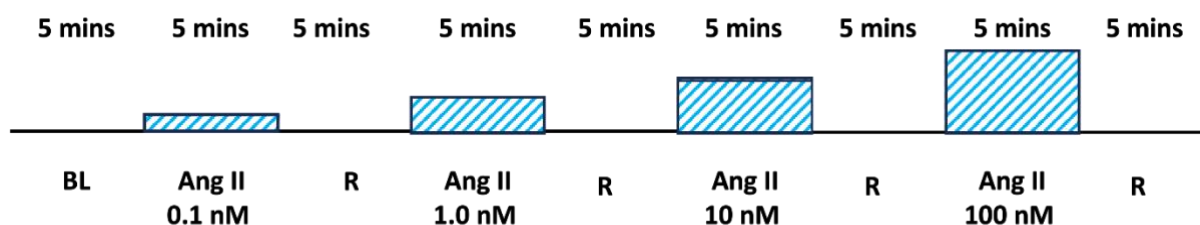
Figure 5.2 Protocol used to evaluate dose dependency of carotid body responses to angiotensin II (Ang II).

In this protocol, a steady-state 5-minute baseline (BL) discharge rate was initially established. After that, 0.1 nM of Ang II was added to the superfusate for 5 minutes and changes in carotid sinus nerve activity was recorded. The drug was then washed out for 5 minutes. Similar recordings were made in response to 5 minutes exposure to 1, 10 and 100 nM Ang II. After each dose, the drug was washed out. A final 5-minute recording was taken in control conditions to assess any long-term potentiation or preparation run-down.

The aim of the first protocol was to identify the optimal concentration to be used in the rest of the experiments in this Chapter, (which was shown to be 1-10 nM). The second protocol in this Chapter was to

measure the influence of mild, steady-state hypoxia on CB responses to 1 and 10 nM Ang II. For these experiments, PO_2 was adjusted to 100 mmHg (mild hypoxia), achieving an approximate rise in baseline nerve activity between 0 and 10 Hz. This high level of variability likely reflects the depth of the type I cell cluster and afferent nerve within the CB, which is being superfused. The change in discharge frequency caused by addition of Ang II was then correlated against the discharge frequency observed in mild hypoxic. This protocol is summarised in Figure 5.3. In this second protocol, 8 normal rats were used.
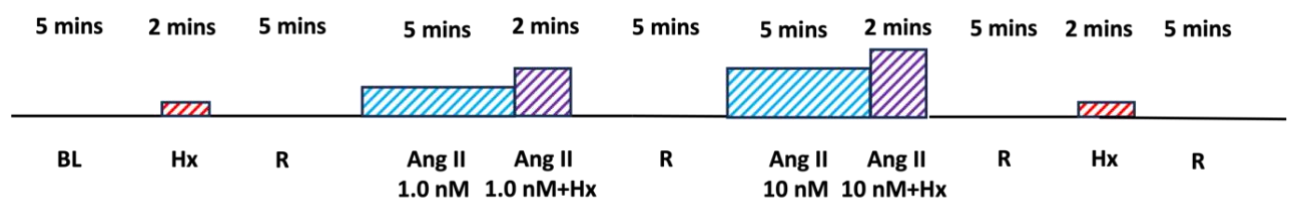
Figure 5.3 Protocol used to assess the influence of mild steady-state hypoxia (100mmHg) on carotid body responses to 1 and 10 nM Ang II.

5 minutes of baseline (normoxic) nerve activity was recorded followed by 2 minutes of steady state mild hypoxia (superfusate PO_2 = 100 mmHg) (Hx) induction. After Hx, the PO_2 was brought back to normoxia for another 5 minutes. 1.0 nM of Ang II was then added for 5 minutes in normoxia, before switching to steady-state Hx with Ang II for 2 minutes. After this point the conditions were reversed and the drug washed out. The protocol is then repeated for 10 nM of Ang II. Lastly, another Hx is given in the absence of Ang II before a final reverse back to normoxia for 5 minutes to monitor any preparation run-down/potentiation.

Similarly, a protocol was used to assess the influence of stead-state hypercapnia on responses to 1-10 nM Ang II. In this protocol, first, control steady state hypercapnic responses were monitored by increasing the superfusate PCO_2 to 80 mmHg for 5 minutes. After recovery, 1 nM of Ang II was added and then nerve discharge frequency was measured in steady-state hypercapnia plus Ang II. Following reverse this was then repeated in the presence of 10 nM Ang II. Finally, another hypercapnic response was performed in the

absence of Ang II to monitor any potentiation or preparation run-down. In this experiment, 8 normal rats were used and the protocol is summarised in Figure 5.4.
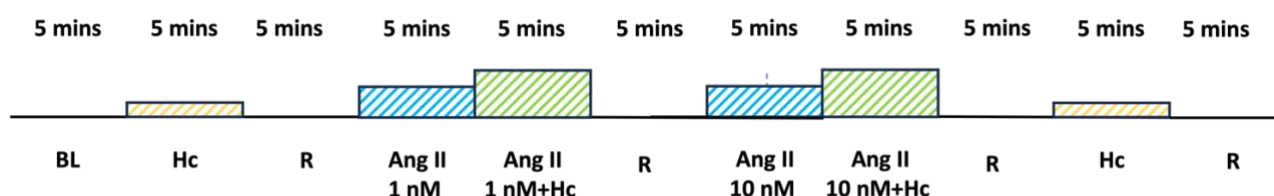
Figure 5.4 Protocol used to monitor the effect of steady state hypercapnia on responses to Ang II.

This Protocol starts with establishing baseline for 5 minutes, followed by 5 minutes exposure to hypercapnia alone (Hc, superfusate PCO_2=80mmHg). After reverse (R), a 5-minute period of 1 nM Ang II will start, followed by 5 minutes of Ang II + Hc. Following reverse and drug washout the same process is repeated for 10nM Ang II. A final control hypercapnic response is given to determine any long-term potentiation or preparation run down.

The next protocol was used to analyse the effect of Ang II on CB hypoxic sensitivity in N and CH animals. This protocol was also devised to determine whether any change in CB O_2 sensitivity caused by Ang II could be reversed by TRPC inhibition with 2-APB. In this protocol, after a baseline discharge frequency is established in normoxia (superfusate PO_2 approximately 300 mmHg) the PO_2 is gradually ramped down to 0 mmHg and the nerve discharge frequency is continuously measured. The PO_2 is then rapidly switched to hyperoxia (95% O_2/5% CO_2) to terminate the response. Normally, this was done before reaching 0 mmHg, at around 10-20 Hz, to decrease the risk of preparation run-down. The discharge frequency is then plotted against superfusate PO_2. This O_2 ramp is first performed under control conditions, then in the presence of 10 nM Ang II, then in presence of 10 nM Ang II plus 10 µM 2-APB and finally after all drugs are washed out to monitor time-dependent preparation run-down. This protocol also allows for comparison of the magnitude of the response to 10 nM Ang II in normoxia, between N and CH animals. Figure 5.5 illustrates the protocol used during this experiment. In this protocol, 8 N rats and 7 CH rats were used.
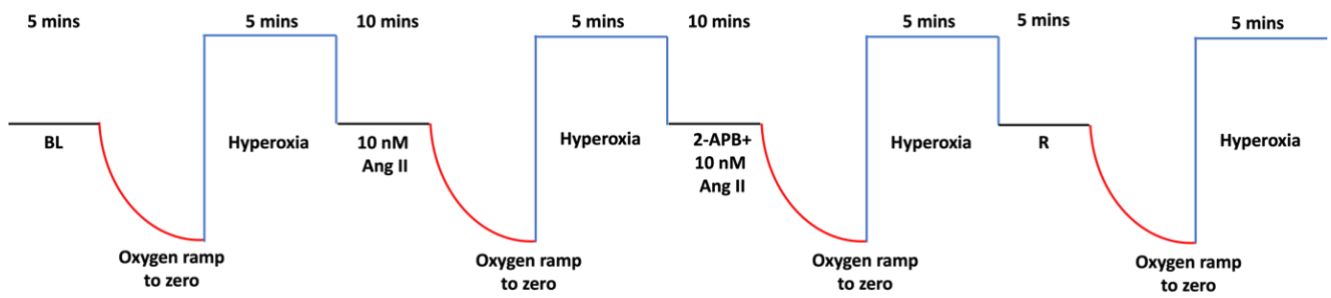
Figure 5.5 Protocol used to compare baseline (BL) responses to Ang II between normoxic (N) and chronic hypoxic (CH) animals and to measure changes in O_2 sensitivity mediated by Ang II and Ang II plus 2-APB in the two animal groups.

For this protocol, an oxygen ramp (PO$_2$: 300 mmHg to 0 mmHg) was induced 4 times- under control conditions, then in the presence of 10 nM Ang II, then in presence of 10 nM Ang II plus 10 µM 2-APB and finally after all drugs are washed out. This protocol was performed on carotid bodies (CBs) isolated from N and CH animals.

The last protocol is used to assess the impact of 2-APB alone on CB hypoxic sensitivity in N and CH animals.

This protocol aimed to assess whether the CB hypoxic sensitivity is altered by 2-APB on its own. Following a baseline discharge frequency establishment in normoxia (superfusate PO$_2$ approximately 300 mmHg), the first O$_2$ ramp will be induced followed by reversal into 5 minutes of hyperoxia (95% O$_2$/5% CO$_2$). 10 µM 2-APB was then added in normoxic conditions for 5 minutes before a second O$_2$ ramp is induced in the presence of 10 µM 2-APB. This is then followed by 10 minutes of hyperoxia, to allow 2-APB washout. At the end, another control O$_2$ ramp is recorded post 2-APB washout to monitor any potential rebound or preparation run-down, Figure 5.6.
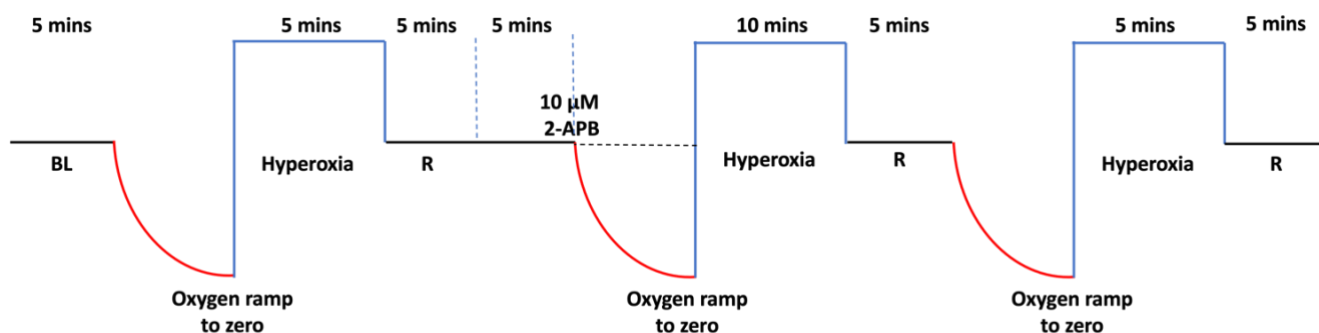
Figure 5.6 Protocol used to compare baseline (BL) responses and changes in O_2 sensitivity caused by 2-APB, in normoxic (N) and chronic hypoxic (CH) animals.

For this protocol, an oxygen ramp (PO_2: 300 mmHg to 0 mmHg) was induced 3 times, under control conditions, then in the presence of 10 µM 2-APB, and after the drug is washed out (rebound). This protocol was performed on carotid bodies (CBs) isolated from N and CH animals.

5.2.4 Data analysis

Data are presented as mean ± SEM or as box-whisker plots with median, the box representing the interquartile range and the whiskers extending to the maximum and minimum points. Individual dots represent single fibre data. Statistical differences were determined using a Student's *t*-test, repeated measures two-way ANOVA, Fisher's exact test or linear regression analysis as appropriate, using Prism v7-10, GraphPad Software, Boston, MA, USA. Significance was taken as p<0.05.

5.3 Results

5.3.1 Ang II causes a brief and unstained rise in carotid sinus nerve activity, independent of concentration

Figure 5.7 A and B show an example raw trace of the carotid sinus nerve activity, measured in response to all Ang II concentrations. During the first 60 seconds of Ang II induction, there was no steady-state change in carotid sinus nerve activity, at any concentration (Figure 5.7 A & B). This was consistent in all fibres tested except for 1 (Figure 5.7 C). When data was grouped together, there was no overall significant increase observed in the first 60 seconds of Ang II induction at any concentration (Figure 5.7 D). It appears that an Ang II response in this experimental preparation needed greater than 60s to reach its peak. Following the first 60s there was usually a brief rise in carotid sinus nerve discharge frequency above baseline, and this was consistent in most of the fibres tested (Figure 5.7 E). This peak response was transient and poorly sustained. Some fibres showed greater peak rises as the concentration of Ang II increased, but not all (Figure 5.7 E). As such the magnitude of the peak response to Ang II was consistent across all concentrations (Figure 5.7 F). Since it appeared that the response to Ang II wore off after a while, the discharge frequency during the last 60 seconds of the 5 minutes exposure were also measured. Although the mean discharge frequency tended to be greater in the presence of Ang II (p=0.1232), the overall effect of Ang II during the last 60 seconds was not significantly different to baseline (Figure 5.7 G & H). This was consistent at all concentrations tested and in most fibres (Figure 5.7 G & H). A key aim of these experiments was to identify a concentration of Ang II to use in the next series of experiments. This was difficult as there was no obvious dose-dependency. However, 100 nM was ruled out due to its limited physiological relevance. In some fibres peak responses were more evident at concentrations greater than 0.1 nM and sometimes responses were slightly better sustained (e.g. Figure 5.7 A & B). Thus, it was decided that 1 and 10 nM Ang II concentrations would be used for the rest of the Chapter.
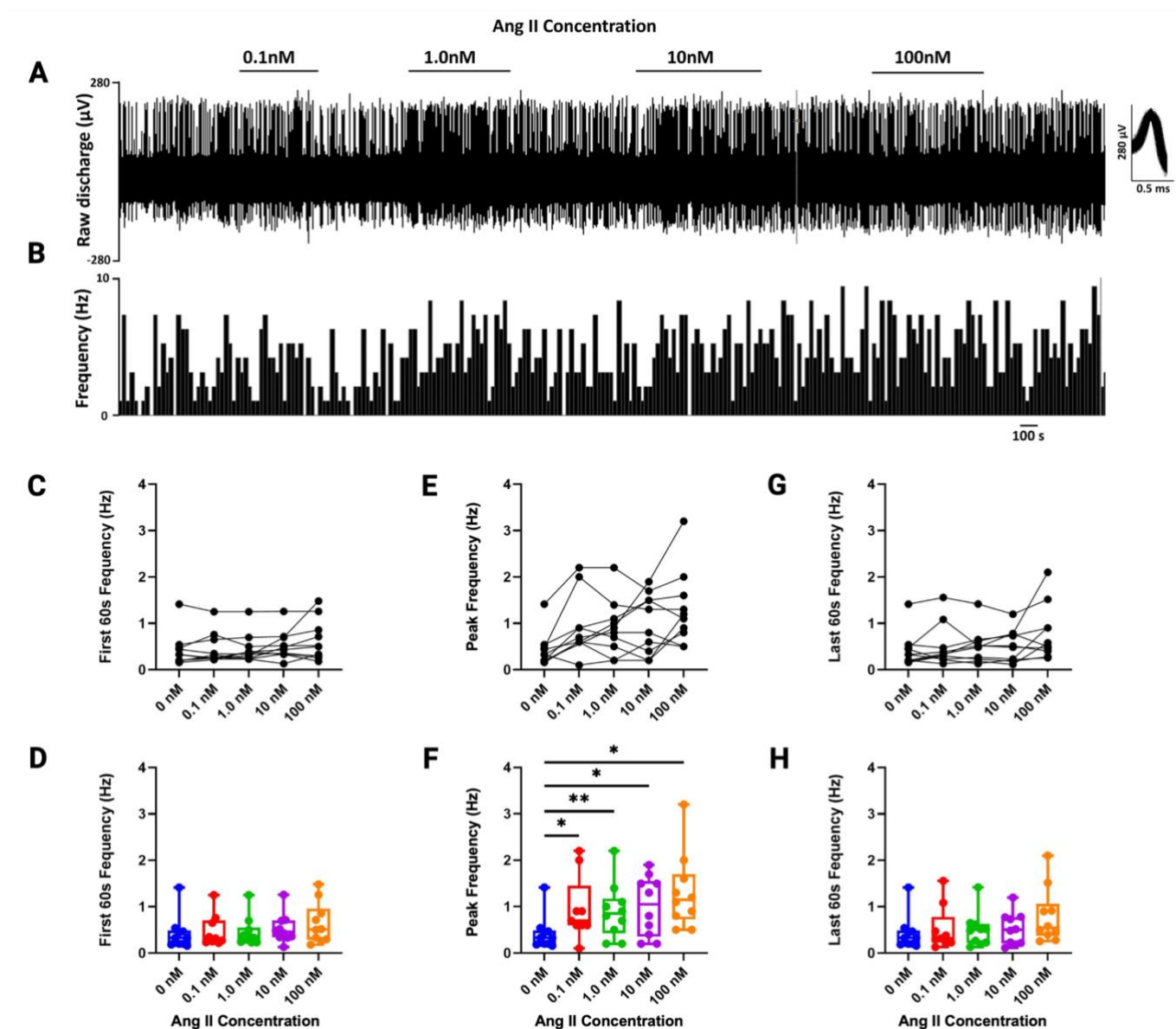
Figure 5.7 Carotid sinus nerve responses to varying concentrations of angiotensin II (Ang II)

A) and B) demonstrate a raw example trace of carotid sinus nerve activity at each Ang II concentration used (0.1, 1, 10 and 100 nM). C) and D) The discharge frequency recorded during the first 60 s of exposure to each concentration of Ang II for each individual fibre (C) and the entire group (D). E) and F) The peak discharge frequency recorded in response to each concentration of Ang II for each individual fibre (E) and the entire group (F). G) and H) The discharge frequency recorded during the last 60 s of exposure to each concentration of Ang II for each individual fibre (G) and the entire group (H). For D, F and H data is presented as box-whisker plots with box denoting the interquartile range, the horizontal line indicating the median and the whiskers extending to minimum and maximum points. Individual data points represent individual fibres (N=10 fibres, n=10 animals). Significance tested using one-way repeated measures ANOVA with Dunett's post-hoc analysis. * and ** denote $p < 0.05$ and $p < 0.01$ respectively.

5.3.2 Ang II exposure induces long term facilitation of the carotid sinus nerve discharge rate

The baseline discharge rate is an indicator of the resting excitability of the carotid sinus nerve and/or basal neurotransmitter release from the type I cells. It was noticed during the nerve recording experiments, that after the exposure to the 4 concentrations of Ang II, the final baseline carotid sinus nerve activity seemed to be higher than the initial baseline, and sometimes even higher that what was measured in the presence of Ang II. Figure 5.8.A demonstrate a raw carotid sinus nerve recording in responses to 4 applications of Ang II. Magnified baseline traces before and after Ang II emphasise the increase in baseline nerve activity following washout of the final application of Ang II (Figure 5.8 B & C). The grouped data shows that before Ang II induction, the mean baseline discharge rate was 0.4267±0.1175 Hz and after the final Ang II was washed out the discharge rate increased to 0.7681±0.1275 Hz (p=0.0280), Figure 5.8. D and E. This rise was present in 8 out of the 10 fibres recorded from (Figure 5.8 D) and appeared to be sustained for at least 5 minutes (Figure 5.8 A). Therefore, these data suggest that repetitive exposure to Ang II causes potentiation of the baseline carotid sinus nerve activity in healthy CBs.
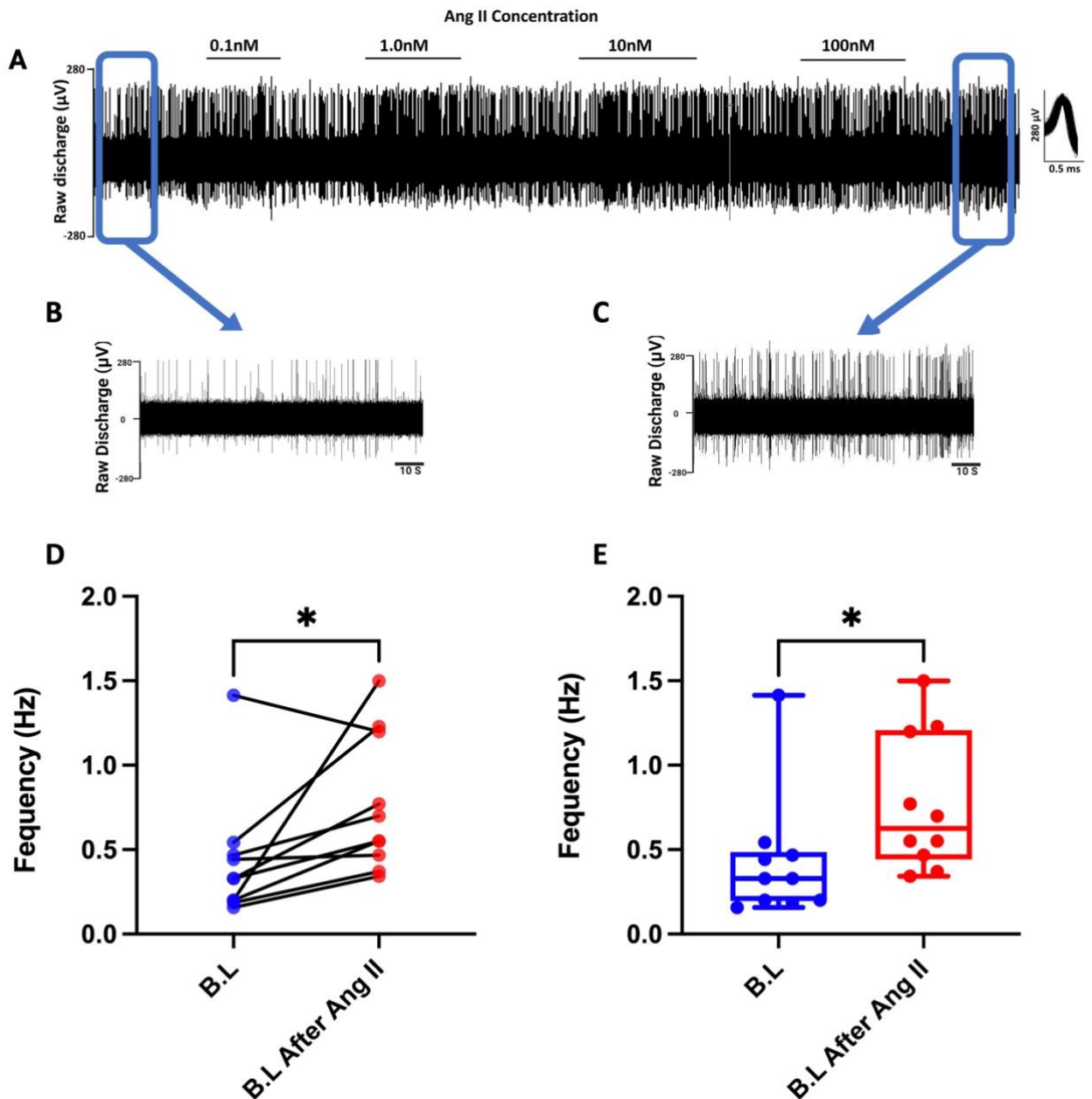
Figure 5.8 Carotid sinus nerve long term facilitation after repetitive exposure to angiotensin II

A) A raw recording of carotid sinus nerve activity in response to 4 applications of Ang II. B) and C) Zoomed-in baseline traces before and after Ang II. D) Individual single fibre baseline comparisons before and after Ang II. E) Group box-whisker plots showing baseline (BL) before and after exposure to Ang II. The box denotes the interquartile range, the horizontal line indicates the median and the whiskers extending to minimum and maximum points. Individual data points represent individual fibres (N=10 fibres, n=10 animals). Significance tested using paired t-test. * denotes $p < 0.05$.

5.3.3 The CB Ang II response depends on the steady-state level of O_2

The next thing was to evaluate the responsiveness of the CB to Ang II at a steady-state level of mild hypoxia. In this experiment two concentrations of Ang II (1 and 10 nM) were tested when the superfusate PO_2 was lowered to 100 mmHg (mild hypoxia) (Figure 5.9 A & B). Comparisons were made between the discharge frequency at 100 mmHg (Hx) without drug (0 nM), Hx plus 1 nM Ang II and Hx plus 10 nM Ang II. When all the data was grouped together, the mean discharge frequency was 2.596±1.044Hz at 100 mm Hg (Hx) without drug, 4.865±2.324 Hz in Hx plus 1 nM Ang II and 6.528±3.457Hz in Hx plus 10 nM (Figure 5.9 C & D). However, a closer look at the data revealed that only two CBs had a large response to either 1 or 10 nM of Ang II during mild hypoxia, whilst the others produced either a slight stimulation of the carotid sinus nerve discharge frequency or rarely, a slight inhibition (Figure 5.9 C & D). These data suggested that the Ang II response could be dependent on the initial rise in baseline activity caused by the exposure to mild hypoxia (Hx), since the ones that responded the most had the highest baseline activity (Figure 5.9 C). To test this in more detail, the rise in activity evoked by Ang II (delta Hz) was plotted against the baseline discharge frequency induced by mild hypoxia for every fibre, and then analysed for a correlation (Figure 5.9 E & F). The plots confirm a significant positive correlation between the baseline mild hypoxic discharge frequency and the rise in discharge frequency caused by Ang II (Figure 5 E & F). This was apparent for both 1 and 10 nM Ang II but the correlation was stronger for 10 nM. This suggests that CB Ang II sensitivity is elevated by steady state, hypoxic induced rises in baseline nerve activity.
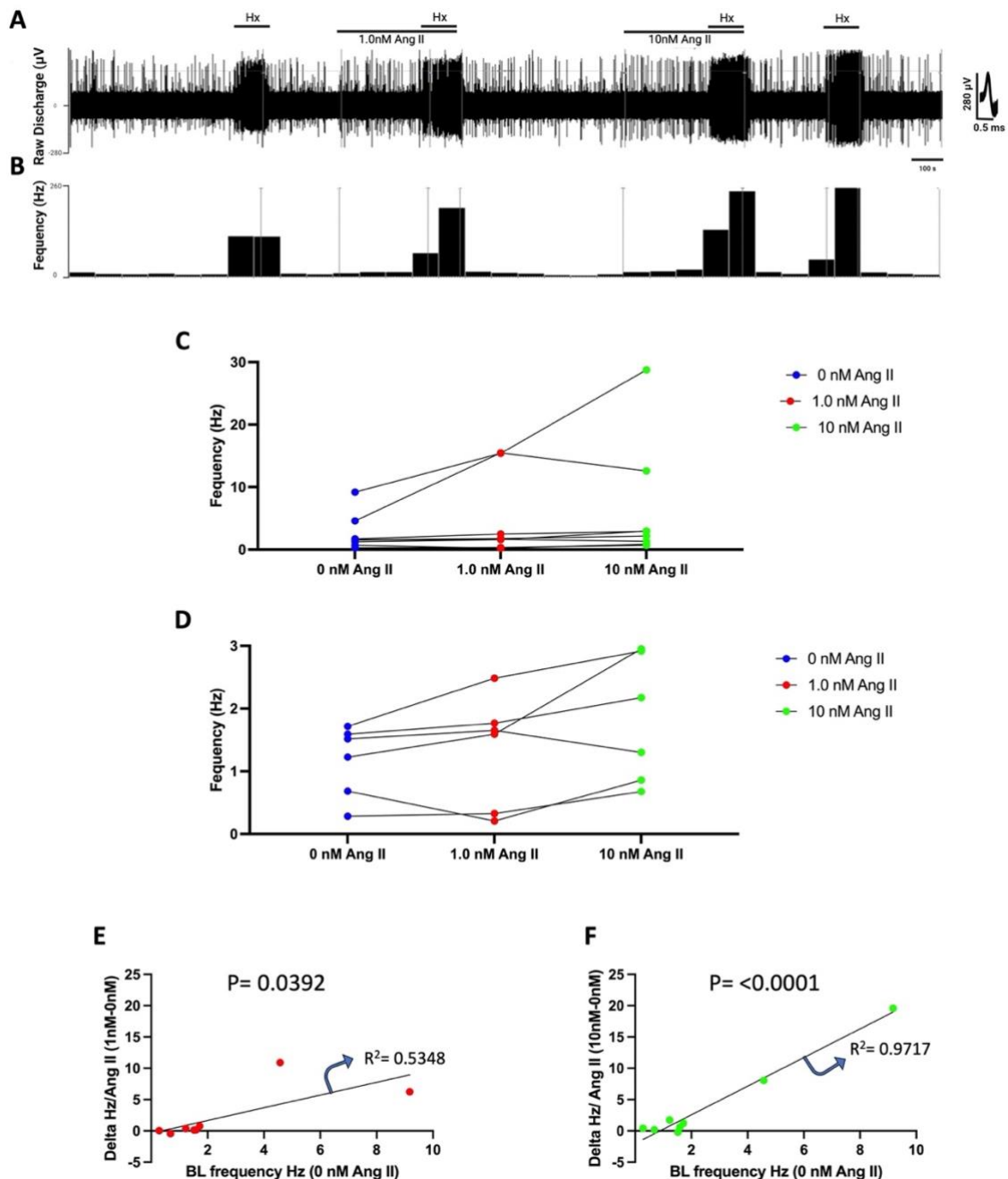
Figure 5.9 Individual variation in carotid sinus nerve response to angiotensin II (Ang II)

A) and B) A raw trace example of the impact of Ang II (1 and 10 nM) when the steady state superfusate PO_2 was lowered to 100 mmHg (mild hypoxia, Hx). C) Every fibre discharge frequency recorded at 100 mmHg (Hx) without drug (0 nM), Hx plus 1 nM Ang II and Hx plus 10 nM Ang II (n=8 fibres from N=8 animals). Only two CBs showed a large response to 1 or 10 nM of Ang II and these seemed to have the largest rise in baseline activity in mild hypoxia. D) As in C, but with a restricted y axis to magnify those fibres with lower baseline hypoxic frequencies. E) and F) Plots of the change in discharge frequency caused by 1 nM (E) and 10 nM (F) Ang II (y axis) against the baseline steady state mild hypoxic discharge frequency (x axis). Significance tested using regression analysis.

5.3.4 Ang II (1 and 10nM) does not affect the carotid sinus nerve sensitivity to hypercapnia

Next it was tested if the CB sensitivity to Ang II was affected by hypercapnia. A raw trace example is shown in Figure 5.10 A and B. The results of this experiment showed that the sensitivity to Ang II did not significantly change during simultaneous exposure to hypercapnia. Nerve discharge frequency was recorded in normocapnia (PCO_2 = 40 mmHg) and hypercapnia (PCO_2 = 80 mmHg) without any drug (0 nM Ang II), in the presence of 1 nM Ang II and in the presence of 10 nM Ang II. The mean steady state discharge frequency was not significantly altered by 1 or 10 nM Ang II in either normocapnia (PCO_2 = 40 mmHg) or hypercapnia (PCO_2 = 80 mmHg) (Figure 5.10 C). This was despite the observation that hypercapnia itself did raise the discharge frequency (p=0.0131, two-way repeated measures ANOVA, Figure 5.10 C). Therefore, a rise in discharge frequency doesn't necessarily mean a larger response to Ang II, rather it seems to depend on what stimulus is causing the rise in discharge frequency. Alternatively, it could be that hypercapnia did not increase the discharge frequency enough to the augment the sensitivity to Ang II.

When the hypercapnic sensitivity itself was analysed (calculated as the change in discharge frequency per mmHg increase in PCO_2), there was no effect of Ang II. The control (0 nM Ang II) CO_2 sensitivity was 0.01067±0.002567 Hz/mmHg PCO_2, and during exposure to 1nM of Ang II the CO_2 sensitivity was 0.01295±0.001864 Hz/mmHg PCO_2, which was not significant (p=0.5056, Figure 5.10.D). During application of 10nM Ang II, the CO_2 sensitivity was 0.01324±0.004174 Hz/mmHg PCO_2, which again was not different to control (0 nM Ang II) (p=0.3173, Figure 5.10.D). Lastly, the post Ang II sensitivity to CO_2 (post control) was 0.01307±0.003345 Hz/mmHg PCO_2 and not significantly altered, suggestive of no run-down in the preparation (p=0.3747, Figure 5.10.D). These results indicate that 1 and 10 nM of Ang II does not affect CB CO_2 sensitivity.
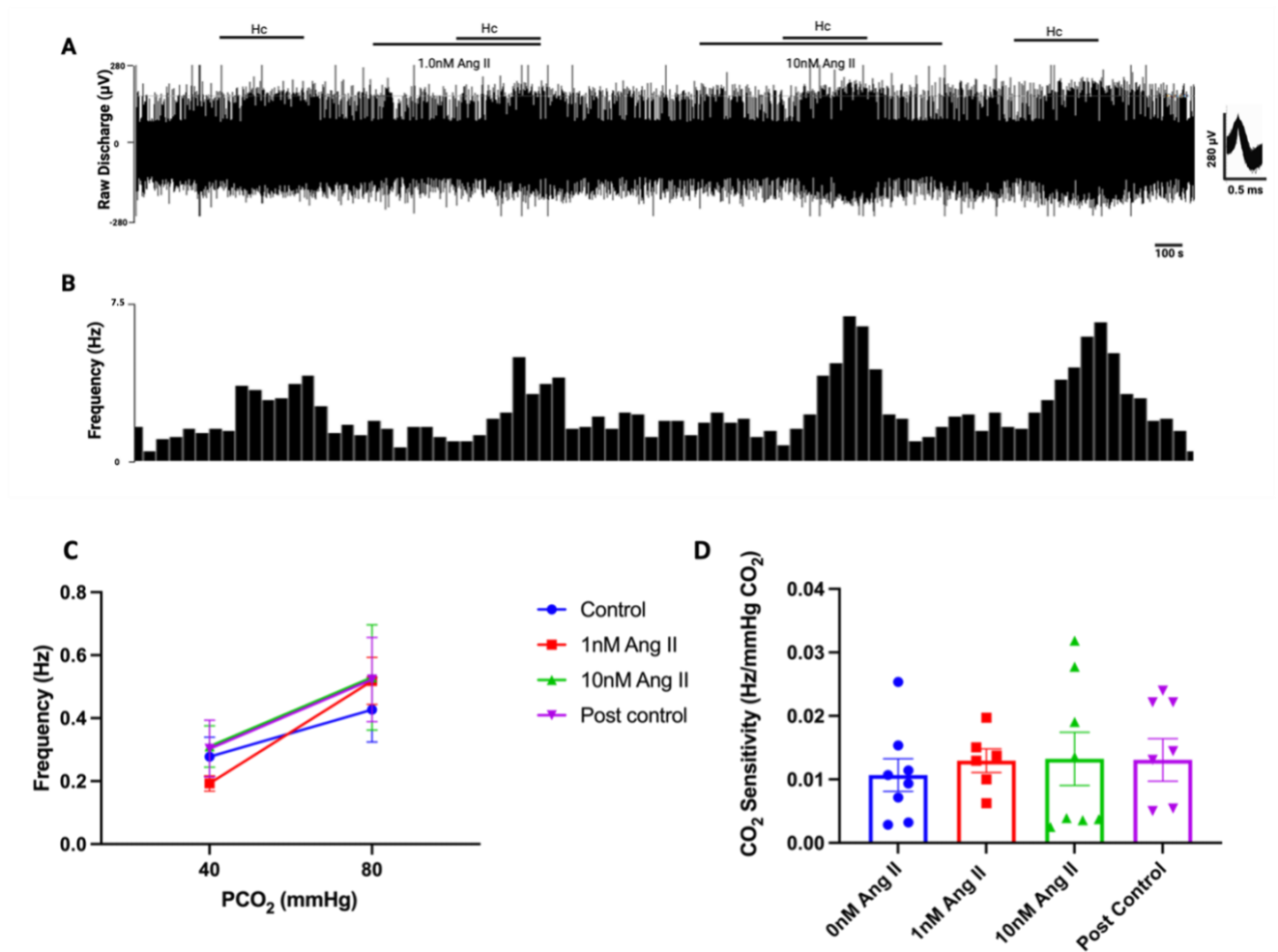
Figure 5.10 1 and 10 nM angiotensin II (Ang II) do not affect the carotid body sensitivity to hypercapnia (Hc).

A) and B) demonstrate a raw trace example. Nerve discharge frequency was recorded in normocapnia (PCO_2 = 40 mmHg) and hypercapnia (PCO_2 = 80 mmHg) without any drug (0 nM Ang II), in the presence of 1 nM Ang II and in the presence of 10 nM Ang II. C) Mean discharge frequency recorded in normocapnia (PCO_2 = 40 mmHg) and hypercapnia (PCO_2 = 80 mmHg) without any drug (0 nM Ang II), in the presence of 1 nM Ang II, in the presence of 10 nM Ang II and following final washout of Ang II (post control). Data presented as mean±SEM. Significance tested using two-way repeated measures ANOVA. D) CO2 sensitivity calculated as change in discharge frequency (Hz) per mmHg increase in PCO_2, for the 4 groups. Data presented as mean±SEM. Individual data points represent single fibre data (N=7/8 fibres, n= 8 animals) Significance tested using a two-way ANOVA.

5.3.5 Ang II responses are larger and more sustained in CH CBs

The next key aim was to investigate if the responses to Ang II were increased in CBs isolated from CH animals. For these comparisons a concentration of 10 nM Ang II was chosen. The response to Ang II in CH CBs took more than 60s to reach its peak. However, in contrast to N CBs, during the first minute, the carotid sinus nerve discharge frequency for CH showed signs of a gradual increase. However, at this time point there was no significant difference between N and CH absolute frequencies (p=0.1245) (Figure 5.11 A). During the second to the fourth minutes of the 5-minute Ang II exposure, the discharge frequency peaks for both N and CH for short period, with the peak discharge frequency observed for CH being significantly greater than for N (p<0.0001) (Figure 5.11 A). The discharge frequency then starts to wear off during the fifth minute but remains significantly higher in the CH group (p=0.0067) (Figure 5.11 A). Specific analysis of the sensitivity to Ang II (Ang II – baseline or 'change in discharge frequency') showed that Ang II induced a larger rise in peak discharge frequency (p=0.0002) and a larger steady state response to Ang II when measured during the fifth minute of exposure (p=0.0223) (Figure 5.11 B).

5.3.6 CH CB sensory fibres are more likely to exhibit a significant response to Ang II

A further analysis was performed to indicate whether or not a fibre demonstrated a significant response to Ang II. A criteria was put forward, outlining that a significant response to Ang II was only counted if the peak discharge frequency achieved in the presence of Ang II was at least 30% greater than the baseline discharge frequency. The response to Ang II in the N group was variable and sometimes barely noticeable, with only 1/5 fibres demonstrating a significant response (Figure 5.12). However, in the 6 CH fibres all showed a measurable response to 10 nM Ang II, Figure 5.12. Therefore, as well as the magnitude and

kinetics of the response to Ang II being greater in CH CBs, there was a greater chance of any single fibre

being sensitive to Ang II.
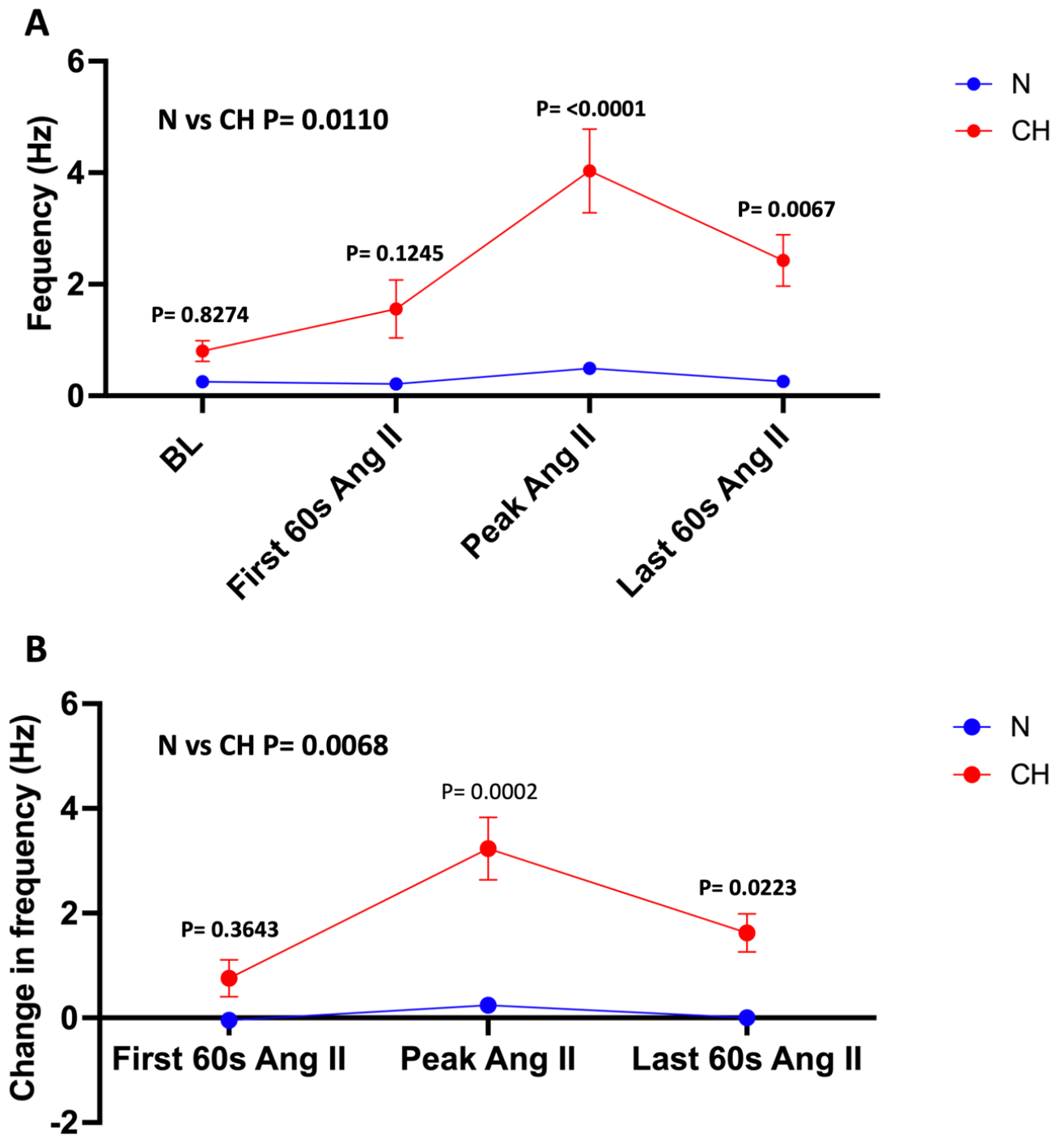
Figure 5.11 Analysis of magnitude and kinetics of the carotid body responses to 10 nM angiotensin II (Ang II) isolated from normoxic (N) and chronic hypoxia (CH) groups.

A) Absolute single fibre discharge frequency measured at baseline (BL), during the first 60 seconds of Ang II exposure, the peak response and during the final 60 seconds of exposure, for N (N=5 fibres, n=5 animals) and CH (N=6 fibres, n=6 animals). B) The change in carotid sinus nerve discharge frequency (Ang II – baseline), calculated during each time point for N and CH. Data presented as mean±SEM. Significance tested using 2-way repeated measures ANOVA with Bonferroni post-hoc analysis.
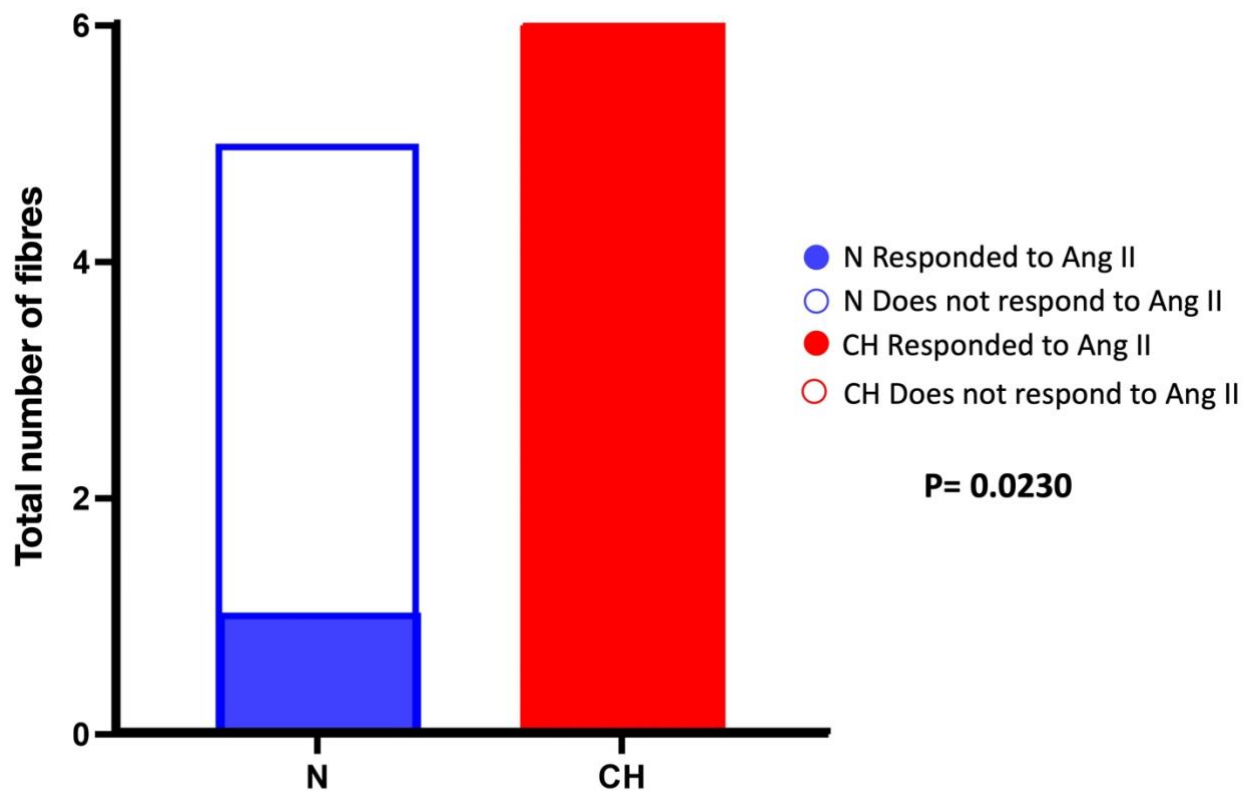
Figure 5.12 Comparing the proportion of carotid body sensory fibres that demonstrated a measurable response to 10 nM angiotensin II (Ang II) in normoxic (N) and chronic hypoxic (CH) groups.

Proportion of fibres that responded to Ang II for N (1/5) vs CH (6/6). A response was determined as a rise in peak discharge frequency at least 30% above baseline. Significance tested using Fisher's exact test.

5.3.7 Chronic hypoxia (CH) induction for 10 days increases CB hypoxic sensitivity

Before evaluating the impact of Ang II on hypoxic sensitivity of N and CH CBs, an initial analysis looked at whether the CH group had a higher intrinsic O_2 sensitivity. In this experiment, an O_2 electrode was placed in the superfusion system, just before the recording bath solution, to continuously measure the PO_2. This allowed for plotting of the PO_2 against the discharge rate as the PO_2 was slowed ramped down from 300 to 0 mmHg. Often the PO_2 was reversed into hyperoxia before reaching 0 mmHg, when the discharge frequency was at around 5-30 Hz, to prevent reaching the maximum response and causing preparation run-down (e.g. neurotransmitter depletion). In these experiments, the CH carotid sinus nerves discharge frequency was significantly higher at 300 mmHg PO_2 normoxic baseline compared with N (2.705 ± 0.4899Hz vs 1.007 ± 0.1988 Hz, p= 0.0033, Student's t test). Furthermore, the discharge frequency response to hypoxia was augmented in the CH group, suggestive of an increase in CB O_2 sensitivity (p=0.0380) (Figure 5.13). This therefore provided additional evidence that the model of CH used (12% F_iO_2 for 10 days) was sufficient to cause CB hyperactivity.
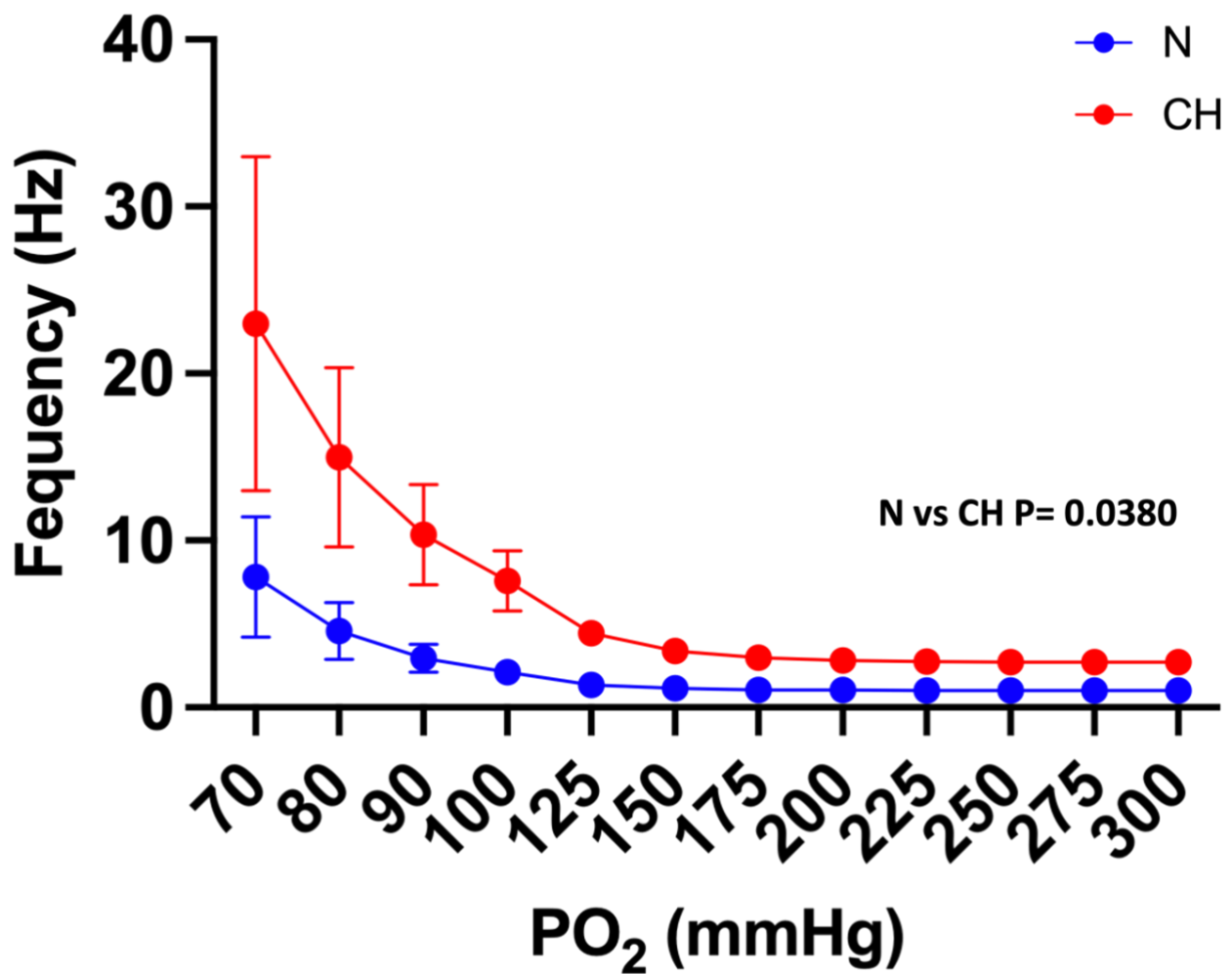
Figure 5.13 Comparing carotid sinus nerve discharge frequency between normoxic (N) and chronic hypoxic (CH) groups at different PO_2s

Calculated single fibre discharge frequency across a range of 300 to 70 mmHg superfusate PO_2s for N (N=8 fibres, n=8 animals) and CH (N=7 fibres, n=7 animals). Data presented as mean±SEM. Statistical differences tested using Two-way repeated measures ANOVA and showed a significant overall effect of CH (p=0.0380).

5.3.8 2-APB reduces the CB hypoxic sensitivity in the presence of Ang II

Acute CB hypoxic sensitivity was evaluated by slowly ramping the O_2 from ca 300mmHg to 0 mmHg and at the same time making continuous measurements of carotid sinus nerve activity. Often the PO_2 was reverse before reaching 0 mmHg once the discharge frequency had reached between 10 to 40 Hz to prevent preparation run-down. Hypoxic responses were recorded in 3 groups: Control, Ang II (10 nM) and Ang II (10 nM) + 2-APB (10 µM). Surprisingly, Ang II alone seemed to inhibit the acute CB hypoxic sensitivity of CH but not N (Figure 5.14 A & B). Calculating the effect of Ang II alone (by subtracting the discharge frequency of the Control group from the Ang II group at all PO_2s) demonstrated that the inhibitory effect of Ang II was significantly larger in the CH group (p= 0.0073, two-way repeated measures ANOVA, Figure 5.14 C). The stronger inhibitory action seems to become more apparent as the PO_2 started to drop below 100 mmHg (Figure 5.14 C).

In the presence of Ang II, 2-APB, a general TRPC channel blocker reduced the hypoxic sensitivity in both N and CH groups (Figure 5.14 A & B). Calculation of the effect of 2-APB in the presence of Ang II (by subtracting the discharge frequency of the Ang II group from the Ang II + 2-APB group at all PO_2s), showed that the inhibitory action of 2-APB is enhanced in the CH group (p=0.0038, two-way repeated measures ANOVA, Figure 5.14 D). This becomes obvious as the PO_2 drops below 100 mmHg (Figure 5.14 C).
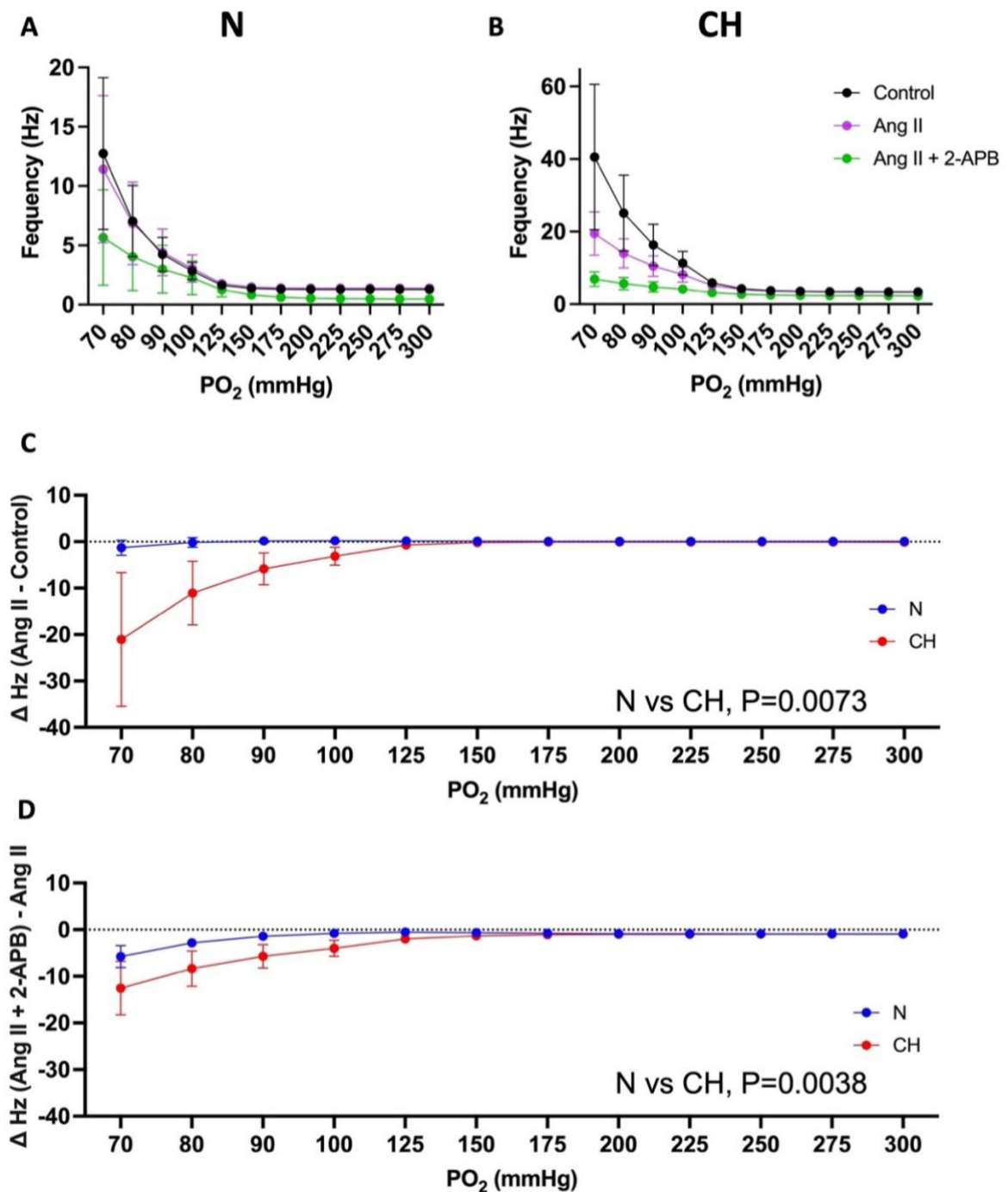
Figure 5.14 2-APB in the presence of angiotensin II (Ang II) causes greater inhibition of the carotid sinus nerve discharge frequency during acute hypoxia in chronic hypoxic (CH) compared with normoxic (N) animals.

A) and B) Mean PO_2 response curves for Control, Ang II (10nM) and Ang II (10 nM) + 2-APB (10 μM) for N (N=8 fibres, n=8 animals) and CH (N=7 fibres, n=7 animals) groups respectively. C) Calculation of the Ang II sensitivity ([Ang II] – [Control]) at different PO_2s for N and CH. D) Calculation of the 2-APB sensitivity in the presence of Ang II ([Ang II + 2-APB] – [Ang II]) at different PO_2s for N and CH. Data presented as mean±SEM. For C and D, significance was tested using a two-way repeated measures ANOVA.

5.3.9 Testing the effect of 2-APB and Vehicle on baseline carotid sinus nerve activity

Since 2-APB is soluble in DMSO, a control Vehicle experiment was performed to confirm that DMSO itself was not responsible for affecting the carotid sinus nerve discharge frequency. Discharge frequency measurements were made in normoxia in N animals, under control, DMSO (0.5%, Vehicle) and 2-APB conditions. In this experiment, the control discharge frequency was 0.2597±0.04789 Hz, after inducing DMSO, this was 0.2736±0.06524 Hz, (p=0.9990, Figure 5.15). When 2-APB was given, the discharge frequency tended to go down to 0.1611±0.04092 Hz (p= 0.1992, Figure 5.15) (N=6 fibres, n= 6 animals). These results indicate that the Vehicle, DMSO, is safe to use in CB preparation and does not alter the carotid sinus nerve discharge frequency by itself, at this concentration.
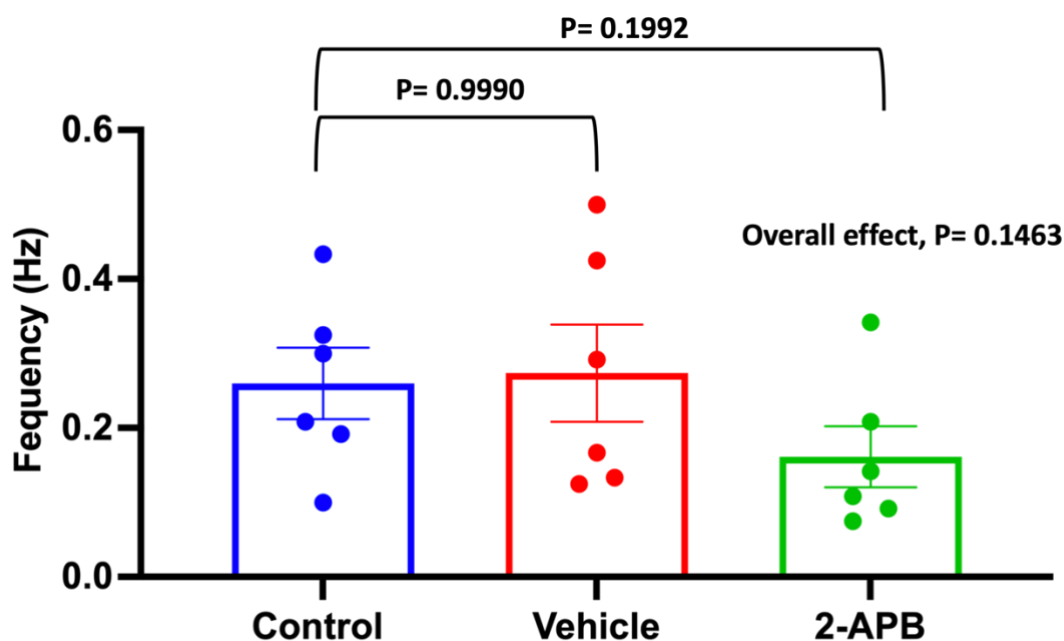
Figure 5.15 Vehicle experiment to confirm that DMSO does not modify the carotid sinus nerve activity.

Mean baseline (normoxic) single fibre discharge frequency recorded from 6 fibres from 6 animals in Control, 0.5% DMSO (Vehicle) and 2-APB (10 µM) conditions. Data presented as mean±SEM, individual datapoints represent single fibre/animal data. Significance was tested using a one-way repeated measures ANOVA with Bonferroni post-hoc analysis.

5.3.10 Identifying differential effects of 2-APB alone on CB hypoxic sensitivity in N and CH groups

To examine if the inhibitory actions of 2-APB on CB hypoxic sensitivity were dependent on the presence of Ang II, a final series of experiments were performed. In this instance, hypoxic responses were measured in Control, 2-APB (10 µM) and washout (Rebound) conditions. In the presence of 2-APB on its own, hypoxic responses were depressed in both N and CH (Figure 5.16 A & B). Calculation of the 2-APB sensitivity ([2-APB] − [Control]) shows that its inhibitory action is enhanced during more severe hypoxic conditions (p<0.0001) but is not different between N and CH (p=0.4544) (Figure 5.16 C). Thus, the greater inhibitory action of 2-APB seen in the CH group in the previous experiments seems to be associated with the presence of Ang II.

It was noticed while conducting the 2-APB experiment protocol, that following washout of 2-APB there appeared to be a rebound increase in discharge frequency. This rebound occurred even after 10 minutes of hyperoxia, when it is very likely that the drug is washed out. Although the rebound increase occurred in both N and CH, it was much larger in the CH group and seemed to be sustained during hypoxia. (Figure 5.16 A & B). Calculation of the size of the rebound across the entire range of PO_2s ([Rebound] − [Control]) showed that this was significantly enhanced in the CH group (p=0.0184), and was not modified by the level of hypoxia (p=0.8517). The different effects of the rebound following 2-APB washout are likely linked to the underlying adaptations that take place on the nerve ending in response to CH.
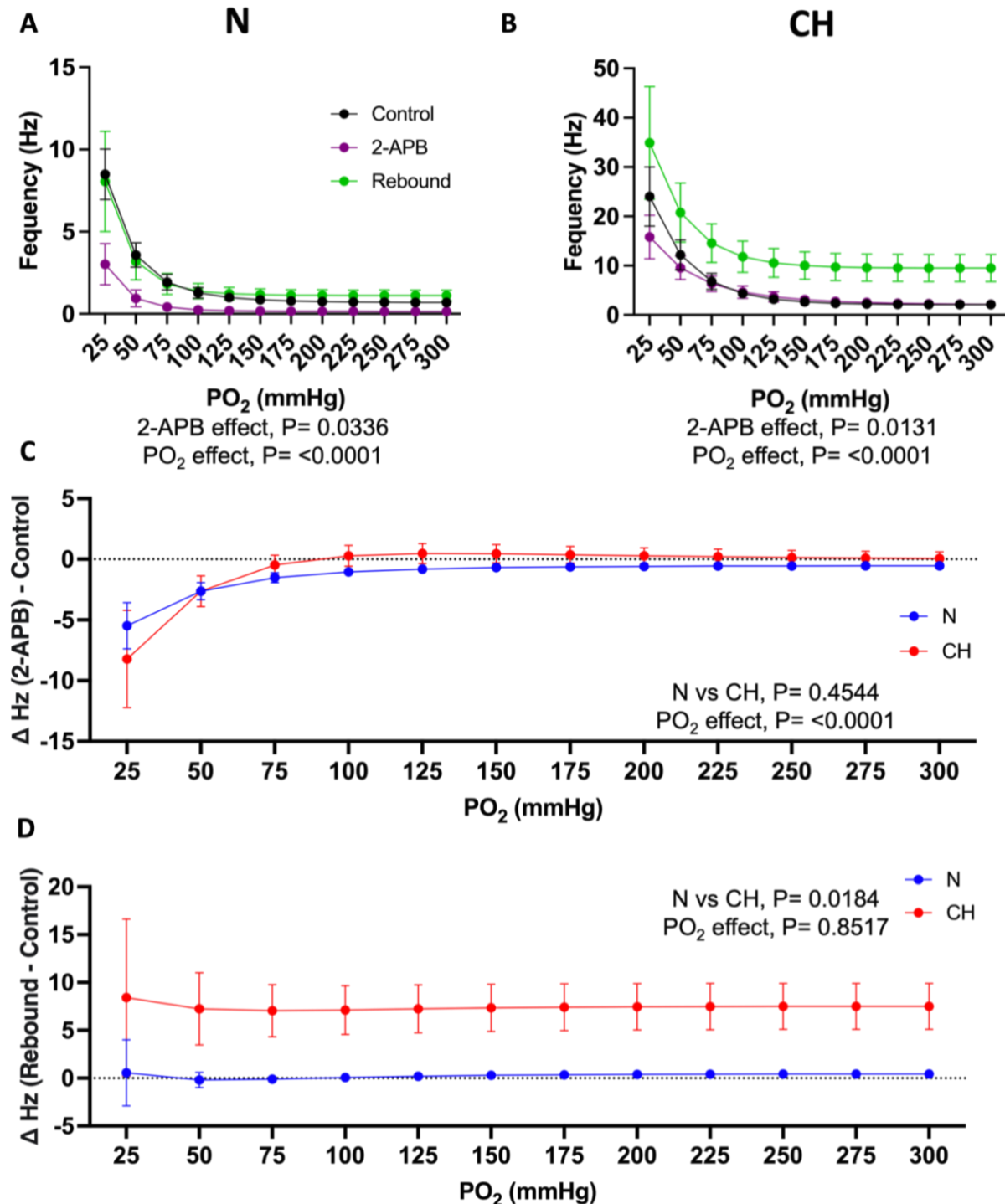
Figure 5.16 2-APB inhibition of carotid body hypoxic sensitivity is consistent in normoxic (N) and chronic hypoxic (CH) groups but rebound following washout is greatly exaggerated in CH.

A) and B) Mean PO_2 response curves for Control, 2-APB (10 μM) and Rebound (washout) for N (N=7 fibres, n=7 animals) and CH (N=8 fibres, n=8 animals) groups respectively. C) Calculation of the 2-APB sensitivity ([2-APB] – [Control]) at different PO_2s for N and CH. D) Calculation of the rebound following 2-APB washout ([Rebound] – [Control]) at different PO_2s for N and CH. Data presented as mean±SEM. For C and D, significance was tested using a two-way ANOVA.

5.4 Chapter synopsis and discussion

5.4.1 List of main findings

- In normal CBs, Ang II causes a modest increase in carotid sinus nerve activity that is poorly sustained

- Repetitive Ang II application induces long term potentiation/facilitation (LTF) of the carotid sinus nerve discharge rate

- The Ang II response depends on baseline activity; it responds more when the baseline activity is elevated by mild hypoxia but not hypercapnia

- CH exposure for 10 days increases the sensitivity to Ang II in normoxia, as evidenced by larger rises in nerve activity and more fibres exhibiting measurable responses

- CH exposure for 10 days increases CB hypoxic sensitivity

- Ang II decreases the acute hypoxic sensitivity of the CB in CH but not N

- In the presence of Ang II, 2-APB decreases CB responses to hypoxia and this is exaggerated in the CH group

- 2-APB alone decreases CB hypoxic sensitivity and this is similar in CH and N

- Washout of 2-APB causes a rebound increase in carotid sinus nerve activity which is greatly enhanced in the CH group

5.4.2 Characterising normal Ang II modulation of carotid sinus nerve activity: response kinetics, response magnitude, impact of baseline activity and induction of LTF

Ang II, known for its crucial role in the renin-angiotensin-aldosterone system, has been shown previously to dose-dependently increase carotid sinus nerve activity (Allen, 1998b, Fung, 2014). However, careful inspection of this data shows that although there is an elevation in intensity between 0.1 and 1 nM further significant stimulation is not observed at 10 nM or 100 nM concentrations (Allen, 1998b). This is largely consistent with the current work. The magnitude of the rise seen by Allen et al., was around 10-50% above baseline which again is in line with what was recorded in the current Chapter. Interestingly, Allen and colleagues reported a transient inhibition of sensory nerve activity upon initial application of Ang II before the excitation. This was not observed in the current work although the presence of both excitatory and inhibitory Ang II mediated pathways could explain why some preparations responded whilst others did not. A key advantage of the current experiments was the longer Ang II exposure time at each concentration. This was able to uncover the overall kinetics of the response to Ang II. Indeed, any rise in nerve activity was short lasting, lasting no more than 1 minute before returning back to basal levels. Again, this could be due to the overall balance between excitatory and inhibitory pathways, or that AT_1Rs were rapidly internalised. Previous work in other tissues (e.g. blood vessels) has shown that in response to agonists, AT_1Rs do internalise leading to alternative intracellular signalling pathways being activated (Hermosilla et al., 2017). It would be interesting to confirm receptor internalization, by visualizing the AT_1Rs before and after Ang II induction, using immunofluorescence microscopy, in N and CH and evaluate the time difference between the groups. However, using the same CB after nerve recording experiment for immunofluorescence experiment would not be ideal due to tissue viability, histological integrity and receptor dynamics.

Interestingly, the findings from this Chapter indicate that repetitive exposure to Ang II followed by washout leads to a persistent rise in baseline carotid sinus nerve discharge rate. Exposure to Ang II has been associated with the development of LTF previously, although this was associated with CBs isolated from animals exposed to CIH (Peng et al., 2011a). The mechanism of Ang II induced LTF in the CIH CB seems to involve persistent activation of NADPH oxidase (Peng et al., 2011a). Although not tested here, an obvious next experiment would be to see if the increase in basal activity following Ang II washout in control CBs is attenuated by an NADPH-oxidase inhibitor or antioxidant. The observation of LTF, a form of neural plasticity, suggests that Ang II not only acutely increases nerve activity but also induces sustained changes in the neural circuitry, through second messenger signalling (Peng et al., 2011a). This could have important implications for understanding the long-term effects of Ang II on the carotid sinus nerve, potentially contributing to sustained alterations in cardiovascular regulation even in healthy subjects.

Another interesting consideration is whether the baseline discharge frequency modifies sensitivity to Ang II. In these experiments baseline discharge frequency was increased by sustained exposure to either mild hypoxia or hypercapnia. Whilst the rise in baseline discharge frequency produced by mild hypoxia seemed to correlate against the response size to Ang II, this was not apparent for hypercapnia. This specific observation indicates a selectivity in Ang II's influence on different aspects of carotid sinus nerve activity, emphasizing the need to distinguish between various physiological stimuli and their respective responses. Although there is some overlap between hypoxic and hypercapnic signalling in the CB (Pepper et al., 1995), there are also likely to be unique pathways such as specific acid-sensing ion channels (Tan et al., 2007). However, for mild hypoxia, the observation that the Ang II response is not uniform but instead depends on baseline activity, demonstrates a sensitivity that increases when the baseline activity is elevated. This dependence on baseline activity implies that the physiological state of the carotid sinus nerve plays a

crucial role in determining the extent of its responsiveness to Ang II. This finding emphasizes the importance of considering the baseline conditions in predicting the dynamics of Ang II-mediated effects on the carotid sinus nerve activity. This may be particularly important in conditions where baseline nerve activity is known to be increased such as CIH, chronic heart failure and essential hypertension (Nanduri et al., 2017a, Peng et al., 2003, Sun et al., 1999, Abdala et al., 2012, Felippe et al., 2023). This relationship between Ang II and the carotid sinus nerve confirms the complexity of neural regulation in cardiovascular physiology and offers potential insights for targeted therapeutic interventions in conditions related to high blood pressure caused by adaptive responses to environmental challenges.

5.4.3 Enhanced responsiveness to Ang II in CH rat CBs

An interesting aspect of Ang II's influence is whether its action on CB function is altered in the context of CH. Previous studies have suggested that CH augments the CB response to Ang II in normoxia (Li et al., 2006). Building on this, in the current experiments, as well as responses to Ang II being larger in CH CBs, they were also more rapidly induced and better sustained. Furthermore, a measurable response to Ang II was observed in a greater proportion of fibres in the CH group (6/6 vs 1/5). This suggests a dynamic relationship between Ang II and CH, where the physiological effects of Ang II are intensified due to adaptive changes brought about by prolonged exposure to low O_2. Furthermore, it suggests that CH induces a more uniform and consistent response to Ang II compared to the more variable responses observed in N animals.

Ang II, a key player in the renin-angiotensin-aldosterone system, exerts its effects through specific receptors, including AT_1Rs (Dasgupta and Zhang, 2011). Therefore, the increased sensitivity in the CH group is potentially due to upregulating AT_1Rs receptor density and/or excitatory intracellular signalling pathways

as suggested previously (Leung et al., 2000, Prabhakar et al., 2009). This idea is supported by earlier findings from Chapter 2 and 3, where AT_1R protein expression and supercluster formation is increased in PC12 cells, a surrogate of CB type 1 cells, after CH. In addition, it may be that type I cells that previously did not express AT_1Rs, start to display AT_1Rs in response to CH. This is a logical explanation for the greater consistency, and it could be explained by the increased expression in Chapter 2 and cluster size reported in Chapter 3.

Furthermore, the heightened response in the CH group may have implications for understanding chronic cardiovascular adaptations to hypoxia. CH and a rise in plasma Ang II are both features of COPD (Zeng, 1989). The observed uniform response to Ang II in the CH group suggests a potential mechanism of carotid sinus nerve hyperactivity which could contribute to the known rise in sympathetic nerve activity to the blood vessels in both COPD patients and CH animal models (Phillips et al., 2018). Exploration of this idea warrants further investigation.

In CH conditions, the persistent activation of the sympathetic nervous system and the CB is a defining feature. This chronic activation initiates a feedback loop, leading to increased production of Ang II and intensified sensitivity of the CB to hypoxia. Elevated levels of circulating Ang II further stimulate carotid body activity, amplifying its discharge rate. This continuous cycle can contribute to the progression of cardiovascular pathologies, including vasoconstriction, neurogenic hypertension, and arrhythmias. The relationship between sympathetic activation, Ang II production, and CB sensitivity emphasises the importance of targeting these pathways in the management of cardiovascular disorders associated with CH.

5.4.4 Targeting TRPC channels with 2-APB: modulating carotid sinus nerve responses to hypoxia and Ang II as a potential therapeutic intervention in CH

CB responses to hypoxia were greater in CH, consistent with an effective CH model. A key observation was the reduction in sensitivity to hypoxia induced by 2-APB, a TRPC channel blocker, in the presence of Ang II. Interestingly this inhibitory action was more apparent in the CH, but only in the presence of Ang II and not when 2-APB was given alone. This effect suggests a merging of signalling pathways or common downstream effectors influenced by 2-APB, most likely TRPC channels. However, there is some evidence that 2-APB also inhibits IP_3 receptors, which are also implicated in Ang II signalling (Splettstoesser et al., 2007).

Ang II binding to AT_1R typically increases excitatory afferent activity in the CB. However, AT_1R activation can also have inhibitory effects, potentially due to Ang II-induced modulation of neurotransmitter release and ion channel activity (Allen, 1998a). These mechanisms can decrease excitatory neurotransmitter release or increase inhibitory signals, balancing the overall chemoreceptor activity under different physiological states (Allen, 1998a).

Surprisingly, Ang II alone caused a reduction in hypoxic sensitivity of CH CBs. It is possible that some AT_1Rs are coupled to inhibitory signalling pathways that are more rapidly activated and tend to predominate (Allen, 1998b). The greater inhibitory action in CH suggests an upregulation of these pathways. During acute hypoxia, excitatory Ang II pathways may still be initiated but are outweighed by Ang II mediated inhibition: i.e. the overall effect is inhibition even though both excitatory and inhibitory pathways are active. 2-APB then causes a further depletion in CH CBs by removing the excitatory actions of Ang II which are mediated via TRPC channels and/or IP_3 receptors.

TRPC channels are a subfamily of transient receptor potential (TRP) channels implicated in various cellular processes, including calcium signalling and sensory transduction (Samanta et al., 2018). These channels have been recognized for their involvement in mediating responses to environmental stimuli and neurohormonal signalling (Numaga-Tomita and Nishida, 2020, Smani et al., 2015). The identification of 2-APB as a TRPC channel blocker suggests that its actions are likely to modulate intracellular Ca^{2+} dynamics and, consequently, the excitability and neurotransmission of neurosecretory cells (Slowik et al., 2023).

The therapeutic implications of blocking TRPC channels with 2-APB in the presence of Ang II during hypoxia might have particular relevance to COPD. In COPD it is expected that the patient is hypoxic and has a rise in circulating Ang II (Gu et al., 1989, Kent et al., 2011, Kaparianos and Argyropoulou, 2011). Furthermore, these patients may experience periods of more severe acute hypoxia. By reducing the hypoxic sensitivity of the CB, 2-APB may reduce excessive neural responses that could contribute to acute cardiovascular complications e.g. stroke or arrhythmia. Whilst more work is needed to establish this, this data opens up possibilities for utilizing TRPC channel blockers as a therapeutic strategy to modulate CB hypersensitivity associated with CH and high Ang II. A summary of the potential mechanism of 2-APB mediated inhibition of type I cell function (in the presence of Ang II) is presented in Figure 5.14.
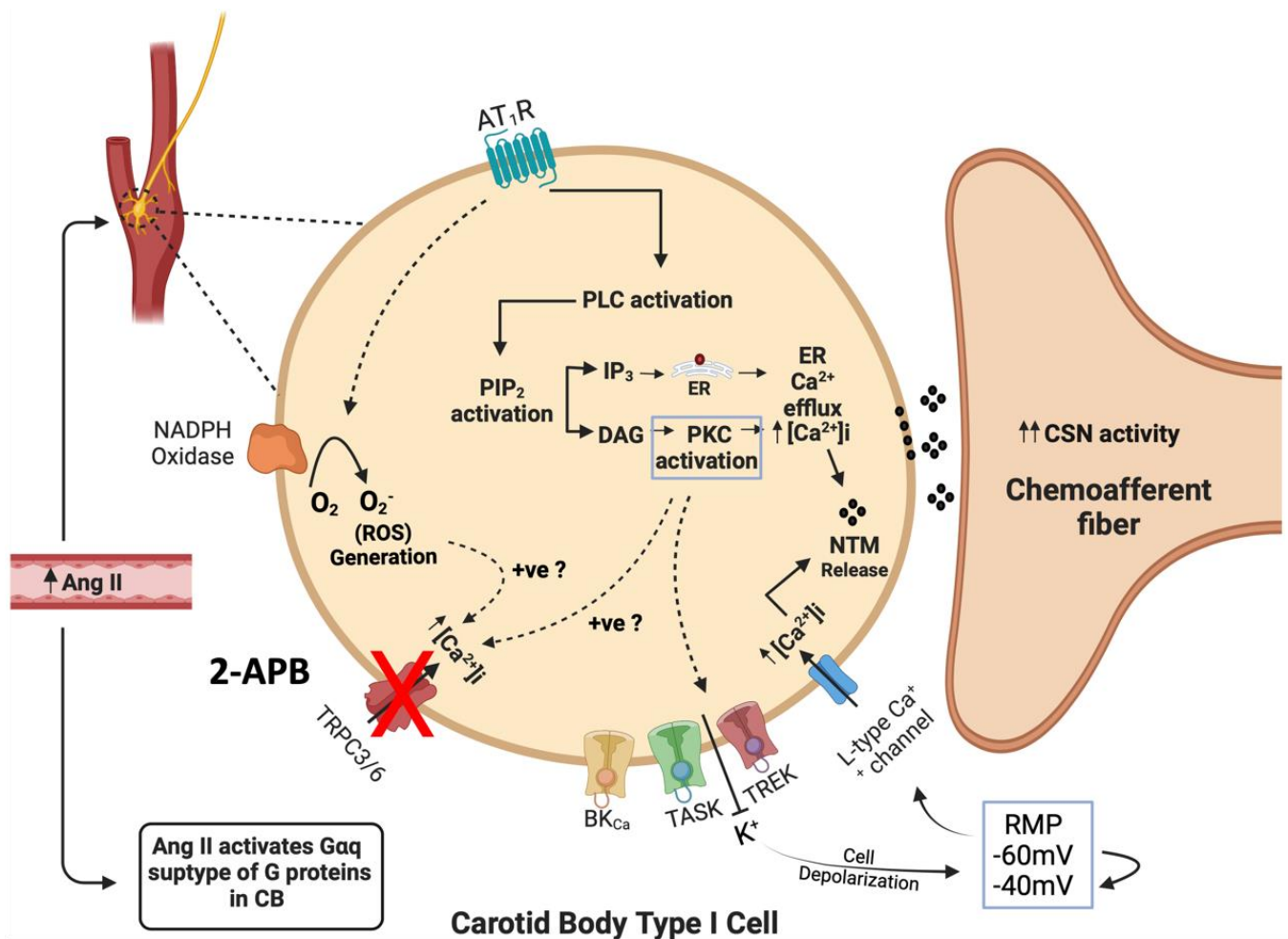
Figure 5.17 Potential mechanism of 2-APB mediated inhibition of type I cell function in the presence of angiotensin II (Ang II).

This figure illustrates the proposed mechanism of the effect of 2-APB on the carotid body (CB) type I cells in the presence of Ang II. After the activation of AT_1R, Ang II may activate TRPC channels via PKC mediated phosphorylation or NADPH-oxidase dependent oxidation. This will contribute to a greater cellular depolarisation and/or rise in intracellular Ca^{2+} promoting enhanced neurotransmitter release. By blocking TRPC channels, 2-APB therefore decreases the intensity of depolarization, Ca^{2+} elevation and neurotransmitter release.

5.4.5 Chapter conclusion

In conclusion, the impact of Ang II on CB function is highly complex; from the short and variable response kinetics to the dependencies on baseline activity, and induction of sensory LTF. Importantly, the overall action of Ang II appears to be exaggerated following CH, producing more consistent and better maintained responses in normoxia and a greater inhibitory action in acute hypoxia. The data also suggests that blocking TRPC channels with 2-APB in the presence of Ang II reduces carotid sinus nerve activity and this effect is more apparent in CH. The prospect of CB-targeted interventions based around TRPC inhibition to improve cardiovascular outcomes in pathologies associated with CH and high Ang II levels (e.g. COPD) is an intriguing future avenue and could offer translation between scientific insights and clinical applications in cardiovascular and respiratory medicine.

Chapter 6. Investigating the influence of TRP channel blockade and CH adaptation on cardiovascular and respiratory responses to acute hypoxia

6.1 Chapter introduction and overview

In vivo cardiovascular/respiratory recording is a crucial method for assessing the dynamic physiological parameters that underlie cardiovascular and respiratory function. This approach involves real-time monitoring and analysis of key parameters, including Arterial Blood Pressure (ABP), Heart Rate (HR), Tidal Volume (Vt) and Respiratory frequency (Rf). These parameters provide valuable insights into the overall cardiovascular and respiratory health of individuals, allow for analysis of responses to different pathophysiological stimuli and help with determination of surgical/pharmacological interventions.

ABP, which is the force exerted by circulating blood against the arterial walls (Gorny, 1993, McGhee and Bridges, 2002), is a fundamental indicator of cardiovascular function (Qammar et al., 2022). Continuous ABP monitoring provides real-time data on pressure fluctuations during the cardiac cycle. CH, a condition characterized by prolonged low O_2 levels in the body's tissues, has been recognized as a significant factor influencing various physiological processes (Pierson, 2000), including cardiovascular function (Abe et al., 2017). One of the notable effects of CH (a common feature of COPD) is its impact on blood pressure (Calbet, 2003). Evidence suggests that one of the main co-morbidities associated with COPD is hypertension (Chatila et al., 2008). Understanding the mechanisms through which CH induces hypertension in COPD can help to guide therapeutic strategies.

Acute hypoxia triggers the inhibition of potassium channels in the CB, leading to cell depolarization, calcium influx, and neurotransmitter release (Kumar, 2007). This activates the glossopharyngeal nerve,

increasing respiratory rate and tidal volume via the medulla oblongata (Zoccal et al., 2024). Concurrently, the sympathetic nervous system releases catecholamines, raising HR and BP through vasoconstriction (Iturriaga et al., 2016a), while peripheral tissues experience vasodilation, and the pulmonary circulation undergoes hypoxic pulmonary vasoconstriction to optimize gas exchange (Ortega-Sáenz and López-Barneo, 2020).

On the other hand, CH stabilizes HIF, increasing erythropoietin and vascular endothelial growth factor, leading to higher red blood cell production and angiogenesis (Ramakrishnan et al., 2014). Chronic sympathetic activation and endothelin-1 production cause persistent hypertension, with renal adaptations influencing the renin-angiotensin-aldosterone system, leading to fluid retention and further elevated BP (Saxena et al., 2018). CH can lead to an elevation in blood pressure, a phenomenon referred to as hypoxia-induced hypertension (Calbet, 2003). This elevation is primarily attributed to the activation of the sympathetic nervous system and the renin-angiotensin-aldosterone system (Calbet, 2003). One of the areas that is less well characterised is the mechanism accounting for this increase in sympathetic nerve activity. In response to acute hypoxia, the body activates reflexes to sustain enough perfusion (and O_2 delivery) to the vital organs (Michiels, 2004, Pierson, 2000). This includes, systemic vasoconstriction, an elevation in HR, the release of hormones (such as adrenaline) and a rise in VE. However, chronic activation of these reflexes in COPD/CH, may contribute to the development of hypertension (Xie et al., 2001, Calbet, 2003, Kumar, 2009). A link between the CB and heightened sympathetic nerve activity has been proposed in COPD patients (Phillips et al., 2018). In the previous Chapter it was shown that the CB is hyperactive in CH subjects. It is therefore hypothesised that reducing CB activity in CH animals will have a larger impact on ABP and HR than in control subjects.

CH could also impair the function of endothelial cells that line blood vessels, which again could contribute to the onset of hypertension (Wong et al., 2017). Mechanisms such as endothelial nitric oxide production as well as an increase in ROS generation could act to induce an imbalance between vasoconstrictive and vasodilatory factors, leading to increased vascular resistance and higher blood pressure (Masaki and Sawamura, 2006, Sandoo et al., 2010, Nadar et al., 2004, Marshall, 2015).

It Is also well-recognized that CH contributes to the development of pulmonary hypertension (Ball et al., 2014), a condition where blood pressure in the pulmonary arteries becomes elevated (Foris et al., 2013). Again, this is very common in individuals with chronic lung diseases such as COPD (Wrobel et al., 2012). The chronically hypoxic environment triggers persistent hypoxic pulmonary vasoconstriction, leading to an increased vascular resistance to blood flow and eventually this can cause right-sided cardiac hypertrophy and failure (Sylvester et al., 2012).

General anaesthesia (GA) plays a critical role in various medical procedures, enabling comfort and co-operation during cardiovascular measurements. While GA can provide benefits, its effects on physiological parameters such as ABP, HR, Rf, and VT must be carefully considered (Albrecht et al., 2014). GAs, to a greater or lesser extent, all depress the central nervous system (Unoki et al., 2009) and may alter autonomic balance which can lead to changes in ABP, HR, Rf and Vt. Some GAs may cause bradycardia or even arrhythmias (Liu et al., 2011), while others might lead to tachycardia due to altered sympathetic and parasympathetic activity (Tobias and Leder, 2011). Respiratory depression is also a concern, with GA potentially reducing Rf and Vt, affecting O_2 saturation and ventilation (Saraswat, 2015).

GA induces depression of the central nervous system and may influence the CBs ability to detect hypoxia, which collectively may restrict the initiation of appropriate reflex responses (Dahan and Teppema, 2003). Depending on the type and depth of GA, the CBs sensitivity to changes in O_2 levels may be blunted, potentially leading to diminished reflex-mediated adjustments in ABP, HR, Rf, and Vt (Pandit, 2014). This can have implications for maintaining adequate oxygenation and ventilation during cardiovascular measurements.

TRP channels play a crucial role in various pathophysiology, including respiratory disorders (Zholos, 2015). Dysregulation of TRP channels has been implicated in respiratory conditions such as asthma, chronic obstructive pulmonary disease (COPD), and pulmonary hypertension, where they contribute to airway inflammation, bronchoconstriction, and pulmonary vascular remodelling (Abbott-Banner et al., 2013). Additionally, TRP channels, particularly those expressed in the CB, participate in respiratory rhythm generation and modulation, influencing breathing patterns and responses to Hx and Hc (Iturriaga et al., 2021). In CH, TRP channels in the CB, undergo alterations in expression and activity, contributing to enhanced sensory responses and adaptive physiological changes to low oxygen levels (Iturriaga et al., 2021). The previous Chapter highlights an important new role of the interaction between AngII signalling and TRPC channel activation in the CB, which appears to be more important in CH animals. A key next aim is to determine if targeting of TRPC channel signalling in the CB *in vivo* induces key cardiovascular alterations, and see if this is exaggerated in CH animals who are proposed to have higher levels of Ang II and increased levels of AT1R expression/supercluster formation.

2-Aminoethoxydiphenyl borate, commonly known as 2-APB, is a chemical compound that acts as an inhibitor of inositol trisphosphate receptors (IP_3Rs) and transient receptor potential (TRP) channels (Maruyama et al., 1997, Colton and Zhu, 2007, Delmas et al., 2002). 2-APB plays a crucial role in modulating intracellular calcium signalling and regulating various cellular processes such as neurotransmitter release (Thyssen et al., 2013). Its ability to manipulate calcium fluxes has made 2-APB a valuable tool to understand the intricacies of cellular signalling pathways. 2-APB is recognized as a modulator of TRP channels, influencing their activity in a complex manner (Colton and Zhu, 2007). Depending on the specific TRP channel subtype and concentration used, 2-APB can either activate or inhibit TRP channels, making it a versatile tool for investigating these channels' diverse roles in sensory perception, cellular signalling, and various physiological processes (Chokshi et al., 2012).

2-APB is known for its ability to block transient receptor potential canonical (TRPC) channels (Colton and Zhu, 2007). TRPC channels are a subgroup of TRP channels, and 2-APB acts as an antagonist for several TRPC channel subtypes (Colton and Zhu, 2007). By blocking TRPC channels, 2-APB can effectively disrupt calcium signalling pathways and inhibit calcium influx into cells (Kim et al., 2015), which is crucial for regulating various cellular processes such neuronal excitability (Rather et al., 2023).

TRPC channels are expressed in the CB, particularly in the type I glomus cells, and they are suggested to play an important role in regulating CB activity (Iturriaga et al., 2021, Buniel et al., 2003a, Kumar et al., 2006c). These channels are proposed to be important in transducing hypoxic and hypercapnic signals into changes in membrane potential and intracellular calcium concentrations within the glomus cells (Iturriaga et al., 2021). When exposed to hypoxia or hypercapnia, TRPC channels are activated, leading to depolarization of the cell membrane and an increase in intracellular calcium (Kumar P. et al., 2006, Kim et

al., 2015) . This depolarization triggers Ca^{2+} influx, the release of neurotransmitters, such as dopamine and ATP, which in turn stimulate the sensory nerve fibres connected to the CB (Iturriaga et al., 2021). These nerve signals are then relayed to the brainstem to initiate the appropriate cardiovascular and respiratory responses, (Lindsey et al., 2018). Understanding the role of TRPC channels in CB activity is crucial in the context of respiratory physiology and my help to explain the body's ability to maintain O_2 and carbon dioxide homeostasis.

In other cell types it has been shown that Ang II can evoke TRPC channel activation, enhancing cell excitability (Dryer et al., 2019, Forrester et al., 2018, Ilatovskaya et al., 2015, Feng et al., 2022, Shi et al., 2010). A similar mechanism may be present in the CB. It was therefore hypothesised that an upregulation of Ang II signalling in CH, would promote exaggerated TRPC activation which could account for CB hyperactivity. In the previous Chapter it was demonstrated that 2-APB had a profound effect on the *ex vivo* CB sensory nerve activity in both N and CH animals. Furthermore, this effect was apparent in the presence of Ang II stimulation of the CB, possibly indicating a link between Ang II signalling and TRPC channel activation in the CB. The primary aim of the current chapter was to explore if 2-APB was able to inhibit the CB *in vivo* leading to a reduction in ABP and HR, an effect that was hypothesised to be exaggerated in CH animals.

6.1.1 Chapter hypotheses

- CH alters cardiovascular parameters, such as increased ABP and HR.

- In CH, an increase in Ang II signalling and exaggerated TRPC channel activity promotes CB hyperactivity and chronic reflex activation accounting for a rise in ABP. This could be restored by 2-APB, a TRPC channel blocker.

6.1.2 Aims of this Chapter

- Using *in vivo* measurements of cardiovascular and respiratory function, I will test whether CH has any influence on the cardiovascular and respiratory systems such as an increase in HR or a rise in ABP.

- Investigate if inhibitory targeting of the CB and TRPC channels using 2-APB, has a greater effect on ABP, HR and VE in CH compared to normal rats, either in normoxia and/or during exposure to acute hypoxia.

6.2 Chapter methods

6.2.1 Animals

All animal procedures were performed in accordance with UK Animals (Scientific Procedures) Act 1986 and approved by the UK Home Office (PPL number PP9019875) and by the Animal Welfare and Ethical Review Body (AWERB) at the University of Birmingham. A total of 13 adult male Wistar rats were randomly split into two groups (normoxia rats (N) n=7 and chronic hypoxia rats (CH) n=6). Animals weighed between 237-350g. All animals were housed in individually ventilated cages, with free access to food and water, and under standard conditions: 12:12 hour light:dark cycle (lights on at 0700), 22°C and 55 % humidity.

CH protocols were the same as those described in Chapters 4 and 5. Briefly, CH rats were exposed to an F_iO_2 of 12% for 10 days using a dynamic O_2 controller and dedicated small animal chamber (BioSpherix, Parish, NY, USA). Animal welfare checks, CO_2 and humidity levels, replacement of silica gel and soda lime, and food and water replenishment were performed daily.

6.2.2 *In vivo* cardiovascular recording procedure

The surgical preparation was not performed by the author of this thesis, but by other members of the research team. The author performed the experimental protocols under supervision, acquired data and performed all data analysis.

Animal weight was recorded before they were taken to the theatre to undergo *in vivo* cardiovascular function measurements. The rat was first anesthetized with 4-5% inhaled isoflurane mixed with O_2 at a flow rate of 1.5 L min^{-1} using an anaesthesia induction chamber. For surgical anaesthesia maintenance, isoflurane inhalation was continued through a rodent face mask, 2-4% isoflurane in O_2, delivered at a flow rate of 1.5 L min^{-1}. Surgical anaesthesia depth was determined as sufficient based on the loss of a pedal withdrawal reflex. The rat was placed on a surgical table, equipped with heating system, to maintain the body temperature at 37°C throughout the whole procedure. A catheter was then inserted into the femoral vein to begin infusion of alfaxalone (Alfaxan®; Vetoquinol UK Ltd, Towcester, UK), at a rate of 17-20 mg per kilogram of body weight per hour, using an infusion pump (Perfusor Space; B.Braun, UK). Once the alfaxalone infusion was started, the isoflurane inhalation was stopped. Surgical anaesthetic levels were continuously monitored throughout the procedure by testing for the absence of a pedal withdrawal reflex and 0.1 mL boluses of alfaxalone was given as needed. After establishing a patent line for alfaxalone, a second femoral vein was cannulated, as a route for 2-APB administration, Figure 6.1.
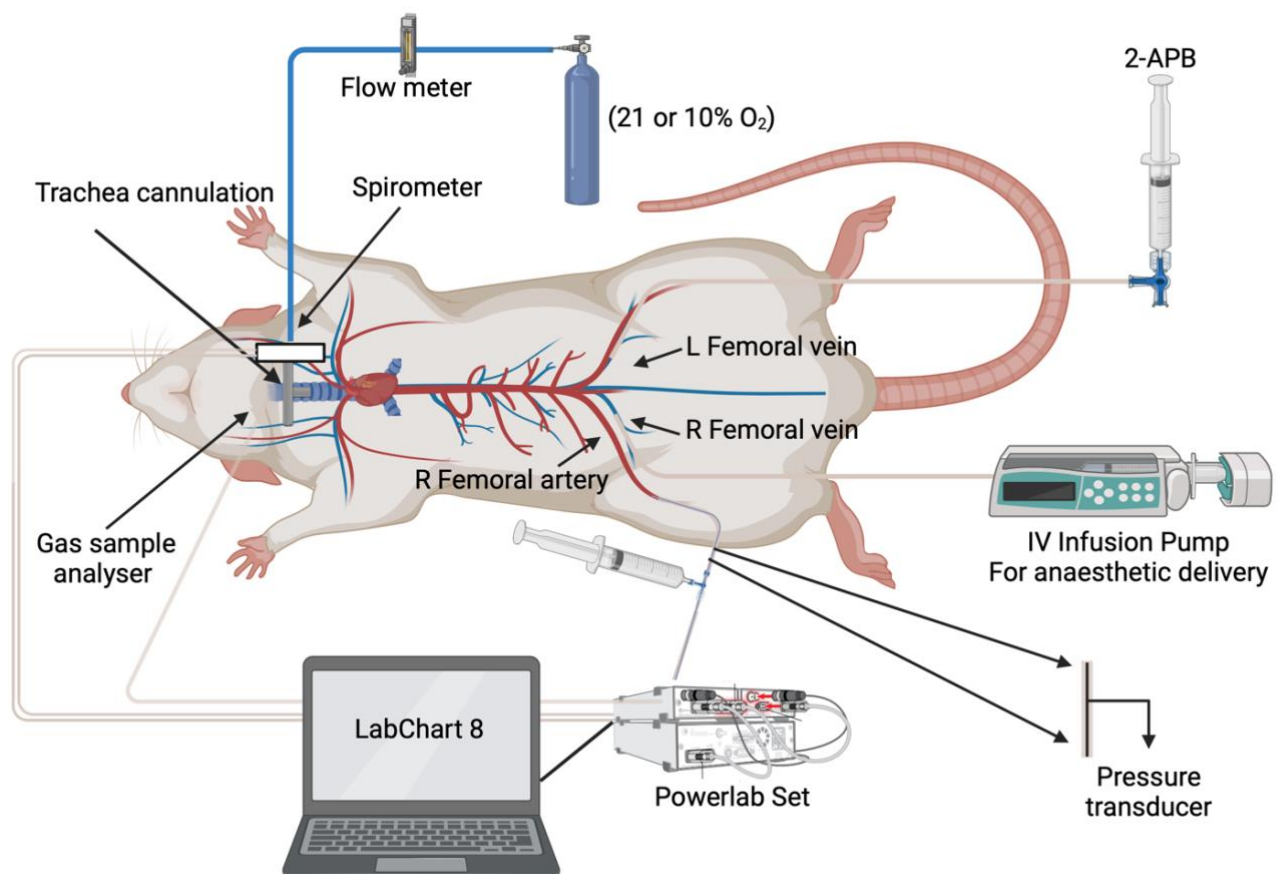
Figure 6.1 A diagram illustrating the in vivo cardiovascular experiment set up.

The figure includes femoral vein cannulations, tracheal cannulation, placement of the spirometer, the site of gas analyser used to measure end tidal O_2 and CO_2, cannulation of the femoral artery and connection of the pressure transducer to measure arterial blood pressure and calculate heart rate. Animals breathed either 21% O_2 (normoxia) or 10% O_2 (hypoxia) delivered via gas cylinders and controlled using flow meters. 2-APB was delivered via bolus through the left femoral vein.

After the two venous cannulas were placed successfully, a femoral artery was then cannulated with a catheter and connected to a pressure transducer (ADInstruments, Oxford, UK) to continually measure the ABP. All catheters were flushed regularly with a heparinised saline to prevent blood clots. The ABP signals were digitised using a PowerLab (ADInstruments, Oxford, UK) at a rate of 100 samples per second. The HR and calculated from the ABP in LabChart by identifying the frequency of repeating cyclic waveforms, while

the MAP was calculated as the derived cyclic mean of the ABP measurements using the following equation (1/3 systolic blood pressure + 2/3 diastolic blood pressure) available in the DataPad window of LabChart version 8 (AD Instruments, Oxford, UK).

A tracheal tube was used to cannulate the trachea to facilitate breathing and to control the desired F_iO_2 delivered to the rat (21% F_iO_2 for normoxia or 10% F_iO_2 for hypoxia). Gas was delivered using cylinders containing pre-mixed gas mixtures at a flow rate of 1.5 L min^{-1}, controlled using a flow meter (Cole-Parmer, St Neots,UK). To measure the airflow, a spirometer was connected to the tracheal tube, and Vt and Rf were derived from the air flow measurement in LabChart 8 (ADInstruments, Oxford, UK). Intermittently, a gas sample analyser (connected to Powerlab) was placed on tracheal tube to obtain end tidal O_2 and CO_2 samples.

6.2.3 *In vivo* cardiovascular recording protocol

The protocol started with 20 to 30 minutes of stabilisation after the surgery, followed by 5 minutes recording of baseline. After obtaining a stable baseline for 5 minutes, a 10% O_2 hypoxic gas mixture was be administered for 5 minutes, followed by 5 minutes of recovery. After 5 minutes of recovery and after ensuring the recording is stable, a 2-APB bolus (10 mg kg^{-1}), dissolved in DMSO (Morihara et al., 2017, Vaidya et al., 2023), was administered intravenously through the left femoral vein, followed by 5 minutes stabilization, to allow enough time for 2-APB to produce its affect. After the 5 minutes, a 5 minute 2-APB baseline was recorded, followed by a 5-minute exposure to 10% O_2 (hypoxia) in the presence of 2-APB. When the hypoxic induction was completed, a final recovery period of 5 minutes was recorded. During the last 30s of each protocol phase, a gas sample was taken to analyse the ETO_2 and $ETCO_2$. This protocol is

summarised in Figure 6.2. All data were collected using a PowerLab (AD Instruments, Oxford, UK) connected to a PC. The baseline cardiovascular data used for analysis at were taken as an average of the last 5 minutes before inducing hypoxia. The data used for analysis of the response to hypoxia was taken as the average once a steady-state had been achieved.
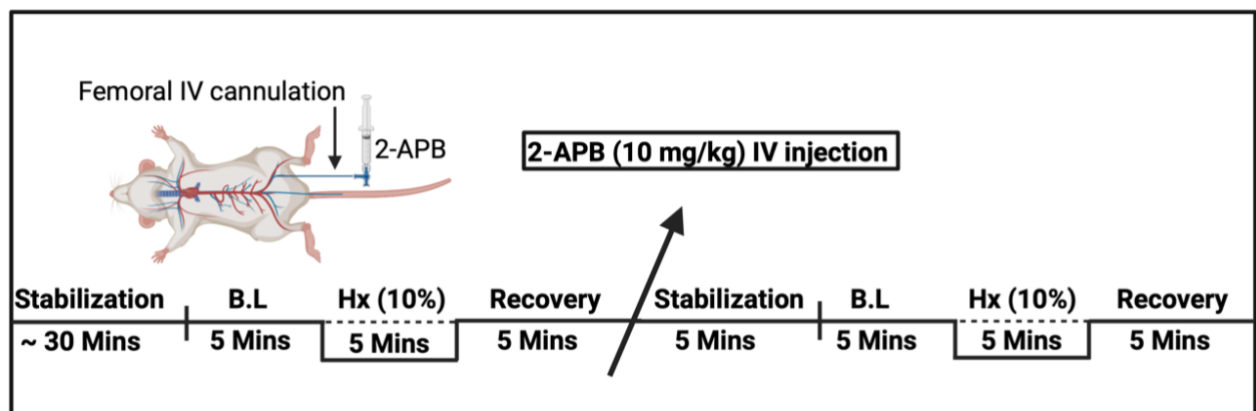
Figure 6.2 A summary of the in vivo protocol used to monitor cardiovascular responses to acute hypoxia (10% F_iO_2) before and after 2-APB administration.

This protocol was performed in normoxic (N) and chronically hypoxic (CH) animal groups.

6.2.4 Data Analysis

Data acquisition was obtained using LabChart 8 software (ADInstruments, Oxford, UK), where the ABP and airflow were measured directly. From LabChart, the HR was calculated from the ABP waveform. The Rf and Vt, were calculated from the air flow trace, using LabChart. ET_{O2} and ET_{CO2} were measured intermittently. Data were presented either as mean±SEM or as box whisker plots with the box representing the interquartile range and the whiskers extending to the maximum and minimum points. The median is also shown as a horizontal line. Individual points denote data from a single animal. Comparisons between N

and CH and/or the effect of 2-APB were tested using 2-way repeated measures ANOVA, or a Student's t test where appropriate using Prism 9 (GraphPad, Boston, MA, USA). Significance was taken as p<0.05.

6.3 Results

6.3.1 Mean arterial pressure (MAP) is not significantly altered during baseline recording in CH rats and is not modified by 2-APB

Mean time courses for N and CH showing baseline MABP and responses to acute hypoxia in the presence and absence of 2-APB are presented in Figure 6.3 A. Across the whole experiment there was no overall effect of CH on MABP (p=0.5734), Figure 6.3 A. Specific comparison of the mean MABP between N and CH at baseline (normoxia) indicates that the MABP of CH rats, (n=6, 146.3±4.916mmHg) was not altered compared to N (n=7, 140.4±6.490, p=0.4986) (Figure 6.3 B). The same results were seen during acute hypoxia (CH, n=6, MABP was 60.32±6.428mmHg, vs 54.03±7.097for N, p=0.5309) (Figure 6.3 C). In the presence of 2-APB, there was no difference in MABP between N and CH, when measured in normoxia or during acute hypoxia (Figure 6.3 D & E). The individual actions of 2-APB on MABP for N and CH are presented in Figure 6.4 A and 6.4 B respectively. When each group was analysed individually, to establish an understanding about the influence of 2-APB on MABP, the data indicates that 2-APB did not significantly modify MABP in either or CH animals, in normoxia or during acute hypoxia (Figure 6.4 A & B). These results indicate that CH does not induce hypertension in rats and 2-APB, when administered at this concentration, does not impact on the ABP.
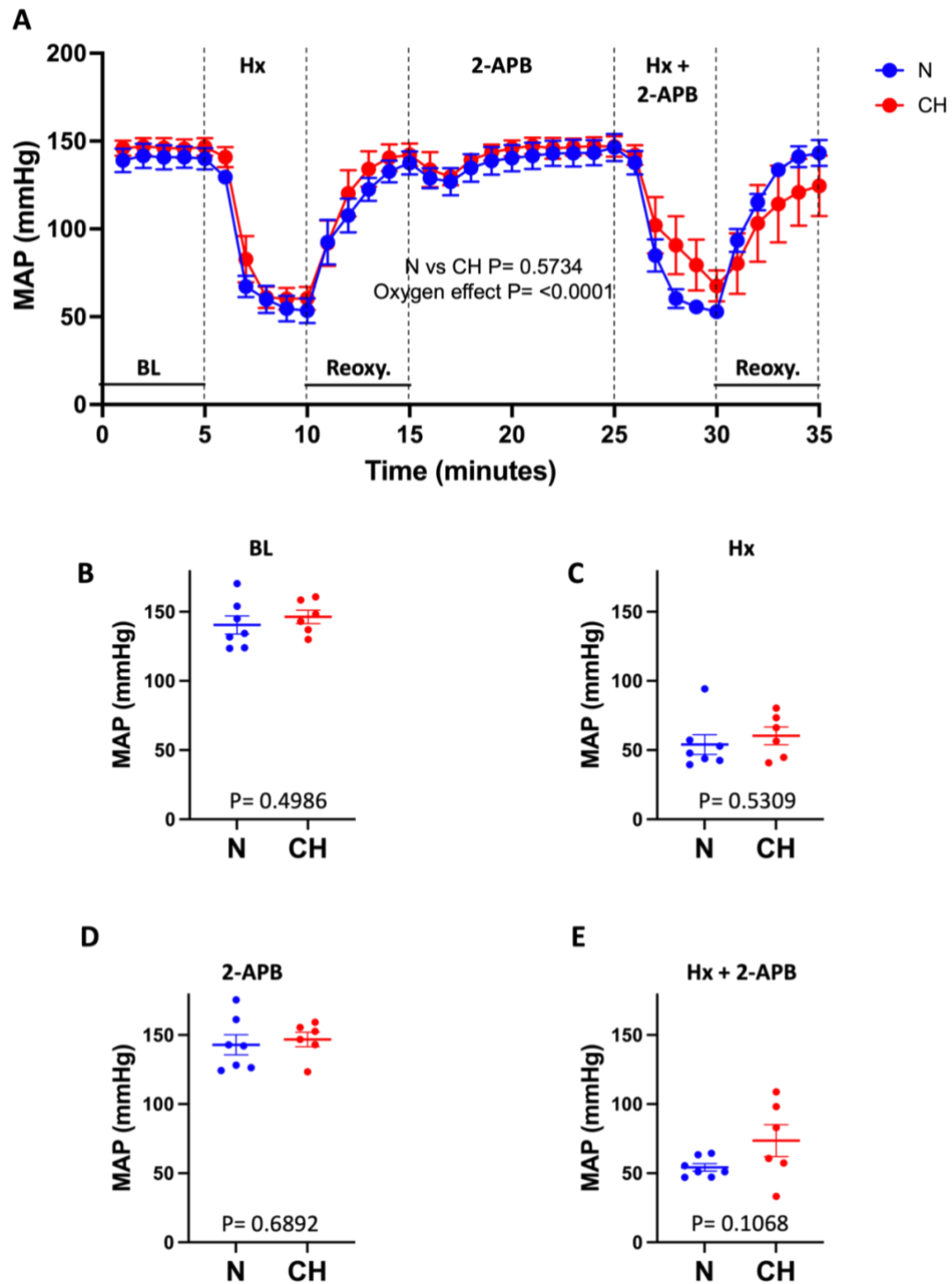
Figure 6.3 Chronic hypoxia (CH) does not significantly increase the mean arterial blood pressure (MABP) in the presence or absence of 2-APB.

A) Demonstrates a minute-to-minute time course of MABP for both groups, (CH n=6, N n=7 B) at baseline (normoxia) and in response to acute hypoxia, in the presence and absence of 2-APB. Data presented as mean±SEM, significance assessed between N and CH using a 2-way repeated measures ANOVA. (B-E) Mean MABP for N and CH animals when measured at baseline (normoxia) (B), in acute hypoxia (C), in normoxia plus 2-APB (D) and in hypoxia plus 2-APB (E). Data presented as mean±SEM. Individual dots represent data from a single animal. Significance tested using an unpaired Student's t-test.
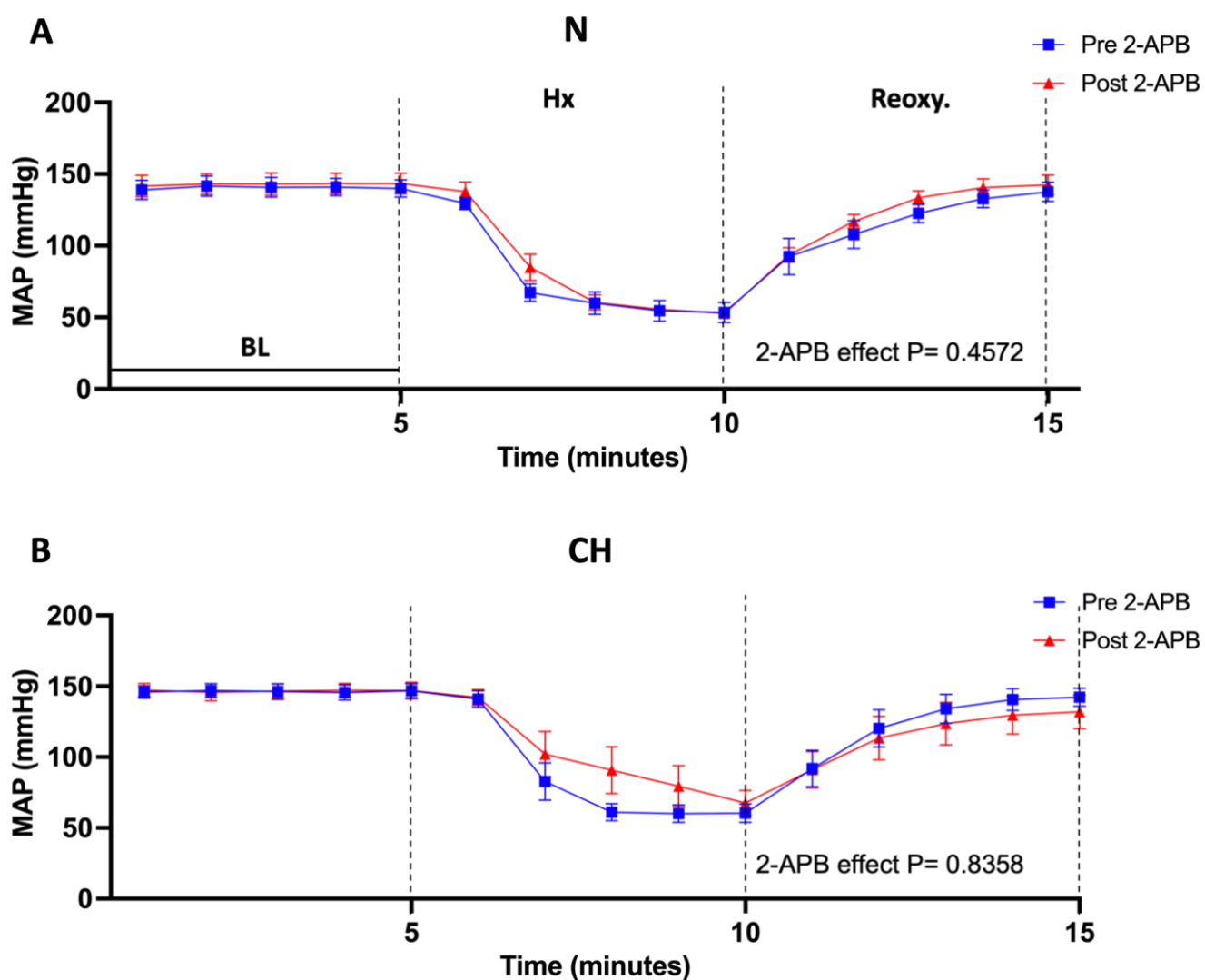
Figure 6.4 2-APB has no influence on mean arterial blood pressure (MABP), in either normoxic (N) or chronic hypoxic (CH) animals.

(A) Comparison of changes in MABP caused by hypoxia pre and post 2-APB administration in the N group, n=7. (B) Comparison of MABP response to hypoxia before and after 2-APB administration in the CH group, n=6. Data presented as mean±SEM, statistical test performed using 2-way repeated measures ANOVA.

6.3.2 The heart rate (HR) is not significantly changed in CH rats, and CH animals display reduced HR sensitivity to 2-APB administration

When measured throughout the entire time course, the overall effect of CH on the HR was not significant (p=0.3693) (figure 6.5 A). To confirm that, a specific time point analysis was performed and the results confirmed that there was no significant alteration in HR between N and CH rats. Despite the lower numerical HR seen in CH rats, in normoxia, the HR in CH group compared to N group was (CH 446.3±12.04bpm vs N 460.9± 9.402bpm, p= 0.3549) and this was not significantly different, Figure 6.5 B. The reduced HR was persistent in the CH group, compared to N group during acute hypoxia and it showed the tendency to be altered (CH 395.9±18.77 vs N 443.1±15.61 bpm, p= 0.0769) (Figure 6.5C). In addition, in the presence of 2-APB, the HR was not significantly different between N and CH when measured in normoxia and hypoxia (Figure 6.5 D & E).

The overall influence of 2-APB on HR was assessed in N and CH. The effect of 2-APB was to significantly depress HR in the N group (p=0.0089) (Figure 6.6 A) but not the CH group although it still tended to be lower throughout (p=0.1666) (Figure 6.6 B).
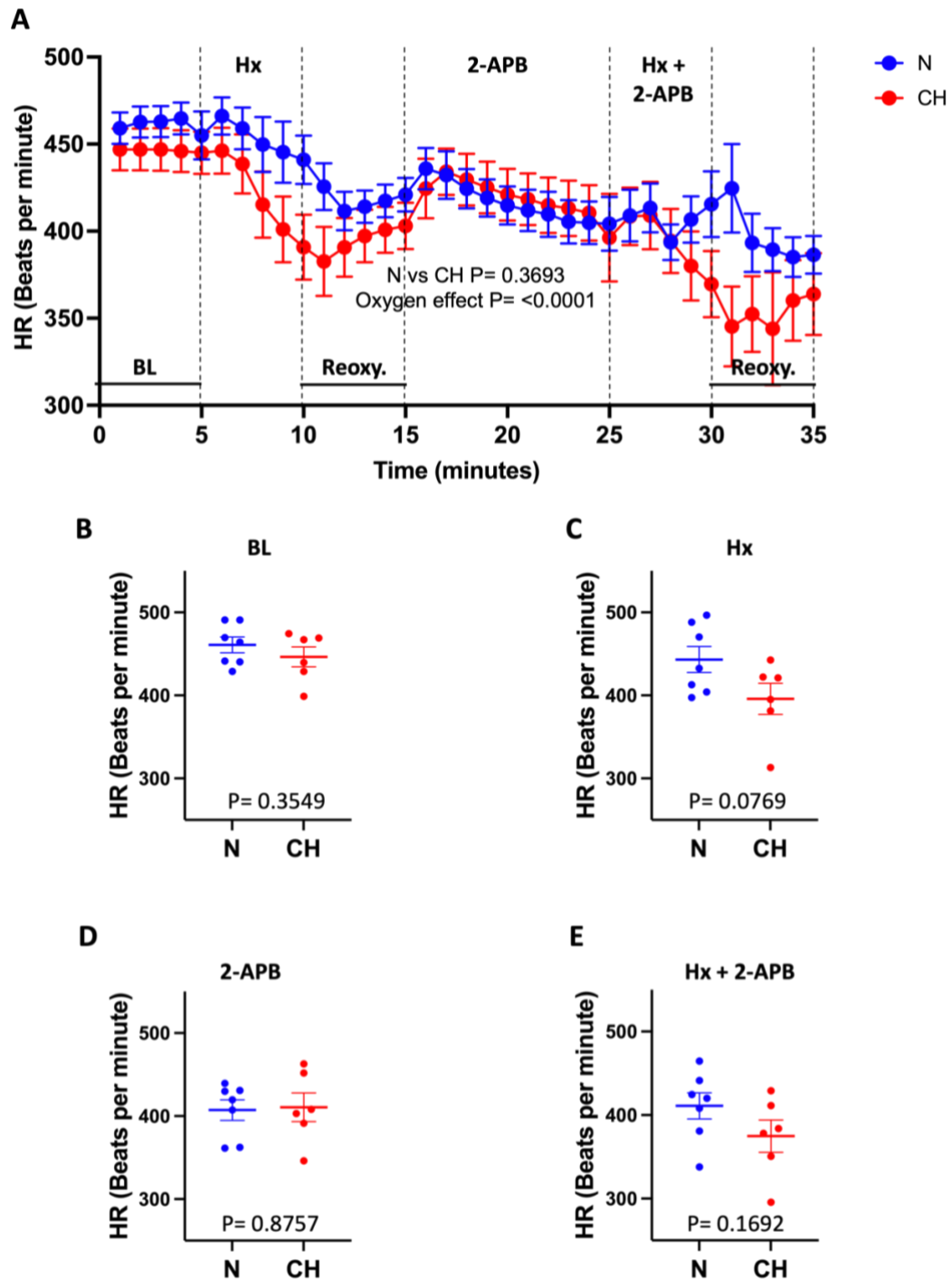
Figure 6.5 Chronic hypoxia (CH) does not impact heart rate (HR) before or after administration of 2-APB.

A) Time course of HR for CH (n=6) and N (n=7) at baseline (normoxia) and in response to acute hypoxia, in the presence and absence of 2-APB. Data presented as mean±SEM, significance assessed between N and CH using a 2-way repeated measures ANOVA. (B-E) Mean HR for N and CH animals when measured at baseline (normoxia) (B), in acute hypoxia (C), in normoxia plus 2-APB (D) and in hypoxia plus 2-APB (E). Data presented as mean±SEM. The horizontal line indicates the mean. Individual dots represent data from a single animal. Significance tested using an unpaired Student's t-test.
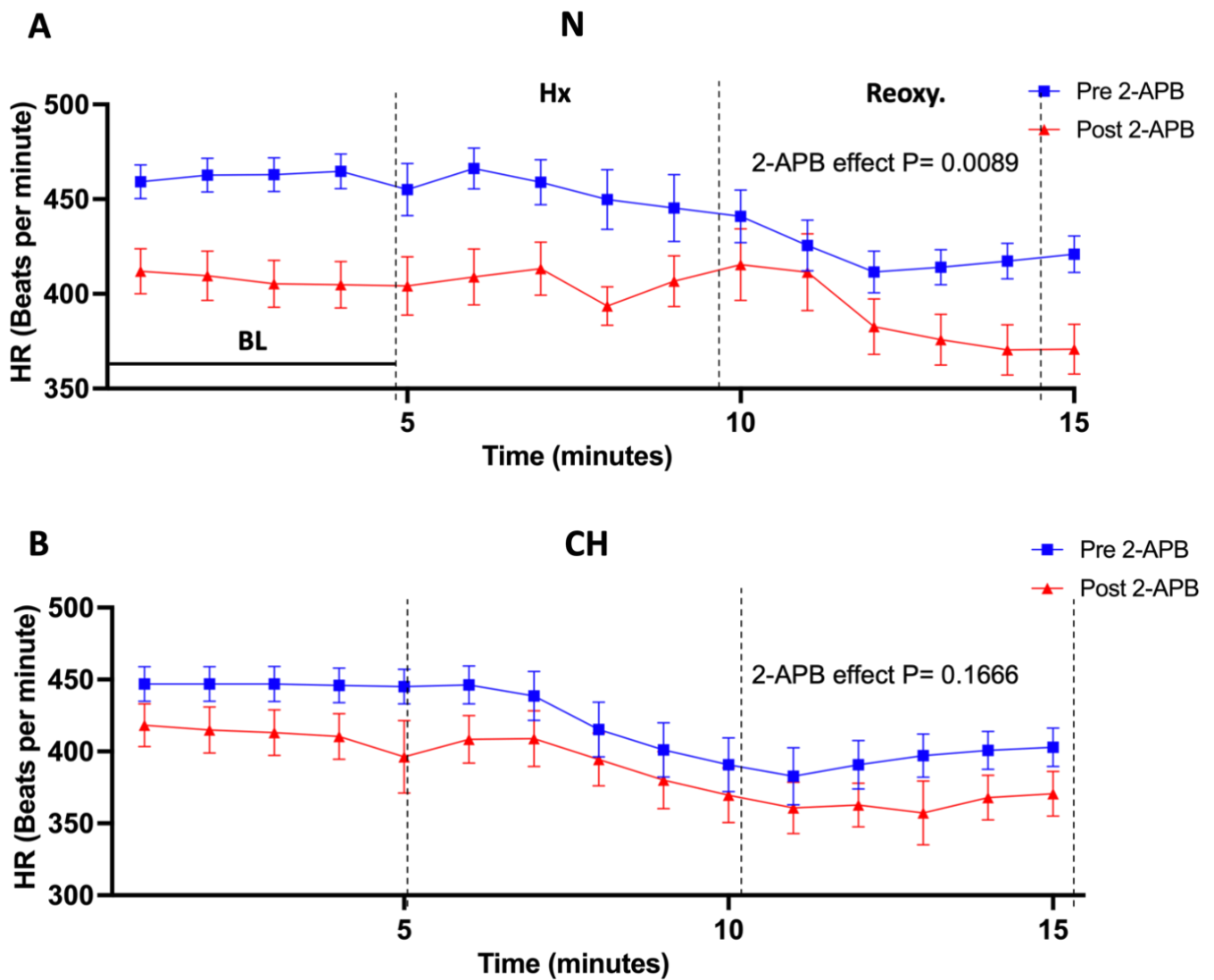
Figure 6.6 The effect of 2-APB on heart rate (HR) responses to hypoxia in chronic hypoxic (CH) and normoxic N animal groups.

(A) Comparison of changes in HR caused by hypoxia pre and post 2-APB administration in the N group, n=7. (B) Comparison of HR response to hypoxia before and after 2-APB administration in the CH group, n=6. Data presented as mean±SEM, statistical test performed using 2-way repeated measures ANOVA.

6.3.3 2-APB does not modify Rf responses to acute hypoxia in N or CH animals

In contrast to the WBP data presented in Chapter 4, *in vivo* recording under anaesthesia showed no overall effect of CH on Rf when measured across the entire experiment (Figure 6.7 A). Furthermore, specific comparisons made at baseline (normoxia) and hypoxia suggested no difference in Rf between N and CH (Figure 6.7 B & C). This was also consistent in the presence of 2-APB (Figure 6.7 D and E). Individual analysis of the overall effect of 2-APB was conducted for N and CH. 2-APB did not the modify the response to hypoxia in either N (p=0.4561) or CH (p=0.3431) (Figure 6.8 A & B).

6.3.4 2-APB does not modify Vt responses to acute hypoxia in N or CH animals

The Vt is one of the most critical indicators of ventilation and it mainly represents the involvement of the central respiratory centres in breathing regulation. *In vivo* recordings of Vt under anaesthesia showed no significant change of Vt in CH animals when measured across the whole experiment although there was a tendency for it to be depressed (p=0.1505) (Figure 6.9 A). Furthermore, more specific analysis indicated that CH rats did not exhibit any significant change in Vt during baseline (normoxic) ventilation or during exposure to acute hypoxia (Figure 6.9B & C). Following administration of 2-APB, CH animals still did not have any significant change in Vt, in normoxia and hypoxia (Figure 6.9 D & E). For a better understanding of the effect of 2-APB on CH and N rat groups, a pre and post 2-APB analysis was performed for each group (Figure 6.10). For both N (p=0.8160) and CH (p=0.9835) 2-APB did not affect the Vt response to acute hypoxia (Figure 6.10 A & B). These findings suggest that under these specific conditions single bolus administration of 2-APB had minimal impact on the ventilatory response to hypoxia in both N and CH animals.
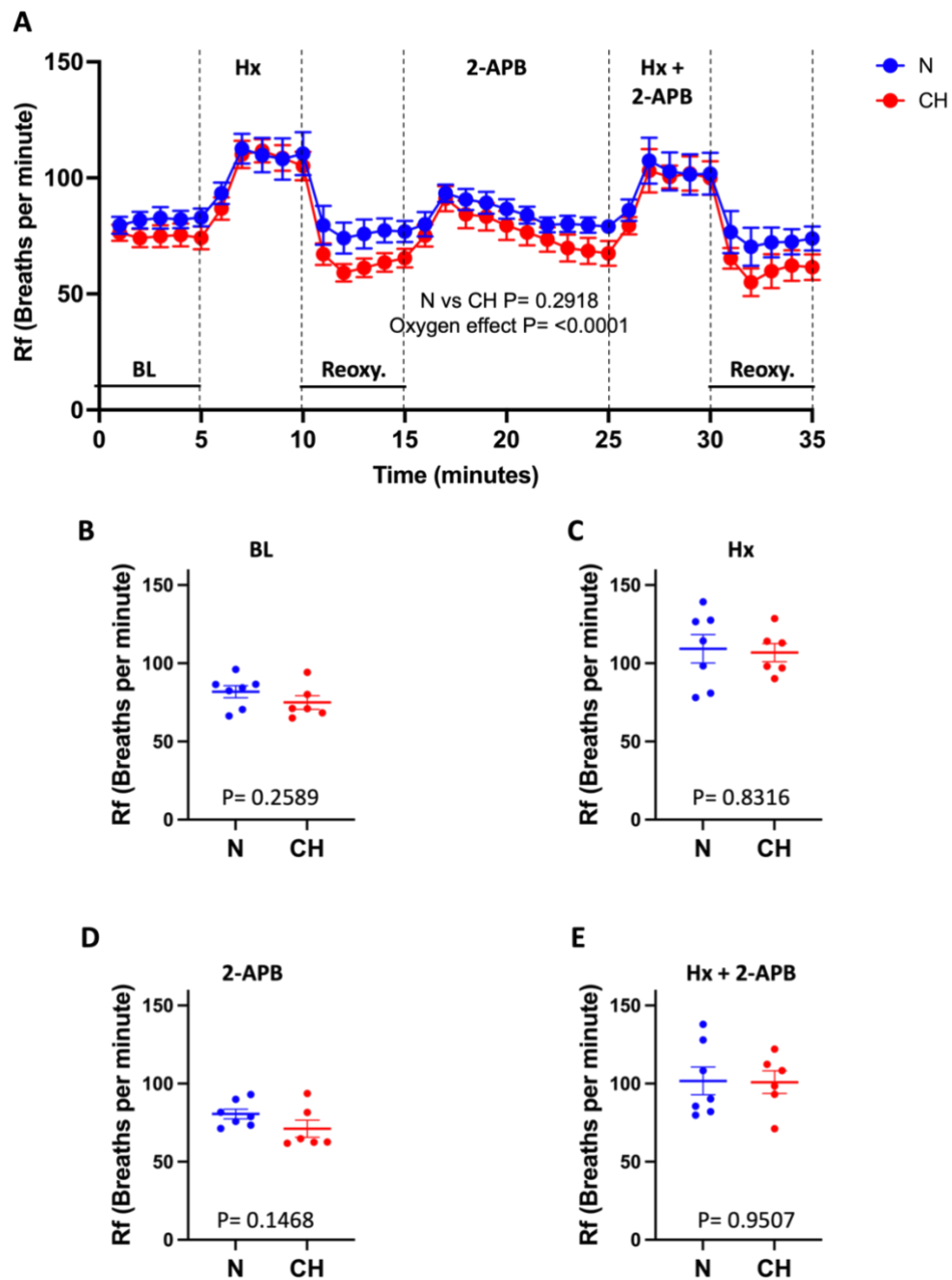
Figure 6.7 When measured under general anaesthesia, chronic hypoxia (CH) does not modify respiratory frequency (Rf) in normoxia, in response to acute hypoxia or following administration of 2-APB.

A) Time course of Rf for CH (n=6) and N (n=7) at baseline (normoxia) and in response to acute hypoxia, in the presence and absence of 2-APB. Data presented as mean±SEM, significance assessed between N and CH using a 2-way repeated measures ANOVA. (B-E) Mean Rf for N and CH animals when measured at baseline (normoxia) (B), in acute hypoxia (C), in normoxia plus 2-APB (D) and in hypoxia plus 2-APB (E). Data presented as box plots with box indicating the interquartile range and the whiskers extending to the maximum and minimum points. The horizontal line indicates the median. Individual dots represent data from a single animal. Significance tested using an unpaired Student's t-test.
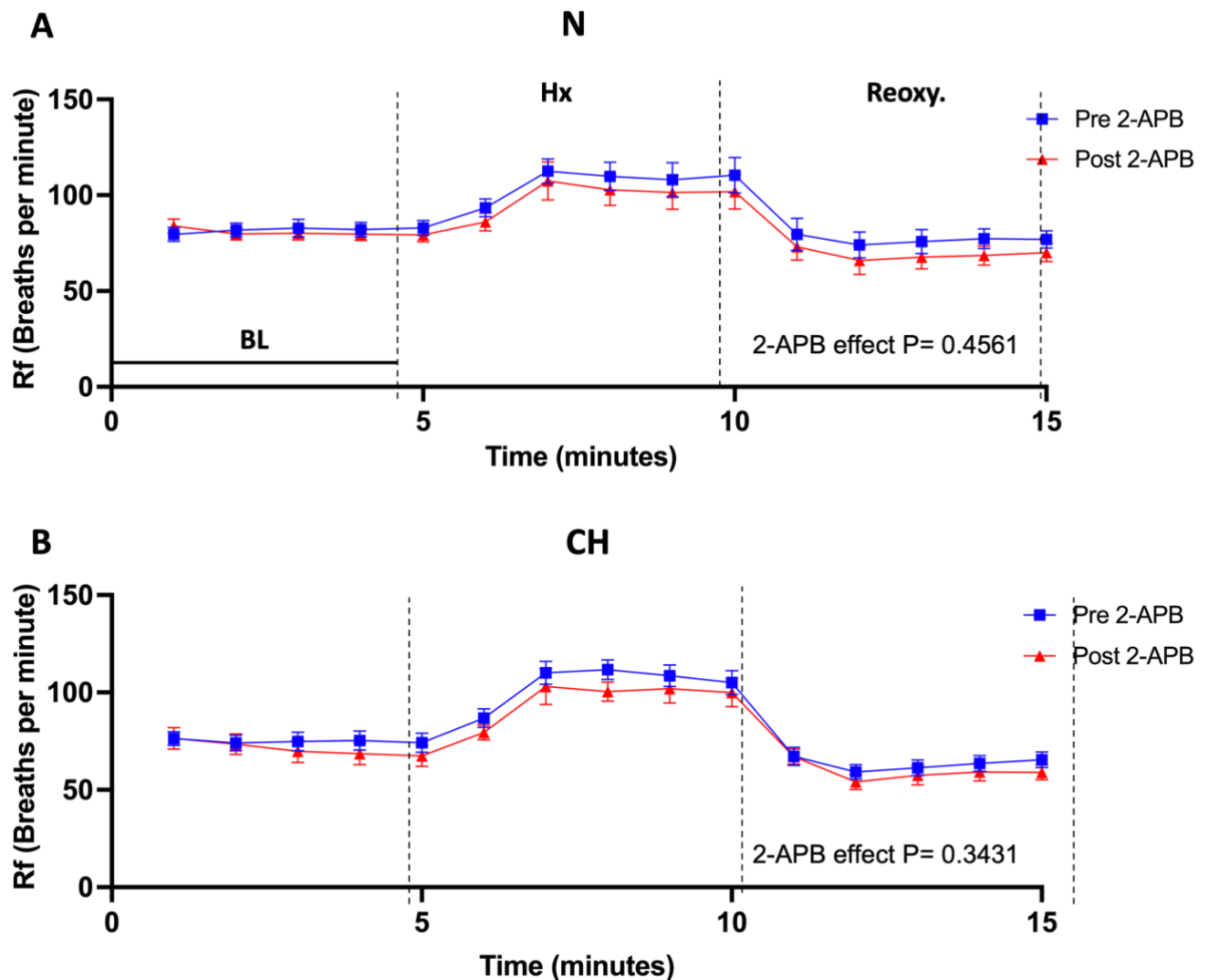
Figure 6.8 2-APB does not attenuate the Rf response to acute hypoxia in normoxic (N) or chronic hypoxic (CH) animals

(A) Rf responses to hypoxia pre and post 2-APB administration in the N group, n=7. (B) Rf responses to hypoxia before and after 2-APB administration in the CH group, n=6. Data presented as mean±SEM, statistical test performed using 2-way repeated measures ANOVA.
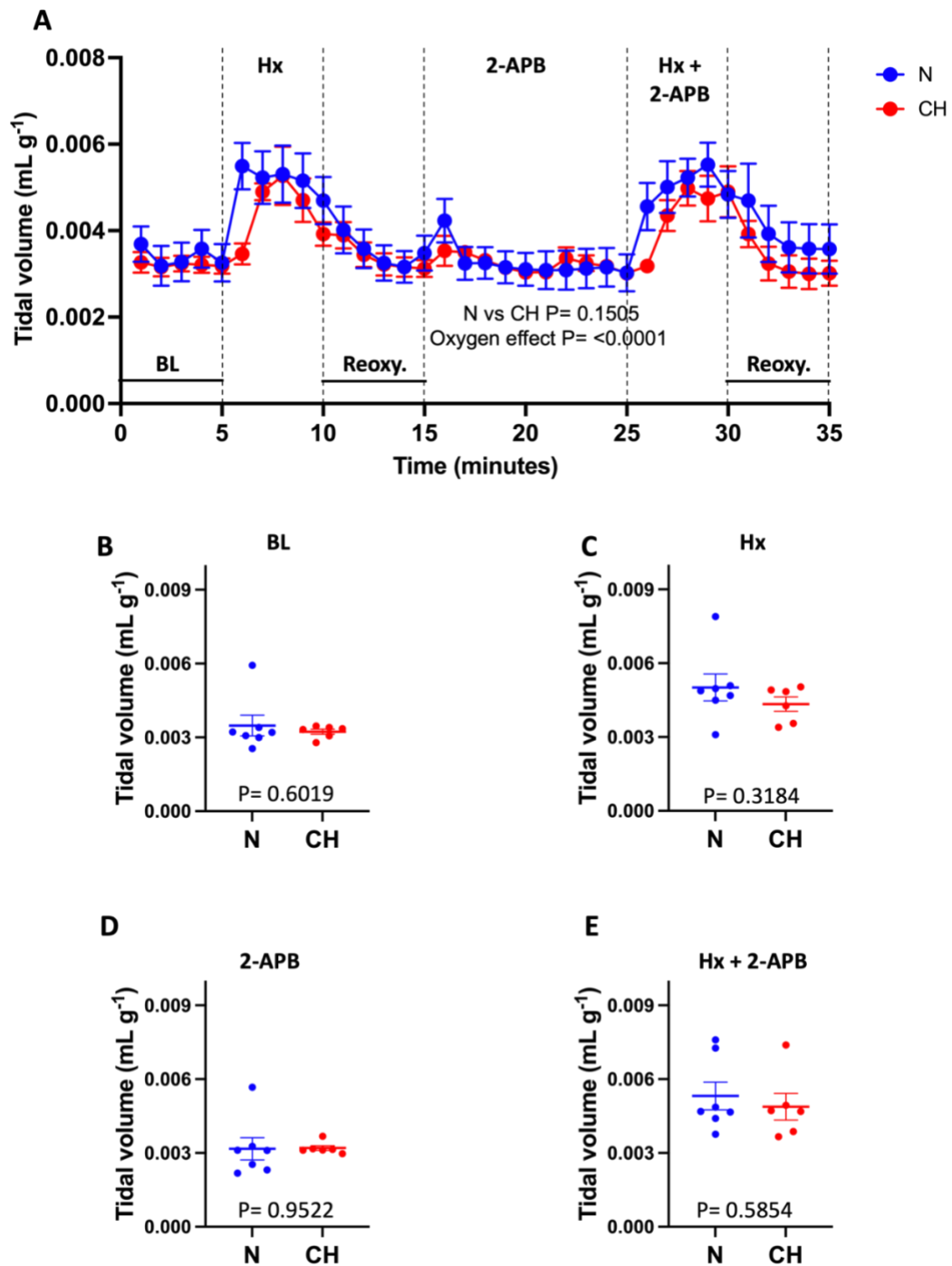
Figure 6.9 When measured under general anaesthesia chronic hypoxia (CH) attenuated tidal volume (Vt) before and after administration of 2-APB.

A) Time course of Vt for CH (n=6) and N (n=7) at baseline (normoxia) and in response to acute hypoxia, in the presence and absence of 2-APB. Data presented as mean±SEM, significance evaluated between N and CH using a 2-way repeated measures ANOVA. (B-E) Grouped Vt data for N and CH animals when measured at baseline (normoxia) (B), in acute hypoxia (C), in normoxia plus 2-APB (D) and in hypoxia plus 2-APB (E). Data presented as mean±SEM, the horizontal line indicates the mean. Individual dots represent data from a single animal. Significance tested using an unpaired Student's t-test.
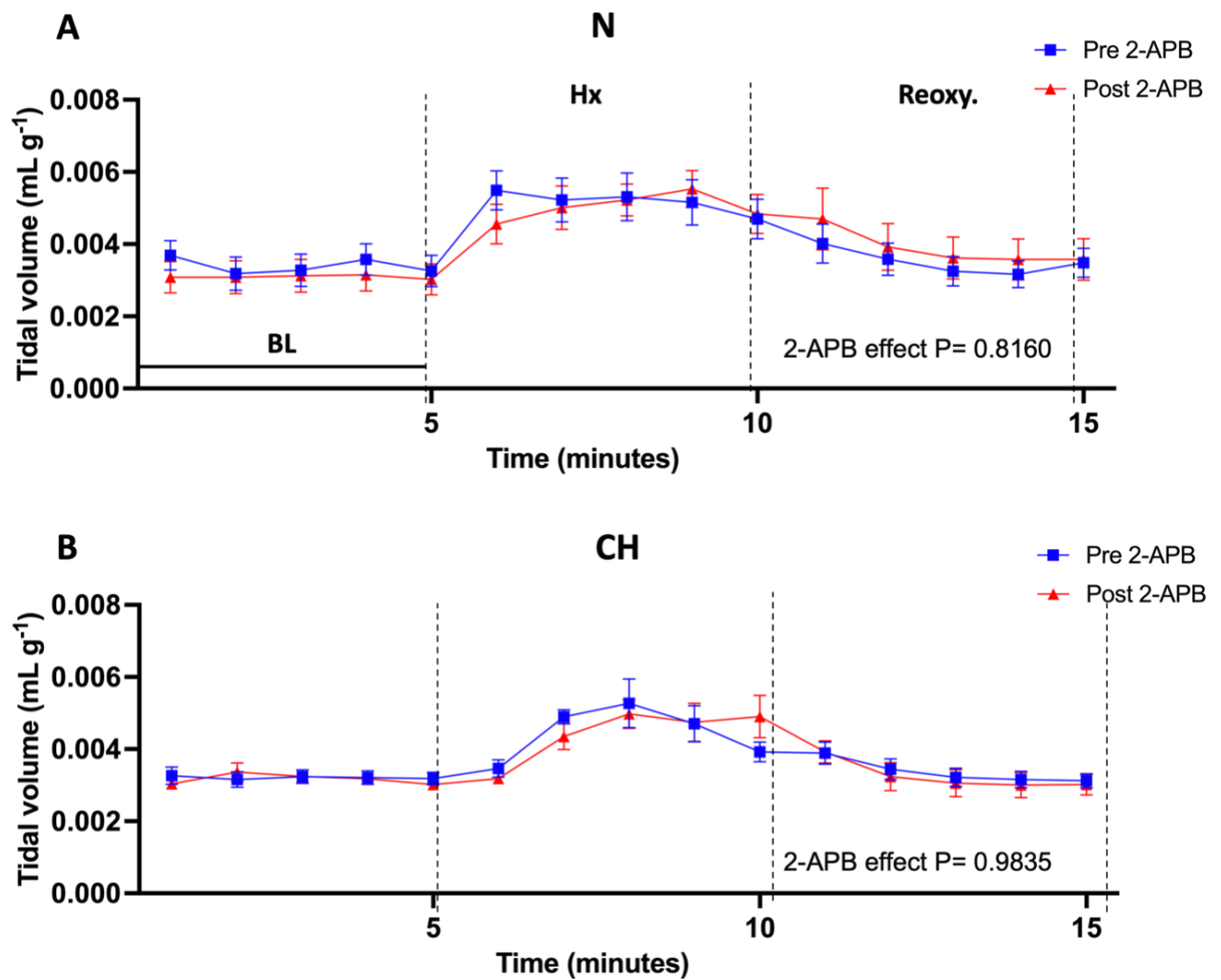
**Figure 6.10 2-APB does not modify the tidal volume (Vt) response to acute hypoxia in normoxic (N) or chronic hypoxic (CH) animals.**

(A) Vt responses to hypoxia pre and post 2-APB administration in the N group, n=7. (B) Vt responses to hypoxia before and after 2-APB administration in the CH group, n=6. Data presented as mean±SEM, statistical test performed using 2-way repeated measures ANOVA.

6.3.5 CH increases the end tidal pO_2 during baseline (normoxic) ventilation, but not during hypoxia, in the presence and absence of 2-APB.

During baseline ventilation, the CH group had an end tidal pO_2 of 18.06±0.1005 kPa, which was significantly greater compared to the end tidal O_2 of the N group measured as 17.52±0.09357 kPa, p=0.0026, Figure 6.11. The end tidal O_2, was reduced in N and CH during acute hypoxia, but there was no significant alteration between the groups measuring 8.474± 0.06383 kPa for the CH group, and 8.440±0.06416 kPa for the N group, p=0.7203, Figure 6.11. After the administration of 2-APB, the end tidal O_2 for CH group was still increased in normoxia (p=0.0218) but not hypoxia (p=0.0963) (Figure 6.11).
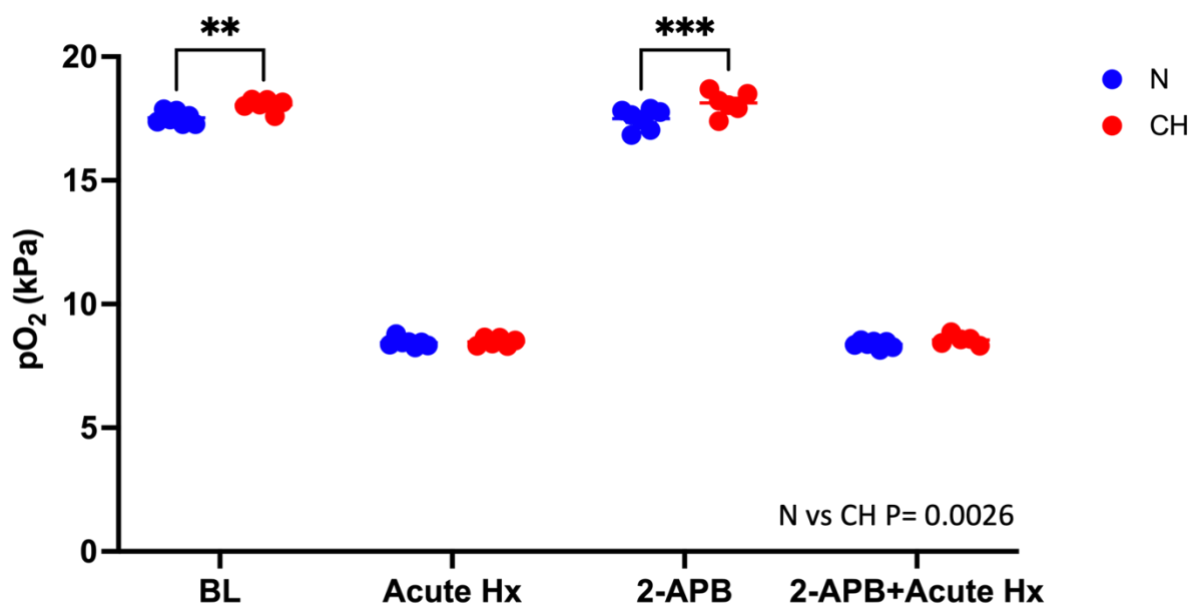
Figure 6.11 The effects of chronic hypoxia (CH) and 2-APB infusion on end tidal O_2 levels

(A) Grouped end tidal pO_2 data for normoxic (N, n=7) and CH (n=6) animals when measured at baseline (BL; normoxia) in acute hypoxia (Hx), in normoxia plus 2-APB and in hypoxia (Hx) plus 2-APB. Data presented as mean±SEM. Individual dots represent data from a single animal. Significance evaluated between N and CH using a 2-way repeated measures ANOVA with Sidak's post hoc analysis. ** and *** denote p<0.01 and p<0.001 respectively.

6.3.6 CH significantly reduces the end tidal pCO$_2$ during baseline (normoxic) ventilation but not in acute hypoxia, both pre and post 2-APB administration

During baseline ventilation the mean end tidal CO$_2$ was 2.157±0.1162 kPa for CH animals and 2.675±0.07497 kPa for N animals, respectively, therefore being significantly lower in the CH group, p=0.0027, Figure 6.12. Although the end tidal pCO$_2$ remained lower in the CH group during acute hypoxia this was not significantly different to N (Figure 6.12). In normoxia, 2-APB administration slightly reduced the mean end tidal CO$_2$ for the CH group, compared to baseline, 2.106±0.1461kPa, while it did not change the end tidal CO$_2$ for the N rat group, 2.676±0.1366 kPa. A significant reduction of end tidal CO$_2$ in normoxia in the CH animals therefore persisted after 2-APB administration, p<0.001), Figure 6.12. Again, although the pCO$_2$ was lower in the CH group during acute hypoxia in the presence of 2-ABP (compared with the N group) this was not statistically significant (Figure 6.12). Collectively, these results are possibly indicative of a slightly greater hyperventilation in the CH animals in normoxia, which persists in the presence of 2-APB.
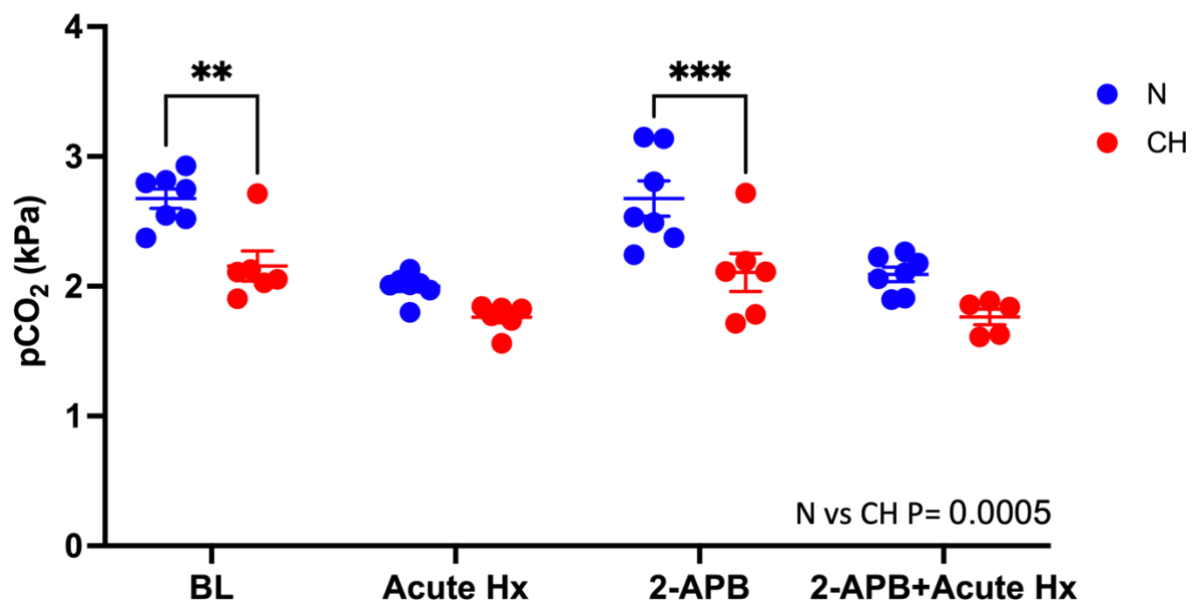
Figure 6.12 The impact of chronic hypoxia (CH) and 2-APB infusion on end tidal CO$_2$ levels

(A) Grouped end tidal pCO$_2$ data for normoxic (N, n=7) and CH (n=6) animals when measured at baseline (BL; normoxia) in acute hypoxia (Hx), in normoxia plus 2-APB and in hypoxia (Hx) plus 2-APB. Data presented as mean±SEM. Individual dots represent data from a single animal. Significance evaluated between N and CH using a 2-way repeated measures ANOVA with Sidak's post hoc analysis. ** and *** denote $p<0.01$ and $p<0.001$ respectively.

6.4 Chapter synopsis and discussion

6.4.1 List of main findings

- In this model of CH and under these recording conditions, CH did not evoke significant changes in cardiovascular parameters including ABP and HR.

- In this model of CH and under these recording conditions CH did not alter Rf or Vt.

- The main effect of 2-APB was to reduce HR, although this was more apparent in N than CH animals

- Single bolus i.v. delivery of 2-APB did not significantly modify cardiovascular or respiratory responses to acute hypoxia in N or CH.

6.4.2 Arterial blood pressure in CH compared to N rats

CH triggers a cascade of adaptations within the cardiovascular system aimed at maintaining tissue O_2 delivery and vital organ function (Essop, 2007). One of the primary responses to hypoxia is the activation of sympathetic nervous system pathways, leading to vasoconstriction and increased heart rate (Xie et al., 2001). These responses induce an increase in blood pressure and facilitate the redirection of blood flow to the brain and other vital organs, by causing vasodilation in their respective vascular beds, while it causes vasoconstrict in less vital organs, such as the gastrointestinal tract (Kuwahira et al., 1993). The absence of a change in ABP in described in this Chapter is therefore perhaps surprising. However, in addition to sympathetic activation, exposure to hypoxia is known to cause peripheral vasodilation, mediated via local endothelial substances (adenosine) and sympatholysis (Edmunds and Marshall, 2003). Indeed, in most animal models of CH that use an exposure time of days to a few weeks, similar to that used here, the animals do not exhibit systemic hypertension despite a robust elevation in sympathetic nerve activity (Coney et al., 2004). Over time as, as the hypoxia is sustained, the production and/or sensitivity to these

local mediators begins to decrease whilst the sympathetic nerve activity remains elevated. Thus, to observe an elevation in ABP, as seen in patients with COPD, it may be necessary to expose animals to CH for much longer periods such as months to years. This could be an interesting area for future investigation. Furthermore, it is unclear how the anaesthesia used (alfaxalone) may have impacted on the ABP observations. In conscious rats, measurements of ABP can be made using telemetry or tail cuff, and these techniques report an MABP much lower than what is reported here (Redfors et al., 2014). Thus, it would appear that alfaxalone itself causes a rise in ABP thereby potentially masking any difference between N and CH. That said, under the same recording conditions and using the same dose of alfaxalone, a significant difference in ABP was detected between N animals and those exposed to CIH (Alzahrani et al., 2021a).

The CBs involvement in initiating reflexive responses to hypoxia contributes to the observed rise in blood pressure (Badoer, 2020). When exposed to hypoxia, the CB detects reduced O_2 levels and initiates reflexive responses to restore O_2 homeostasis (Cummins et al., 2020). These responses often involve increased sympathetic outflow and blunted vagal activity, resulting in vasoconstriction and elevated HR, all of which are proposed to increase in MABP in COPD patients (Xie et al., 2001, Calbet, 2003). However, there are other factors that might contribute to hypertension in COPD patients that are not necessarily seen in this CH model. While the CB role is likely important, other mechanisms also come into play during CH. The renin-angiotensin-aldosterone system (May et al.), for instance, can be activated to increase blood volume and systemic vascular resistance (Nangaku and Fujita, 2008). This can further contribute to the observed rise in MABP in COPD patients. A key limitation of the work presented here is that serum concentrations of Ang II were not measured. Additionally, alterations in vascular remodelling and increased production of vasoconstrictors like endothelin-1 may be at play (Ambalavanan et al., 2007).

6.4.3 The potential influence of anaesthesia on heart rate in CH rats during baseline and acute hypoxia

CH typically leads to an increase in HR (Kuwahira et al., 1993). This response is a part of the body's adaptive mechanism to cope with the reduced O_2 availability in the environment (Cowburn et al., 2017). Sympathetic activation is one of the primary drivers behind the increase in HR during CH (Prabhakar et al., 2022). In response to low O_2 levels, the body initiates a series of physiological changes to enhance O_2 delivery to vital organs. One of these changes involves the release of noradrenaline from sympathetic fibres, a neurotransmitter that increases HR by stimulating the heart's pacemaker cells at the SA node and enhances ventricular contractility (Adeoye et al., 2015).

The observation of no alteration in HR in anaesthetised CH rats during normoxia or acute hypoxia conditions underscores the intricate interplay between anaesthesia, CH, and cardiovascular regulation. The role of anaesthesia in modulating cardiovascular responses is a complex factor that must be considered when interpreting these findings.

Anaesthesia is known to exert profound effects on the autonomic nervous system, particularly by dampening sympathetic and parasympathetic influences on the heart (Liu et al., 2019). Reduced sympathetic outflow, which typically increases HR, is often observed under anaesthesia (Liu et al., 2019). This effect can be accentuated in the presence of CH, where sympathetic activation is already heightened due to the body's adaptation to low O_2 levels. CH elicits a series of cardiovascular adaptations to enhance O_2 delivery, including increased sympathetic activity (Calbet, 2003). In the context of anaesthesia, which reduces sympathetic drive, the interaction between the two factors can result in a blunted HR. Thus, excessive inhibition of sympathetic nerve activity to the heart in the CH group is a likely explanation for the lack of effect on HR in the CH group.

6.4.4 Effects of CH on Vt, Rf and end tidal gases in anaesthetised CH rats

In response to CH, the respiratory system undergoes various adaptations to optimize O_2 delivery to tissues (Brinkman et al., 2023). One of the key adjustments is an increase in Rf (Wilkinson et al., 2010). Accordingly, there was a clear increase in Rf observed in this CH model in normoxia and hypoxia observed in Chapter 4 in awake animals. The increased Rf allows for more gas exchange by increasing alveolar ventilation, facilitating the removal of CO_2 and aiding O_2 uptake from the lungs (Deveci et al., 2001). The CBs, which are sensitive to changes in arterial O_2 levels, play a crucial role in this response (Powell, 2007). They initiate reflexes that lead to enhanced respiratory drive, manifested as an increased Rf, when O_2 levels are low (Brinkman et al., 2023). These findings all appeared to be present in the current CH model when measurements were made in awake animals using WBP (Chapter 4). Furthermore, in Chapter 5, there was clear evidence of basal increases in CB nerve activity and sensitivity to acute hypoxia, again validating the CH model. Moreover, the same rats underwent the WBP experiment one day before the *in vivo* experiment and revealed altered ventilation in the CH group.

The observation of no alteration in Rf and Vt in anaesthetised CH rats in this Chapter, suggests complex interactions between CH, anaesthesia, and respiratory control. Anaesthesia can suppress peripheral as well as central nerve activity (Liu et al., 2019). This suppression can extend to the sensory nerve activity of the CB, as well as the central processing of the sensory signals and the downstream motor output (Dahan and Teppema, 2003). Anaesthesia can also blunt the sensitivity of the CBs to changes in arterial O_2 levels (Saraswat, 2015). Thus, what is seen in the current work is probably a strong suppression of reflexes mediated by the CB which would normally contribute to enhanced inspiratory drive and Rf in in CH (Powell, 2007). This is probably sufficient to abolish any measurable differences in Rf between N and CH that were seen in awake animals. This may be further complicated by the impact of anaesthesia on ventilation

metabolism matching. End-tidal O_2 and CO_2 are parameters that reflect the concentration of O_2 and CO_2 in the exhaled breath and are equivalent to the alveolar gases (Casey and Semler, 2019) (Aminiahidashti et al., 2018). Analysis of end tidal O_2 and CO_2 are highly suggestive of a hyperventilation in both N and CH, which seems to be more apparent in CH animals. Measurements of metabolic rate weren't taken but would be expected to be depressed under anaesthesia. At the same time, depression of the central nervous system, including the respiratory centres (Saraswat, 2015) and sites responsible for ventilation/metabolism matching could have resulted in overall changes in the relationship between alveolar ventilation and O_2 consumption (Hedenstierna and Rothen, 2012). Anaesthesia could also have impacted on ventilation perfusion matching and/or pulmonary gas exchange, influencing the composition of the exhaled breath (Hedenstierna and Rothen, 2012). It would be particularly interesting to explore the effect of CH on metabolic rate and ventilation/metabolism matching, along with subsequent analysis of the effect of anaesthetics which could be greater in CH animals.

6.4.5 2-APB decreases HR but did not alter cardiovascular and respiratory responses to acute hypoxia.

In Chapter 5, 2-APB produced significant depression of CB sensory nerve activity isolated from both N and CH. This was apparent in both normoxia and acute hypoxia and also in the presence and absence of Ang II. Thus, it was hypothesised that a similar depression of CB function *in vivo* should decrease the chemoreflex and possibly lower the ABP. However, the only clear effect of 2-APB was to lower the HR in N animals. This likely reflects a direct effect on the SAN rather than the CB due to the absence of other changes in cardiovascular or respiratory parameters (such as ABP or end tidal gases).

There is however no evidence that the recommended 2-APB IV bolus of (10 mg kg^{-1}), inhibited CB function when delivered in this manner. A major limitation was that 2-APB was delivered as a single bolus rather than a continuous infusion. Given the powerful effect that 2-APB had *ex vivo*, it can only be suggested that the bolus delivery method meant that 2-APB did not reach a sufficient local concentration within the CB tissue to adequately inhibit its sensory nerve activity. These results are therefore useful preliminary findings and rather than discounting the potential targeting of TRPC channels in the CB to reduce chemoreflex activity and ABP; future studies are warranted to test higher *in vivo* concentrations of 2-APB than those used here and using alternative delivery methods e.g. continuous i.v. infusion or oral administration. Using the same CB for immunohistochemistry immediately after an *in vivo* experiment could have offered a direct link between physiological responses and molecular changes.

TRP channels play a crucial role in modulating heart rate via the SA node, the heart's natural pacemaker (Wen et al., 2020). These non-selective cation channels facilitate the influx of ions such as Ca^{2+} and Na$^+$, essential for the rhythmic depolarization and repolarization of SA node cells that generate action potentials (Worley et al., 2007, Avila-Medina et al., 2018). Specific TRP channel subtypes, such as TRPM4, TRPV1, TRPC3, and TRPC6, contribute to the pacemaker potential by regulating membrane potential and calcium dynamics (Gees et al., 2010). The autonomic nervous system further influences these channels; sympathetic stimulation increases heart rate by enhancing TRP channel activity (Michlig et al., 2016). Blocking TRP channels reduces cation influx, slows depolarization, and alters membrane potential dynamics, leading to a decreased heart rate. Furthermore, inhibition of CB function by 2-APB, could lead to a reduction in sympathetic drive to the heart, although this would have expected to co-inside with a reduction in respiratory frequency which was not observed. Nevertheless, this complex relationship could explain why the TRP channel blocker used here (2-APB) reduced the heart rate in the current experiments.

The lack of change in blood pressure despite the decrease in heart rate could be explained by compensatory mechanisms. When heart rate decreases, the body can maintain blood pressure by adjusting stroke volume and vascular resistance (Kobe et al., 2019). Additionally, TRP channels in blood vessels may not be as significantly affected, allowing the vascular tone to remain stable and thus preserving blood pressure. This balance between cardiac output and vascular resistance ensures that blood pressure remains constant despite changes in heart rate. The decrease in HR but not BP in response to 2-APB could be justified by the hypothesis that the local effect of Hx in the vasculature may mask any sympathetic effects mediated by the CB (Cowburn et al., 2017).

6.4.6 Conclusion

The results of this chapter have revealed that CH failed to induce alterations in MABP, HR, Rf, and Vt, when recorded under GA. Some differences may have been masked by the use of GA, or the cardiovascular adaptations in CH animals may need longer to develop than 10 days. Surprisingly, administration of 2-APB had no impact on MAP, Rf and Vt in both N and CH. 2-APB did have a significant effect on HR although this is likely mediated via the sino atrial node and not the CB. It is likely that the concentration of 2-APB used was not sufficient to inhibit *in vivo* CB activity. Future studies are needed to test higher *in vivo* concentrations of 2-APB and different delivery methods to target the CB more effectively.

Chapter 7. Overall discussion

7.1 Main findings

- In PC12 cells, (an O_2-sensitive surrogate of the CB type I cell), exposure to CH increases protein expression of AT_1R as well as cell size

- In PC12 cells, AT_1Rs localise to form distinct clusters on the cell membrane

- Exposure to CH increases AT_1R supercluster formation

- The CH animal model used successfully produced CB hyperactivity and an increase in VE in normoxia and hypoxia

- CH animals had greatly reduced inspiratory and expiratory times as well as overall elevations in inspiratory and expiratory drive

- CH animals also displayed a less variable breathing pattern

- *Ex vivo* CH CBs are more sensitive to Ang II, generating larger and more consistent responses

- In the presence of Ang II, TRPC channel inhibition with 2-APB reduced *ex vivo* CB hypoxic sensitivity to a greater extent in the CH group

- Single bolus administration of 2-APB *in vivo* was not sufficient to modify cardiorespiratory reflexes in N or CH animals, underlining the need for more refined approaches for targeting AngII-TRPC signalling in the CB *in vivo*

7.2 Adaptive responses in PC12 cell size, AT_1R protein expression and AT_1R clustering: implications for CH

The observed increase in PC12 cell size in response to CH is likely to involve a switch in the delicate balance between processes such as cell growth, proliferation, and apoptosis, under prolonged O_2 depletion

(Amodeo and Skotheim, 2016). CH induces a series of adaptive changes, including altering protein synthesis, altered gene expression, and increased organelle biogenesis, collectively resulting in cellular hypertrophy (Lee et al., 2020). This hypertrophic response is very likely to involve HIF stabilisation and signalling, and may serve as a mechanism to optimize survival in O_2 deprived conditions, by boosting cellular functions such as amplified sensitivity to extracellular signals like Ang II and changes in cell metabolism (Fung and Bergmann, 2023).

This increase in PC12 cell size is likely interconnected with the upregulation of AT_1R and TH protein expression, all of which may be governed by HIF. The rise in AT_1R protein expression may be linked to the need for enhanced cellular functions in response to CH. Indeed, the Ang II signalling pathway, mediated through AT_1R, is known to influence cell growth, intracellular Ca^{2+} homeostasis and survival (Dasgupta and Zhang, 2011). The increased AT_1R expression may contribute by promoting cellular responses associated with growth and adaptation. This could be achieved through IP_3 mediated modifications in Ca^{2+} store release, PKC mediated changes in ion channel function (possibly including TRPC channels) and/or secondary β-arrestin mediated signalling following AT_1R internalisation and localisation to the nucleus.

Simultaneously, the observed increase in TH expression in CH suggests a collaborative effort to augment catecholamines and neurotransmitter levels. The upregulation of TH may reflect an adaptive response aimed at increasing neurosecretion thereby affecting extracellular signalling.

A very interesting finding was that AT_1Rs were not randomly expressed in PC12 cells but rather formed distinct clusters or hotspots on the cell membrane. This is suggestive of highly localised microdomain Ang II signalling within the PC12 cell. The observed increase in maximum AT_1R cluster size (indicative of

increased super cluster formation) is likely to greatly enhance the local intensity of the Ang II signal, but only in specialised compartments throughout the cell. The overall functional importance of this change in cluster characteristics is unclear, but could be related to enhanced sensitivity to Ang II seen in later parts of this thesis. A generalised increase in GPCR cluster size may reflect an adaptive mechanism to enhance the overall sensitivity of PC12 cells to extracellular signals, such as those mediated by Ang II and other ligands, in response to CH. In the future it would be good to observe if similar changes in clustering are observed for other GPCRs, in addition to AT_1Rs e.g. D_2Rs.

The mechanism accounting for increased supercluster formation is unknown. However, it could involve alterations in cytoskeleton rearrangement and receptor trafficking in response to CH, possibly driven by HIF. More work in this area is clearly needed to allow for a better understanding of what causes changes in AT_1R (and other GPCR) single-molecule organisation and clustering. Moreover, the coordinated increase in both cell size and AT_1R superclusters adds another layer of complexity. This integrated response involves not only alterations in cellular morphology/growth but also dynamic changes in receptor expression and clustering, pointing towards a complex adaptive strategy by PC12 cells to thrive during CH. The most obvious extension of this work is to evaluate AT_1R clustering in CB type I cells isolated from N and CH animals. This may include examining the spatial relationship between AT_1Rs and TRPC channels.

7.3 CB and cardiopulmonary responses to CH: a novel role for Ang II-TRPC signalling

The findings from this thesis offer a comprehensive insight into the interconnected CB and ventilatory adaptations to CH in rats. In CH animals, there was an elevation in carotid sinus nerve activity, inspiratory drive and VE in both normoxia and hypoxia. It is very likely that these respiratory adaptations are driven

by CB hyperactivity. The heightened CB activity is also likely to account for the reduction in inspiratory time. What is less clear is if the increased output from the CB is responsible for reduction in breathing variability and SD1 on the Poincare plots. It would be interesting to establish if the patterning of CB sensory nerve activity was more regular in CH animals, possibly providing a clear link with the more regular breathing pattern and decreased short term variability. It would also be interesting to deduce whether the reduction in breathing variability directly correlates with the level of CB hyperactivity, in CH animals and maybe also COPD patients. If true then this could offer a novel marker of CB hyperactivity, helping to determine those who would benefit most from CB targeted therapy.

In conjunction with the augmented carotid sinus nerve activity, CH rats display an increased sensitivity to Ang II. Responses were larger, better sustained, and present in a larger proportion of sensory fibres. This supports the findings from earlier parts of the thesis, where PC12 cells showed an increased AT_1R expression and cluster size. Interestingly, the administration of 2-APB successfully attenuated carotid sinus nerve activity in the presence of Ang II and this effect is more apparent in CH rats. Since the inhibitory action of 2-APB alone was consistent between N and CH, this implies an upregulation of Ang II-TRPC signalling in the CH CB. Precisely how this interaction takes place and what causes it to be increased in CH is still to be determined. However, this work highlights the potential for modulation of CB hyperactivity in the context of CH by targeting Ang II-TRPC signalling. The effectiveness of 2-APB suggests that specific TRPC channel inhibitors may hold promise in reducing the CB hyperactivity in response to the increased levels of Ang II in CH and COPD.

Despite the positive impact of 2-APB on CB hyperactivity displayed *ex vivo*, it was observed that single bolus administration of 2-APB *in vivo* did not alter the ABP or HR in CH rats. It could be that whilst 2-APB

may influence CB responses, this does not translate to changes in cardiovascular parameters. It was also observed that this dose and method of 2-APB administration did not affect baseline breathing or responses to acute hypoxia in either N or CH animals. Thus, what is more likely is that the 2-APB did not reach a high enough concentration within the CB tissue to produce inhibition of the carotid sinus nerve activity. Thus, targeting TRPC in the CB to alleviate cardiovascular dysfunction remains an intriguing possibility, but clearly more effective drug delivery approaches are needed.

Overall, these findings collectively emphasise a complex and integrated physiological adaptation to CH in rats. The augmented carotid sinus nerve activity, amplified responsiveness to Ang II, more regular breathing pattern, and increased efficacy of 2-APB in reducing some these effects, illustrate the complex interplay between the CB, cardiovascular and respiratory adaptations when challenged by CH.

7.4 Limitations

7.4.1 Disruption of laboratory work due to the COVID-19 pandemic

The COVID-19 pandemic, with its far-reaching implications, has left a huge mark on scientific research, introducing unprecedented challenges and setbacks. Prior to the enforcement of the national lockdown in the UK, experiments were planned to measure AT_1R protein expression and single-molecule arrangement in CB type I cells isolated from N and CH animals. However, the imposition of the national lockdown suddenly disrupted the research plan. With the complete closure of some laboratory facilities, and severely restricted access to others, it was not possible at that time to proceed with the N and CH animal models. Instead, experiments were performed on PC12 cells, a cell line that shares many features with type I cells. Even these experiments were disrupted during COVID-19, with cell cultures often having to be discarded

after multiple passages and experiments started from the beginning due to lockdowns, restricted access to lab facilities and limited working hours.

Upon full re-opening of facilities, it was decided to proceed with the physiological experiments presented in Chapters 4, 5 and 6 rather than perform the same cellular imaging experiments (as in Chapters 2 and 3) but in CB type I cells. This allowed for development of a broader range of techniques and allowed for generation of functional data.

7.4.2 Maintaining the baseline F_iO_2 at 12% in CH animals for WBP recordings as a more relevant model of COPD

Maintaining rats in a 12% F_iO_2 in the recording chamber during WBP at baseline before inducing acute hypoxia would have presented a more physiologically relevant approach, particularly in the context of studying adaptive respiratory responses similar to those observed in conditions like COPD (Garrod et al., 2006). The use of an F_iO_2 of 21% O_2, is likely to have created a more hyperoxic environment in the CB (and elsewhere) in animals that have spent 10 days adapting to a much lower O_2 environment. As such, some of the breathing measurements at baseline may have been underestimated, e.g. Rf, VT/Ti and VE, and alterations are likely to have been much more substantial had CH baselines been measured at 12% F_iO_2.

CH induces adaptive changes in respiratory physiology, a phenomenon well-documented in COPD where patients often experience prolonged periods of reduced O_2 levels (Kent et al., 2011, Akgul et al., 2007, Thomas and Marshall, 1995). Maintaining rats in a 12% WBP chamber during baseline recordings (their new 'normoxic environment') would offer the advantage of being able to isolate the effects of CH in normoxia from those of acute hypoxia. This approach would allow for a clearer description of the adaptive

changes that occur specifically due to CH exposure in normoxia, providing more valuable insights into the long-term consequences of sustained low O_2 levels. This would not only enhance the physiological validity of the experimental model but also contribute to a more comprehensive understanding of respiratory adaptations in CH conditions, better mirroring the challenges faced by COPD patients.

7.5 Future directions

7.5.1 Investigating the colocalization between AT_1R and TRP channels in CB type I cells and PC12 cells.

Observing how the AT_1R might colocalize or be in close proximity with TRP channels within CB type I cells and PC12 cells (using super-resolution microscopy) holds promise for identifying a potential close spatial association that could be relevant to the complex mechanisms governing the overall response to Ang II. This includes imaging and measuring members of the TRPC, TRPV, TRPM and maybe TRPA subtypes. The diverse roles played by these TRP channels in cellular signalling make them candidates for potential interaction with AT_1R, with TRPC being the most likely due to its known involvement in Ang II signalling in other tissues (Ma et al., 2016, Ilatovskaya et al., 2014). Better insights into the colocalization between AT_1R and specific TRP channels could improve target identification for pharmacological interventions, and provide a more precise understanding of how these molecular interactions contribute to CB hyperactivity in pathological conditions such as CH/COPD. Such imaging could also be performed on CB tissue isolated from CIH and HF animals, conditions where CB hyperactivity is again associated with pathological Ang II signalling.

7.5.2 Identifying which subtypes of TRPC channels are involved in Ang II signalling in the CB

Investigating the specific subtype of TRPC channels involved in Ang II signalling in the CB would add a crucial layer to our understanding of cellular signalling in this pathophysiological setting. While it was confirmed that 2-APB reduces sinus nerve activity in the presence of Ang II in CH CBs, pinpointing the TRPC subtype responsible for this modulation remains an essential point for further exploration. This could be done by using specific TRPC channel subtype inhibitors/activators, in addition to the imaging studies described above. The use of genetic KO animal models with single or multiple depletion of TRPC channels in the CB would also offer mechanistic insight. Unravelling the relative contributions of TRPC channels in Ang II signalling in the CB will offer valuable insights into the molecular complexities governing this regulatory mechanism. Such studies hold the potential to refine the pharmacological strategies used to reduce CB hyperactivity, promoting the use of specific TRPC subtype inhibitors, rather than general TRPC blockers. This should help facilitate the development of more targeted interventions to better optimize therapeutic outcomes whilst at the same time limiting non-specific actions, in conditions characterized by increased Ang II signalling such as CH/COPD.

7.5.3 Examining the effect of 2-APB on breathing in awake N and CH animals.

It will be a priority to measure the effect of 2-APB on breathing and breathing patterns in awake N and CH animals using WBP. In this thesis, it was confirmed that 2-APB did reduce the effect of Ang II on carotid sinus nerve activity in CH animals. A next step would be to use 2-APB to effectively inhibit the CB *in vivo* to evaluate changes in respiratory timings and patterning in CH animals. Testing 2-APB's ability to affect the breathing parameters and/or the breathing patterns is an important question to ask. A similar protocol could be followed as that described in Chapter 4, except that baseline breathing and hypoxic responses

would be evaluated pre and post administration of 2-APB (IP), for both N and CH rat groups, Figure 7.1.

For these experiments it would be important to administer a dose of 2-APB that achieves a similar local

concentration within the CB tissue to that used in the *ex vivo* experiments (10 µM). This may require some

optomisation.
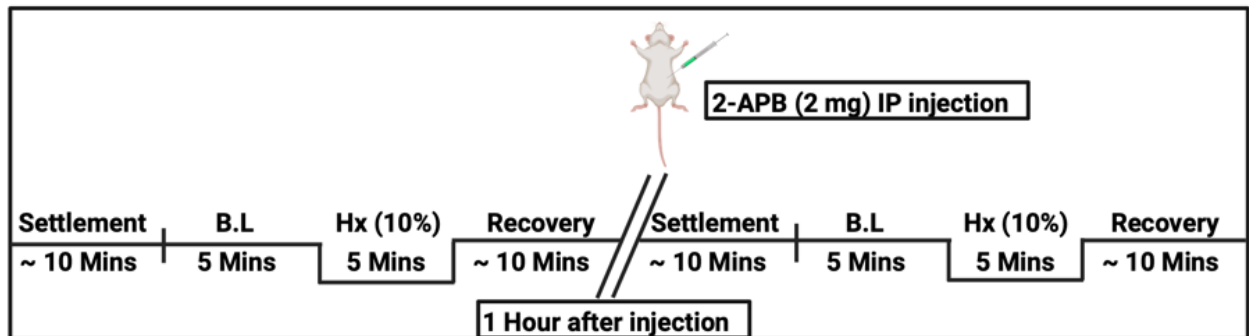
Figure 7.1 Measuring respiratory responses to hypoxia using WBP before and after administration of 2-APB.

The protocol illustrates the proposed protocol for the experiment. Two rounds of recording will be performed, one before and one after the IP injection of 2-APB.

7.6 Thesis summary:

Pathological conditions characterized by CH lead to altered physiological adaptations, starting at the cellular level and progressing to organs and systems, ultimately causing multisystem changes to maintain oxygen delivery. COPD exemplifies such conditions, featuring chronic activation of the sympathetic nervous system and increased circulatory Ang II. Both hypoxia and Ang II stimulate the CB, an early responder to CH. In PC12 cells, a model for CB type I cells, CH increases AT_1R and TH expression, cell size, and the organization of AT_1R clusters. In CH rats, baseline ventilation driven by the CB increases to ensure oxygen delivery. These findings were corroborated in vitro, with heightened CB sinus nerve sensitivity to Ang II, mediated by TRPC channels. Blocking TRPC channels with 2-APB reduced Ang II sensitivity *in vitro*, but *in vivo* experiments showed no significant effects. The involvement of TRPC channels suggests their potential as therapeutic targets in CH characterized pathology. Further investigation into these channels could reveal new strategies for managing neurogenic hypertension associated with CH and the CB hyperactivity.

Appendix

List of peer-reviewed research articles published throughout the PhD Studentship

Aldossary HS, Alzahrani AA, Nathanael D, Alhuthail EA, Ray CJ, Batis N, Kumar P, Coney AM, Holmes AP. G-Protein-Coupled Receptor (GPCR) Signaling in the Carotid Body: Roles in Hypoxia and Cardiovascular and Respiratory Disease. Int J Mol Sci. 2020 Aug 20;21(17):6012. doi: 10.3390/ijms21176012. PMID: 32825527; PMCID: PMC7503665.

Aldossary HS, Nieves DJ, Kavanagh DM, Owen D, Ray CJ, Kumar P, Coney AM, Holmes AP. Analyzing Angiotensin II Receptor Type 1 Clustering in PC12 Cells in Response to Hypoxia Using Direct Stochastic Optical Reconstruction Microscopy (dSTORM). Adv Exp Med Biol. 2023;1427:175-184. doi: 10.1007/978-3-031-32371-3_19. PMID: 37322348.

Alzahrani AA, Cao LL, **Aldossary HS**, Nathanael D, Fu J, Ray CJ, Brain KL, Kumar P, Coney AM, Holmes AP. β-Adrenoceptor blockade prevents carotid body hyperactivity and elevated vascular sympathetic nerve density induced by chronic intermittent hypoxia. Pflugers Arch. 2021 Jan;473(1):37-51. doi: 10.1007/s00424-020-02492-0. Epub 2020 Nov 19. PMID: 33210151; PMCID: PMC7782391.

Swiderska A, Coney AM, Alzahrani AA, **Aldossary HS**, Batis N, Ray CJ, Kumar P, Holmes AP. Mitochondrial Succinate Metabolism and Reactive Oxygen Species Are Important but Not Essential for Eliciting Carotid Body and Ventilatory Responses to Hypoxia in the Rat. Antioxidants (Basel). 2021 May 25;10(6):840. doi: 10.3390/antiox10060840. PMID: 34070267; PMCID: PMC8225218.

Holmes AP, Swiderska A, Nathanael D, **Aldossary HS**, Ray CJ, Coney AM, Kumar P. Are Multiple Mitochondrial Related Signalling Pathways Involved in Carotid Body Oxygen Sensing? Front Physiol. 2022 May 31;13:908617. doi: 10.3389/fphys.2022.908617. PMID: 35711317; PMCID: PMC9194093.

Review

G-Protein-Coupled Receptor (GPCR) Signaling in the Carotid Body: Roles in Hypoxia and Cardiovascular and Respiratory Disease

Hayyaf S. Aldossary [1,2], Abdulaziz A. Alzahrani [1,3], Demitris Nathanael [1], Eyas A. Alhuthail [1,4], Clare J. Ray [1], Nikolaos Batis [5], Prem Kumar [1], Andrew M. Coney [1] and Andrew P. Holmes [1,6,*]

[1] Institute of Clinical Sciences, University of Birmingham, Birmingham B15 2TT, UK; HXA807@student.bham.ac.uk (H.S.A.); AAA717@student.bham.ac.uk (A.A.A.); demitris.nathanael@gmail.com (D.N.); EXA833@student.bham.ac.uk (E.A.A.); c.j.ray@bham.ac.uk (C.J.R.); p.kumar@bham.ac.uk (P.K.); a.m.coney@bham.ac.uk (A.M.C.)

[2] College of Medicine, Basic Medical Sciences, King Saud bin Abdulaziz University for Health Sciences, Riyadh 11481, Saudi Arabia

[3] Respiratory Care Department, Faculty of Applied Medical Sciences, Umm Al-Qura University, Makkah 24381, Saudi Arabia

[4] Collage of Sciences and Health Professions, Basic Sciences Department, King Saud bin Abdulaziz University for Health Sciences, Riyadh 11481, Saudi Arabia

[5] Institute of Cancer and Genomic Sciences, University of Birmingham, Birmingham B15 2TT, UK; N.Batis@bham.ac.uk

[6] Institute of Cardiovascular Sciences, University of Birmingham, Birmingham B15 2TT, UK

* Correspondence: a.p.holmes@bham.ac.uk; Tel.: +44-121-415-8161

check for updates

Abstract: The carotid body (CB) is an important organ located at the carotid bifurcation that constantly monitors the blood supplying the brain. During hypoxia, the CB immediately triggers an alarm in the form of nerve impulses sent to the brain. This activates protective reflexes including hyperventilation, tachycardia and vasoconstriction, to ensure blood and oxygen delivery to the brain and vital organs. However, in certain conditions, including obstructive sleep apnea, heart failure and essential/spontaneous hypertension, the CB becomes hyperactive, promoting neurogenic hypertension and arrhythmia. G-protein-coupled receptors (GPCRs) are very highly expressed in the CB and have key roles in mediating baseline CB activity and hypoxic sensitivity. Here, we provide a brief overview of the numerous GPCRs that are expressed in the CB, their mechanism of action and downstream effects. Furthermore, we will address how these GPCRs and signaling pathways may contribute to CB hyperactivity and cardiovascular and respiratory disease. GPCRs are a major target for drug discovery development. This information highlights specific GPCRs that could be targeted by novel or existing drugs to enable more personalized treatment of CB-mediated cardiovascular and respiratory disease.

Keywords: G-protein; GPCR; carotid body; hypoxia; hypertension; drug-discovery

1. Introduction

The carotid body (CB) is a vital sensory organ, located near the carotid bifurcation, that constantly monitors blood supplying the brain [1]. The CB is stimulated by acute hypoxia, upon which it rapidly activates vital cardiovascular and respiratory reflexes, including peripheral vasoconstriction, elevated heart rate and increased breathing [2]. These ensure that sufficient blood-oxygen is delivered to

Analyzing Angiotensin II Receptor Type 1 Clustering in PC12 Cells in Response to Hypoxia Using Direct Stochastic Optical Reconstruction Microscopy (dSTORM)

19

Hayyaf S. Aldossary, Daniel J. Nieves, Deirdre M. Kavanagh, Dylan Owen, Clare J. Ray, Prem Kumar, Andrew M. Coney, and Andrew P. Holmes

Abstract

Angiotensin II (Ang II) is a hormone that plays a major role in maintaining homeostasis. The Ang II receptor type 1 (AT_1R) is expressed in acute O_2 sensitive cells, including carotid body (CB) type I cells and pheochromocytoma 12 (PC12) cells, and Ang II increases cell activity. While a functional role for Ang II and AT_1Rs in increasing the activity of O_2 sensitive cells has been established, the nanoscale distribution of AT_1Rs has not. Furthermore, it is not known how exposure to hypoxia may alter the single-molecule arrangement and clustering of AT_1Rs. In this study, the AT_1R nanoscale distribution under control normoxic conditions in PC12 cells was determined using direct stochastic optical reconstruction microscopy (dSTORM). AT_1Rs were arranged in distinct clusters with measurable parameters. Across the entire cell surface there averaged approximately 3 AT_1R clusters/μm^2 of cell membrane. Cluster area varied in size ranging from 1.1×10^{-4} to 3.9×10^{-2} μm^2. Twenty-four hours of exposure to hypoxia (1% O_2) altered clustering of AT_1Rs, with notable increases in the maximum cluster area, suggestive of an increase in supercluster formation. These observations could aid in

H. S. Aldossary (✉)
School of Biomedical Sciences, Institute of Clinical Sciences, University of Birmingham, Birmingham, UK

College of Medicine, Basic Medical Sciences, King Saud bin Abdulaziz University for Health Sciences, Riyadh, Saudi Arabia
e-mail: hxa807@student.bham.ac.uk

D. J. Nieves
Institute of Immunology and Immunotherapy and Centre of Membrane Proteins and Receptors (COMPARE), University of Birmingham, Birmingham, UK

D. M. Kavanagh
Micron Bioimaging Facility, University of Oxford, Oxford, UK

D. Owen
School of Mathematics, University of Birmingham, Birmingham, UK

C. J. Ray · P. Kumar · A. M. Coney
A. P. Holmes (✉)
School of Biomedical Sciences, Institute of Clinical Sciences, University of Birmingham, Birmingham, UK
e-mail: a.p.holmes@bham.ac.uk

175

INTEGRATIVE PHYSIOLOGY

β-Adrenoceptor blockade prevents carotid body hyperactivity and elevated vascular sympathetic nerve density induced by chronic intermittent hypoxia

Abdulaziz A. Alzahrani[1,2] · Lily L. Cao[1,3] · Hayyaf S. Aldossary[1,4] · Demitris Nathanael[1] · Jiarong Fu[1] · Clare J. Ray[1] · Keith L. Brain[1,3] · Prem Kumar[1] · Andrew M. Coney[1] · Andrew P. Holmes[1,3]

Abstract

Carotid body (CB) hyperactivity promotes hypertension in response to chronic intermittent hypoxia (CIH). The plasma concentration of adrenaline is reported to be elevated in CIH and our previous work suggests that adrenaline directly activates the CB. However, a role for chronic adrenergic stimulation in mediating CB hyperactivity is currently unknown. This study evaluated whether beta-blocker treatment with propranolol (Prop) prevented the development of CB hyperactivity, vascular sympathetic nerve growth and hypertension caused by CIH. Adult male Wistar rats were assigned into 1 of 4 groups: Control (N), N + Prop, CIH and CIH + Prop. The CIH paradigm consisted of 8 cycles h^{-1}, 8 h day^{-1}, for 3 weeks. Propranolol was administered via drinking water to achieve a dose of 40 mg kg^{-1} day^{-1}. Immunohistochemistry revealed the presence of both β_1 and β_2-adrenoceptor subtypes on the CB type I cell. CIH caused a 2–3-fold elevation in basal CB single-fibre chemoafferent activity and this was prevented by chronic propranolol treatment. Chemoafferent responses to hypoxia and mitochondrial inhibitors were attenuated by propranolol, an effect that was greater in CIH animals. Propranolol decreased respiratory frequency in normoxia and hypoxia in N and CIH. Propranolol also abolished the CIH mediated increase in vascular sympathetic nerve density. Arterial blood pressure was reduced in propranolol groups during hypoxia. Propranolol exaggerated the fall in blood pressure in most (6/7) CIH animals during hypoxia, suggestive of reduced sympathetic tone. These findings therefore identify new roles for β-adrenergic stimulation in evoking CB hyperactivity, sympathetic vascular hyperinnervation and altered blood pressure control in response to CIH.

Keywords Carotid body · Hypoxia · Adrenaline · β-Adrenoceptors · Chronic intermittent hypoxia · Hypertension · Beta-blockers · Vascular sympathetic nerves

Abbreviations

CB	Carotid body
MABP	Mean arterial blood pressure
HR	Heart rate
V_E	Minute ventilation
V_t	Tidal volume
R_f	Respiratory frequency
HVR	Hypoxic ventilatory response
CIH	Chronic intermittent hypoxia
OSA	Obstructive sleep apnoea
MA	Mesenteric artery

✉ Andrew M. Coney
a.m.coney@bham.ac.uk

✉ Andrew P. Holmes
a.p.holmes@bham.ac.uk

1 Institute of Clinical Sciences, University of Birmingham, Edgbaston, Birmingham B15 2TT, UK

2 Respiratory Care Department, Faculty of Applied Medical Sciences, Umm Al-Qura University, Makkah, Saudi Arabia

3 Institute of Cardiovascular Sciences, University of Birmingham, Edgbaston, Birmingham B15 2TT, UK

4 College of Medicine, Basic Medical Sciences, King Saud bin Abdulaziz University for Health Sciences, Riyadh, Saudi Arabia

Introduction

The carotid body (CB) is the major sensory organ in the human body that responds to acute hypoxic stress [30, 50]. When stimulated the CB activates vital protective reflexes including hyperventilation, systemic vasoconstriction and elevated heart rate [29, 30]. CB activation in hypoxia is critical

 Springer

226

Article

Mitochondrial Succinate Metabolism and Reactive Oxygen Species Are Important but Not Essential for Eliciting Carotid Body and Ventilatory Responses to Hypoxia in the Rat

Agnieszka Swiderska [1,2], Andrew M. Coney [1], Abdulaziz A. Alzahrani [1,3], Hayyaf S. Aldossary [1,4], Nikolaos Batis [5], Clare J. Ray [1], Prem Kumar [1] and Andrew P. Holmes [1,6,*]

[1] Institute of Clinical Sciences, University of Birmingham, Edgbaston, Birmingham B15 2TT, UK; agnieszka.swiderska@postgrad.manchester.ac.uk (A.S.); a.m.coney@bham.ac.uk (A.M.C.); AAA717@student.bham.ac.uk (A.A.A.); HXA807@student.bham.ac.uk (H.S.A.); c.j.ray@bham.ac.uk (C.J.R.); p.kumar@bham.ac.uk (P.K.)
[2] Manchester Academic Health Sciences Centre, Unit of Cardiac Physiology, 3.26 Core Technology Facility, Institute of Cardiovascular Sciences, The University of Manchester, 46 Grafton Street, Manchester M13 9NT, UK
[3] Respiratory Care Department, Faculty of Applied Medical Sciences, Umm Al-Qura University, Makkah 24381, Saudi Arabia
[4] Basic Medical Sciences, College of Medicine, King Saud bin Abdulaziz University for Health Sciences, Riyadh 11481, Saudi Arabia
[5] Institute of Cancer and Genomic Sciences, University of Birmingham, Edgbaston, Birmingham B15 2TT, UK; N.Batis@bham.ac.uk
[6] Institute of Cardiovascular Sciences, University of Birmingham, Edgbaston, Birmingham B15 2TT, UK
* Correspondence: a.p.holmes@bham.ac.uk; Tel.: +44-121-415-8161

Abstract: Reflex increases in breathing in response to acute hypoxia are dependent on activation of the carotid body (CB)—A specialised peripheral chemoreceptor. Central to CB O_2-sensing is their unique mitochondria but the link between mitochondrial inhibition and cellular stimulation is unresolved. The objective of this study was to evaluate if ex vivo intact CB nerve activity and in vivo whole body ventilatory responses to hypoxia were modified by alterations in succinate metabolism and mitochondrial ROS (mitoROS) generation in the rat. Application of diethyl succinate (DESucc) caused concentration-dependent increases in chemoafferent frequency measuring approximately 10–30% of that induced by severe hypoxia. Inhibition of mitochondrial succinate metabolism by dimethyl malonate (DMM) evoked basal excitation and attenuated the rise in chemoafferent activity in hypoxia. However, approximately 50% of the response to hypoxia was preserved. MitoTEMPO (MitoT) and 10-(6'-plastoquinonyl) decyltriphenylphosphonium (SKQ1) (mitochondrial antioxidants) decreased chemoafferent activity in hypoxia by approximately 20–50%. In awake animals, MitoT and SKQ1 attenuated the rise in respiratory frequency during hypoxia, and SKQ1 also significantly blunted the overall hypoxic ventilatory response (HVR) by approximately 20%. Thus, whilst the data support a role for succinate and mitoROS in CB and whole body O_2-sensing in the rat, they are not the sole mediators. Treatment of the CB with mitochondrial selective antioxidants may offer a new approach for treating CB-related cardiovascular–respiratory disorders.

Keywords: carotid body; hypoxia; succinate; mitochondrial reactive oxygen species; succinate dehydrogenase; hypoxic ventilatory response

1. Introduction

The ability for humans to sense and respond to a fall in blood oxygen (hypoxia/hypoxaemia) has never been so apparent as in the current COVID-19 pandemic, in which millions of people have experienced this life-threatening stressor [1]. When challenged by hypoxia, the carotid body (CB) is the major peripheral chemoreceptor that detects this stimulus within seconds [2,3]. In contrast to almost all other cell types, the CB type I

Check for updates

Are Multiple Mitochondrial Related Signalling Pathways Involved in Carotid Body Oxygen Sensing?

Andrew P. Holmes[1]*, Agnieszka Swiderska[2], Demitris Nathanael[1], Hayyaf S. Aldossary[1,3], Clare J. Ray[1], Andrew M. Coney[1] and Prem Kumar[1]*

[1]School of Biomedical Sciences, Institute of Clinical Sciences, College of Medical and Dental Sciences, University of Birmingham, Birmingham, United Kingdom, [2]Unit of Cardiac Physiology, Division of Cardiovascular Sciences, Faculty of Biology, Medicine and Health, University of Manchester, Manchester, United Kingdom, [3]College of Medicine, Basic Medical Sciences, King Saud bin Abdulaziz University for Health Sciences, Riyadh, Saudi Arabia

It is generally acknowledged that the carotid body (CB) type I cell mitochondria are unique, being inhibited by relatively small falls in P_aO_2 well above those known to inhibit electron transport in other cell types. This feature is suggested to allow for the CB to function as an acute O_2 sensor, being stimulated and activating systemic protective reflexes before the metabolism of other cells becomes compromised. What is less clear is precisely how a fall in mitochondrial activity links to type I cell depolarisation, a process that is required for initiation of the chemotransduction cascade and post-synaptic action potential generation. Multiple mitochondrial/metabolic signalling mechanisms have been proposed including local generation of mitochondrial reactive oxygen species (mitoROS), a change in mitochondrial/cellular redox status, a fall in MgATP and an increase in lactate. Although each mechanism is based on compelling experimental evidence, they are all not without question. The current review aims to explore the importance of each of these signalling pathways in mediating the overall CB response to hypoxia. We suggest that there is unlikely to be a single mechanism, but instead multiple mitochondrial related signalling pathways are recruited at different P_aO_2s during hypoxia. Furthermore, it still remains to be determined if mitochondrial signalling acts independently or in partnership with extra-mitochondrial O_2-sensors.

Keywords: carotid body, hypoxia, mitochondria, succinate, arterial chemoreceptor, O_2 sensor, metabolism, mitochondrial inhibitors

INTRODUCTION—A ROLE FOR MITOCHONDRIA IN CAROTID BODY O_2 SENSING

The carotid body (CB) type I or glomus cell has an extraordinary ability to be stimulated by relatively small falls in P_aO_2, well above those that start to impact on the metabolism of other cell types (Kumar and Prabhakar, 2012). This allows the CB to act as a protective peripheral chemoreceptor that detects and responds to arterial hypoxia, leading to downstream reflex activation (Kumar, 2009). Of the proposed O_2 sensors within the CB, including the mitochondria, haem-oxygenase 2, NADPH-oxidase and O_2-dependent K^+ ion channels, only the mitochondria have been identified as having a unique phenotype in comparison with other O_2-insensitive cell types (Holmes et al., 2018a) and it has become increasingly apparent that the type I cell mitochondria have an important role in CB O_2 sensing.

228

References

ABBOTT-BANNER, K., POLL, C. & VERKUYL, J. M. 2013. Targeting TRP Channels in Airway Disorders. *Current Topics in Medicinal Chemistry,* 13**,** 310-321.

ABDALA, A. P., MCBRYDE, F. D., MARINA, N., HENDY, E. B., ENGELMAN, Z. J., FUDIM, M., SOBOTKA, P. A., GOURINE, A. V. & PATON, J. F. 2012. Hypertension is critically dependent on the carotid body input in the spontaneously hypertensive rat. *J Physiol,* 590**,** 4269-77.

ABE, H., SEMBA, H. & TAKEDA, N. 2017. The Roles of Hypoxia Signaling in the Pathogenesis of Cardiovascular Diseases. *J Atheroscler Thromb,* 24**,** 884-894.

ABRAMOWITZ, J., YILDIRIM, E. & BIRNBAUMER, L. 2007. The TRPC Family of Ion Channels: Relation to the TRP Superfamily and Role in Receptor- and Store-Operated Calcium Entry. *In:* LIEDTKE, W. B. & HELLER, S. (eds.) *TRP Ion Channel Function in Sensory Transduction and Cellular Signaling Cascades.* Boca Raton (FL).

ADEOYE, O. O., SILPANISONG, J., WILLIAMS, J. M. & PEARCE, W. J. 2015. Role of the sympathetic autonomic nervous system in hypoxic remodeling of the fetal cerebral vasculature. *J Cardiovasc Pharmacol,* 65**,** 308-16.

AGUSTI, A. & FANER, R. 2012. Systemic inflammation and comorbidities in chronic obstructive pulmonary disease. *Proc Am Thorac Soc,* 9**,** 43-6.

AKGUL, F., BATYRALIEV, T., KARBEN, Z. & PERSHUKOV, I. 2007. Effects of acute hypoxia on left and right ventricular contractility in chronic obstructive pulmonary disease. *Int J Chron Obstruct Pulmon Dis,* 2**,** 77-80.

ALBERT, P. & CALVERLEY, P. 2007. Chronic obstructive pulmonary disease. *Journal of the Royal College of Physicians of Edinburgh,* 37**,** 213-217.

ALBRECHT, M., HENKE, J., TACKE, S., MARKERT, M. & GUTH, B. 2014. Influence of repeated anaesthesia on physiological parameters in male Wistar rats: a telemetric study about isoflurane, ketamine-xylazine and a combination of medetomidine, midazolam and fentanyl. *BMC Vet Res,* 10**,** 310.

ALDOSSARY, H. S., ALZAHRANI, A. A., NATHANAEL, D., ALHUTHAIL, E. A., RAY, C. J., BATIS, N., KUMAR, P., CONEY, A. M. & HOLMES, A. P. 2020. G-Protein-Coupled Receptor (GPCR) Signaling in the Carotid Body: Roles in Hypoxia and Cardiovascular and Respiratory Disease. *Int J Mol Sci,* 21.

ALDOSSARY, H. S., NIEVES, D. J., KAVANAGH, D. M., OWEN, D., RAY, C. J., KUMAR, P., CONEY, A. M. & HOLMES, A. P. 2023. Analyzing Angiotensin II Receptor Type 1 Clustering in PC12 Cells in Response to Hypoxia Using Direct Stochastic Optical Reconstruction Microscopy (dSTORM). *Adv Exp Med Biol,* 1427**,** 175-184.

ALLEN, A. M. 1998a. Angiotensin AT1 receptor-mediated excitation of rat carotid body chemoreceptor afferent activity. *J Physiol,* 510 (Pt 3)**,** 773-81.

ALLEN, A. M. 1998b. Angiotensin AT1 receptor-mediated excitation of rat carotid body chemoreceptor afferent activity. *J Physiol,* 510 (Pt 3)**,** 773-81.

ALLEN, A. M. 1998c. Angiotensin AT(1) receptor-mediated excitation of rat carotid body chemoreceptor afferent activity. *Journal of Physiology-London,* 510**,** 773-781.

ALZAHRANI, A. A., CAO, L. L., ALDOSSARY, H. S., NATHANAEL, D., FU, J., RAY, C. J., BRAIN, K. L., KUMAR, P., CONEY, A. M. & HOLMES, A. P. 2021a. beta-Adrenoceptor blockade prevents carotid body hyperactivity and elevated vascular sympathetic nerve density induced by chronic intermittent hypoxia. *Pflugers Arch,* 473**,** 37-51.

ALZAHRANI, A. A., CAO, L. L., ALDOSSARY, H. S., NATHANAEL, D., FU, J., RAY, C. J., BRAIN, K. L., KUMAR, P., CONEY, A. M. & HOLMES, A. P. 2021b. β-Adrenoceptor blockade prevents carotid body hyperactivity and elevated vascular sympathetic nerve density induced by chronic intermittent hypoxia. *Pflugers Arch,* 473**,** 37-51.

AMBALAVANAN, N., LI, P., BULGER, A., MURPHY-ULLRICH, J., OPARIL, S. & CHEN, Y. F. 2007. Endothelin-1 mediates hypoxia-induced increases in vascular collagen in the newborn mouse lung. *Pediatr Res,* 61**,** 559-64.

AMINIAHIDASHTI, H., SHAFIEE, S., ZAMANI KIASARI, A. & SAZGAR, M. 2018. Applications of End-Tidal Carbon Dioxide (ETCO2) Monitoring in Emergency Department; a Narrative Review. *Emerg (Tehran),* 6**,** e5.

AMODEO, A. A. & SKOTHEIM, J. M. 2016. Cell-Size Control. *Cold Spring Harb Perspect Biol,* 8**,** a019083.

ANDREAS, S., HERRMANN-LINGEN, C., RAUPACH, T., LUTHJE, L., FABRICIUS, J. A., HRUSKA, N., KORBER, W., BUCHNER, B., CRIEE, C. P., HASENFUSS, G. & CALVERLEY, P. 2006. Angiotensin II blockers in obstructive pulmonary disease: a randomised controlled trial. *Eur Respir J,* 27**,** 972-9.

ARAKAWA, K., ARAKAWA, H., HUESTON, C. M. & DEAK, T. 2014. Effects of the estrous cycle and ovarian hormones on central expression of interleukin-1 evoked by stress in female rats. *Neuroendocrinology,* 100**,** 162-77.

ARIAS-MAYENCO, I., GONZALEZ-RODRIGUEZ, P., TORRES-TORRELO, H., GAO, L., FERNANDEZ-AGUERA, M. C., BONILLA-HENAO, V., ORTEGA-SAENZ, P. & LOPEZ-BARNEO, J. 2018. Acute O(2) Sensing: Role of Coenzyme QH(2)/Q Ratio and Mitochondrial ROS Compartmentalization. *Cell Metab,* 28**,** 145-158 e4.

ATANASOVA, D. Y., DANDOV, A. D., DIMITROV, N. D. & LAZAROV, N. E. 2018a. Immunohistochemical localization of angiotensin AT1 receptors in the rat carotid body. *Acta Histochem,* 120**,** 154-158.

ATANASOVA, D. Y., DANDOV, A. D., DIMITROV, N. D. & LAZAROV, N. E. 2018b. Immunohistochemical localization of angiotensin AT(1) receptors in the rat carotid body. *Acta Histochem,* 120**,** 154-158.

ATANASOVA, D. Y., DANDOV, A. D., DIMITROV, N. D. & LAZAROV, N. E. 2018c. Immunohistochemical localization of angiotensin AT(1) receptors in the rat carotid body. *Acta Histochemica,* 120**,** 154-158.

AVILA-MEDINA, J., MAYORAL-GONZALEZ, I., DOMINGUEZ-RODRIGUEZ, A., GALLARDO-CASTILLO, I., RIBAS, J., ORDOÑEZ, A., ROSADO, J. A. & SMANI, T. 2018. The Complex Role of Store Operated Calcium Entry Pathways and Related Proteins in the Function of Cardiac, Skeletal and Vascular Smooth Muscle Cells. *Front Physiol,* 9**,** 257.

BADDELEY, D., JAYASINGHE, I., CREMER, C., CANNELL, M. B. & SOELLER, C. 2009. Light-induced dark states of organic fluochromes enable 30 nm resolution imaging in standard media. *Biophys J,* 96**,** L22-4.

BADOER, E. 2020. The Carotid Body a Common Denominator for Cardiovascular and Metabolic Dysfunction? *Front Physiol,* 11**,** 1069.

BALL, M. K., WAYPA, G. B., MUNGAI, P. T., NIELSEN, J. M., CZECH, L., DUDLEY, V. J., BEUSSINK, L., DETTMAN, R. W., BERKELHAMER, S. K., STEINHORN, R. H., SHAH, S. J. & SCHUMACKER, P. T. 2014. Regulation of hypoxia-induced pulmonary hypertension by vascular smooth muscle hypoxia-inducible factor-1alpha. *Am J Respir Crit Care Med,* 189**,** 314-24.

BARALDO, S., TURATO, G. & SAETTA, M. 2012. Pathophysiology of the small airways in chronic obstructive pulmonary disease. *Respiration, 84*, 89-97.

BARER, G. R., HERGET, J., SLOAN, P. J. & SUGGETT, A. J. 1978. The effect of acute and chronic hypoxia on thoracic gas volume in anaesthetized rats. *J Physiol, 277*, 177-92.

BARNES, L. A., MESARWI, O. A. & SANCHEZ-AZOFRA, A. 2022. The Cardiovascular and Metabolic Effects of Chronic Hypoxia in Animal Models: A Mini-Review. *Front Physiol, 13*, 873522.

BARNES, P. J. & CELLI, B. R. 2009. Systemic manifestations and comorbidities of COPD. *Eur Respir J, 33*, 1165-85.

BAVIS, R. W., SONG, M. J., SMACHLO, J. P., HULSE, A., KENISON, H. R., PERALTA, J. N., PLACE, J. T., TRIEBWASSER, S., WARDEN, S. E. & MCDONOUGH, A. B. 2020. Ventilatory and carotid body responses to acute hypoxia in rats exposed to chronic hypoxia during the first and second postnatal weeks. *Respir Physiol Neurobiol, 275*, 103400.

BECKHAUSER, T. F., FRANCIS-OLIVEIRA, J. & DE PASQUALE, R. 2016. Reactive Oxygen Species: Physiological and Physiopathological Effects on Synaptic Plasticity. *J Exp Neurosci, 10*, 23-48.

BERNARDINI, A., WOLF, A., BROCKMEIER, U., RIFFKIN, H., METZEN, E., ACKER-PALMER, A., FANDREY, J. & ACKER, H. 2020. Carotid body type I cells engage flavoprotein and Pin1 for oxygen sensing. *Am J Physiol Cell Physiol, 318*, C719-C731.

BIAN, J., LEI, J., YIN, X., WANG, P., WU, Y., YANG, X., WANG, L., ZHANG, S., LIU, H. & FU, M. L. X. 2019. Limited AT1 Receptor Internalization Is a Novel Mechanism Underlying Sustained Vasoconstriction Induced by AT1 Receptor Autoantibody From Preeclampsia. *J Am Heart Assoc, 8*, e011179.

BIN-JALIAH, I., MASKELL, P. D. & KUMAR, P. 2004. Indirect sensing of insulin-induced hypoglycaemia by the carotid body in the rat. *J Physiol, 556*, 255-66.

BISGARD, G. E. 2000. Carotid body mechanisms in acclimatization to hypoxia. *Respir Physiol, 121*, 237-46.

BISHOP, T., TALBOT, N. P., TURNER, P. J., NICHOLLS, L. G., PASCUAL, A., HODSON, E. J., DOUGLAS, G., FIELDING, J. W., SMITH, T. G., DEMETRIADES, M., SCHOFIELD, C. J., ROBBINS, P. A., PUGH, C. W., BUCKLER, K. J. & RATCLIFFE, P. J. 2013. Carotid body hyperplasia and enhanced ventilatory responses to hypoxia in mice with heterozygous deficiency of PHD2. *J Physiol, 591*, 3565-77.

BOERS, E., BARRETT, M., SU, J. G., BENJAFIELD, A. V., SINHA, S., KAYE, L., ZAR, H. J., VUONG, V., TELLEZ, D., GONDALIA, R., RICE, M. B., NUNEZ, C. M., WEDZICHA, J. A. & MALHOTRA, A. 2023. Global Burden of Chronic Obstructive Pulmonary Disease Through 2050. *JAMA Netw Open, 6*, e2346598.

BORK, K., WURM, F., HALLER, H., STRAUSS, C., SCHELLER, C., GNANAPRAGASSAM, V. S. & HORSTKORTE, R. 2015. Neuroprotective and neuroregenerative effects of nimodipine in a model system of neuronal differentiation and neurite outgrowth. *Molecules, 20*, 1003-13.

BOUTILIER, R. G. 2001. Mechanisms of cell survival in hypoxia and hypothermia. *Journal of Experimental Biology, 204*, 3171-3181.

BOYLE, R. & POMPEIANO, O. 1981. Relation between cell size and response characteristics of vestibulospinal neurons to labyrinth and neck inputs. *J Neurosci, 1*, 1052-66.

BRASSINGTON, K., SELEMIDIS, S., BOZINOVSKI, S. & VLAHOS, R. 2022. Chronic obstructive pulmonary disease and atherosclerosis: common mechanisms and novel therapeutics. *Clin Sci (Lond), 136*, 405-423.

BRINKMAN, J. E., TORO, F. & SHARMA, S. 2023. Physiology, Respiratory Drive. *StatPearls.* Treasure Island (FL) ineligible companies. Disclosure: Fadi Toro declares no relevant financial relationships with ineligible companies. Disclosure: Sandeep Sharma declares no relevant financial relationships with ineligible companies.

BROWN, C. V., BOULET, L. M., VERMEULEN, T. D., SANDS, S. A., WILSON, R. J. A., AYAS, N. T., FLORAS, J. S. & FOSTER, G. E. 2020. Angiotensin II-Type I Receptor Antagonism Does Not Influence the Chemoreceptor Reflex or Hypoxia-Induced Central Sleep Apnea in Men. *Frontiers in Neuroscience,* 14**,** 13.

BUCKLER, K. J. 2015a. TASK channels in arterial chemoreceptors and their role in oxygen and acid sensing. *Pflugers Archiv-European Journal of Physiology,* 467**,** 1013-1025.

BUCKLER, K. J. 2015b. TASK channels in arterial chemoreceptors and their role in oxygen and acid sensing. *Pflugers Arch,* 467**,** 1013-25.

BUCKLER, K. J. & TURNER, P. J. 2013. Oxygen sensitivity of mitochondrial function in rat arterial chemoreceptor cells. *J Physiol,* 591**,** 3549-63.

BUNIEL, M. C., SCHILLING, W. P. & KUNZE, D. L. 2003a. Distribution of transient receptor potential channels in the rat carotid chemosensory pathway. *J Comp Neurol,* 464**,** 404-13.

BUNIEL, M. C. F., SCHILLING, W. P. & KUNZE, D. L. 2003b. Distribution of transient receptor potential channels in the rat carotid chemosensory pathway. *Journal of Comparative Neurology,* 464**,** 404-413.

CABELLO-RIVERA, D., ORTEGA-SAENZ, P., GAO, L., MUNOZ-CABELLO, A. M., BONILLA-HENAO, V., SCHUMACKER, P. T. & LOPEZ-BARNEO, J. 2022. Oxygen regulation of breathing is abolished in mitochondrial complex III-deficient arterial chemoreceptors. *Proc Natl Acad Sci U S A,* 119**,** e2202178119.

CALBET, J. A. 2003. Chronic hypoxia increases blood pressure and noradrenaline spillover in healthy humans. *J Physiol,* 551**,** 379-86.

CASEY, J. D. & SEMLER, M. W. 2019. Beginning of the End? End-tidal Oxygen as an Outcome in Airway Management Research. *EClinicalMedicine,* 13**,** 10-11.

CASTELLO, P. R., WOO, D. K., BALL, K., WOJCIK, J., LIU, L. & POYTON, R. O. 2008. Oxygen-regulated isoforms of cytochrome c oxidase have differential effects on its nitric oxide production and on hypoxic signaling. *Proc Natl Acad Sci U S A,* 105**,** 8203-8.

CHANG, A. J., ORTEGA, F. E., RIEGLER, J., MADISON, D. V. & KRASNOW, M. A. 2015. Oxygen regulation of breathing through an olfactory receptor activated by lactate. *Nature,* 527**,** 240-4.

CHANG, T. B., HSU, J. C. & YANG, T. T. 2023. Single-molecule localization microscopy reveals the ultrastructural constitution of distal appendages in expanded mammalian centrioles. *Nat Commun,* 14**,** 1688.

CHATILA, W. M., THOMASHOW, B. M., MINAI, O. A., CRINER, G. J. & MAKE, B. J. 2008. Comorbidities in chronic obstructive pulmonary disease. *Proc Am Thorac Soc,* 5**,** 549-55.

CHEN, S., KUHN, M., PRETTNER, K., YU, F., YANG, T., BARNIGHAUSEN, T., BLOOM, D. E. & WANG, C. 2023. The global economic burden of chronic obstructive pulmonary disease for 204 countries and territories in 2020-50: a health-augmented macroeconomic modelling study. *Lancet Glob Health,* 11**,** e1183-e1193.

CHEN, S., TAKAHASHI, N., CHEN, C., PAULI, J. L., KUROKI, C., KAMINOSONO, J., KASHIWADANI, H., KANMURA, Y., MORI, Y., OU, S., HAO, L. & KUWAKI, T. 2020a. Transient Receptor Potential Ankyrin 1 Mediates Hypoxic Responses in Mice. *Front Physiol,* 11**,** 576209.

CHEN, X., SOOCH, G., DEMAREE, I. S., WHITE, F. A. & OBUKHOV, A. G. 2020b. Transient Receptor Potential Canonical (TRPC) Channels: Then and Now. *Cells,* 9.

CHENG, X. Y., BISWAS, S., LI, J., MAO, C. J., CHECHNEVA, O., CHEN, J., LI, K., ZHANG, J. R., LIU, C. F. & DENG, W. B. 2020. Human iPSCs derived astrocytes rescue rotenone-induced mitochondrial dysfunction and dopaminergic neurodegeneration in vitro by donating functional mitochondria. *Transl Neurodegener,* 9**,** 13.

CHERNIACK, N. S., VON EULER, C., GLOGOWSKA, M. & HOMMA, I. 1981. Characteristics and rate of occurrence of spontaneous and provoked augmented breaths. *Acta Physiol Scand,* 111**,** 349-60.

CHIOCCHIO, S. R., BISCARDI, A. M. & TRAMEZZANI, J. H. 1966. Catecholamines in the carotid body of the cat. *Nature,* 212**,** 834-5.

CHO, Y. J., MA, J. E., YUN, E. Y., KIM, Y. E., KIM, H. C., LEE, J. D., HWANG, Y. S. & JEONG, Y. Y. 2011. Serum angiopoietin-2 levels are elevated during acute exacerbations of COPD. *Respirology,* 16**,** 284-90.

CHOKSHI, R., FRUASAHA, P. & KOZAK, J. A. 2012. 2-aminoethyl diphenyl borinate (2-APB) inhibits TRPM7 channels through an intracellular acidification mechanism. *Channels (Austin),* 6**,** 362-9.

CHUA, P. & LIM, W. K. 2023. The strategic uses of collagen in adherent cell cultures. *Cell Biol Int,* 47**,** 367-373.

COLLINGRIDGE, G. L., ISAAC, J. T. & WANG, Y. T. 2004. Receptor trafficking and synaptic plasticity. *Nat Rev Neurosci,* 5**,** 952-62.

COLTON, C. K. & ZHU, M. X. 2007. 2-Aminoethoxydiphenyl borate as a common activator of TRPV1, TRPV2, and TRPV3 channels. *Handb Exp Pharmacol***,** 173-87.

CONDE, S. V., GONZALEZ, C., BATUCA, J. R., MONTEIRO, E. C. & OBESO, A. 2008. An antagonistic interaction between A2B adenosine and D2 dopamine receptors modulates the function of rat carotid body chemoreceptor cells. *J Neurochem,* 107**,** 1369-81.

CONEY, A. M., BISHAY, M. & MARSHALL, J. M. 2004. Influence of endogenous nitric oxide on sympathetic vasoconstriction in normoxia, acute and chronic systemic hypoxia in the rat. *J Physiol,* 555**,** 793-804.

CONEY, A. M., HOLMES, A., RAY, C. J., JOHNSTON, J., WILLIAMS, N. & KUMAR, P. 2022. Poster Communications: Severe hypoxia reduces the randomness and variability of carotid body (CB) sensory patterning. *The Physiological Society* 50, C20.

CONFORTI, L., BODI, I., NISBET, J. W. & MILLHORN, D. E. 2000. O2-sensitive K+ channels: role of the Kv1.2 -subunit in mediating the hypoxic response. *J Physiol,* 524 Pt 3**,** 783-93.

COWBURN, A. S., MACIAS, D., SUMMERS, C., CHILVERS, E. R. & JOHNSON, R. S. 2017. Cardiovascular adaptation to hypoxia and the role of peripheral resistance. *Elife,* 6.

CRAMER, T. & JOHNSON, R. S. 2003. A Novel Role for the Hypoxia Inducible Transcription Factor HIF-1α Critical Regulation of Inflammatory Cell Function. *Cell Cycle,* 2**,** 192-193.

CRIÉE, C. P., SORICHTER, S., SMITH, H. J., KARDOS, P., MERGET, R., HEISE, D., BERDEL, D., KÖHLER, D., MAGNUSSEN, H., MAREK, W., MITFESSEL, H., RASCHE, K., ROLKE, M., WORTH, H., JÖRRES, R. A. & CARE, W. G. F. B. P. O. T. G. S. F. P. A. R. 2011. Body plethysmography--its principles and clinical use. *Respir Med,* 105**,** 959-71.

CUKIC, V. 2014. The changes of arterial blood gases in COPD during four-year period. *Med Arch,* 68**,** 14-8.

CUMMINS, E. P., STROWITZKI, M. J. & TAYLOR, C. T. 2020. Mechanisms and Consequences of Oxygen and Carbon Dioxide Sensing in Mammals. *Physiol Rev,* 100**,** 463-488.

CZYZYK-KRZESKA, M. F., BAYLISS, D. A., LAWSON, E. E. & MILLHORN, D. E. 1992. Regulation of tyrosine hydroxylase gene expression in the rat carotid body by hypoxia. *J Neurochem,* 58**,** 1538-46.

DAHAN, A. & TEPPEMA, L. J. 2003. Influence of anaesthesia and analgesia on the control of breathing. *Br J Anaesth,* 91**,** 40-9.

DASGUPTA, C. & ZHANG, L. 2011. Angiotensin II receptors and drug discovery in cardiovascular disease. *Drug Discov Today,* 16**,** 22-34.

DAUBNER, S. C., LE, T. & WANG, S. Z. 2011. Tyrosine hydroxylase and regulation of dopamine synthesis. *Archives of Biochemistry and Biophysics,* 508**,** 1-12.

DELMAS, P., WANAVERBECQ, N., ABOGADIE, F. C., MISTRY, M. & BROWN, D. A. 2002. Signaling microdomains define the specificity of receptor-mediated InsP(3) pathways in neurons. *Neuron,* 34**,** 209-20.

DEMPSEY, J. A. & FORSTER, H. V. 1982. Mediation of Ventilatory Adaptations. *Physiol Rev,* 62**,** 262-346.

DEVAUX, C. A. & LAGIER, J. C. 2023. Unraveling the Underlying Molecular Mechanism of 'Silent Hypoxia' in COVID-19 Patients Suggests a Central Role for Angiotensin II Modulation of the AT1R-Hypoxia-Inducible Factor Signaling Pathway. *J Clin Med,* 12.

DEVECI, D., MARSHALL, J. M. & EGGINTON, S. 2001. Relationship between capillary angiogenesis, fiber type, and fiber size in chronic systemic hypoxia. *Am J Physiol Heart Circ Physiol,* 281**,** H241-52.

DEVINE, J. F. 2008. Chronic obstructive pulmonary disease: an overview. *Am Health Drug Benefits,* 1**,** 34-42.

DRAKE, M. T., SHENOY, S. K. & LEFKOWITZ, R. J. 2006. Trafficking of G protein-coupled receptors. *Circ Res,* 99**,** 570-82.

DRYER, S. E., ROSHANRAVAN, H. & KIM, E. Y. 2019. TRPC channels: Regulation, dysregulation and contributions to chronic kidney disease. *Biochim Biophys Acta Mol Basis Dis,* 1865**,** 1041-1066.

DUKE, T. & GRAHAM, I. 2009. Equilibrium mechanisms of receptor clustering. *Prog Biophys Mol Biol,* 100**,** 18-24.

DUNHAM-SNARY, K. J., WU, D., SYKES, E. A., THAKRAR, A., PARLOW, L. R. G., MEWBURN, J. D., PARLOW, J. L. & ARCHER, S. L. 2017. Hypoxic Pulmonary Vasoconstriction: From Molecular Mechanisms to Medicine. *Chest,* 151**,** 181-192.

DWINELL, M. R. & POWELL, F. L. 1999. Chronic hypoxia enhances the phrenic nerve response to arterial chemoreceptor stimulation in anesthetized rats. *J Appl Physiol (1985),* 87**,** 817-23.

EDMUNDS, N. J. & MARSHALL, J. M. 2003. The roles of nitric oxide in dilating proximal and terminal arterioles of skeletal muscle during systemic hypoxia. *J Vasc Res,* 40**,** 68-76.

ENDESFELDER, U. & HEILEMANN, M. 2015. Direct stochastic optical reconstruction microscopy (dSTORM). *Methods Mol Biol,* 1251**,** 263-76.

ESSOP, M. F. 2007. Cardiac metabolic adaptations in response to chronic hypoxia. *J Physiol,* 584**,** 715-26.

ESTER, M., KRIEGEL, H.-P., SANDER, J. & XU, X. A density-based algorithm for discovering clusters in large spatial databases with noise. kdd, 1996. 226-231.

FASCIANI, I., CARLI, M., PETRAGNANO, F., COLAIANNI, F., ALOISI, G., MAGGIO, R., SCARSELLI, M. & ROSSI, M. 2022. GPCRs in Intracellular Compartments: New Targets for Drug Discovery. *Biomolecules,* 12.

FELIPPE, I. S. A., ZERA, T., DA SILVA, M. P., MORAES, D. J. A., MCBRYDE, F. & PATON, J. F. R. 2023. The sympathetic nervous system exacerbates carotid body sensitivity in hypertension. *Cardiovasc Res,* 119**,** 316-331.

FELLERS.T.J.; & DAVIDSON.M.W. 2021. *Introduction to Confocal Microscopy* [Online]. Tallahassee, Florida: OLYMPUS CORPORATION. Available: https://www.olympus-lifescience.com/en/microscope-resource/primer/techniques/confocal/confocalintro/ [Accessed 4 June 2021].

FENG, Y., LI, M., WANG, Y., YANG, M., SHI, G., YIN, D., XUAN, Z. & XU, F. 2022. Activation of TRPC6 by AngⅡ Induces Podocyte Injury and Participates in Proteinuria of Nephrotic Syndrome. *Front Pharmacol,* 13**,** 915153.

FERNANDEZ-AGUERA, M. C., GAO, L., GONZALEZ-RODRIGUEZ, P., PINTADO, C. O., ARIAS-MAYENCO, I., GARCIA-FLORES, P., GARCIA-PERGANEDA, A., PASCUAL, A., ORTEGA-SAENZ, P. & LOPEZ-BARNEO, J. 2015. Oxygen Sensing by Arterial Chemoreceptors Depends on Mitochondrial Complex I Signaling. *Cell Metab,* 22**,** 825-37.

FIDONE, S., GONZALEZ, C. & YOSHIZAKI, K. 1982. Effects of low oxygen on the release of dopamine from the rabbit carotid body in vitro. *J Physiol,* 333**,** 93-110.

FIELDING, J. W., HODSON, E. J., CHENG, X., FERGUSON, D. J. P., ECKARDT, L., ADAM, J., LIP, P., MATON-HOWARTH, M., RATNAYAKA, I., PUGH, C. W., BUCKLER, K. J., RATCLIFFE, P. J. & BISHOP, T. 2018. PHD2 inactivation in Type I cells drives HIF-2alpha-dependent multilineage hyperplasia and the formation of paraganglioma-like carotid bodies. *J Physiol,* 596**,** 4393-412.

FINKS, S. W., RUMBAK, M. J. & SELF, T. H. 2020. Treating Hypertension in Chronic Obstructive Pulmonary Disease. *N Engl J Med,* 382**,** 353-363.

FISH, K. N. 2009. Total internal reflection fluorescence (TIRF) microscopy. *Curr Protoc Cytom,* Chapter 12**,** Unit12.18.

FISHMAN, M., JACONO, F. J., PARK, S., JAMASEBI, R., THUNGTONG, A., LOPARO, K. A. & DICK, T. E. 2012. A method for analyzing temporal patterns of variability of a time series from Poincare plots. *J Appl Physiol (1985),* 113**,** 297-306.

FORIS, V., KOVACS, G., TSCHERNER, M., OLSCHEWSKI, A. & OLSCHEWSKI, H. 2013. Biomarkers in pulmonary hypertension: what do we know? *Chest,* 144**,** 274-283.

FORRESTER, S. J., BOOZ, G. W., SIGMUND, C. D., COFFMAN, T. M., KAWAI, T., RIZZO, V., SCALIA, R. & EGUCHI, S. 2018. Angiotensin II Signal Transduction: An Update on Mechanisms of Physiology and Pathophysiology. *Physiol Rev,* 98**,** 1627-1738.

FUNG, H. F. & BERGMANN, D. C. 2023. Function follows form: How cell size is harnessed for developmental decisions. *Eur J Cell Biol,* 102**,** 151312.

FUNG, M. L. 2014. The role of local renin-angiotensin system in arterial chemoreceptors in sleep-breathing disorders. *Front Physiol,* 5**,** 336.

FUNG, M. L., LAM, S. Y., CHEN, Y., DONG, X. & LEUNG, P. S. 2001. Functional expression of angiotensin II receptors in type-I cells of the rat carotid body. *Pflugers Arch,* 441**,** 474-80.

GAO, L., BONILLA-HENAO, V., GARCIA-FLORES, P., ARIAS-MAYENCO, I., ORTEGA-SAENZ, P. & LOPEZ-BARNEO, J. 2017. Gene expression analyses reveal metabolic specifications in acute O(2) -sensing chemoreceptor cells. *J Physiol,* 595**,** 6091-6120.

GARRIDO, A. M. & GRIENDLING, K. K. 2009. NADPH oxidases and angiotensin II receptor signaling. *Mol Cell Endocrinol,* 302**,** 148-58.

GARROD, R., MARSHALL, J., BARLEY, E. & JONES, P. W. 2006. Predictors of success and failure in pulmonary rehabilitation. *Eur Respir J,* 27**,** 788-94.

GEES, M., COLSOUL, B. & NILIUS, B. 2010. The role of transient receptor potential cation channels in Ca^{2+} signaling. *Cold Spring Harb Perspect Biol,* 2, a003962.

GOLD, O. M. S., BARDSLEY, E. N., PONNAMPALAM, A. P., PAUZA, A. G. & PATON, J. F. R. 2022. Cellular basis of learning and memory in the carotid body. *Frontiers in Synaptic Neuroscience,* 14.

GORNY, D. A. 1993. Arterial blood pressure measurement technique. *AACN Clin Issues Crit Care Nurs,* 4**,** 66-80.

GREEN, K. N., BOYLE, J. P. & PEERS, C. 2002. Hypoxia potentiates exocytosis and Ca^{2+} channels in PC12 cells via increased amyloid beta peptide formation and reactive oxygen species generation. *J Physiol,* 541**,** 1013-23.

GREENE, L. A. & TISCHLER, A. S. 1976. Establishment of a noradrenergic clonal line of rat adrenal pheochromocytoma cells which respond to nerve growth factor. *Proc Natl Acad Sci U S A,* 73**,** 2424-8.

GREULICH, T., WEIST, B. J. D., KOCZULLA, A. R., JANCIAUSKIENE, S., KLEMMER, A., LUX, W., ALTER, P. & VOGELMEIER, C. F. 2017. Prevalence of comorbidities in COPD patients by disease severity in a German population. *Respir Med,* 132**,** 132-138.

GU, Y. Q., HUANG, D. J. & HU, B. X. 1989. [Influence of acute respiratory failure on plasma renin activity and plasma angiotensin II level in advanced chronic obstructive pulmonary disease and chronic cor pulmonale]. *Zhonghua Nei Ke Za Zhi,* 28**,** 347-50, 381.

GUYENET, P. G., STORNETTA, R. L. & BAYLISS, D. A. 2010. Central respiratory chemoreception. *J Comp Neurol,* 518**,** 3883-906.

HAASE, V. H. 2010. Hypoxic regulation of erythropoiesis and iron metabolism. *Am J Physiol Renal Physiol,* 299**,** F1-13.

HAMDOLLAH ZADEH, M. A., GLASS, C. A., MAGNUSSEN, A., HANCOX, J. C. & BATES, D. O. 2008. VEGF-mediated elevated intracellular calcium and angiogenesis in human microvascular endothelial cells in vitro are inhibited by dominant negative TRPC6. *Microcirculation,* 15**,** 605-14.

HEDENSTIERNA, G. & ROTHEN, H. U. 2012. Respiratory function during anesthesia: effects on gas exchange. *Compr Physiol,* 2**,** 69-96.

HEINDL, S., LEHNERT, M., CRIEE, C. P., HASENFUSS, G. & ANDREAS, S. 2001. Marked sympathetic activation in patients with chronic respiratory failure. *Am J Respir Crit Care Med,* 164**,** 597-601.

HEMPLEMAN, S. C. 1996. Increased calcium current in carotid body glomus cells following in vivo acclimatization to chronic hypoxia. *J Neurophysiol,* 76**,** 1880-6.

HERMOSILLA, T., ENCINA, M., MORALES, D., MORENO, C., CONEJEROS, C., ALFARO-VALDES, H. M., LAGOS-MEZA, F., SIMON, F., ALTIER, C. & VARELA, D. 2017. Prolonged AT(1)R activation induces Ca(V)1.2 channel internalization in rat cardiomyocytes. *Sci Rep,* 7**,** 10131.

HESS, D. R. & BIGATELLO, L. M. 2002. Lung recruitment: the role of recruitment maneuvers. *Respir Care,* 47**,** 308-17; discussion 317-8.

HOGG, J. C. & TIMENS, W. 2009. The pathology of chronic obstructive pulmonary disease. *Annu Rev Pathol,* 4**,** 435-59.

HOLMES, A. P., RAY, C. J., CONEY, A. M. & KUMAR, P. 2018a. Is Carotid Body Physiological O(2) Sensitivity Determined by a Unique Mitochondrial Phenotype? *Front Physiol,* 9**,** 562.

HOLMES, A. P., RAY, C. J., PEARSON, S. A., CONEY, A. M. & KUMAR, P. 2018b. Ecto-5'-nucleotidase (CD73) regulates peripheral chemoreceptor activity and cardiorespiratory responses to hypoxia. *J Physiol,* 596**,** 3137-3148.

HOLMES, A. P., RAY, C. J., THOMPSON, E. L., ALSHEHRI, Z., CONEY, A. M. & KUMAR, P. 2019. Adrenaline activation of the carotid body: Key to CO(2) and pH homeostasis in hypoglycaemia and potential pathological implications in cardiovascular disease. *Respir Physiol Neurobiol,* 265**,** 92-99.

HOLMES, A. P., SWIDERSKA, A., NATHANAEL, D., ALDOSSARY, H. S., RAY, C. J., CONEY, A. M. & KUMAR, P. 2022. Are Multiple Mitochondrial Related Signalling Pathways Involved in Carotid Body Oxygen Sensing? *Front Physiol,* 13**,** 908617.

HOLMES, A. P., TURNER, P. J., CARTER, P., LEADBEATER, W., RAY, C. J., HAUTON, D., BUCKLER, K. J. & KUMAR, P. 2014. Glycogen metabolism protects against metabolic insult to preserve carotid body function during glucose deprivation. *J Physiol,* 592**,** 4493-506.

HU, C. J., WANG, L. Y., CHODOSH, L. A., KEITH, B. & SIMON, M. C. 2003. Differential roles of hypoxia-inducible factor 1α (HIF-1α) and HIF-2α in hypoxic gene regulation. *Molecular and Cellular Biology,* 23**,** 9361-9374.

HUGHES, M. J., MCGETTRICK, H. M. & SAPEY, E. 2020. Shared mechanisms of multimorbidity in COPD, atherosclerosis and type-2 diabetes: the neutrophil as a potential inflammatory target. *Eur Respir Rev,* 29.

IKEDA, K., KAWAKAMI, K., ONIMARU, H., OKADA, Y., YOKOTA, S., KOSHIYA, N., OKU, Y., IIZUKA, M. & KOIZUMI, H. 2017. The respiratory control mechanisms in the brainstem and spinal cord: integrative views of the neuroanatomy and neurophysiology. *J Physiol Sci,* 67**,** 45-62.

ILATOVSKAYA, D. V., LEVCHENKO, V., LOWING, A., SHUYSKIY, L. S., PALYGIN, O. & STARUSCHENKO, A. 2015. Podocyte injury in diabetic nephropathy: implications of angiotensin II-dependent activation of TRPC channels. *Sci Rep,* 5**,** 17637.

ILATOVSKAYA, D. V., PALYGIN, O., CHUBINSKIY-NADEZHDIN, V., NEGULYAEV, Y. A., MA, R., BIRNBAUMER, L. & STARUSCHENKO, A. 2014. Angiotensin II has acute effects on TRPC6 channels in podocytes of freshly isolated glomeruli. *Kidney Int,* 86**,** 506-14.

ITURRIAGA, R., ALCAYAGA, J., CHAPLEAU, M. W. & SOMERS, V. K. 2021. Carotid body chemoreceptors: physiology, pathology, and implications for health and disease. *Physiol Rev,* 101**,** 1177-1235.

ITURRIAGA, R., DEL RIO, R., IDIAQUEZ, J. & SOMERS, V. K. 2016a. Carotid body chemoreceptors, sympathetic neural activation, and cardiometabolic disease. *Biological Research,* 49.

ITURRIAGA, R., DEL RIO, R., IDIAQUEZ, J. & SOMERS, V. K. 2016b. Carotid body chemoreceptors, sympathetic neural activation, and cardiometabolic disease. *Biol Res,* 49**,** 13.

JENDZJOWSKY, N. G., ROY, A., IFTINCA, M., BARIONI, N. O., KELLY, M. M., HERRINGTON, B. A., VISSER, F., ALTIER, C. & WILSON, R. J. A. 2021. PKCepsilon stimulation of TRPV1 orchestrates carotid body responses to asthmakines. *J Physiol,* 599**,** 1335-1354.

JENSEN, E. & CROSSMAN, D. J. 2014. Technical review: types of imaging-direct STORM. *Anat Rec (Hoboken),* 297**,** 2227-31.

JOSHI, S., WOLLENZIEN, H., LECLERC, E. & JARAJAPU, Y. P. 2019. Hypoxic regulation of angiotensin-converting enzyme 2 and Mas receptor in human CD34. *J Cell Physiol,* 234**,** 20420-20431.

KAMEDA, Y. 1996. Immunoelectron microscopic localization of vimentin in sustentacular cells of the carotid body and the adrenal medulla of guinea pigs. *J Histochem Cytochem,* 44**,** 1439-49.

KAPARIANOS, A. & ARGYROPOULOU, E. 2011. Local renin-angiotensin II systems, angiotensin-converting enzyme and its homologue ACE2: their potential role in the pathogenesis of chronic obstructive pulmonary diseases, pulmonary hypertension and acute respiratory distress syndrome. *Curr Med Chem,* 18**,** 3506-15.

KARNATI, S., SEIMETZ, M., KLEEFELDT, F., SONAWANE, A., MADHUSUDHAN, T., BACHHUKA, A., KOSANOVIC, D., WEISSMANN, N., KRUGER, K. & ERGUN, S. 2021. Chronic Obstructive Pulmonary Disease and the Cardiovascular System: Vascular Repair and Regeneration as a Therapeutic Target. *Front Cardiovasc Med,* 8**,** 649512.

KATO, K., YAMAGUCHI-YAMADA, M. & YAMAMOTO, Y. 2010. Short-term Hypoxia Increases Tyrosine Hydroxylase Immunoreactivity in Rat Carotid Body. *Journal of Histochemistry & Cytochemistry,* 58**,** 839-846.

KENT, B. D., MITCHELL, P. D. & MCNICHOLAS, W. T. 2011. Hypoxemia in patients with COPD: cause, effects, and disease progression. *Int J Chron Obstruct Pulmon Dis,* 6**,** 199-208.

KIM, D., HOGAN, J. O. & WHITE, C. 2020. Ca(2+) oscillations in rat carotid body type 1 cells in normoxia and hypoxia. *Am J Physiol Cell Physiol,* 318**,** C430-C438.

KIM, H., KIM, J., JEON, J. P., MYEONG, J., WIE, J., HONG, C., KIM, H. J., JEON, J. H. & SO, I. 2012. The roles of G proteins in the activation of TRPC4 and TRPC5 transient receptor potential channels. *Channels (Austin),* 6**,** 333-43.

KIM, I., FITE, L., DONNELLY, D. F., KIM, J. H. & CARROLL, J. L. 2015. Possible Role of TRP Channels in Rat Glomus Cells. *Adv Exp Med Biol,* 860**,** 227-32.

KIM, S. H., PARK, J. H., LEE, J. K., HEO, E. Y., KIM, D. K. & CHUNG, H. S. 2017. Chronic obstructive pulmonary disease is independently associated with hypertension in men: A survey design analysis using nationwide survey data. *Medicine (Baltimore),* 96**,** e6826.

KIM, S. J., FONG, A. Y., PILOWSKY, P. M. & ABBOTT, S. B. G. 2018. Sympathoexcitation following intermittent hypoxia in rat is mediated by circulating angiotensin II acting at the carotid body and subfornical organ. *Journal of Physiology-London,* 596**,** 3217-3232.

KING, P. T. 2015. Inflammation in chronic obstructive pulmonary disease and its role in cardiovascular disease and lung cancer. *Clin Transl Med,* 4**,** 68.

KLEIN, T., SAUER, M., ERGUN, S. & KARNATI, S. 2023. Direct Stochastic Optical Reconstruction Microscopy (dSTORM) of Peroxisomes. *Methods Mol Biol,* 2643**,** 85-92.

KOBAYASHI, S., NISHIMURA, M., YAMOMOTO, M., AKIYAMA, Y., MIYAMOTO, K. & KAWAMAKI, Y. 1996. Relationship between breathlessness and hypoxic and hypercapnic ventilatory response in patients with COPD. *Eur Respir J,* 9**,** 2340-5.

KOBE, J., MISHRA, N., ARYA, V. K., AL-MOUSTADI, W., NATES, W. & KUMAR, B. 2019. Cardiac output monitoring: Technology and choice. *Ann Card Anaesth,* 22**,** 6-17.

KOIZUMI, S., ROSA, P., WILLARS, G. B., CHALLISS, R. A., TAVERNA, E., FRANCOLINI, M., BOOTMAN, M. D., LIPP, P., INOUE, K., RODER, J. & JEROMIN, A. 2002. Mechanisms underlying the neuronal calcium sensor-1-evoked enhancement of exocytosis in PC12 cells. *J Biol Chem,* 277**,** 30315-24.

KRAEMER, R., SMITH, H. J., REINSTAEDTLER, J., GALLATI, S. & MATTHYS, H. 2024. Predicting parameters of airway dynamics generated from inspiratory and expiratory plethysmographic airway loops, differentiating subtypes of chronic obstructive diseases. *BMJ Open Respir Res,* 11.

KROCK, B. L., SKULI, N. & SIMON, M. C. 2011. Hypoxia-induced angiogenesis: good and evil. *Genes Cancer,* 2**,** 1117-33.

KUMAR, P. 2007. Sensing hypoxia in the carotid body: from stimulus to response. *Oxygen Sensing and Hypoxia-Induced Responses,* 43**,** 43-60.

KUMAR, P. 2009. Systemic effects resulting from carotid body stimulation-invited article. *Adv Exp Med Biol,* 648**,** 223-33.

KUMAR, P., PEARSON, S. & GU, Y. 2006a. A role for TRP channels in carotid body chemotransduction? *FASEB J,* 20:A12–29.

KUMAR, P., PEARSON, S. & GU, Y. 2006b. A role for TRP channels in carotid body chemotransduction? *FASEB J* 20:A12–29.

KUMAR, P., PEARSON, S. & GU, Y. 2006c. A role for TRP channels in carotid body chemotransduction? *FASEB J,* 20**,** A1229-A1229.

KUMAR, P. & PRABHAKAR, N. R. 2012a. Peripheral Chemoreceptors: Function and Plasticity of the Carotid Body. *Comprehensive Physiology***,** 141–219.

KUMAR, P. & PRABHAKAR, N. R. 2012b. Peripheral chemoreceptors: function and plasticity of the carotid body. *Compr Physiol,* 2**,** 141-219.

KUMAR P., PEARSON S. & C., G. Y. 2006. A role for TRP channels in carotid body chemotransduction? . *FASEB J* 20**,** A1229-A1229.

KUWAHIRA, I., HEISLER, N., PIIPER, J. & GONZALEZ, N. C. 1993. Effect of chronic hypoxia on hemodynamics, organ blood flow and O2 supply in rats. *Respir Physiol,* 92**,** 227-38.

LAM, S. Y., FUNG, M. L. & LEUNG, P. S. 2004a. Regulation of the angiotensin-converting enzyme activity by a time-course hypoxia in the carotid body. *J Appl Physiol (1985),* 96**,** 809-13.

LAM, S. Y., FUNG, M. L. & LEUNG, P. S. 2004b. Regulation of the angiotensin-converting enzyme activity by a time-course hypoxia in the carotid body. *J Appl Physiol,* 96**,** 809-13.

LAM, S. Y. & LEUNG, P. S. 2003. Chronic hypoxia activates a local angiotensin-generating system in rat carotid body. *Mol Cell Endocrinol,* 203**,** 147-53.

LAM, S. Y., LIU, Y., NG, K. M., LIONG, E. C., TIPOE, G. L., LEUNG, P. S. & FUNG, M. L. 2014. Upregulation of a local renin-angiotensin system in the rat carotid body during chronic intermittent hypoxia. *Exp Physiol,* 99**,** 220-31.

LEE, P., CHANDEL, N. S. & SIMON, M. C. 2020. Cellular adaptation to hypoxia through hypoxia inducible factors and beyond. *Nat Rev Mol Cell Biol,* 21**,** 268-283.

LELEK, M., GYPARAKI, M. T., BELIU, G., SCHUEDER, F., GRIFFIE, J., MANLEY, S., JUNGMANN, R., SAUER, M., LAKADAMYALI, M. & ZIMMER, C. 2021. Single-molecule localization microscopy. *Nat Rev Methods Primers,* 1.

LEONARD, E. M., SALMAN, S. & NURSE, C. A. 2018. Sensory Processing and Integration at the Carotid Body Tripartite Synapse: Neurotransmitter Functions and Effects of Chronic Hypoxia. *Front Physiol,* 9**,** 225.

LEUNG, P. S., FUNG, M. L. & TAM, M. S. 2003. Renin-angiotensin system in the carotid body. *Int J Biochem Cell Biol,* 35**,** 847-54.

LEUNG, P. S., LAM, S. Y. & FUNG, M. L. 2000. Chronic hypoxia upregulates the expression and function of AT(1) receptor in rat carotid body. *J Endocrinol,* 167**,** 517-24.

LEUNG, P. S., YAO, X. Q., CHAN, H. C., FU, L. X. & WONG, P. Y. 1998. Differential gene expression of angiotensin II receptor subtypes in the epididymides of mature and immature rats. *Life Sci,* 62**,** 461-8.

LEVER, J. D., LEWIS, P. R. & BOYD, J. D. 1959. Observations on the fine structure and histochemistry of the carotid body in the cat and rabbit. *J Anat,* 93**,** 478-90.

LI, D., SHAO, L., CHEN, B. C., ZHANG, X., ZHANG, M., MOSES, B., MILKIE, D. E., BEACH, J. R., HAMMER, J. A., PASHAM, M., KIRCHHAUSEN, T., BAIRD, M. A., DAVIDSON, M. W., XU, P. & BETZIG, E. 2015. ADVANCED IMAGING. Extended-resolution structured illumination imaging of endocytic and cytoskeletal dynamics. *Science,* 349**,** aab3500.

LI, L., LIU, W., SUN, Q., ZHU, H., HONG, M. & QIAN, S. 2021. Decitabine Downregulates TIGAR to Induce Apoptosis and Autophagy in Myeloid Leukemia Cells. *Oxid Med Cell Longev,* 2021**,** 8877460.

LI, Y. L., GAO, L., ZUCKER, I. H. & SCHULTZ, H. D. 2007. NADPH oxidase-derived superoxide anion mediates angiotensin II-enhanced carotid body chemoreceptor sensitivity in heart failure rabbits. *Cardiovasc Res,* 75**,** 546-54.

LI, Y. L. & SCHULTZ, H. D. 2006. Enhanced sensitivity of Kv channels to hypoxia in the rabbit carotid body in heart failure: role of angiotensin II. *J Physiol,* 575**,** 215-27.

LI, Y. L., XIA, X. H., ZHENG, H., GAO, L., LI, Y. F., LIU, D., PATEL, K. P., WANG, W. & SCHULTZ, H. D. 2006. Angiotensin II enhances carotid body chemoreflex control of sympathetic outflow in chronic heart failure rabbits. *Cardiovasc Res,* 71**,** 129-38.

LINDSEY, B. G., NUDING, S. C., SEGERS, L. S. & MORRIS, K. F. 2018. Carotid Bodies and the Integrated Cardiorespiratory Response to Hypoxia. *Physiology (Bethesda),* 33**,** 281-297.

LIU, D., YANG, D., HE, H., CHEN, X., CAO, T., FENG, X., MA, L., LUO, Z., WANG, L., YAN, Z., ZHU, Z. & TEPEL, M. 2009. Increased transient receptor potential canonical type 3 channels in vasculature from hypertensive rats. *Hypertension,* 53**,** 70-6.

LIU, Q., KONG, A. L., CHEN, R., QIAN, C., LIU, S. W., SUN, B. G., WANG, L. X., SONG, L. S. & HONG, J. 2011. Propofol and arrhythmias: two sides of the coin. *Acta Pharmacol Sin,* 32**,** 817-23.

LIU, X., RABIN, P. L., YUAN, Y., KUMAR, A., VASALLO, P., 3RD, WONG, J., MITSCHER, G. A., EVERETT, T. H. T. & CHEN, P. S. 2019. Effects of anesthetic and sedative agents on sympathetic nerve activity. *Heart Rhythm,* 16**,** 1875-1882.

LOPEZ-BARNEO, J., GONZALEZ-RODRIGUEZ, P., GAO, L., FERNANDEZ-AGUERA, M. C., PARDAL, R. & ORTEGA-SAENZ, P. 2016. Oxygen sensing by the carotid body: mechanisms and role in adaptation to hypoxia. *Am J Physiol Cell Physiol,* 310**,** C629-42.

LOPEZ-BARNEO, J., LOPEZ-LOPEZ, J. R., URENA, J. & GONZALEZ, C. 1988. Chemotransduction in the carotid body: K+ current modulated by PO2 in type I chemoreceptor cells. *Science,* 241**,** 580-2.

LOPEZ-BARNEO, J., ORTEGA-SAENZ, P., PARDAL, R., PASCUAL, A. & PIRUAT, J. I. 2008. Carotid body oxygen sensing. *Eur Respir J,* 32**,** 1386-98.

LOPEZ-BARNEO, J., PARDAL, R. & ORTEGA-SAENZ, P. 2001. Cellular mechanism of oxygen sensing. *Annu Rev Physiol,* 63**,** 259-87.

LOVICK, T. A. & ZANGROSSI, H. 2021. Effect of Estrous Cycle on Behavior of Females in Rodent Tests of Anxiety. *Front Psychiatry,* 12**,** 711065.

LUONGO, F., PIETROPAOLO, G., GAUTIER, M., DHENNIN-DUTHILLE, I., OUADID-AHIDOUCH, H., WOLF, F. I. & TRAPANI, V. 2018. TRPM6 is Essential for Magnesium Uptake and Epithelial Cell Function in the Colon. *Nutrients,* 10.

MA, R., CHAUDHARI, S. & LI, W. 2016. Canonical Transient Receptor Potential 6 Channel: A New Target of Reactive Oxygen Species in Renal Physiology and Pathology. *Antioxid Redox Signal,* 25**,** 732-748.

MACIAS, D., COWBURN, A. S., TORRES-TORRELO, H., ORTEGA-SAENZ, P., LOPEZ-BARNEO, J. & JOHNSON, R. S. 2018. HIF-2alpha is essential for carotid body development and function. *Elife,* 7.

MARCUS, N. J., LI, Y. L., BIRD, C. E., SCHULTZ, H. D. & MORGAN, B. J. 2010. Chronic intermittent hypoxia augments chemoreflex control of sympathetic activity: role of the angiotensin II type 1 receptor. *Respir Physiol Neurobiol,* 171**,** 36-45.

MARSHALL, J. M. 2015. Interactions between local dilator and sympathetic vasoconstrictor influences in skeletal muscle in acute and chronic hypoxia. *Exp Physiol,* 100**,** 1400-11.

MARUYAMA, T., KANAJI, T., NAKADE, S., KANNO, T. & MIKOSHIBA, K. 1997. 2APB, 2-aminoethoxydiphenyl borate, a membrane-penetrable modulator of Ins(1,4,5)P3-induced Ca2+ release. *J Biochem,* 122**,** 498-505.

MARXSEN, J. H., STENGEL, P., DOEGE, K., HEIKKINEN, P., JOKILEHTO, T., WAGNER, T., JELKMANN, W., JAAKKOLA, P. & METZEN, E. 2004. Hypoxia-inducible factor-1 (HIF-1) promotes its degradation by induction of HIF-alpha-prolyl-4-hydroxylases. *Biochem J,* 381**,** 761-7.

MASAKI, T. & SAWAMURA, T. 2006. Endothelin and endothelial dysfunction. *Proc Jpn Acad Ser B Phys Biol Sci,* 82**,** 17-24.

MAY, V., LUTZ, E., MACKENZIE, C., SCHUTZ, K. C., DOZARK, K. & BRAAS, K. M. 2010. Pituitary adenylate cyclase-activating polypeptide (PACAP)/PAC1HOP1 receptor activation coordinates multiple neurotrophic signaling pathways: Akt activation through phosphatidylinositol 3-kinase gamma and vesicle endocytosis for neuronal survival. *J Biol Chem,* 285**,** 9749-61.

MAZIA, D., SCHATTEN, G. & SALE, W. 1975. Adhesion of cells to surfaces coated with polylysine. Applications to electron microscopy. *J Cell Biol,* 66**,** 198-200.

MCELROY, G. S. & CHANDEL, N. S. 2017. Mitochondria control acute and chronic responses to hypoxia. *Exp Cell Res,* 356**,** 217-222.

MCGHEE, B. H. & BRIDGES, E. J. 2002. Monitoring arterial blood pressure: what you may not know. *Crit Care Nurse,* 22**,** 60-4, 66-70, 73 passim.

MCMORROW, C., FREDSTED, A., CARBERRY, J., O'CONNELL, R. A., BRADFORD, A., JONES, J. F. & O'HALLORAN, K. D. 2011. Chronic hypoxia increases rat diaphragm muscle endurance and sodium-potassium ATPase pump content. *Eur Respir J,* 37**,** 1474-81.

MCMURRAY, J. J., PACKER, M., DESAI, A. S., GONG, J., LEFKOWITZ, M. P., RIZKALA, A. R., ROULEAU, J. L., SHI, V. C., SOLOMON, S. D., SWEDBERG, K., ZILE, M. R., INVESTIGATORS, P.-H. & COMMITTEES 2014. Angiotensin-neprilysin inhibition versus enalapril in heart failure. *N Engl J Med,* 371**,** 993-1004.

MICHIELS, C. 2004. Physiological and pathological responses to hypoxia. *Am J Pathol,* 164**,** 1875-82.

MICHLIG, S., MERLINI, J. M., BEAUMONT, M., LEDDA, M., TAVENARD, A., MUKHERJEE, R., CAMACHO, S. & LE COUTRE, J. 2016. Effects of TRP channel agonist ingestion on metabolism and autonomic nervous system in a randomized clinical trial of healthy subjects. *Sci Rep,* 6**,** 20795.

MILLER, A. J. & ARNOLD, A. C. 2019. The renin-angiotensin system in cardiovascular autonomic control: recent developments and clinical implications. *Clinical Autonomic Research,* 29**,** 231-243.

MILLS, L. & NURSE, C. 1993. Chronic hypoxia in vitro increases volume of dissociated carotid body chemoreceptors. *Neuroreport,* 4**,** 619-22.

MIRABILE, V. S., SHEBL, E., SANKARI, A. & BURNS, B. 2023. Respiratory Failure. *StatPearls.* Treasure Island (FL) ineligible companies. Disclosure: Eman Shebl declares no relevant financial relationships with ineligible companies. Disclosure: Abdulghani Sankari declares no relevant financial relationships with ineligible companies. Disclosure: Bracken Burns declares no relevant financial relationships with ineligible companies.

MISHRA, M., TIWARI, S. & GOMES, A. V. 2017. Protein purification and analysis: next generation Western blotting techniques. *Expert Review of Proteomics,* 14**,** 1037-1053.

MORGAN, A. D., ZAKERI, R. & QUINT, J. K. 2018a. Defining the relationship between COPD and CVD: what are the implications for clinical practice? *Ther Adv Respir Dis,* 12**,** 1753465817750524.

MORGAN, B. J., TEODORESCU, M., PEGELOW, D. F., JACKSON, E. R., SCHNEIDER, D. L., PLANTE, D. T., GAPINSKI, J. P., HETZEL, S. J. & DOPP, J. M. 2018b. Effects of losartan and allopurinol on cardiorespiratory regulation in obstructive sleep apnoea. *Experimental Physiology,* 103**,** 941-955.

MORI, Y., TAKAHASHI, N., KUROKAWA, T. & KIYONAKA, S. 2017. TRP channels in oxygen physiology: distinctive functional properties and roles of TRPA1 in O(2) sensing. *Proc Jpn Acad Ser B Phys Biol Sci,* 93**,** 464-482.

MORI, Y., TAKAHASHI, N., POLAT, O. K., KUROKAWA, T., TAKEDA, N. & INOUE, M. 2016. Redox-sensitive transient receptor potential channels in oxygen sensing and adaptation. *Pflugers Arch,* 468**,** 85-97.

MOSQUEIRA, M. & ITURRIAGA, R. 2019. Chronic hypoxia changes gene expression profile of primary rat carotid body cells: consequences on the expression of NOS isoforms and ET-1 receptors. *Physiol Genomics,* 51**,** 109-124.

MOUROT, L., BOUHADDI, M., PERREY, S., ROUILLON, J. D. & REGNARD, J. 2004. Quantitative Poincare plot analysis of heart rate variability: effect of endurance training. *Eur J Appl Physiol,* 91**,** 79-87.

NADAR, S., BLANN, A. D. & LIP, G. Y. 2004. Endothelial dysfunction: methods of assessment and application to hypertension. *Curr Pharm Des,* 10**,** 3591-605.

NAGATSU, T. 2007. The catecholamine system in health and disease -Relation to tyrosine 3-monooxygenase and other catecholamine-synthesizing enzymes. *Proc Jpn Acad Ser B Phys Biol Sci,* 82**,** 388-415.

NANDURI, J., PENG, Y. J., WANG, N., KHAN, S. A., SEMENZA, G. L., KUMAR, G. K. & PRABHAKAR, N. R. 2017a. Epigenetic regulation of redox state mediates persistent cardiorespiratory abnormalities after long-term intermittent hypoxia. *J Physiol,* 595**,** 63-77.

NANDURI, J., PENG, Y. J., WANG, N., KHAN, S. A., SEMENZA, G. L., KUMAR, G. K. & PRABHAKAR, N. R. 2017b. Epigenetic regulation of redox state mediates persistent cardiorespiratory abnormalities after long-term intermittent hypoxia. *Journal of Physiology-London,* 595**,** 63-77.

NANGAKU, M. & FUJITA, T. 2008. Activation of the renin-angiotensin system and chronic hypoxia of the kidney. *Hypertens Res,* 31**,** 175-84.

NATTIE, E. & LI, A. 2012. Central chemoreceptors: locations and functions. *Compr Physiol,* 2**,** 221-54.

NAVARRO-LOMAS, G., DE-LA, O. A., JURADO-FASOLI, L., CASTILLO, M. J., FEMIA, P. & AMARO-GAHETE, F. J. 2020. Assessment of autonomous nerve system through non-linear heart rate variability outcomes in sedentary healthy adults. *PeerJ,* 8**,** e10178.

NEUNHAUSERER, D., PATTI, A., NIEDERSEER, D., KAISER, B., CADAMURO, J., LAMPRECHT, B., ERMOLAO, A., STUDNICKA, M. & NIEBAUER, J. 2021. Systemic Inflammation, Vascular

Function, and Endothelial Progenitor Cells after an Exercise Training Intervention in COPD. *Am J Med,* 134**,** e171-e180.

NISHIDA, M., KUWAHARA, K., KOZAI, D., SAKAGUCHI, R. & MORI, Y. 2015. TRP Channels: Their Function and Potentiality as Drug Targets. *In:* NAKAO, K., MINATO, N. & UEMOTO, S. (eds.) *Innovative Medicine: Basic Research and Development.* Tokyo.

NUMAGA-TOMITA, T. & NISHIDA, M. 2020. TRPC Channels in Cardiac Plasticity. *Cells,* 9.

NUMATA, T., OGAWA, N., TAKAHASHI, N. & MORI, Y. 2013. TRP channels as sensors of oxygen availability. *Pflugers Arch,* 465**,** 1075-85.

NUNES, A. R., HOLMES, A. P., CONDE, S. V., GAUDA, E. B. & MONTEIRO, E. C. 2014. Revisiting cAMP signaling in the carotid body. *Front Physiol,* 5**,** 406.

NUNES, A. R., HOLMES, A. P., SAMPLE, V., KUMAR, P., CANN, M. J., MONTEIRO, E. C., ZHANG, J. & GAUDA, E. B. 2013. Bicarbonate-sensitive soluble and transmembrane adenylyl cyclases in peripheral chemoreceptors. *Respir Physiol Neurobiol,* 188**,** 83-93.

NURSE, C. A. & FEARON, I. M. 2002. Carotid body chemoreceptors in dissociated cell culture. *Microsc Res Tech,* 59**,** 249-55.

O'DRISCOLL, C. M. & GORMAN, A. M. 2005. Hypoxia induces neurite outgrowth in PC12 cells that is mediated through adenosine A2A receptors. *Neuroscience,* 131**,** 321-9.

OPIE, L. H. & SACK, M. N. 2001. Enhanced angiotensin II activity in heart failure: reevaluation of the counterregulatory hypothesis of receptor subtypes. *Circ Res,* 88**,** 654-8.

OPREA, D., SANZ, C. G., BARSAN, M. M. & ENACHE, T. A. 2022. PC-12 Cell Line as a Neuronal Cell Model for Biosensing Applications. *Biosensors (Basel),* 12.

ORTEGA-SAENZ, P., MORENO-DOMINGUEZ, A., GAO, L. & LOPEZ-BARNEO, J. 2020. Molecular Mechanisms of Acute Oxygen Sensing by Arterial Chemoreceptor Cells. Role of Hif2alpha. *Front Physiol,* 11**,** 614893.

ORTEGA-SÁENZ, P. & LÓPEZ-BARNEO, J. 2020. Physiology of the Carotid Body: From Molecules to Disease. *Annual Review of Physiology, Vol 82,* 82**,** 127-149.

PAGEON, S. V., NICOVICH, P. R., MOLLAZADE, M., TABARIN, T. & GAUS, K. 2016. Clus-DoC: a combined cluster detection and colocalization analysis for single-molecule localization microscopy data. *Mol Biol Cell,* 27**,** 3627-3636.

PANDIT, J. J. 2014. Volatile anaesthetic depression of the carotid body chemoreflex-mediated ventilatory response to hypoxia: directions for future research. *Scientifica (Cairo),* 2014**,** 394270.

PARDAL, R., ORTEGA-SAENZ, P., DURAN, R. & LOPEZ-BARNEO, J. 2007. Glia-like stem cells sustain physiologic neurogenesis in the adult mammalian carotid body. *Cell,* 131**,** 364-77.

PATEL, A. J. & HONORÉ, E. 2001. Molecular physiology of oxygen-sensitive potassium channels. *Eur Respir J,* 18**,** 221-7.

PAULDING, W. R., SCHNELL, P. O., BAUER, A. L., STRIET, J. B., NASH, J. A., KUZNETSOVA, A. V. & CZYZYK-KRZESKA, M. F. 2002. Regulation of gene expression for neurotransmitters during adaptation to hypoxia in oxygen-sensitive neuroendocrine cells. *Microscopy Research and Technique,* 59**,** 178-187.

PENG, Y. J., NANDURI, J., RAGHURAMAN, G., SOUVANNAKITTI, D., GADALLA, M. M., KUMAR, G. K., SNYDER, S. H. & PRABHAKAR, N. R. 2010. H2S mediates O2 sensing in the carotid body. *Proc Natl Acad Sci U S A,* 107**,** 10719-24.

PENG, Y. J., OVERHOLT, J. L., KLINE, D., KUMAR, G. K. & PRABHAKAR, N. R. 2003. Induction of sensory long-term facilitation in the carotid body by intermittent hypoxia: implications for recurrent apneas. *Proc Natl Acad Sci U S A,* 100**,** 10073-8.

PENG, Y. J., RAGHURAMAN, G., KHAN, S. A., KUMAR, G. K. & PRABHAKAR, N. R. 2011a. Angiotensin II evokes sensory long-term facilitation of the carotid body via NADPH oxidase. *J Appl Physiol (1985),* 111**,** 964-70.

PENG, Y. J., RAGHURAMAN, G., KHAN, S. A., KUMAR, G. K. & PRABHAKAR, N. R. 2011b. Angiotensin II evokes sensory long-term facilitation of the carotid body via NADPH oxidase. *J Appl Physiol,* 111**,** 964-70.

PEPPER, D. R., LANDAUER, R. C. & KUMAR, P. 1995. Postnatal development of CO2-O2 interaction in the rat carotid body in vitro. *J Physiol,* 485 (Pt 2)**,** 531-41.

PHAN, M. N., LEDDY, H. A., VOTTA, B. J., KUMAR, S., LEVY, D. S., LIPSHUTZ, D. B., LEE, S. H., LIEDTKE, W. & GUILAK, F. 2009. Functional characterization of TRPV4 as an osmotically sensitive ion channel in porcine articular chondrocytes. *Arthritis Rheum,* 60**,** 3028-37.

PHILLIPS, D. B., COLLINS, S. E., BRYAN, T. L., WONG, E. Y. L., MCMURTRY, M. S., BHUTANI, M. & STICKLAND, M. K. 2019. The effect of carotid chemoreceptor inhibition on exercise tolerance in chronic obstructive pulmonary disease: A randomized-controlled crossover trial. *Respir Med,* 160**,** 105815.

PHILLIPS, D. B., STEINBACK, C. D., COLLINS, S. E., FUHR, D. P., BRYAN, T. L., WONG, E. Y. L., TEDJASAPUTRA, V., BHUTANI, M. & STICKLAND, M. K. 2018. The carotid chemoreceptor contributes to the elevated arterial stiffness and vasoconstrictor outflow in chronic obstructive pulmonary disease. *J Physiol,* 596**,** 3233-3244.

PIERSON, D. J. 2000. Pathophysiology and clinical effects of chronic hypoxia. *Respir Care,* 45**,** 39-51; discussion 51-3.

PLANT, L. D., XIONG, D., ROMERO, J., DAI, H. & GOLDSTEIN, S. A. N. 2020. Hypoxia Produces Pro-arrhythmic Late Sodium Current in Cardiac Myocytes by SUMOylation of Na(V)1.5 Channels. *Cell Rep,* 30**,** 2225-2236 e4.

PLATERO-LUENGO, A., GONZALEZ-GRANERO, S., DURAN, R., DIAZ-CASTRO, B., PIRUAT, J. I., GARCIA-VERDUGO, J. M., PARDAL, R. & LOPEZ-BARNEO, J. 2014. An O2-sensitive glomus cell-stem cell synapse induces carotid body growth in chronic hypoxia. *Cell,* 156**,** 291-303.

POWELL, F. L. 2007. The influence of chronic hypoxia upon chemoreception. *Respir Physiol Neurobiol,* 157**,** 154-61.

POWELL, F. L. & FU, Z. 2008. HIF-1 and ventilatory acclimatization to chronic hypoxia. *Respir Physiol Neurobiol,* 164**,** 282-7.

PRABHAKAR, N. R. 2016. Carotid body chemoreflex: a driver of autonomic abnormalities in sleep apnoea. *Exp Physiol,* 101**,** 975-85.

PRABHAKAR, N. R. & JACONO, F. J. 2005. Cellular and molecular mechanisms associated with carotid body adaptations to chronic hypoxia. *High Alt Med Biol,* 6**,** 112-20.

PRABHAKAR, N. R., PENG, Y. J., KUMAR, G. K., NANDURI, J., DI GIULIO, C. & LAHIRI, S. 2009. Long-term regulation of carotid body function: acclimatization and adaptation--invited article. *Adv Exp Med Biol,* 648**,** 307-17.

PRABHAKAR, N. R., PENG, Y. J. & NANDURI, J. 2022. Adaptive cardiorespiratory changes to chronic continuous and intermittent hypoxia. *Handb Clin Neurol,* 188**,** 103-123.

PRIETO-LLORET, J., OLEA, E., GORDILLO-CANO, A., DOCIO, I., OBESO, A., GOMEZ-NINO, A., AARONSON, P. I. & ROCHER, A. 2021. Maladaptive Pulmonary Vascular Responses to Chronic Sustained and Chronic Intermittent Hypoxia in Rat. *Antioxidants (Basel),* 11.

PULGAR-SEPULVEDA, R., VARAS, R., ITURRIAGA, R., DEL RIO, R. & ORTIZ, F. C. 2018. Carotid Body Type-I Cells Under Chronic Sustained Hypoxia: Focus on Metabolism and Membrane Excitability. *Front Physiol,* 9**,** 1282.

QAMMAR, N. W., ORINAITE, U., SIAUCIUNAITE, V., VAINORAS, A., SAKALYTE, G. & RAGULSKIS, M. 2022. The Complexity of the Arterial Blood Pressure Regulation during the Stress Test. *Diagnostics (Basel),* 12.

RAMAKRISHNAN, S., ANAND, V. & ROY, S. 2014. Vascular endothelial growth factor signaling in hypoxia and inflammation. *J Neuroimmune Pharmacol,* 9**,** 142-60.

RAMIREZ, J. M. 2014. The integrative role of the sigh in psychology, physiology, pathology, and neurobiology. *Prog Brain Res,* 209**,** 91-129.

RANDHAWA, P. K. & JAGGI, A. S. 2015. TRPV4 channels: physiological and pathological role in cardiovascular system. *Basic Res Cardiol,* 110**,** 54.

RATHER, M. A., KHAN, A., WANG, L., JAHAN, S., REHMAN, M. U., MAKEEN, H. A. & MOHAN, S. 2023. TRP channels: Role in neurodegenerative diseases and therapeutic targets. *Heliyon,* 9**,** e16910.

REDFORS, B., SHAO, Y. & OMEROVIC, E. 2014. Influence of anesthetic agent, depth of anesthesia and body temperature on cardiovascular functional parameters in the rat. *Lab Anim,* 48**,** 6-14.

REEVES, S. R., GOZAL, E., GUO, S. Z., SACHLEBEN, L. R., JR., BRITTIAN, K. R., LIPTON, A. J. & GOZAL, D. 2003. Effect of long-term intermittent and sustained hypoxia on hypoxic ventilatory and metabolic responses in the adult rat. *J Appl Physiol (1985),* 95**,** 1767-74.

REQUEJO-ISIDRO, J. 2013. Fluorescence nanoscopy. Methods and applications. *J Chem Biol,* 6**,** 97-120.

ROOK, W., JOHNSON, C. D., CONEY, A. M. & MARSHALL, J. M. 2014. Prenatal hypoxia leads to increased muscle sympathetic nerve activity, sympathetic hyperinnervation, premature blunting of neuropeptide Y signaling, and hypertension in adult life. *Hypertension,* 64**,** 1321-7.

ROSENKRANZ, S., GIBBS, J. S., WACHTER, R., DE MARCO, T., VONK-NOORDEGRAAF, A. & VACHIERY, J. L. 2016. Left ventricular heart failure and pulmonary hypertension. *Eur Heart J,* 37**,** 942-54.

ROY, A., FARNHAM, M. M. J., DERAKHSHAN, F., PILOWSKY, P. M. & WILSON, R. J. A. 2018. Acute intermittent hypoxia with concurrent hypercapnia evokes P2X and TRPV1 receptor-dependent sensory long-term facilitation in naive carotid bodies. *J Physiol,* 596**,** 3149-3169.

SAMANTA, A., HUGHES, T. E. T. & MOISEENKOVA-BELL, V. Y. 2018. Transient Receptor Potential (TRP) Channels. *Subcell Biochem,* 87**,** 141-165.

SANDOO, A., VAN ZANTEN, J. J., METSIOS, G. S., CARROLL, D. & KITAS, G. D. 2010. The endothelium and its role in regulating vascular tone. *Open Cardiovasc Med J,* 4**,** 302-12.

SARASWAT, V. 2015. Effects of anaesthesia techniques and drugs on pulmonary function. *Indian J Anaesth,* 59**,** 557-64.

SARKAR, M., BHARDWAZ, R., MADABHAVI, I. & MODI, M. 2019. Physical signs in patients with chronic obstructive pulmonary disease. *Lung India,* 36**,** 38-47.

SAXENA, T., ALI, A. O. & SAXENA, M. 2018. Pathophysiology of essential hypertension: an update. *Expert Review of Cardiovascular Therapy,* 16**,** 879-887.

SCHERER, K. 2019. *Olympus FV1200 Quick Start Guide* [Online]. ULC WIKI: ULC WIKI. Available: https://wiki.ucl.ac.uk/display/LMCBLMic/Olympus+FV1200+Quick+Start+Guide [Accessed].

SCHMITT, P., GARCIA, C., SOULIER, V., PUJOL, J. F. & PEQUIGNOT, J. M. 1992. Influence of long-term hypoxia on tyrosine hydroxylase in the rat carotid body and adrenal gland. *J Auton Nerv Syst,* 40**,** 13-9.

SCHULTZ, H. D. & LI, Y. L. 2007. Carotid body function in heart failure. *Respir Physiol Neurobiol,* 157**,** 171-85.

SEMENZA, G. L. & PRABHAKAR, N. R. 2018. The role of hypoxia-inducible factors in carotid body (patho) physiology. *J Physiol,* 596**,** 2977-2983.

SENA, L. A. & CHANDEL, N. S. 2012. Physiological roles of mitochondrial reactive oxygen species. *Mol Cell,* 48**,** 158-67.

SETA, K., KIM, H. W., FERGUSON, T., KIM, R., PATHROSE, P., YUAN, Y., LU, G., SPICER, Z. & MILLHORN, D. E. 2002. Genomic and physiological analysis of oxygen sensitivity and hypoxia tolerance in PC12 cells. *Ann N Y Acad Sci,* 971**,** 379-88.

SEVERS, L. J., VLEMINCX, E. & RAMIREZ, J. M. 2022. The psychophysiology of the sigh: I: The sigh from the physiological perspective. *Biol Psychol,* 170**,** 108313.

SHANKS, J. & RAMCHANDRA, R. 2021. Angiotensin II and the Cardiac Parasympathetic Nervous System in Hypertension. *Int J Mol Sci,* 22.

SHETH, S., BRITO, R., MUKHERJEA, D., RYBAK, L. P. & RAMKUMAR, V. 2014. Adenosine receptors: expression, function and regulation. *Int J Mol Sci,* 15**,** 2024-52.

SHI, J., JU, M., SALEH, S. N., ALBERT, A. P. & LARGE, W. A. 2010. TRPC6 channels stimulated by angiotensin II are inhibited by TRPC1/C5 channel activity through a Ca^{2+}- and PKC-dependent mechanism in native vascular myocytes. *J Physiol,* 588**,** 3671-82.

SHIRAHATA, M., TANG, W. Y., SHIN, M. K. & POLOTSKY, V. Y. 2015. Is the Carotid Body a Metabolic Monitor? *Adv Exp Med Biol,* 860**,** 153-9.

SLOWIK, E. J., STANKOSKA, K., BUI, N. N., PASIEKA, B., CONRAD, D., ZAPP, J., HOTH, M., BOGESKI, I. & KAPPL, R. 2023. The calcium channel modulator 2-APB hydrolyzes in physiological buffers and acts as an effective radical scavenger and inhibitor of the NADPH oxidase 2. *Redox Biol,* 61**,** 102654.

SMANI, T., SHAPOVALOV, G., SKRYMA, R., PREVARSKAYA, N. & ROSADO, J. A. 2015. Functional and physiopathological implications of TRP channels. *Biochim Biophys Acta,* 1853**,** 1772-82.

SMITH, C. A., BISGARD, G. E., NIELSEN, A. M., DARISTOTLE, L., KRESSIN, N. A., FORSTER, H. V. & DEMPSEY, J. A. 1986. Carotid bodies are required for ventilatory acclimatization to chronic hypoxia. *J Appl Physiol (1985),* 60**,** 1003-10.

SOBRINO, V., GONZALEZ-RODRIGUEZ, P., ANNESE, V., LOPEZ-BARNEO, J. & PARDAL, R. 2018. Fast neurogenesis from carotid body quiescent neuroblasts accelerates adaptation to hypoxia. *EMBO Rep,* 19.

SOLAIMAN, A. Z., FEEHAN, R. P., CHABITNOY, A. M., LEUENBERGER, U. A. & MONAHAN, K. D. 2014. Ventilatory responses to chemoreflex stimulation are not enhanced by angiotensin II in healthy humans. *Autonomic Neuroscience-Basic & Clinical,* 183**,** 72-79.

SORBELLO, M., MICAGLIO, M., ZDRAVKOVIC, I., GAÇONNET, C. & SKINNER, M. 2018. Pressure, volume and temperature: Boyle's law rules airways. *Minerva Anestesiol,* 84**,** 1112-1114.

SOULAGE, C., PASCUAL, O., ROUX, J. C., DENAVIT-SAUBIE, M. & PEQUIGNOT, J. M. 2004. Chemosensory inputs and neural remodeling in carotid body and brainstem catecholaminergic cells. *Adv Exp Med Biol,* 551**,** 53-8.

SPLETTSTOESSER, F., FLOREA, A. M. & BUSSELBERG, D. 2007. IP(3) receptor antagonist, 2-APB, attenuates cisplatin induced Ca2+-influx in HeLa-S3 cells and prevents activation of calpain and induction of apoptosis. *Br J Pharmacol,* 151**,** 1176-86.

SRINIVASAN, S. & AVADHANI, N. G. 2012. Cytochrome c oxidase dysfunction in oxidative stress. *Free Radic Biol Med,* 53**,** 1252-63.

SU, S., YUDIN, Y., KIM, N., TAO, Y. X. & ROHACS, T. 2021. TRPM3 Channels Play Roles in Heat Hypersensitivity and Spontaneous Pain after Nerve Injury. *J Neurosci,* 41**,** 2457-2474.

SUN, S. Y., WANG, W., ZUCKER, I. H. & SCHULTZ, H. D. 1999. Enhanced activity of carotid body chemoreceptors in rabbits with heart failure: role of nitric oxide. *J Appl Physiol (1985),* 86**,** 1273-82.

SUNDIN, L., BURLESON, M. L., SANCHEZ, A. P., AMIN-NAVES, J., KINKEAD, R., GARGAGLIONI, L. H., HARTZLER, L. K., WIEMANN, M., KUMAR, P. & GLASS, M. L. 2007. Respiratory chemoreceptor function in vertebrates comparative and evolutionary aspects. *Integr Comp Biol,* 47**,** 592-600.

SUNGKAWORN, T., JOBIN, M. L., BURNECKI, K., WERON, A., LOHSE, M. J. & CALEBIRO, D. 2017. Single-molecule imaging reveals receptor-G protein interactions at cell surface hot spots. *Nature,* 550**,** 543-547.

SWIDERSKA, A., CONEY, A. M., ALZAHRANI, A. A., ALDOSSARY, H. S., BATIS, N., RAY, C. J., KUMAR, P. & HOLMES, A. P. 2021. Mitochondrial Succinate Metabolism and Reactive Oxygen Species Are Important but Not Essential for Eliciting Carotid Body and Ventilatory Responses to Hypoxia in the Rat. *Antioxidants (Basel),* 10.

SYLVESTER, J. T., SHIMODA, L. A., AARONSON, P. I. & WARD, J. P. 2012. Hypoxic pulmonary vasoconstriction. *Physiol Rev,* 92**,** 367-520.

TAKAHASHI, Y., WATANABE, H., MURAKAMI, M., OHBA, T., RADOVANOVIC, M., ONO, K., IIJIMA, T. & ITO, H. 2007. Involvement of transient receptor potential canonical 1 (TRPC1) in angiotensin II-induced vascular smooth muscle cell hypertrophy. *Atherosclerosis,* 195**,** 287-96.

TAN, Z. Y., LU, Y., WHITEIS, C. A., BENSON, C. J., CHAPLEAU, M. W. & ABBOUD, F. M. 2007. Acid-sensing ion channels contribute to transduction of extracellular acidosis in rat carotid body glomus cells. *Circ Res,* 101**,** 1009-19.

TAYLOR-CLARK, T. E. 2016. Role of reactive oxygen species and TRP channels in the cough reflex. *Cell Calcium,* 60**,** 155-62.

TAYLOR-CLARK, T. E., MCALEXANDER, M. A., NASSENSTEIN, C., SHEARDOWN, S. A., WILSON, S., THORNTON, J., CARR, M. J. & UNDEM, B. J. 2008. Relative contributions of TRPA1 and TRPV1 channels in the activation of vagal bronchopulmonary C-fibres by the endogenous autacoid 4-oxononenal. *J Physiol,* 586**,** 3447-59.

THEODORAKOPOULOU, M. P., ALEXANDROU, M. E., BAKALOUDI, D. R., PITSIOU, G., STANOPOULOS, I., KONTAKIOTIS, T. & BOUTOU, A. K. 2021. Endothelial dysfunction in COPD: a systematic review and meta-analysis of studies using different functional assessment methods. *ERJ Open Res,* 7.

THOMAS, T. & MARSHALL, J. M. 1995. A study on rats of the effects of chronic hypoxia from birth on respiratory and cardiovascular responses evoked by acute hypoxia. *J Physiol,* 487 (Pt 2)**,** 513-25.

THOMPSON, E. L., RAY, C. J., HOLMES, A. P., PYE, R. L., WYATT, C. N., CONEY, A. M. & KUMAR, P. 2016. Adrenaline release evokes hyperpnoea and an increase in ventilatory CO2 sensitivity during hypoglycaemia: a role for the carotid body. *J Physiol,* 594**,** 4439-52.

THYSSEN, A., STAVERMANN, M., BUDDRUS, K., DOENGI, M., EKBERG, J. A., ST JOHN, J. A., DEITMER, J. W. & LOHR, C. 2013. Spatial and developmental heterogeneity of calcium signaling in olfactory ensheathing cells. *Glia,* 61**,** 327-37.

TIPOE, G. L. & FUNG, M. L. 2003. Expression of HIF-1alpha, VEGF and VEGF receptors in the carotid body of chronically hypoxic rat. *Respir Physiol Neurobiol,* 138**,** 143-54.

TOBIAS, J. D. & LEDER, M. 2011. Procedural sedation: A review of sedative agents, monitoring, and management of complications. *Saudi J Anaesth,* 5**,** 395-410.

TOUYZ, R. M. 2008. Transient receptor potential melastatin 6 and 7 channels, magnesium transport, and vascular biology: implications in hypertension. *Am J Physiol Heart Circ Physiol,* 294**,** H1103-18.

TUTEJA, N. 2009. Signaling through G protein coupled receptors. *Plant Signaling & Behavior,* 4**,** 942-947.

UNOKI, T., GRAP, M. J., SESSLER, C. N., BEST, A. M., WETZEL, P., HAMILTON, A., MELLOTT, K. G. & MUNRO, C. L. 2009. Autonomic nervous system function and depth of sedation in adults receiving mechanical ventilation. *Am J Crit Care,* 18**,** 42-50; quiz 51.

URENA, J., FERNANDEZ-CHACON, R., BENOT, A. R., ALVAREZ DE TOLEDO, G. A. & LOPEZ-BARNEO, J. 1994. Hypoxia induces voltage-dependent Ca2+ entry and quantal dopamine secretion in carotid body glomus cells. *Proc Natl Acad Sci U S A,* 91**,** 10208-11.

VALLI, J., GARCIA-BURGOS, A., ROONEY, L. M., VALE DE MELO, E. O. B., DUNCAN, R. R. & RICKMAN, C. 2021. Seeing beyond the limit: A guide to choosing the right super-resolution microscopy technique. *J Biol Chem,* 297**,** 100791.

VAN DE WAL, R. M., PLOKKER, H. W., LOK, D. J., BOOMSMA, F., VAN DER HORST, F. A., VAN VELDHUISEN, D. J., VAN GILST, W. H. & VOORS, A. A. 2006. Determinants of increased angiotensin II levels in severe chronic heart failure patients despite ACE inhibition. *Int J Cardiol,* 106**,** 367-72.

VAN GESTEL, A. J. & STEIER, J. 2010. Autonomic dysfunction in patients with chronic obstructive pulmonary disease (COPD). *J Thorac Dis,* 2**,** 215-22.

VAN GESTEL, A. J. R., KOHLER, M. & CLARENBACH, C. F. 2012. Sympathetic Overactivity and Cardiovascular Disease in Patients with Chronic Obstructive Pulmonary Disease. *Discovery Medicine,* 14**,** 359-368.

VANDENBERG, P., KERN, A., RIES, A., LUCKENBILL-EDDS, L., MANN, K. & KUHN, K. 1991. Characterization of a type IV collagen major cell binding site with affinity to the alpha 1 beta 1 and the alpha 2 beta 1 integrins. *J Cell Biol,* 113**,** 1475-83.

VARAS, R., WYATT, C. N. & BUCKLER, K. J. 2007. Modulation of TASK-like background potassium channels in rat arterial chemoreceptor cells by intracellular ATP and other nucleotides. *J Physiol,* 583**,** 521-36.

VENKATARAMANI, V., KARDORFF, M., HERRMANNSDORFER, F., WIENEKE, R., KLEIN, A., TAMPE, R., HEILEMANN, M. & KUNER, T. 2018. Enhanced labeling density and whole-cell 3D dSTORM imaging by repetitive labeling of target proteins. *Sci Rep,* 8**,** 5507.

WAKAI, J., TAKAYAMA, A., YOKOYAMA, T., NAKAMUTA, N., KUSAKABE, T. & YAMAMOTO, Y. 2015. Immunohistochemical localization of dopamine D2 receptor in the rat carotid body. *Acta Histochem,* 117**,** 784-9.

WALSH, M. P. & MARSHALL, J. M. 2006. The early effects of chronic hypoxia on the cardiovascular system in the rat: role of nitric oxide. *J Physiol,* 575**,** 263-75.

WANG, J., HOGAN, J. O. & KIM, D. 2017a. Voltage- and receptor-mediated activation of a non-selective cation channel in rat carotid body glomus cells. *Respir Physiol Neurobiol,* 237**,** 13-21.

WANG, J. J., HOGAN, J. O. & KIM, D. 2017b. Voltage- and receptor-mediated activation of a non-selective cation channel in rat carotid body glomus cells. *Respiratory Physiology & Neurobiology,* 237**,** 13-21.

WANG, Z. Y. & BISGARD, G. E. 2002. Chronic hypoxia-induced morphological and neurochemical changes in the carotid body. *Microsc Res Tech,* 59**,** 168-77.

WEIHE, E., DEPBOYLU, C., SCHUTZ, B., SCHAFER, M. K. & EIDEN, L. E. 2006. Three types of tyrosine hydroxylase-positive CNS neurons distinguished by dopa decarboxylase and VMAT2 co-expression. *Cell Mol Neurobiol,* 26**,** 659-78.

WEN, H., GWATHMEY, J. K. & XIE, L. H. 2020. Role of Transient Receptor Potential Canonical Channels in Heart Physiology and Pathophysiology. *Front Cardiovasc Med,* 7**,** 24.

WESTERINK, R. H. & EWING, A. G. 2008. The PC12 cell as model for neurosecretion. *Acta Physiol (Oxf),* 192**,** 273-85.

WIATRAK, B., KUBIS-KUBIAK, A., PIWOWAR, A. & BARG, E. 2020. PC12 Cell Line: Cell Types, Coating of Culture Vessels, Differentiation and Other Culture Conditions. *Cells,* 9.

WILKINSON, K. A., HUEY, K., DINGER, B., HE, L., FIDONE, S. & POWELL, F. L. 2010. Chronic hypoxia increases the gain of the hypoxic ventilatory response by a mechanism in the central nervous system. *J Appl Physiol (1985),* 109**,** 424-30.

WONG, B. W., MARSCH, E., TREPS, L., BAES, M. & CARMELIET, P. 2017. Endothelial cell metabolism in health and disease: impact of hypoxia. *EMBO J,* 36**,** 2187-2203.

WORLEY, P. F., ZENG, W., HUANG, G. N., YUAN, J. P., KIM, J. Y., LEE, M. G. & MUALLEM, S. 2007. TRPC channels as STIM1-regulated store-operated channels. *Cell Calcium,* 42**,** 205-11.

WROBEL, J. P., THOMPSON, B. R. & WILLIAMS, T. J. 2012. Mechanisms of pulmonary hypertension in chronic obstructive pulmonary disease: a pathophysiologic review. *J Heart Lung Transplant,* 31**,** 557-64.

WU, Y., HAN, X., SU, Y., GLIDEWELL, M., DANIELS, J. S., LIU, J., SENGUPTA, T., REY-SUAREZ, I., FISCHER, R., PATEL, A., COMBS, C., SUN, J., WU, X., CHRISTENSEN, R., SMITH, C., BAO, L., SUN, Y., DUNCAN, L. H., CHEN, J., POMMIER, Y., SHI, Y. B., MURPHY, E., ROY, S., UPADHYAYA, A., COLON-RAMOS, D., LA RIVIERE, P. & SHROFF, H. 2021. Multiview confocal super-resolution microscopy. *Nature,* 600**,** 279-284.

XIE, A., SKATRUD, J. B., PULEO, D. S. & MORGAN, B. J. 2001. Exposure to hypoxia produces long-lasting sympathetic activation in humans. *J Appl Physiol (1985),* 91**,** 1555-62.

XING, H., LEE, H., LUO, L. & KYRIAKIDES, T. R. 2020. Extracellular matrix-derived biomaterials in engineering cell function. *Biotechnol Adv,* 42**,** 107421.

XU, F., GU, Q. H., ZHOU, T. & LEE, L. Y. 2003. Acute hypoxia prolongs the apnea induced by right atrial injection of capsaicin. *J Appl Physiol (1985),* 94**,** 1446-54.

XU, J., MA, H. & LIU, Y. 2017. Stochastic Optical Reconstruction Microscopy (STORM). *Curr Protoc Cytom,* 81**,** 12 46 1-12 46 27.

YAMAMOTO, Y., KONIG, P., HENRICH, M., DEDIO, J. & KUMMER, W. 2006. Hypoxia induces production of nitric oxide and reactive oxygen species in glomus cells of rat carotid body. *Cell Tissue Res,* 325**,** 3-11.

YAO, Y., CHEN, J., LI, X., CHEN, Z. F. & LI, P. 2023. A carotid body-brainstem neural circuit mediates sighing in hypoxia. *Curr Biol,* 33**,** 827-837 e4.

YENTES, J. M., FALLAHTAFTI, F., DENTON, W. & RENNARD, S. I. 2020. COPD Patients Have a Restricted Breathing Pattern That Persists with Increased Metabolic Demands. *COPD,* 17**,** 245-252.

ZAPATA, P., HESS, A., BLISS, E. L. & EYZAGUIRRE, C. 1969. Chemical, electron microscopic and physiological observations on the role of catecholamines in the carotid body. *Brain Res,* 14**,** 473-96.

ZENG, G. B. 1989. [The renin-angiotensin-aldosterone system changes in chronic obstructive pulmonary disease]. *Zhonghua Jie He He Hu Xi Za Zhi,* 12**,** 265-7, 317.

ZHANG, M., MA, Y., YE, X., ZHANG, N., PAN, L. & WANG, B. 2023. TRP (transient receptor potential) ion channel family: structures, biological functions and therapeutic interventions for diseases. *Signal Transduct Target Ther,* 8**,** 261.

ZHDANOV, A. V., WARD, M. W., PREHN, J. H. & PAPKOVSKY, D. B. 2008. Dynamics of intracellular oxygen in PC12 Cells upon stimulation of neurotransmission. *J Biol Chem,* 283**,** 5650-61.

ZHOLOS, A. V. 2015. TRP Channels in Respiratory Pathophysiology: The Role of Oxidative, Chemical Irritant and Temperature Stimuli. *Current Neuropharmacology,* 13**,** 279-291.

ZHOU, T., CHIEN, M.-S., KALEEM, S. & MATSUNAMI, H. 2016. Single cell transcriptome analysis of mouse carotid body glomus cells. *The Journal of physiology,* 594**,** 4225-51.

ZOCCAL, D. B., VIEIRA, B. N., MENDES, L. R., EVANGELISTA, A. B. & LEIRAO, I. P. 2024. Hypoxia sensing in the body: An update on the peripheral and central mechanisms. *Experimental Physiology,* 109**,** 461-469.